PB86-194099

Physics of the Earthquake Focus

Editor
M. A. SADOVSKII

REPRODUCED BY
NATIONAL TECHNICAL
INFORMATION SERVICE

PHYSICS OF THE EARTHQUAKE FOCUS

1.a

TT 76-52028

AKADEMIYA NAUK SSSR
Trudy Ordena Lenina Instituta Fiziki Zemli im. O.Yu. Shmidta

ACADEMY OF SCIENCES OF THE USSR
Transactions of the Order of Lenin O.Yu. Shmidt Institute of Physics of the Earth

Physics of the Earthquake Focus

[*Fizika Ochaga Zemletryaseniya*]

Editor
M.A. SADOVSKII

Nauka Publishers,
Moscow, 1975

Translated from Russian

Published for the United States Department of the Interior,
and the National Science Foundation, Washington, D.C., by
Amerind Publishing Co. Pvt. Ltd., New Delhi
1985

Preceding page blank

NTIS is authorized to reproduce and sell this report. Permission for further reproduction must be obtained from the copyright owner.

© 1985 Oxonian Press Pvt. Ltd., New Delhi

Translated for the United States Department of the Interior, pursuant to an agreement with the National Science Foundation, Washington, D.C., by Amerind Publishing Co. Pvt. Ltd., 66 Janpath, New Delhi 110001

Translator: Dr. S. Guha
General Editor: Dr. V.S. Kothekar

Available from the U.S. Department of Commerce,
National Technical Information Service,
Springfield, Virginia 22161

Printed at Gidson Printing Works, New Delhi, India

UDC 550.348.098.43

In this volume, for the first time, the physics of fractures is used to examine and generalize certain aspects of the processes preparatory to an earthquake and concomitant changes in the physical state of the medium in the region of the earthquake focus. The book covers a wide range of problems including theoretical studies and laboratory and field experiments, as formulated by the Section of Physics of the Focus and Forerunners of Earthquakes at the Institute of Physics of the Earth, Academy of Sciences of the USSR.

The book is intended for a wide range of geophysicists, geologists and specialists working on the physics of fractures.

Preceding page blank

for understanding earthquake precursors is rated high in some foreign works. V.I. Myachkin and O.D. Voevoda's paper gives a statistical description of destructive processes in heterogeneous medium and discusses the scope for its use in the study of earthquake precursors. The concluding paper in Section I, by S.I. Zubkov and V.I. Myachkin, examines the validity of the laws of endurance limit for ascertaining the time of appearance of forerunners and establishes an empirical relationship between the earthquake energy and the magnitude of the stress drop.

Section II, devoted to laboratory studies, begins with an introductory article by G.A. Sobolev and O.G. Shamina, where the most pertinent experimental results on destruction of rocks and materials under compression are analyzed. They identify the key problems whose solution is essential for an insight into the physics of earthquake preparation, which substantiates the program of laboratory studies drawn up by the IFZ. The subsequent articles elucidate the results of some studies carried out under this program. We may mention first the article by O.G. Shamina and co-workers describing successful experiments on controlled shear fractures, which permit the observation of changes in the physical properties of materials responsible for the appearance of certain forerunners of earthquakes observed prior to the development of the main shear crack. No less fascinating are the analogies between the development of seismic processes and processes of fracturing of laboratory specimens drawn in S.D. Vinogradov's article. Here certain arguments for the similarity of these processes are advanced, of course not so much to clarify the essence of the matter as much to stress its significance. Some information on the phenomena accompanying straining and fracturing of rocks is given in the articles by I.S. Tomashevskaya, E.I. Parkhomenko, and others. The nature of such effects as triboluminescence of the air and triboelectrification of rocks during earthquakes is discussed. It is shown that during hydration and dehydration of rocks there is a possibility of redistribution of mechanical stresses in the rock mass.

Studies on seismic prospecting and mechanoelectric phenomena in seismoactive areas of Kamchatka are described in detail in Section III, dealing with field studies. The article by O.I. Silaeva et al. on the ultrasonic sounding of the surface layer of tectonically dislocated ground is included here. It provides a new approach to the study of the earthquake focus. Mention must be made of G.A. Sobolev's note on the inter-relations of strong earthquakes in the Kurile-Kamchatka area.

As already noted, this collection does not claim to be an exhaustive treatment of the present state of the art of the Physics of Earthquake Focus. Nor does it cover all the research in progress at the IFZ. Its object is only to highlight the most pertinent broad directions of this research, which as experience has shown, have been appreciated not only in our country but also abroad.

It is quite probable that the material furnished here will require substantial revision very soon. For instance, our understanding of the processes occurring at the earthquake focus may be broadened substantially by studies in the electric conductivity of the crust in the area of an imminent earthquake. Geodesic observations of the epicentral zones of future earthquakes also seem to be highly promising. We also feel that the study of residual strains and dislocations in this zone has been rather neglected. The energetics of a seismic focus can hardly be understood without a clear comprehension of the magnitude and nature of residual phenomena. Lastly, it cannot be ruled out that the crack-forming process will have to be studied in two-phase media, taking note of the presence of water in cracks that has either intruded from outside or has appeared in the process of dehydration. All this, of course, is a matter for the future. Right now we hope that the material presented in this volume will be useful to scientists engaged in the study of seismic foci.

M.A. Sadovskii

III. TECHNIQUES AND SOME RESULTS OF FIELD STUDIES

UDC 550.34.01.013

Fundamentals of Physics of the Earthquake Focus Forerunners

V.I. Myachkin, B.V. Kostrov, G.A. Sobolev and O.G. Shamina

The paper examines the general postulates of the physics of the earthquake focus and basic data for these postulates available from observations, laboratory experiments and theoretical calculations in the field of fracture mechanics. It formulates concepts relating to the process of building up of fractures in the earthquake focus. These concepts offer a possible explanation for the overall nature of the change in earthquake forerunners with time as confirmed by field observations.

Interest in the earthquake focus is as old as seismology itself. As far back as 1910 Reid advanced a hypothesis correlating earthquakes and fracturing of the earth's material. However, seismology subsequently developed mainly along the lines of study of the earth's structure. This is explained not only by the great scientific and economic importance of the study of the earth's interior, but also by the fact that a knowledge of the structure of the medium and of the laws of propagation of seismic wave is an essential prerequisite for studies on the focus. Moreover, it was impossible to study the earthquake focus as a factor of rupture of the medium without an adequately developed physics of rupture of solid bodies. As is well known, mechanics of rupture originated in the mid-twenties, began to develop vigorously only in the post-war years in the context of growing constructional requirements, and is developing particularly rapidly now.

Developments in seismology, particularly the discovery of its key lines in the thirties, permitted the initiation of studies on earthquake. These studies for long proceeded independently of fracture physics (parallel with its development). They involved building what are called "seismologic" models of the focus based more on observational data than on well-formulated physical concepts of rupture processes. The classical works of Byerly, Keilis-Borok, Vvedenskaya, Honda, and others are well known as the principal sources of information on the focus from seismologic observations. The work of A.V. Vvedenskaya and co-workers, who developed methods for determining the orientations of the axes of the major stresses in the earthquake foci, deserves

special attention. Contemporaneously a large group of seismologists at the IFZ continued to develop Academician G.A. Gamburtsev's ideas on earthquake physics. These studies, conducted in "natural" laboratories, i.e. in seismoactive areas of the country and in mines, provided extremely useful data on various physical characteristics of earthquakes: the energetics of individual earthquakes and their sum total, space-time correlations, changes in the properties of the medium, etc. (Yu.V. Riznichenko, I.L. Nersesov, S.D. Vinogradov, V.I. Myachkin, O.G. Shamina and others). Geologic and tectonophysical concepts of the formation and development of crustal faults (V.V. Belousov, M.V. Gzovskii and K.I. Kuznetsov) and of the seismic flow of rock masses (Yu.V. Riznichenko) developed further.

A theory of the earthquake focus based on a combination of certain results of fracture mechanics and achievements of seismology began to develop in the mid-sixties (Knopoff, Burridge, Holmes and B.V. Kostrov). Extensive exploratory studies of earthquake prognosis demanded a much deeper knowledge of the processes leading up to earthquakes. Therefore in many organizations the scope of laboratory experiments on the physics of material fracturing was widened with a special emphasis on "seismologic" investigations. The main attention was directed to the processes of formation of micro- and macrocracks due to shear fracturing and the concomitant changes in the physico-mechanical properties of specimens and models.

The most revealing result of prognostic field studies in recent years is that prognostic symptoms (at least some of them) are detected in quite diverse areas of the globe and have a similar time-dependent course related to earthquake energy [1–3].

Advances in fracture mechanics and, in particular, seismologic type special laboratory experiments now allow a qualitative interpretation of the field results obtained and offer new opportunities for prognostic studies. In our view, the level of development of the fracture theory and concepts of earthquake focus, recent laboratory experiments, and field observations, allow us to formulate a theory of preparatory earthquake processes. Such a theory is essential for solving several fundamental problems of modern geophysics and, primarily, for such national tasks as prognosis of the time of occurrence of strong earthquakes, prognosis of the real impact of earthquakes on the ground surface and man-made structures, development of new methods for seismic zonation, etc.

FUNDAMENTAL CONCEPTS IN PHYSICS OF THE EARTHQUAKE FOCUS

The term "earthquake focus" is interpreted in seismological literature in most diverse ways. It is a point (hypocenter) having definite coordinates, a center, or an area (volume) bounded by after-shock coordinates.

According to recent data, the focus of a tectonic earthquake is a dynamic (rapid) break in the continuity of the earth's material resulting from strain built up in the process of tectonic shear deformations. This break occurs on some surface. The subject matter of the physics of earthquake focus is in effect the study of dynamic and quasistatic processes of growth and healing of faults. In essence, *the physics of earthquake focus is the physics of the collapse of rock masses (earth's matter) in the environment of the earth's interior.** It is obvious that the earthquake focus as a process of rapid fault propagation cannot be comprehended and physically described without an understanding of the circumstances of the inception and cessation of the fault. That is why the physics of focus transcends the framework of the earthquake in action and is logically divided into three major sections (see Table): 1) physics of earthquake preparation; 2) physics of earthquake in action; and 3) physics of residual phenomena.

Table

Physics of earthquake focus		
Precursors, month	Dynamic faulting, sec	Residual phenomena, month
Stressed state in space and time	Loss of resistance to macrofaulting	Redistribution of stresses in space and time
Accumulation and development of minor flaws	Widening of fault and radiation of seismic waves	Appearance of secondary faults
Formation of macrofaults	Cessation of fault	Healing of macrofaults

An identical approach to the classification of the seismic process was earlier suggested by Kasahara [4]. He divided it into three stages, viz. preseismic, seismic proper (fault), and postseismic. M.V. Gzovskii [19] differentiated similar stages in tectonic faulting. Later, M.V. Rats and S.N. Chernyshev [5], who "modernized" M.V. Gzovskii's classification, brought the tectonic faulting stages into direct correspondence with the scheme now accepted in physics [5, p. 76] and noted uniform fracturing throughout the strained body, concentration and merger of cracks, formation and expansion of faults, etc.

M.V. Gzovskii combines the first two stages into one and adds a terminal stage of retarded expansion of the fault formed.

*We will confine ourselves to this earthquake mechanism and refrain from discussing the probability of earthquakes of a different type as, for instance, ones caused by changes in specific volume due to phase transitions.

In our classification the stage of uniform fracturing in space, though significant for an insight into the causes of earthquakes, may not be formally discussed in the framework of the physics of earthquake focus.

The preparation of the earthquake proper begins with an avalanchelike increase in the number and dimensions of cracks after they attain a "critical" density in some space and culminate with the formation of several "starting" cracks in the plane of what will be the main fault. This process, which alters the effective (integral) physico-mechanical properties of the medium involves a specific space-time course of seismic energy release and is the basis for prognosis of the probable space, time and magnitude of the earthquake.

The formation of the main fault and the circumstances of its inception, rapid spread and cessation are included in the section on the physics of the earthquake in action. Segregation of this stage from the subsequent expansion of the fault (as also according to M.V. Gzovskii) is essential for seismology, since a knowledge of the circumstances of the inception and cessation of an isolated fault is an important clue to an understanding of the preparatory processes and the residual phenomena.

Study of the residual phenomena (penetration, branching and healing of the main fault) permits a rapid, purposeful addition to our knowledge of earthquake and is therefore treated as a separate discipline.

FUNDAMENTAL CONCEPTS OF DESTRUCTIVE PROCESSES

Three types of destructive phenomena are now distinguished under different circumstances of stress application, e.g. the instant at which a constant stress is applied (rapid destruction), the impact of repeated stresses (fatigue), and the impact of prolonged stresses (delayed destruction and endurance limit).

The classical theories of ultimate strength were based on the concept that a definite stress, critical for the material (its endurance limit or ultimate resistance), has to be applied to the material to bring about its rapid collapse. The number of cycles or the duration of the stress is a characteristic of the process of fatigue or delayed collapse of the material. It was assumed that the strained medium is continuous and homogeneous. This precludes the probability of the dependence of physical mechanism of the collapse on the structure of the material. Progress in solid state physics permitted the inclusion in resistance theory models of the material of an ideal crystal lattice. But it raised certain issues: for instance, theoretical strength was found to be higher by many orders than the actual strength Griffith [6], Irwin [7], Orowan [8] and others tried to overcome these issues.

Fracturing of solid material is correlated with the occurrence and appearance of numerous microcracks in the material. Cracks spread (grow) when the rise in surface energy is compensated by a fall in the elastic energy stored

in the medium. The effective specific surface energy (i.e. the resistance to crack growth) γ_{eff} includes all the mechanical energy spent irreversibly (particularly for plastic deformation) around the crack margin per unit of recreated surface.

Isolated (*solitary*) *crack*. The condition of its movement is given by

$$G = 2\gamma_{eff}, \tag{1}$$

where G is the crack-moving force.

In a homogeneous stress field in an elastic homogeneous medium the crack-moving force is related to the stress and the size of the crack by the equation

$$G = c\,\sigma^2 l/2\mu, \tag{2}$$

where c is a dimensionless coefficient dependent on the shape of the crack and the type of stress, and μ is the shear modulus of the medium. The critical stress for an isolated crack is derived from (1) and (2) as

$$\sigma = \sqrt{\frac{4\mu\gamma_{eff}}{c\,l}}.$$

The correlation between the critical stress and the length of the crack is expressed by curve 1 in Fig. 1. Upon increase of stress to the value

$$\sigma_{0.1}(\sigma_{0.1}) = 2\sqrt{\mu\gamma_{eff}/c\,l_1}$$

a crack of length l_1 begins to spread dynamically, unrestrained until complete disintegration of the body. Arrest of a fast crack is possible if the stress field or the medium is heterogeneous. The critical stress in a heterogeneous medium is depicted in Fig. 1 by curve 2. The crack passes into the equilibrium stage after attaining the length l_2 and grows steadily with further quasistatic increase of stress.

Crack growth may be slow even at constant stress. The fact that γ_{eff} is dependent on the rate of crack movement is the basis for understanding this

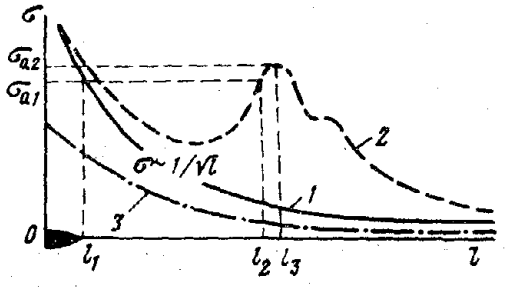

Fig. 1. Variation in breaking stress with crack length.

process (Fig. 2). Part of the energy needed for the disintegration of the material at the margins of the crack may be supplied by nonmechanical means, for instance, through fluctuations in the thermal motion of molecules, a fall in the surface tension of the active medium (Rebinder effect) [9], or the corrosive action of the medium (corrosion under stress). The mechanical work done in all these processes is less, the longer the destructive process at the margins of the cracks, i.e. the slower the growth of the crack. The irrecoverable losses involved in disintegration diminish at fairly high growth rates. Rapid disintegration sets in at a crack-moving force equaling the maximum value of $2\gamma_{eff}$, denoted by G_c (critical) in Fig. 2. Crack growth is slow when $G < G_c$. If γ_{eff} has a finite value (not defined so far) at zero rate, then there should be a range of safe G values and correspondingly a range of safe stresses dependent on the size of the crack (curve 3 in Fig. 1).

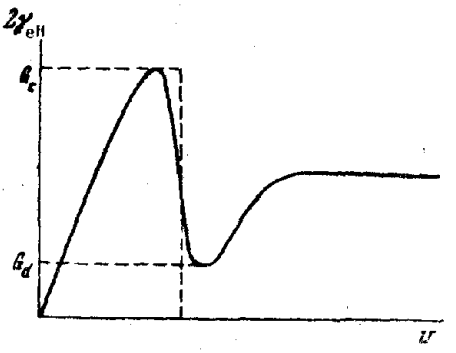

Fig. 2. Variation in effective surface energy with rate of crack movement.

Description of materials with the help of model of continuous medium that ignored the structure of the material of lower ranks and typical size, which is much smaller than the size of the crack, was successful only within certain limits. It was found that the spread of a crack of any size is facilitated by the formation and growth of defects and the destruction of structures of a lower order. Therefore the hierarchy of models has to be discussed right from the molecular level, i.e. from the structure and defects of the crystal lattice, and going on to models of continuous media that altogether ignore the inner structure of the material. Such a hierarchy of structures for metallic structural materials is shown in Fig. 3.

In geological studies dealing with faults running for hundreds or thousands of kilometers the following categories of fractures are identified: Microcracks splitting isolated crystals and parts of rocks (0.01 mm–10 cm); macrocracks visible in exposures (10–100 cm); fractures ripping rock massifs (100 m–10 km); and large tectonic faults right up to deep faults breaching whole blocks of the lithosphere [5]. It should be noted here that the char-

acteristics of the medium vary with the scale but are determined by the properties of the material at the lower (micro) levels. In particular, the resistance to crack growth $2\gamma_{eff}$ mounts at each higher level, for it includes losses entailed in microcrack formation, i.e. it includes losses entailed in failure at the preceding level. This fact offers an easy explanation of the known experi-

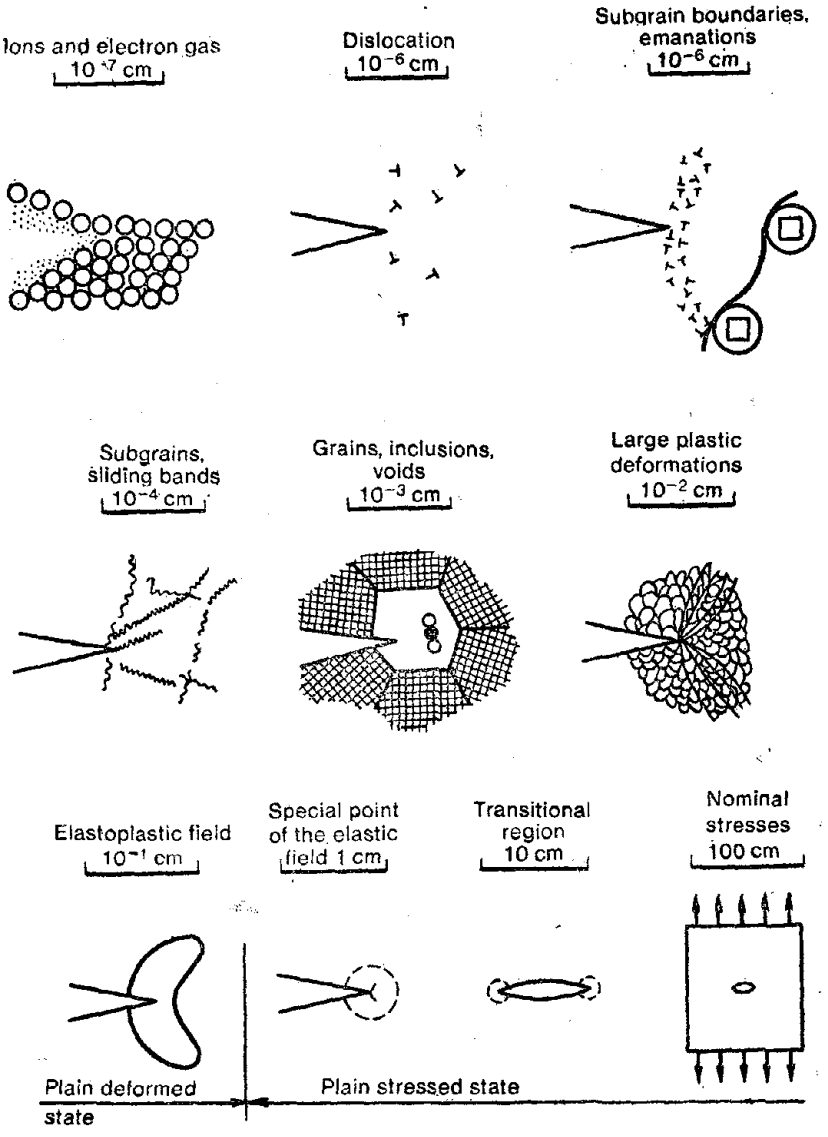

Fig. 3. Characteristic scales of structural heterogeneity of material [10].

mental data, the discreteness of slow crack growth, and the arrest of fast cracks when they attain some characteristic length [11].

Crack arrays. Numerous experiments have shown that collapse generally occurs due to formation of microcrack arrays and their merger into a main fault with the disintegration of the bridges linking them. Disintegration by an isolated crack is nothing but a graphic theoretical approximation [11]. Analysis of experimental and theoretical results shows that the avalanchelike disintegration stage is caused by interception of defects (cracks) when a definite microcrack concentration is reached in the material, which is dependent on the conditions of stresses and the structural heterogeneity of the medium [11, 12]. Attainment of a definite crack concentration under prolonged stresses can be explained by the delayed growth of cracks, which forestalls the growth of the remaining cracks at the strength barriers of the microstructure of the material. In the case of fast stresses "diffusional" disintegration occurs due to the steady growth of tensile cracks at the shear crack boundaries.

The part played by interaction of cracks in the acceleration and instability of the crack-forming process is well illustrated by theoretical correlations of critical stresses for crack arrays in a homogeneous field (Fig. 4). For the interaction of two unequal cracks it was found that the growth of minor cracks is retarded or altogether arrested when these cracks occur above or under the plane of a major crack. It is obvious that cases of mutually accelerating rather than retarding disposition (at least at the initial stage of interaction) should be more common when the microcracks are scattered in space with statistical uniformity and oriented in a predominant direction. From the macroscopic standpoint rupturing dislocation in cracks contributes to the

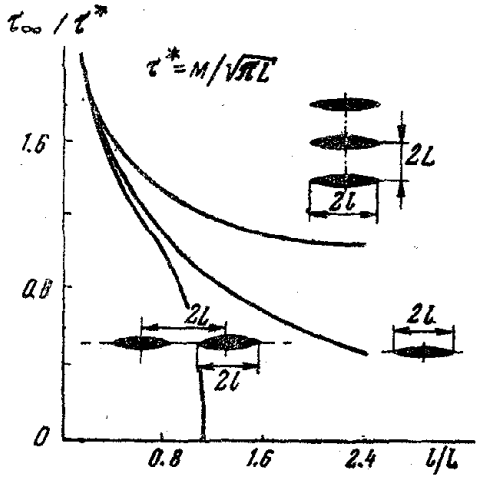

Fig. 4. Stability of crack array in a homogeneous medium [13].

straining of the material. This contribution is proportional to the stress and the cube of the average crack size. The avalanchelike process of crack formation and, correspondingly, macrodeformations, are unstable, i.e. acceleration may occur even on lowering the macrostress level. Due to the microheterogeneity of the medium the unstable accelerated crack-forming process is increasingly dispersed and localized in narrow cracklike zones [11, 12] giving rise to the main fault. Mogi's experiments [14] are an excellent illustration of the dynamics of such a process under progressive stress.

The time base of places and the energy of acoustic impulses corresponding to rapid dynamic cracks are shown in Fig. 5.

Concentration of cracks approaching the main fault was also noted in geologic studies (Fig. 6). The process of localization of macrodeformation

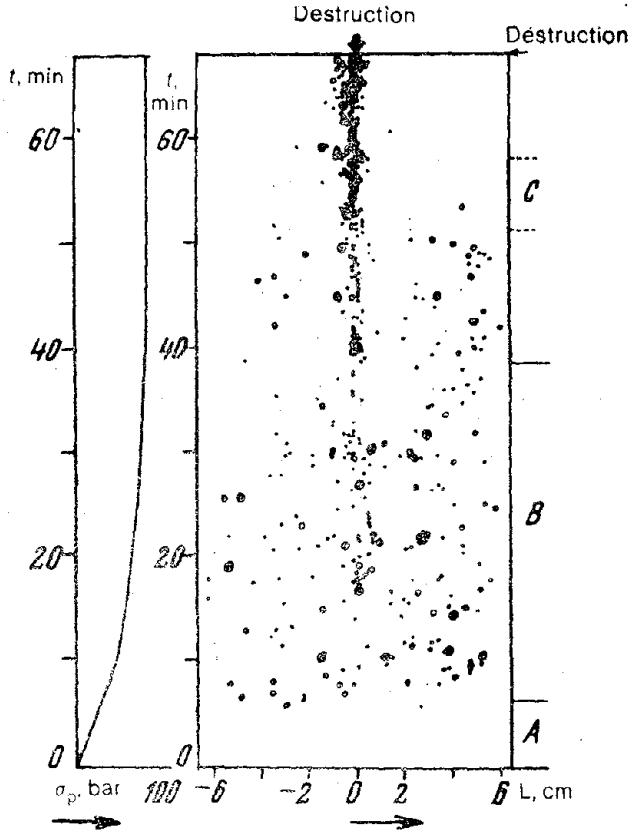

Fig. 5. Space-time distribution of sources of elastic impulses in strained granite specimen [14]:

A—Absence of microfissures; B—Their diffusional distribution in space; C—Their concentration in the direction of the future main fault.

in a narrow zone is shown diagrammatically in Fig. 7.

The avalanchelike unstable process begins in the hatched area when the stress becomes σ_0 and the strain becomes ϵ_0. The strain rises to ϵ_1' as the stress throughout the space drops to σ_1. At all other points of the body remaining in an elastic state the strain is "restored" to ϵ_1. The instability of the crack-forming process is illustrated in Fig. 7 from the macroscopic standpoint.

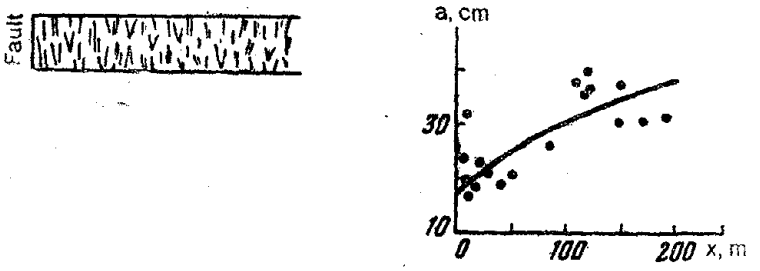

Fig. 6. Variation in density of advancing cracks with proximity to fault [2].

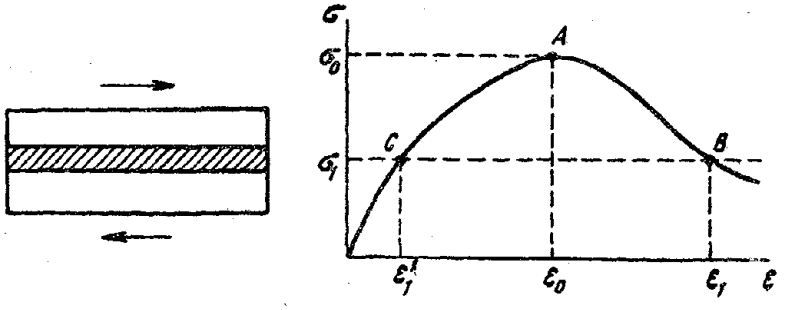

Fig. 7. Stress-strain diagram for internal fracturing of material.

Let us also state that at a constant strain rate the acceleration of the process may reduce the applied stress and correspondingly retard the process to such an extent that dynamic growth of the macrofault formed would become impossible. In such a case the dynamic phenomena (fissures) become markedly intense in the preparatory phase of macrofracturing and abate with the release of macrostress.

Factors affecting the rate of crack formation. Higher stress gives rise to a larger number of fractures and accelerates their formation. In polymers the longest microfractures appear with a smaller number of microcracks at lower stresses [11, 12]. Correspondingly, the avalanche stage is accelerated under

increased stresses. It is certain that the rate of the process is affected by the nature of the stressed state, in particular by the correlation of the major compressive stresses. It was found that the links between cracks disintegrate at a lower rate than isolated cracks spread dynamically. For instance, the retardation factor is nearly 5 for steel [11].

Faster fracturing at higher temperatures can be explained in a similar way [12]. Because of irreversible changes in the resistance of the stressed material as well as in the surface-active media containing matter liable to be strongly absorbed on the surface of the crack the impact of the surrounding medium is very strong [9, 12]. The nature of the impact of these factors on the rate of the avalanche stage is largely dependent on the correlation of the rates of crack growth and diffusion of the corrosive medium.

It is known that "old" healed cracks in a material delay fracturing [11]. Perhaps it is right to say that these cracks are simply parts of the structure of the material and conform to the general concepts of the effect of strength barriers.

The following postulates of fracture mechanics as applied to the physics of the earthquake focus are most important:

1. Fracturing of statistically homogeneous materials under prolonged stresses occurs due to a rise in the number and size of crack-forming defects.
2. Defects increase under practically any stress and are formed faster with increased stress (crack kinetics).
3. Total deformation is made up of elastic and effective deformation caused by relative shifting of crack boundaries.
4. Macrofracturing (formation of main fault) results from avalanchelike growth and instability of total deformation attained at a critical crack density and demands a definite time span.
5. Formation of the main fault causes a reduction in the stress level in the surrounding space, such that the growth of new defects is delayed and the number of active cracks decreases.

The translation of these concepts into the seismologic scale demands that the description of the process of delayed fracturing in essential outline should be independent of the structural level.

Thus fracture mechanics offers a vivid qualitative picture of the destructive process under prolonged stresses. However, the quantitative theory for this process in media heterogeneous in strength is very complex and is, indeed, only now being formulated.

PHYSICS OF EARTHQUAKE PRECURSORS

In geophysics and geology the main attention of the student of preparatory earthquake processes was long diverted to the correlations between stresses and strains. It was generally supposed that the role of cracks and

defects was confined to dissipating the potential energy of elastic stresses in rheological models of the medium [15] and to contributing to the average tectonic straining [16, 17] and the seismic flow of rock masses [18]. Heterogeneity of the stress field was correlated mainly with the difference in the rate of straining of crustal blocks or with the concentration of stresses in geological heterogeneities. The tectonic and physical concepts of M.V. Gzovskii and co-workers [19], who stressed the role of ruptures as stress concentrators, did not develop far enough in the sixties.

These concepts would hardly lead us to expect any striking features in the behavior of the stress and strain field and corresponding changes in the physico-mechanical properties of the medium just before the earthquake. We believe that the very popularity of the concepts of monotonous changes in stresses and strains throughout build-up to the earthquake led to gross underestimation of the magnitudes of the earthquake preparatory phenomena. For instance, Hayakawa [20] believed that it was almost impossible to record changes in velocities of elastic waves even though specialists in rock fracture argued the great importance of crack formation [20], and the results of numerous laboratory, mining, and field observations testifying to sharp changes in the physico-mechanical properties of rocks and to the time-dependent course of seismic processes [21, 22] were known by them.

It is quite obvious now that the appearance and development of cracks in time and space with changes in the stressed state are decisive factors in the forerunners of any fault, including earthquakes.

Space- and time-dependent course of processes in focal zones of earthquakes and physical foundation of earthquake forerunners. Let us examine from the premises of fracture physics the general time-dependent course of earthquake forerunners involving development of microfractures at lower levels, as also the salient external features (microprocesses), i.e. deformations and effective parameters, of the state and physical properties of the medium.

Real rocks always contain defects or microcracks scattered at random in space.

Definitely oriented tectonic shear stresses induce the slow growth of statistically evenly dispersed defects and the formation of new ones. At a definite level of average stresses, which in our view changes slowly in time, the growth and appearance of new microcracks are accelerated and begin to prevail over the process of closure. The displacements along fracture sides in each defect contribute to the total deformation of the entire space. This fracturing is likely to occur statistically evenly throughout the space with the development and formation of shear and tensile cracks [11, 23].

In principle there should also be a change in the properties of the medium, e.g. the effective modulus of elasticity, and an additional anisotropy at this stage which corresponds to the precritical stage of fracture of the specimen. This is stage I in Fig. 8 showing the rate of average strain with time. Stage I

does not seem to depict phenomena of the forerunner type.

The irreversible avalanchelike preparatory stage of an earthquake begins after a certain average critical microcrack density is reached throughout a volume or in a large part thereof. The process is markedly accelerated throughout the volume due to microcrack interaction. Rapid stress redistribution in spasmodically increasing microcracks (one may perhaps refer to microcracks of the next "rank" in size) also promotes acceleration of the process as a whole. The areas "lagging" a little in density of defects are activated and a large part of the volume is gradually involved in the process of avalanchelike microfracturing. The rate of inelastic deformation and variation in integral physical properties of the medium markedly rises accordingly.

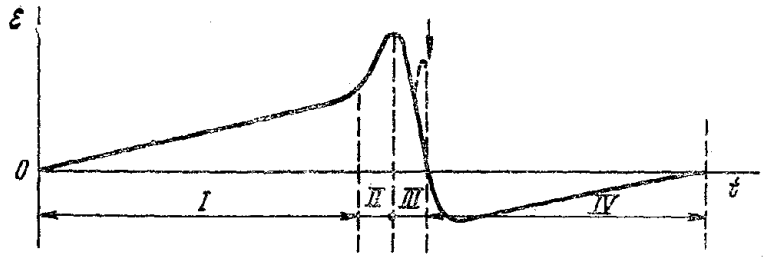

Fig. 8. Variation in rate of average strain during seismic cycle.

As the forerunner of an earthquake such a process would be unstable, and because of the heterogeneity of the medium would be confined to a small number of narrow zones, in each one of which several relatively large cracks would be formed in closely lying planes. In such a case minor cracks cease to develop in a large part of the volume due to stress release in the zone and perhaps partially heal up. The integral rate of straining of the entire zone diminishes because it is now regulated mainly by crack growth, initially in several narrow zones and subsequently in only one of them (Fig. 8, stage III). There is an apparent "restoration" of many integral characteristics of the zone in general. This ray-shaped course of the strain rate at stages II and III shows the trend of change of the total area of microfractures. Understandably, time-dependent changes are in reality not smooth and should assume an abrupt form flaired like a bay.

A narrow zone of unstable deformation involves an increased concentration of fractures and serves as the surface of the future main fault. This earthquake fault is formed upon the rupture of links between embryonal cracks. The process of link rupture is qualitatively analogous to the entire process as such and therefore should be preceded by a brief, narrower variation of the strain rate. Since rupture of one of the links may not be enough

for the entire main fault to rip open, there should be several such brief variations in the strain rate. These fluctuations may be regarded as forerunners of strong foreshocks.

The entire zone adjoining the fracture plane is relaxed immediately after the earthquake. The stresses shift to the margin of this new fracture. The strain rate may be negative after the earthquake because many local fractures relieved of stresses may give rise to reverse shoves.

It should be pointed out that the instant of the earthquake, i.e. the ripping open of the main fault, is provisionally referred in Fig. 8 to zero strain rate. In reality, the magnitude and sign of strain rate at the instant of the earthquake depend on the extent of relaxation of the entire area of the earthquake prepared by a narrow zone of starting fractures and, consequently, on the number of these fractures and the size of the links between them.

The above concepts of the general course of crack-forming processes allow us to explain the behavior of various earthquake forerunners with time. Examples of pre-earthquake variations in geophysical and other fields observed by different observers are given in Fig. 9. It is striking that these forerunners follow a somewhat bay-shaped course.

The course of the forerunners conforming to the process discussed above is diagrammatically shown in Fig. 10.

All forerunners dependent on the magnitude of total strain (variations in distance and heights between points on the earth's surface, slopes) should be proportional to the average magnitude of directed shoves and, consequently, to the sum of the fractured areas. Their general course is derived by simple integration of strain rates, depicted in Fig. 8.

The velocity of elastic waves is dependent mainly on the effective modulus of elasticity of the medium. It is known that during avalanchelike crack growth (Fig. 8, stage II) the effective modulus of elasticity (wavelength greater than crack size) diminishes with a concomitant sharp fall in the velocity of elastic waves. At stage III (Fig. 8), when most of the minor cracks heal up, the effective modulus of elasticity is restored because it remains almost unaffected by a small number of large cracks. The correlation of velocities of longitudinal and transverse waves will assume the same appearance.

The energy of weak earthquakes of magnitudes 2 or 3 aggregated for a certain time that is much shorter than the duration of the main fault preparation is proportional to the aggregate area of fractures formed in that time. The curve for $E^{2/3}$ would simulate the average strain rate curve provided the average variation in the aggregate area of dynamic fractures in unit time is proportional to the variation in aggregate area of slowly growing fractures. The decrease in the slope of the earthquake repetition curve γ (higher proportion of strong earthquakes) should be fairely sharp at stage II and somewhat gentler at stage III.

The increase in the content of radon and other products of radioactive decay and in spring discharge is dependent on the extent of rock fracturing which, consequently, increases markedly at stage II and continues to do so till stage III when large, but few, fractures are formed. The curve for this

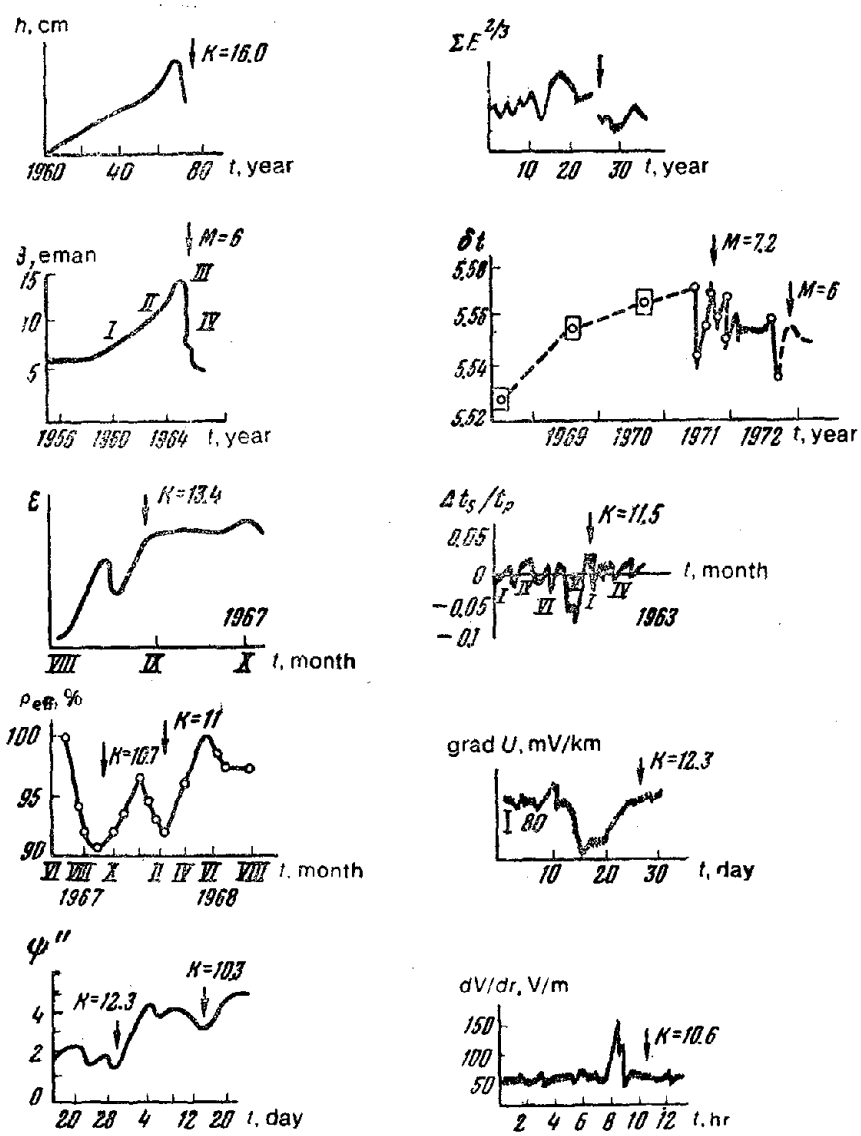

Fig. 9. Variation in geophysical fields in earthquake preparatory process [1].

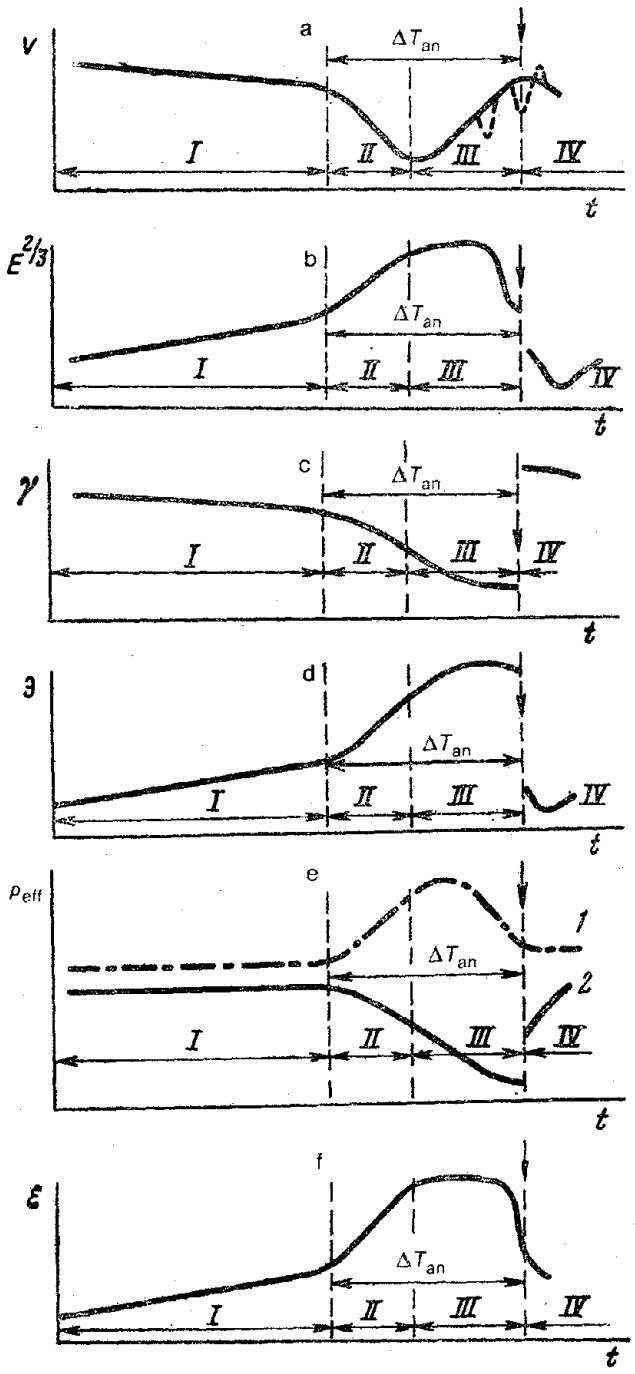

Fig. 10. General time-dependent course of earthquake forerunners corresponding to course in Fig. 8:

a—Velocity of elastic waves; b—Earthquake energy; c—Slope of repetition curve; d—Radon concentration; e—Elastic resistance and telluric potentials; f—Dislocation of earth's surface. 1—Dry rocks; 2—water-saturated rocks.

forerunner is also likely to show a fall prior to the earthquake, when many minor cracks heal up.

The electrical resistance of dry rocks should increase at stage II and diminish at stage III. On the contrary, the electrical resistance of water-saturated rocks should fall sharply at stage II and diminish progressively, of course at a lower rate, at stage III, provided water diffuses into the formed cracks. Perhaps the gradients of electrotelluric currents should change likewise.

The above behavior of the forerunners corresponds to their conduct during measurements right in the zone where avalanchelike crack growth and subsequent formation of fracture planes occur. Measurements of the strains and physical properties of the medium beyond this zone show the effects to be dependent not so much on crack formation as on the relatively sharp change in the stressed state. Perhaps an analogy with mining operations is appropriate here. The pressure (stress) borne by a block of rock away from the mining area (in the particular case this block loses its bearing capacity) is transferred to contiguous areas. In that case certain properties of the medium will change differently. For instance, at stage II the velocity of elastic waves should increase but the electrical resistance in dry rocks should decrease. At the same time, the deformation and electrical resistance of water-saturated rocks may follow a time-dependent course akin to that in the focal zone, but may be induced by different physical factors. The increase in strain will be induced by the elastic part, whereas electrical resistance will fall due to the rise of capillary water.

Reference should also be made to the course of the curves (Fig. 10) at stage IV immediately after the earthquake. The major part of the aftershocks occurs outside the preparation zone of a particular earthquake. Therefore, if the technique for measuring the physical properties of the medium fails to differentiate the processes within the zone from those beyond, the course of the curves after the earthquake will not correspond to the curves in Fig. 10.

Energy dependence of the time of earthquake preparation. The earliest experimental data on the energy dependence of the time of earthquake preparation were obtained in the study of the correlations of anomalous longitudinal and transverse wave velocities [24] and strain rates [25]. The average curve showing dependence of the logarithm of the time of appearance of anomalies ΔT_{an} on the logarithm of energy $K = \log E$ [1] is plotted in Fig. 11. Ignoring anomalous slopes, we get the equation

$$\log \Delta T_{an} \cong 0.48\,K + c.$$

As a first approximation this equation can be explained from the standpoint of endurance limit, i.e. under the lower average stresses typical of strong earthquakes the rate of crack growth and interaction diminishes [11]. On

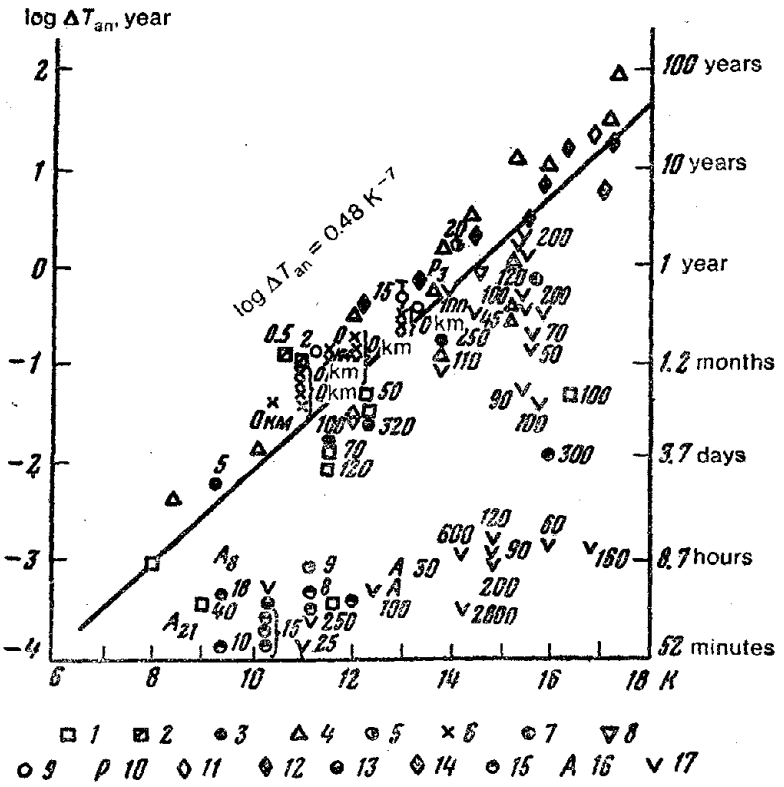

Fig. 11. Average curve showing dependence of time of earthquake preparation on energy [1]:

1—Grad U; 2—ρ_{eff}; 3-5—ϵ; 6—$\Delta t_S/t_P$; 7—V_P; 8—log $P_{5.0}/P_{2.5}$; 9—t_P, t_S, A_P; 10—Mach unit; 11—A_{10}; 12—$\Sigma E^{2/3}$; 13—W/t; 14—$Az°$; 15—dU/dr; 16—N_{ae}; 17—ψ. Figures next to symbols in graph indicate hypocentral distances.

the other hand, the processes of avalanchelike growth and formation of the narrow zone of the future main fault resulting in a strong earthquake may be prolonged simply because of the size of the preparation zone.

Several experiments of polymers [12] have shown that average crack dimensions under constant stresses increase with time logarithmically. In [26, 27] the correlation of time ΔT_{an} and magnitude M has the same slope in logarithmic coordinates upon conversion of magnitudes into energy. In explaining this correlation (and the forerunners themselves) the authors of [26, 27] emphasize the process of rock expansion and contraction (dilatancy) and the diffusional intrusion of water into the cracks. These views, often contradictory, demand separate and detailed examination. Here we will confine ourselves to a brief consideration of certain aspects.

The rate of diffusion of water in conjunction with the area of the pro-

pagation zone permits quantitative computation of the time of appearance of a forerunner while rock dilatancy coupled with subsequent filling of cracks with water enables us to build suitable qualitative models of the behavior of the forerunners by varying the proportion of dry and wet pores. The long-known effect of water on rock strength is also a valuable guide. However, dilatancy as a general mechanism of earthquake preparation should be treated with great caution, for this phenomenon [28] manifests itself under definite hydrostatic and other stresses.

Let us also note that in these studies dilatancy is mechanically transferred from the scale level of the specimen to be fractured to the scale level of the forerunners of earthquakes of any energy. Thus the increase in seismic activity and in the proportion of earthquakes of high magnitudes up to the strongest depends only on the statistical dispersal of the density of dilatancy in the medium.

How to substantiate the "supply" of sufficient water at great depths is not clear. In our view, it is more logical to link the influence of water on the earthquake preparation time with the size of the cracks that precede earthquakes at stages II and III.

Corrosion under stress was referred to above. The time required for the supply of water to the crack mouth (basing on the same concepts of diffusion) is proportional to the size of the crack formed dynamically on interaction. Consequently, the growth of large cracks is promoted by corrosion to a lesser extent than that of small cracks.

This explains why the V_P/V_S curves are asymmetric and the average size of the cracks formed is smaller at stage II than at stage III. This factor should also be considered in explaining and computing the preparation time of various classes of earthquakes.

Detection of the bay-shaped course of forerunners in laboratory experiments of dry material [29] does not allow us to agree with the necessity of diffused overflow of water in the process of preparation of the earthquake.

Referring to Fig. 11 again, let us note the concentration of points lying below the principal equation $\log \Delta T_{an} = 0.48 \log E + c$. The authors of [1]

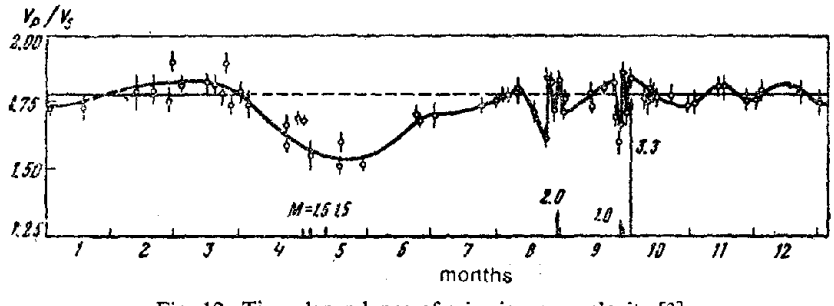

Fig. 12. Time dependence of seismic wave velocity [3].

suggest cautiously that these can be interpreted, at least for some cases, as brief forerunners. The concept developed in this article of brief forerunners as forerunners of strong foreshocks that rip open intercrack bridges may be illustrated by Fig. 12. It is striking that in the setting of reversion of the V_P/V_S curve to the previous level there are two bays accompanied by foreshocks relatively strong for the main event. Similar, "minor" bays showing foreshocks occur in other curves [3] and were observed earlier in Garm [2, 24]. Marked variations in the wave velocity were also noted before the earthquake of $M = 7.2$ on November 24, 1971 in Kamchatka [30]. In the same way we can also interpret the numerous anomalies in the electrotelluric field in Kamchatka [31].

PHYSICS OF ACTIVE EARTHQUAKES AND RESIDUAL PHENOMENA

Physical concepts of fracture of materials are used in the study of the seismic stage and earthquake in action. The question of the point source of waves equated with the earthquake focus has been decisively resolved; the focus has been described in physical terms, i.e. in terms of orientation and area of fault, magnitude of strain release, distribution of shoves on the fault surface, etc. [32]. The possibilities of determining these quantities from seismic observations have been ascertained.

On the basis of prolonged observations the dislocation model permitting introduction of new empirical characteristics of the focus, i.e. seismic moment and tensor of seismic moment of the focus, into seismology was found to be best suited to describing the focus in general [33, 34]. Seismic moment allows evaluation of certain integral properties of the focus independently of the fault area measured from observations on the surface of the earth, from macroseismic data [35], and from the dimensions of the aftershock area. The magnitudes of strain release at the focus of shallow earthquakes were astonishingly small (of the order of a few bars). This can easily be explained by the laws of fracture mechanics. Strain releases of the order of several kilobars in deep-focus earthquakes can often be attributed to an increase in the strength and homogeneity of material with depth. There is, however, a possibility of the dimensions of the foci of deep-focus earthquakes being underestimated.

Seismic moment is a measure of the contribution of an earthquake to the average strain [33] or, if the seismicity is caused by movement along an isolated fracture, to the average shove along the fracture [36]. Thus determination of seismic moments for an earthquake series enables us to study the correlation of seismicity and tectonic process as well as the peculiarities of the process in the preparatory stages of strong earthquakes. "Purer" prognosticators of the deformation type may perhaps be obtained this way.

Seismic radiations (their orientation, distribution of amplitudes and frequencies of P and S waves, energy, etc.) are dependent on the parameters of the fault (shape and size, rate of propagation, circumstances of interaction of sides of the fault, etc.). There are great theoretical possibilities for studying the peculiarities of radiation dependent on the structure and physical properties of the environment of various seismoactive areas and, consequently, for predicting the specific impact of destructive earthquakes. Experimental studies in rock strength and frictional characteristics under conditions simulating the process at the earthquake foci are called for. Theory here encounters formidable mathematical problems. Attempts were made in [37, 38] to provide a theoretical explanation of the form of spectra.

Let us point out that a study of the physical features of faults under diverse thermodynamic conditions is extremely important for the pre- and postseismic stages of earthquakes because these features determine the rate of the process as a whole and the correlation of the energies liberated and dissipated [39].

Like the preparation, the cessation of faults drags on, and due to the concentration of stresses the growth of defects is markedly accelerated and new earthquakes or aftershocks occur at the ends of the arrested fault. Conditions are created that are analogous to material testing under thrust.

Let us note that the familiar difference in the correlation of classes of energy and of the time of aftershocks of comparable energies can easily be explained by the postulates of fracture mechanics. Arrest of the fault by the strength barrier, beyond which is an area under higher stresses, causes the process to linger with strong aftershocks. Extension of the fault to the area under lower average stresses is responsible for fault cessation without significant residual phenomena. Generally the whole series of aftershocks is studied in seismology regardless of their location relative to the main fault. Yet it is obvious that the aftershock processes in the space where the earthquake was under preparation and in the space beyond are basically different.

Extensive experimental studies were conducted on the residual phenomena in the focal zone of large earthquakes. The paramount importance of such studies for seismology and physics of focus is shown in the recent monumental studies of the Dagestan earthquake [40, 41].

CONCLUSION

1. It was shown that a review of fracture mechanics in the context of microheterogeneity of the medium, the effect of high pressures, and endurance limit is necessary for an understanding of the processes of preparation, development, and residual phenomena of earthquakes.

2. The concept of the preparation of the main fault with the growth and interaction of microfractures at a lower scale level is supported by a whole

series of physical facts. This qualitative theory provides an explanation of all the major phenomena of earthquake preparation, in particular, the nature of the prognosticators and the relationship of the time of appearance of prognosticators with the earthquake energy.

3. The development of physics of earthquake focus as a synthesis of laboratory, field, and theoritical studies of destructive process promises to resolve fundamental problems of seismology and the associated problems of applied economics, i.e. prediction of strong earthquakes, their impact on construction, and seismic zonation.

REFERENCES

1. Myachkin, V.I. and S.I. Zubkov. 1973. Svodnyi grafik predvestnikov zemletryasenii (Tentative graph for earthquake forerunners). *Izv. AN SSSR, Fizika Zemli*, No. 6.
2. Nersesov, I.L. et al. 1973. Vozmozhnosti prognozirovaniya zemletryasenii na primere Garmskogo raiona Tadzhikskoi SSR (Scope of earthquake prediction from the example of the Garm region of the Tadzhik SSR). In: *Predvestniki Zemletryasenii* (*Tr. IFZ AN SSSR*). VINITI, Moscow.
3. Aggarwal, J.P. et al. 1973. *Nature*, **241**, 101.
4. Kasahara, K. 1969. Focal processes and various approaches to the mechanism thereof. *Publ. Dominion Obs.*, **37**.
5. Rats, M.V. and S.N. Chernyshev. 1970. Treshchinovatost i svoistva treshchinovatykh gornykh porod (Jointing and Properties of Jointed Rocks). Nedra, Moscow.
6. Griffith, A.A. 1921. The phenomenon of rupture and flow in solids. *Philos. Trans. Roy. Soc. London*, **A-221**.
7. Irwin, G.R. 1969. Basic concepts for dynamic fracture testing. *Trans. ASME, ser. D.* **91**, No. 3.
8. Orowan, E. 1950. Fundamentals of brittle behavior of metals. In: *Fatigue and Fracture of Metals*, J. Wiley, N.Y.
9. Rebinder, P.A. and E.D. Shchukin. 1972. Poverkhnostnye yavleniya v tverdykh telakh v protsessakh ikh deformatsii i razrusheniya (Surface phenomena in solid bodies in the process of deformation and fracture). *Usp. Fiz. Nauk*, **108**, No. 1.
10. Makklintok, F. and A. Argon. 1970. Deformatsiya i razrusheniya materialov (Deformation and Fracture of Materials). Mir, Moscow.
11. Finkel', V.M. 1970. Fizika razrusheniya (Fracture Physics). Metallurgia, Moscow.
12. Regel', V.R., A.I. Slutsker and E'.E. Tomashevskii. 1974. Kineticheskaya priroda prochnosti tverdykh tel (Kinetic Strength Characteristics

of Solid Bodies). Nauka, Moscow.
13. Barenblatt, G.I. and G.P. Cherepanov. 1961. O khrupkikh treshchinakh prodol'nogo Sdviga (Brittle fractures in longitudinal dislocation). *PMM*, **25**, No. 6.
14. Mogi, K. 1968. Source locations of elastic shocks in the fracturing process in rocks. *Bull. Seismol. Soc. Japan*, **46**, 5.
15. Zubkov, S.I. and V.I. Myachkin. 1971. Vremennoi khod uprugikh i neuprugikh deformatsii v period podgotovki zemletryaseniya (Time-dependent course of elastic and rigid deformation during earthquake preparation). *Geofiz. Sb.*, No. 42.
16. Kuznetsov, K.I. 1967. Zakonomernosti razrusheniya uprugovyazkikh tel k nekotorye vomozhnosti prilozheniya ikh i seismologii (Laws of Fracture of Elastoviscous Bodies and Some Prospects of Their Applications to Seismology). Nauka, Moscow.
17. Belousov, V.V. 1962. Osnovnye voprosy geotektoniki (Basic Problems of Geotectonics). Gosgeoltekhizdat, Moscow.
18. Riznichenko, Yu.V. 1965. O seismicheskom techenii gornykh mass (Seismic flow of rock masses). In: *Dinamika Zemnoi Kory*. Izd-vo AN SSSR, Moscow.
19. Gzovskii, M.V. 1960. Fizicheskaya teoriya obrazovaniya tektonicheskikh razryvov (Physical theory of formation of tectonic faults). In: *Problemy Tektonofiziki*. Gosgeoltekhizdat, Moscow.
20. Savarenskii, E.F. (Ed.). 1968. Sb. Predskazanie Zemletryasenii (Collection: Prediction of Earthquakes). Mir, Moscow.
21. Riznichenko, Yu.V. et al. 1956. Seismoakusticheskie metody izucheniya napryazhennogo sostoyaniya gornykh porod na obraztsakh i v massive (Seismoacoustic methods of studying the stressed state of rocks in specimens and massifs). *Tr. Geofiz. in-ta.*, No. 34 (161).
22. Issledovanie gornogo davleniya geofizicheskimi metodami (Study of Rock Pressure by Geophysical Methods). 1967. Nauka, Moscow.
23. Sb. Razrushenie, t. 1. Mikroskopicheskie i makroskopicheskie osnovy mekhaniki razrusheniya (Collection: Fracture, Vol. 1. Microscopic and Macroscopic Principles of Fracture Mechanics). 1973. Mir, Moscow.
24. Semenov, A.N. 1969. Izmenenie otnosheniya vremen probega poperechnykh i prodol'nykh voln pered sil'nymi zemletryaseniyami (Variation in travel time of transverse and longitudinal waves before strong earthquakes). *Izv. AN SSSR, Fizika Zemli*, No. 4.
25. Rikhitake, T. 1969. An approach to prediction of magnitude and occurrence time of earthquakes. *Tectonophysics*, **8**, No. 2.
26. Scholz, H., R. Sykes and J.P. Aggarwal. 1973. Development of rock dilatancy and subsequent diffusion of water into newly opened cracks may explain a class of phenomena precursory to earthquakes. *Science*, **20**, No. 6.

27. Anderson, D.L. and J.H. Whitcomb. 1973. Time-depended Seismology. *Contrib. Div. Geol. and Planet. Sci., Calif. Inst. Technol. Pas.*, No. 2363.
28. Stavrogin, A.N. 1968. Analiz eksperimental'nykh resul'tatov po deformatsii i razrusheniyu gornykh porod (Analysis of experimental data on deformation and fracture of rocks). In: *Gornoe Davlenie, Sdvizhenie Gornykh Porod i Metodika Marksheiderskikh Rabot*, VNIMI, Leningrad.
29. Shamina, O.G. and S.A. Strizhkov. 1974. Seismicheskie predvestniki zemletryasenii (Seismic forerunners of earthquakes). *Dokl. AN SSSR*, **247**, No. 6.
30. Myachkin, V.I. et al. Otsenka tochnosti i nekotorye rezul'taty nablyudenii po prosvechivaniyu ochagovykh zon na Kamchatka (Some observational data on sounding focal zones in Kamchatka and their accuracy). Present book, p. 174.
31. Sobolev, G.A. et al. Izuchenie mekhanoelektricheskikh yavlenii v seismoaktivnom raione (Study of mechanoelectric records in a seismic region). Present book, p 196.
32. Kostrov, B.V. 1970. Teoriya ochagov tektonicheskikh zemletryasenii (A theory of tectonic earthquake foci). *Izv. AN SSSR, Fizika Zemli*, No. 1.
33. Kostrov, B.V. 1974. Seismicheskii moment, energiya zemletryaseniya i seismicheskoe techenie gornykh mass (Seismic moment, energy of earthquake, and seismic flow). *Izv. AN SSSR, Fizika Zemli*, No. 4.
34. Aki, K. 1972. Earthquake mechanism. *Tectonophysics*, **13**, Nos. 1–4.
35. Shebalin, N.V. 1969. Makroseismicheskoe pole i ochag sil'nogo zemletryaseniya (Macroseismic Field and Focus of Strong Earthquake). Author's abstract of Doctoral Thesis, *IFZ AN SSSR*, Moscow.
36. Brune, J.N. 1971. Seismic sources, fault-plane studies and tectonics. XV General Assembly IUGG U.S. Nat. Report.
37. Aki, K. 1967. Scaling law of seismic spectrum. *J. Geophysics Res.*, **72**.
38. Haskell, N.A. 1966. Total energy and energy of spectral density of elastic wave radiation from propagating faults. Pt. 2. A statistical source model. *Bull. Seismol. Soc. America*, **56**.
39. Tomashevskaya, I.S. Izmenenie razlichnykh fizicheskikh parametrov v protsesse deformatsii i razrusheniya obraztsov gornykh porod (Change of various physical parameters during straining and fracturing of rock specimens). Present book, p. 134.
40. Shebalin, N.V. 1970. Dagestanskoe zemletryasenie 14 maya 1970 goda (Dagestan Earthquake of May 14, 1970). Datknigoizdat, Makhachkala.
41. Magomedov, A.M., N.V. Shebalin and V.N. Sholpo. 1971. Zemletryasenie v Dagestane (Earthquake in Dagestan). *Zemlya i Vselennaya*, No. 1.

I. Theoretical Aspects of Fracture

Preceding page blank

UDC 550.34.01.013

Mechanics of Brittle Fracture on Compression

B.V. Kostrov and V.N. Friedmann

The present paper examines the quasistatic growth of tensile cracks formed under compression at the tips of initial shear cracks with sides subjected to friction. It is shown that in compression critical load is not the ultimate strength of material. Initial direction of crack growth has been studied.

1. INTRODUCTION

Linear elastic fracture mechanics, whose foundations were laid by Griffith [1], attributes the real strength of solid bodies to the formation of a host of cracklike defects in the body, catastrophic development of one or several of which brings about disintegration of the body. The model of the brittle body is conceived in this case as a linear elastic (generally homogeneous and isotropic) matrix containing a certain number of cracks. To describe the behavior of the crack-bearing medium it is additionally necessary to assign to the elasticity theory equations boundary conditions on crack surfaces in the form

$$\sigma_{ij} n_j = 0 \quad \text{for} \quad [u_i n_i] > 0, \tag{1.1a}$$

where

$$\left.\begin{aligned} &[u_i n_i] = 0 \\ &\sigma_{ij} n_j - n_i \sigma_{jk} n_j n_k = f_i \end{aligned}\right\} \quad \text{for} \quad \sigma_{ik} n_i n_k < 0, \tag{1.1b}$$

where σ_{ij} is the stress tensor; n_i is the unit normal to the crack surface; u_i is the displacement vector; f_i is the frictional stress. The square brackets indicate a jump of the bracketed value on the crack surface. Repeated indices are summed. Case (1.1a) refers to an open crack and case (1.1b) to an overlying or closed crack. If we confine ourselves to the model of an ideally brittle body [2] we have to assign an additional condition, viz. the fracturing criterion, to the crack peripheries to describe crack growth. In fact, formulation of the fracturing criterion transfers the problem of the crack-bearing body from elasticity theory to fracture mechanics. Griffith's energy criterion [1], implying that a crack spreads when the fall in potential energy of the body caused by crack growth compensates the rise in crack

surface energy, is physically the soundest fracturing criterion. Wide application of fracture mechanics to real materials became possible when Irwin [3] and Orowan [4] proposed to replace the surface energy in Griffith's criterion by effective surface energy involving all the energy losses caused by the fracturing. Griffith's criterion is formulated quantitatively as follows: the crack spreads provided the following equation holds good for any part of the body containing part of the crack periphery:

$$\delta E + \delta A + 2\gamma_{\text{eff}}\,\delta S = 0 \quad (\delta S > 0), \tag{1.2}$$

where δE is the change in the energy of the body; δA is the action of external forces; γ_{eff} is the specific effective surface energy; δS is the increment in crack surface. If the crack-moving force is

$$G = \lim_{\Delta V \to 0} \lim_{\delta S \to 0} \frac{\delta E + \delta A}{\delta S}, \tag{1.3a}$$

then Griffith's criterion can be expressed in the local form as

$$G = 2\gamma_{\text{eff}}^{\text{def}} \equiv G_*, \tag{1.3b}$$

i.e. the crack spreads when the crack-moving force attains the critical value

$$G_* = 2\gamma_{\text{eff}}.$$

In conformity with (1.3a) the crack-moving force is expressed by local features of the elastic field around each point of the crack periphery. It is known [2] that stresses near the crack periphery have, in general, an exponential factor of the order of $\frac{1}{2}$ and their distribution is determined unambiguously by the coefficient of stress intensity along the crack in the plane tangential to the crack, according to the equation

$$k_i = \lim_{r \to 0} \sqrt{2r}\,\sigma_{ij}\,n_j, \tag{1.4}$$

where $r \to$ is the distance from the crack periphery along the normal to the crack periphery in the tangential plane; n_j is the normal to the crack surface.

The asymptotic behavior of all stress components is described as:

$$\sigma_{ij} = O\left(\frac{k_{ij}(\varphi)}{\sqrt{2r}}\right) \text{ for } r \to 0, \tag{1.5}$$

where φ is the angle between a fixed direction along the normal to the crack periphery and the tangential plane. Evidently, $k_i = k_{ij}(0)\,n_j$. The expressions $k_{ij}(\varphi)$ through k_I and the rate of dynamic crack growth in general can be obtained from the formulas given in [5] for a static case, e.g. in [6].

Let us denote by N_i the unit vector of the normal to the plane drawn through the tangent to the crack periphery at an angle φ with respect to the tangential plane ($N_i\,n_i = \cos\varphi$). Then the coefficients of stress intensity in this plane can be derived as

$$k_j(\varphi) = k_{ij}(\varphi)\,N_i. \tag{1.6}$$

Pure forms of fracture, i.e. tensile fracture ($k_1 \neq 0$, $k_2 = k_3 = 0$), transverse shear ($k_1 = k_3 = 0$; $k_2 \neq 0$) and transverse shear fracture ($k_1 = k_2 = 0$, $k_3 \neq 0$), can be derived by introducing a local coordinate system originating from a fixed point of the crack periphery with axis x_1 perpendicular to the crack fracture, x_2 perpendicular to the periphery in the tangential plane, and axis x_3 tangential to the crack periphery. It may be assumed that the process of destruction of the medium is entirely dependent on the behavior of the stress field around the crack periphery. In that case, since γ_{eff} or G_* accounts for the total energy consumed for destruction, it should generally speaking depend on the destructive process, i.e. on the rate at which the crack spreads and on the correlation of coefficients of stress intensity at the crack periphery (of the destructive type), according to the relation

$$2\gamma_{\text{eff}} = G_*(\alpha, \beta, v). \tag{1.7}$$

where $\alpha = \tan^{-1} k_2/k_1$; $\beta = \tan^{-1} k_3/k_1$; v is the rate of spread of crack periphery; this relation is determined by the properties of the material.

In this paper we will discuss the quasistatic problems of fracture under the impact of relatively brief stresses digressing from dynamic as well as fatigue phenomena. Therefore we hereinafter take $v = 0$ and ignore the dependence on the rate in correlations of the type (1.7).

To correlate force G moving the crack with the coefficient of stress intensity it is necessary to consider a small increment in crack surface in some direction and calculate the limit (1.3a). This readily yields the expression

$$G = \lim_{\delta l \to 0} \frac{1}{2\delta l} \int_0^{\delta l} (\sigma_{ij} N_j + f_i)[u_i]\, dl,$$

where δl is the dislocation of the crack periphery in a direction normal to its initial position in the plane bearing the normal N_i. The integration is carried out along the new crack surface. Taking (1.5) into account and assuming that the frictional forces are limited, we obtain

$$G = \lim_{\delta l \to 0} \frac{k_i(\varphi)}{2\delta l} \int_0^{\delta l} \frac{[u_i]\, dl}{\sqrt{2l}}. \tag{1.8}$$

Further refinement of this expression is possible only when the jump in crack growth can be correlated with the coefficients of intensity $k_i(\varphi)$. This means solving the asymptotic problem of elasticity theory involving a semi-infinite (the ratio of initial crack size to δl can be ignored) crack with a fracture of length δl in the field of initial stresses given by (1.5). This is easy if the crack grows in its tangential plane. As a result, we get Irwin's formula [7]:

$$G = \frac{1}{2\mu}\{(1-\nu)(k_1^2 + k_2^2) + k_3^2\}, \tag{1.9}$$

where μ is the shear modulus; ν is Poisson's ratio; k_1, k_2 and k_3 are the coefficients of stress intensity for tensile, transverse shear, and transverse shear fracture respectively.

For pure type of fracture (1.9) enables us to express the fracturing criterion directly through the coefficients of intensity (force approach). For instance, for pure tensile fracture we get the Irwin criterion as:

$$k_1 = K_1^{\text{def}} \equiv \sqrt{\frac{2\mu G_1}{1-\nu}}, \tag{1.10}$$

where G_1 is the critical crack-moving force for tensile fracture. Criterion (1.10) can also be considered independently of the Griffith energy criterion. In that case K_1 should be taken as a constant of the material.

Formulas (1.9) and (1.10) fully satisfy the general theory of the mechanics of fracture under tensile stresses. This is because the most dangerous cracks in the body are those oriented along the normal to the maximum tensile stress. Experiments show that they spread in their own plane (this is also to be expected from symmetry considerations) if the external stresses are uniform. It is generally assumed that the initial cracks are scattered quite sparsely, so that their interaction can be neglected. In that case we readily find that the coefficient of intensity k_1 is related to the maximum tensile stress and the typical dimension of the initial crack by the equation

$$k_1 = \lambda p \sqrt{l}, \tag{1.11}$$

where λ is a dimensionless constant dependent on the crack shape. Equations (1.10) and (1.11) give the critical stress p_* at which the crack begins to spread according to the equation

$$p_* = \frac{K_1}{\lambda \sqrt{l}}. \tag{1.12}$$

As the stress p attains the value given by (1.12), the crack begins to spread and the equilibrium is disturbed, for k_1 rises with the increase in crack size. Thus activation of the most dangerous defect under tensile stresses causes destruction of the body, whose strength is, however, not affected by the remaining defects.

Griffith's criterion alone cannot substantiate the fracturing criterion [eq. (1.10)]. However, it is the most popular one from the physical standpoint because it is based on the law of conservation of energy and the assumption that the fracture of material is dependent on such macroscopic characteristics of the state of material as the coefficients of stress intensity.

Other approaches involve construction of some specific model of the peripheral zone of the crack and, in general, include unobservable parameters. Reference should be made here to Barenblatt [8] and Leonov-Panasyuk's [6] models which consider the forces of locking of the sides of

the crack, and to the model proposed by Griffith [9] to describe fracturing upon compression, based on the assumption that the initial crack is an elliptical cavity with the minor but finite radius of curvature at the crack periphery. Griffith believed that fracturing starts when the tensile stress arising from stress concentration reaches the breaking point at some location on the crack surface. On the basis of this criterion Griffith found the most dangerous crack orientation and the angle between the direction of crack spread and the initial direction of the crack. For tension this approach (as also the other models) yields the same result as the energy criterion, provided the dimensions of the peripheral zone or the radius of curvature can be ignored in comparison with the crack size; all these approaches converge in the Irwin criterion (1.10). This led to postulation of the criterion (1.10), ignoring the consideration that fracture occurs in the direction in which the coefficient of stress intensity for tensile fracture $k_1(\varphi) = k_{ij}(\varphi) N_i N_j$ attains the critical value.

Panasyuk [6] applied this criterion to compression fracturing and deduced the direction of crack spread and the correlation of critical tensile and compression stresses. But Griffith's force approach and Panasyuk's approach were found to yield divergent results [10].

Cherepanov [11] advanced another criterion for choosing the direction of an open crack, i.e. the principle of local symmetry, whereby the crack spreads in a direction such that $k_2 = 0$ after the coefficient k_1 attains the critical value. For closed cracks he postulated that they spread rectilinearly when the coefficient k_2 attains the critical value K_{II} as distinct from K_I. This approach approximates Panasyuk's approach and yields comparable results. Griffith had to reject the energy criterion he himself proposed for compression fracturing for lack of a solution of the problem of fractured cracks, which left no means of deducing the force moving the crack in the rectilinear direction.

Several solutions have recently been worked out [12–14] for open fractured cracks, allowing a more comprehensive examination of the question of direction of crack spread under tensile stresses. The data obtained are not qualitatively new, nor are they sufficient for analysis of compressional fracture, because closed cracks, whose role may be taken by sliding bands and other shear dislocations, should be regarded as the initial defects. In this article compressional fracture is discussed in the light of Griffith's energy criterion.

Brittle fracture under compression has some characteristics that differentiate it from tensile fracture. In the case of uniaxial compression of some brittle materials with a greased pressplate the main crack extends in a direction parallel to the direction of the load on the specimen. This is highly paradoxical inasmuch as no stress operates in the plane of the crack. In the case of uniaxial compression supplemented by hydrostatic pressure the direc-

tion of crack spread tends to attain the direction of the plane of maximum tangential stress [15].

Another important characteristic of compression fracture is the expansion of material under stresses exceeding roughly one-half of the ultimate strength (dilatancy) [15, 16]. This phenomenon was recently used by American researchers [17, 18] as one of the probable explanations of the earthquake forewarnings. These characteristics of compression failure are attributed to the fact that under compressive loads cracks spread as a result of the concentration of tensile stresses at their periphery and diverge from the direction of the initial closed crack [15, 16].

To determine the direction of propagation of an open crack radiating from the periphery of an initial overlying crack, let us consider, in the light of Griffith's criterion, a case where the stress operates on the body bearing the initial crack quasistatically and all stresses increase in proportion to some parameter p (simple stress). Then in (1.8) $k_i(\varphi)$ and $[u_i]$ will be proportional to p, i.e. $k_i(\varphi) = pk_i^1(\varphi)$, $[u_i] = p[u_i^1]$, and we will have

$$G = p^2 G^1(\varphi), \tag{1.13}$$

where $G^1(\varphi)$ is the crack-moving force in the direction φ with $p = 1$. Further, under these conditions k_2/k_1 and k_3/k_1 will also depend only on the direction of crack spread φ, i.e. $G_* = G_*(\varphi)$ according to (1.7). Equation (1.3) will then acquire the form

$$p^2 G^1(\varphi) = G_*(\varphi). \tag{1.14}$$

It is logical to assume that the fracture will also start in the direction φ_*, for which (1.14) takes the following form when p is minimum:

$$G^1(\varphi_*)/G_*(\varphi_*) = \max. \tag{1.15}$$

An essential condition for this is

$$\frac{\partial}{\partial \varphi}\left(\frac{G}{G_*}\right)\Big|_{\varphi = \varphi_*} = 0. \tag{1.16}$$

It is assumed that this condition is satisfied when a crack spreads along the smooth curve; i.e. the ratio of force of a moving crack to elasticity of deformation G_* is maximum.

The dependence of G_* on the parameters α find β giving the type of fracture is governed by the properties of the material and can be ascertained only experimentally. Appropriate experimental data are still lacking, so this dependence can only be guessed. The guess that G_* is constant is the simplest. In such case the crack should spread in the direction of the maximum crack-moving force. This guess amounts to the guess that γ_{eff} coincides with the true surface energy. When substantial irrecoverable losses are entailed in the fracture γ_{eff} depends on the types of fracture, and it may be assumed that it is minimum for pure tensile fracture. Granted that the depend-

ence of $G_* = 2\gamma_{\text{eff}}$ on φ is greater than that of G on φ, the angle φ_* should differ little from the angle for which G_* is minimum, i.e. for which $k_2 = k_3 = 0$ at the periphery of a recreated crack. This conforms to Cherepanov's principle of local symmetry.

In this article we discuss the major aspect of the mechanics of compressional fracture, i.e. the plane problem of quasistatic spread in a homogeneous field of initial stresses, the inititial crack being a closed frictional crack. This aspect plays a part analogous to Griffith's criterion for tension.

2. STATEMENT OF THE PROBLEM

Let us consider the plane problem of elasticity theory affecting the equilibrium of a finite medium having the shear modulus μ and Poisson's ratio ν and weakened by a three-segment crack. Let this consist of a rectilinear segment of a closed crack of length $2l_1$ and two more or less curvilinear segments of an open crack of length l_2 oriented centrosymmetrically relative to the middle of the rectilinear segment. Let us take the Cartesian coordinate system (x_1, x_2) with the axis x_1 coinciding with the rectilinear segment of the crack (Fig. 1). Let us introduce the complex variable $z = x_1 + ix_2$. Hence the position of the crack will be described by the equations

$$\text{Limit } z = 0, \; -l_1 < \operatorname{Re} z < l_1 \quad (\text{segment } a) \tag{2.1}$$

$$z = \pm \zeta(s), \; 0 < s < l_2 \quad (\text{segment } b) \tag{2.2}$$

where $\zeta(s)$ is the differentiated function of the real variable s such that $\zeta(0) = l_1, |\zeta'(s)| = 1$. The crack is closed in the segment a, i.e.

$$[\sigma_{22} + i\sigma_{12}] = 0, \qquad [u_2] = 0, \tag{2.3}$$

and its sides interact according to Coulomb-Mohr's law as follows:

$$\sigma_{12} - k\sigma_{22} = -r_0 \operatorname{sgn}[u_1], \tag{2.4}$$

where k is the coefficient of friction; r_0 is the locking.

The closed segment may represent, for instance, a sliding band. Then $k = 0$ and r_0 implies yield limit. The condition (1.1b) also requires that $\sigma_{22} \leqslant 0$. This condition is supposed to be satisfied and should be verified after the problem is solved. The condition (1.1a) should be satisfied in segment b, i.e.

$$\sigma_{n2} + i\sigma_{n1} = 0 \qquad (\text{segment } b), \tag{2.5}$$

where σ_{n1} and σ_{n2} are the components of the frictional stress vector.

The stressed state is supposed to be uniform at infinity. The principal stresses at infinity are equal to σ_1^∞ and σ_2^∞. The major axis corresponding to σ_1 forms the angle α with the axis x_1, and $\sigma_1^\infty < \sigma_2^\infty < 0$. The stress and dislocation components are expressed by two extra-crack analytic functions

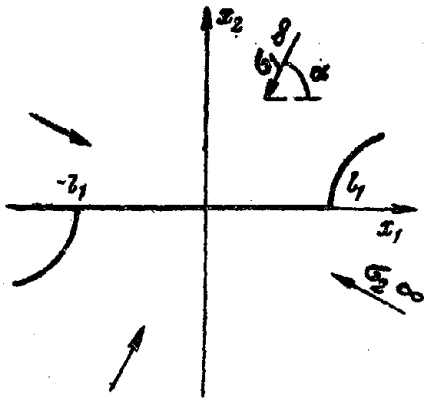

Fig. 1. Crack of centrosymmetric shape in compressive stress field.

of the complex variable z, using the Kolosov-Muskhelishvili formulas [19]:

$$\sigma_{11}+\sigma_{22}=2\left(\Phi(z)+\overline{\Phi(z)}\right)+2p,$$
$$\sigma_{22}-\sigma_{11}+2i\sigma_{12}=2\left(\bar{z}\Phi'(z)+\Psi(z)\right)+2\tau e^{2i\alpha},$$
$$2\mu\frac{\partial}{\partial x_1}(u_1-iu_2)=\chi\overline{\Phi(z)}-\Phi(z)-z\Phi'(z)-\Psi(z), \tag{2.6}$$

where $\chi=3-4\nu$ for planar deformation and $\chi=\frac{3-\nu}{1+\nu}$ for the planar stressed state; p and r are related to the principal stresses at infinity as follows:

$$p=\frac{1}{2}(\sigma_1^\infty+\sigma_2^\infty),\quad r=\frac{1}{2}(\sigma_1^\infty-\sigma_2^\infty). \tag{2.7}$$

The functions $\Phi(z)$ and $\Psi(z)$ should diminish at infinity as z^{-2}.

Equation (2.6) gives us the expression for the stresses on the crack and for the derivatives of dislocations in the direction of the crack as

$$\sigma_{n2}+i\sigma_{n1}=\bar{\zeta}'\overline{\Phi(\zeta)}+\bar{\zeta}'\Phi(\zeta)+\bar{\zeta}\zeta'\Phi'(z)+\zeta'\Psi(z)+p\zeta'+\tau\zeta'e^{2i\alpha},$$
$$2\mu(u_1'-iu_2')=\chi\bar{\zeta}'\overline{\Phi(\zeta)}-\bar{\zeta}'\Phi(\zeta)-\bar{\zeta}\zeta'\Phi'(\zeta)-\zeta\Psi(\zeta), \tag{2.8}$$

where the derivative with respect to s is denoted by a dash. The relation $\zeta=s\equiv x_1$ holds good for the segment a.

3. REDUCTION OF THE PROBLEM TO A SINGULAR INTEGRAL EQUATION

Let us represent the functions $\Phi(z)$ and $\Psi(z)$ as the sums $\Phi=\Phi_1+\Phi_2$, and $\Psi=\Psi_1+\Psi_2$, all the characteristics of the function Φ_1 and Ψ_1 being confined to segment a and those of Φ_2 and Ψ_2 to segment b. Taking into

account the jumps in stresses and displacements in the segment a, and considering the expansion of Φ_2 and Ψ_2 in this segment, we readily find from (2.3) that

$$\Psi_1(z) = -2\Phi_1(z) - z\Phi_1'(z), \quad \overline{\Phi_1(z)} = -\Phi_1(\bar{z}). \tag{3.1}$$

Considering the symmetry of the problem and the continuity of the stress vector in segment b, the functions Φ_2 and Ψ_2 can be expressed in the form of Cauchy-type integrals:

$$\Phi_2(z) = \frac{1}{\pi i}\int_0^{l_2}\left(\frac{1}{\zeta(s)-z} + \frac{1}{\zeta(s)+z}\right)\zeta'(s)\,g(s)\,ds, \tag{3.2}$$

$$\Psi_2(z) = \frac{-1}{\pi i}\int_0^{l_2}\left(\frac{1}{\zeta(s)-z} + \frac{1}{\zeta(s)+z}\right)\bar{\zeta}'(s)\,\bar{g}(s)\,ds$$

$$-\frac{1}{\pi i}\int_0^{l_2}\left(\frac{1}{(\zeta(s)-z)^2} + \frac{1}{(\zeta(s)+z)^2}\right)\bar{\zeta}(s)\,\zeta'(s)\,g(s)\,ds,$$

where

$$g(s) = \frac{\mu}{\chi+1}\bar{\zeta}'\,[u_1' + iu_2']. \tag{3.3}$$

Here the square brackets, as usual, denote a jump of the displacement derivative with respect to s in segment b.

Thus the problem boils down to finding $\Phi_1(z)$ and $g(s)$ from the boundary conditions given by (2.4) and (2.5).

Equation (2.4) can be rewritten as:

$$\mathrm{Re}\,(k+i)(\sigma_{22} + i\sigma_{12}) = \tau_0 \quad \text{(segment } a\text{)}. \tag{3.4}$$

Putting $\sigma_{22} + i\sigma_{12}$ from (2.8) in this expression, considering (3.1) and (3.2), and granting the function $g(s)$ to be known, we arrive at the Riemann problem for $\Phi_1(z)$ which can be readily solved as:

$$\Phi_1(z) = \frac{1}{2}iT\left(1 - z(z^2 - l_1^2)^{-1/2}\right) + \frac{1}{\pi i}\int_0^{l_2}[X(\zeta, z)\,\zeta' g + \overline{X}(\zeta, \bar{z})\,\bar{\zeta}'\bar{g}]\,ds, \tag{3.5}$$

where

$$T = \tau_0 - kp - k\tau\cos 2\alpha + \tau\sin 2\alpha, \tag{3.6}$$

$$X(\zeta, z) = -\frac{ik+1}{4}(P(\zeta, z) - P(-\zeta, z) + P(\bar{\zeta}, z) - P(-\bar{\zeta}, z))$$

$$+\frac{ik-1}{4}(\zeta - \bar{\zeta})\frac{\partial}{\partial\zeta}(P(\zeta, z) + P(-\zeta, z)). \tag{3.7}$$

Here

$$P(\zeta, z) = \frac{1}{\sqrt{z^2-l_1^2}}\left(1-\frac{z+\zeta}{\sqrt{\zeta^2-l_1^2}+\sqrt{z^2-l_1^2}}\right). \tag{3.8}$$

The branches of the radicals are so chosen that $\operatorname{Re}\sqrt{z^2-l_1^2} \geqslant 0$ outside segment a.

Putting the expressions (3.2), (3.5) and (3.1) in the expression for stresses in segment b from (2.8) and using the condition (2.5), we derive the singular integral equation with reference to $g(s)$ as

$$\frac{2}{\pi i}\,\text{v.p.}\int_0^{l_2}\left(\operatorname{Re}\frac{\zeta'(t)}{\zeta(s)-\zeta(t)}\right)\bar{\zeta}'(s)\,g(s)\,ds-\frac{1}{\pi i}\int_0^{l_2}(Z_1(s,t)\,\zeta'(s)\,g(s)$$
$$+Z_2(s,t)\,\bar{\zeta}'(s)g(s))\,ds = F(t), 0<t<l_2, \tag{3.9}$$

where

$$Z_1(s,t) = 2i\,\frac{\bar{\zeta}(s)+\bar{\zeta}(t)}{\zeta(s)-\zeta(t)}\operatorname{Im}\left(\text{v.p.}\frac{\zeta'(t)}{\zeta(s)-\zeta(t)}\right)$$
$$+2i\,\frac{\bar{\zeta}(s)+\bar{\zeta}(t)}{\zeta(s)+\zeta(t)}\operatorname{Im}\frac{\zeta'(t)}{\zeta(s)+\zeta(t)}-\bar{\zeta}'(t)\,X(\zeta(s),\bar{\zeta}(t))$$
$$+(\bar{\zeta}(t)-\zeta(t))\frac{\partial}{\partial t}X(\zeta(s),\zeta(t)),$$

$$Z_2(s,t) = -2\operatorname{Re}\frac{\zeta'(t)}{\zeta(t)+\zeta(s)}-\bar{\zeta}'(t)\,\bar{X}\left(\zeta(s),\zeta(t)+\left\{\bar{\zeta}'(t)\right.\right.$$
$$\left.\left.-2\zeta'(t)\,\bar{X}(\zeta(s),\bar{\zeta}(t))+(\bar{\zeta}(t)-\zeta(t)\right\}\frac{\partial}{\partial t}\bar{X}(\zeta(s),\bar{\zeta}(t)\right), \tag{3.10}$$

$$F(t) = -\frac{iT}{2}\left[\zeta'(t)(\zeta(t)-\bar{\zeta}(t))\frac{l_1^2}{(\zeta^2(t)-l_1^2)^{3/2}}\right.$$
$$+\left(1-\frac{\zeta(t)}{(\bar{\zeta}^2(t)-l_1^2)^{1/2}}\right)\bar{\zeta}'(t)+(2\zeta'(t)-\bar{\zeta}'(t))\left(1-\frac{\zeta(t)}{(\zeta^2(t)-l_1^2)^{1/2}}\right)$$
$$\left.+p\,\bar{\zeta}'(t)+\tau\zeta'(t)\,e^{2i\alpha}\right].$$

To ensure a unique solution it is necessary to add the following supplementary condition to (3.9):

$$\frac{1}{\pi}\operatorname{Im}\int_0^{l_2} g(s)\,\zeta'(s)\,ds = 0, \tag{3.11}$$
$$\lim_{s\to 0}\operatorname{Im}(2(k-i)\,\zeta'(s)+1-\bar{\zeta}'(s))\,\sqrt{s}\,g(s) = 0.$$

The first of these expresses continuity of displacement jump at the point $z = l_1$, and the second the condition where the stresses at this point have an exponential factor not exceeding 1/2.

The singular equation (3.9) can be solved as

$$\zeta'(s)\, g(s) = \frac{V(s)}{\sqrt{s(l_2 - s)}}, \tag{3.12}$$

where $V(s)$ is the piecewise differentiable function. The function $V(s)$ can be considered as a segment of the first type of Chebyshev polynomial series, where the Hermitian quadrature equation holds good for the regular integral [this is the second integral in eq. (3.9)] and an analogous quadrature equation for the singular integral. Quadrature equations of this type are used repeatedly, for instance, in [20, 21].

A numeration schedule was prepared to resolve the derived closed system of linear algebraic equations.

4. DIRECTION OF TENSILE CRACK PROPAGATION

Let us consider an isolated closed crack located in a field of quasistatically growing compressive stresses at an angle α_0 realizing the maximum $T(\alpha)$, i.e.

$$T'(\alpha_0) = 0. \tag{4.1}$$

From (3.6) we get

$$\cot 2\alpha_0 = -k. \tag{4.2}$$

The trajectory of the growing tensile crack may be determined thus: let us raise the stress a little such that the length l_2 increases by δl. Let us find the angle φ_* at which $G(\varphi_*, l_2)$ is maximum (we assume G_* to be a constant here). To get a smooth curve the segments on which the curvilinear crack is constructed are taken as conjugate arcs of circles, the initial segment being regarded as rectilinear. Thus the coordinate of the point on the tensile crack can be expressed as:

$$w(s) = se^{i\varphi} m, \qquad m = 1,$$

$$w(s) = w(l_m) + \frac{i\Delta l_{m+1}}{\Delta\varphi_{m+1}}\left(1 - e^{\,i\,\frac{s-l_m}{\Delta l_{m+1}}\,\Delta\varphi_{m+1}}\right), \quad m > 1, \tag{4.3}$$

where m is the number of the segment of the curvilinear crack given by the equation

$$\Delta l_{m+1} = l_{m+1} - l_m, \quad \Delta\varphi_{m+1} = \varphi_{m+1} - \varphi_m.$$

The initial stage of a tensile crack originating from the tip of a shear

crack is our foremost concern. Analysis of (3.9), when $\frac{l_2}{l_1} \ll 1$, shows that the coefficients of stress intensity at the end of a tensile crack and its length are correlated as:

$$k_i(\varphi, l_2) \approx k_i'(\varphi) + k_i''(\varphi)\sqrt{l_2}, \tag{4.4}$$

$k_i'(\varphi)$ being dependent only on the coefficient of stress intensity at the tip of a shear crack, as follows:

$$k_2^0 = T\sqrt{l_1}. \tag{4.5}$$

The crack-moving force bears the same relationship with l_2 as in (4.4). From (1.2) and (1.3a) we derive

$$\delta E + \delta A = \int_0^{\delta l} G(l_2)\, dl_2 = \frac{1-\nu}{2\mu} \int_0^{\delta l} \left(k_1^2(l_2) + k_2^2(l_2) \right) dl_2. \tag{4.6}$$

Using (4.4) we get for the asymptotic expression of the force $G(\varphi)$

$$G^\circ(\varphi) \approx \frac{1-\nu}{2\mu} \left(k_1'^2(\varphi) + k_2'^2(\varphi) \right). \tag{4.7}$$

Assuming G_* to be constant, we should find max $G^\circ(\varphi)$ or $-$ max $(k_1'^2(\varphi) + k_2'^2(\varphi))$ in conformity with (1.15).

The function $\frac{G^\circ(\varphi)}{G^\circ(0)}$ for $k = 0$ and $k = 1$ are represented graphically in Fig. 2.

In the absence of friction numerical calculation gives the angle between the direction of a shear crack and the initial direction of a tensile crack as

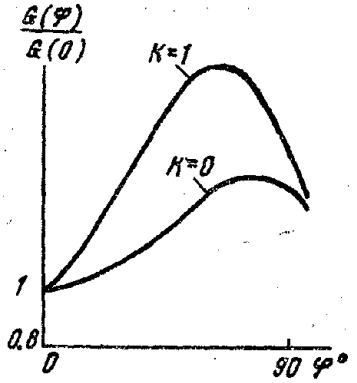

Fig. 2. Relation of crack-moving force with dip angle of tensile segment in asymptotic case.

nearly 79°, rather than the 90° obtained by Griffith [9] and about 70° reported by Panasyuk [6].

The angle at which the tensile cracks begin to develop is expected to diminish if the sides of the crack interact with friction. In fact, when $k = 1$, maximum $G^\circ(\varphi)$ is attained at $\varphi = 60°$.

CONCLUSION

In this paper calculations have been made for short tensile cracks. The results obtained enable us to draw the following conclusions regarding the behavior of matter under compression.

Under constant stress the coefficients of stress-intensity as given by (4.4) fall with an increase in l_2, i.e. k_I'' in this expression is negative. The crack moving force G^1 also diminishes with an increase in l_2. Therefore higher stresses are necessary to sustain a quasistatically increasing crack in limiting equilibrium.

The relation of G^1 to l_2 is shown in Fig. 3. Smaller G means that under critical stress tensile cracks develop steadily, at least initially. Here lies the essential difference in the nature of brittle fracture under compression and brittle fracture under tension. Under tensile stresses the limiting state induces dynamic crack growth and specimen failure (provided the tip of the developing crack does not encounter obstacles), so that the critical stress in this case is actually the ultimate strength.

The situation is different under compression when the critical compressive stress is not the ultimate strength of the material.

The ratio of critical compressive and tensile stresses can be deduced mathematically; Griffith found it to be nearly 8 and Panasyuk 2.66 [10]. The ratio is 2 for a crack [22] growing according to Griffith's criterion in its own plane. It is to be noted that in these studies this value is identical with the

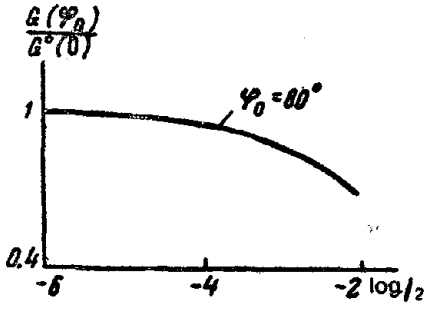

Fig. 3. Relation of crack-moving force with length of tensile segment.

ratio of ultimate strengths, although in reality it is not so. In our case the ratio of critical compressive and tensile stresses is roughly 1.38.

Let us conceive a real body with a high density of shear-type cracks that is subjected to quasistatic compression. Cracks with critical length and orientation are activated under stresses conforming to the failure condition (1.14). New cracks reaching the limiting state with increasing stress are thereupon involved in this steadily advancing process. Thus, defects accumulate as quasistatically growing tensile cracks from the tips of shear cracks, causing an increase in the specific volume of the material. Other moduli of the medium alter in the process if the medium is taken as continuous. Hence there are grounds for studying the macroscopic characteristics, e.g. volume expansion, variation of wave velocity in the medium, etc., as premonitors of the dynamic development of the main cracklike defect under the impact of high pressures [15, 16].

The problem discussed in this paper does not offer a comprehensive answer to the question how a brittle body fractures under compression, but the solution derived enables us to analyze the process of fracturing of bodies with predetermined length- and anglewise crack distribution, to compute the dilatancy and to make a quantitative study of fracture forerunners.

REFERENCES

1. Griffith, A.A. 1920. *Philos. Trans. Roy. Soc. London*, A **221**, 163.
2. Kostrov, B.V. and L.V. Nikitin. 1970. Some general problems of mechanics of brittle fracture. *Arch. Mech. Stosowanej*, No. 22.
3. Irwin, G.R. 1948. Fracture dynamics. *Fracturing of Metals*. ASM, Cleveland.
4. Orowan, E. 1950. Fundamentals of brittle behavior of metals. *Fatigue and Fracture of Metals*. J. Wiley, N.Y.
5. Kostrov, B.V. and L.V. Nikitin. 1970. Primenenie metodov mekhaniki khrupkogo razrusheniya k izucheniyu mekhanizma ochaga zemletryaseniya (Application of techniques of brittle fracture mechanics to study of the mechanism of the earthquake focus). In: *Fizicheskie Osnovaniya Poiskov Metodov Prognoza Zemletryasenii. Tr. IFZ AN SSSR*, Nauka, Moscow, p. 9.
6. Panasyuk, V.V. 1968. Predel'noe ravnovesie khrupkikh tel s treshchinami (Limiting Equilibrium of Crack-Bearing Brittle Bodies). Naukova Dumka, Kiev.
7. Prikladnye voprosy vyazkosti razrusheniya (Applied Aspects of Fracturing Viscosity). Mir, Moscow, 1968.
8. Barenblatt, G.I. 1959. O ravnovesnykh treshchinakh, obrazuyushchikhsya pri khrupkom razrushenii (Equilibrium cracks formed upon brittle fracture). *Dokl. AN SSSR*, **127**, No. 1.

9. Griffith, A.A. 1924. The theory of rupture. *Proc. I. Internat. Congr. Appl. Mech.*, Delft.
10. Lin'kov, A.M. 1972. Zamechanie k vychisleniyam predela prochnosti na szhatie (A note on calculations of ultimate compression strength). *Izv. AN SSSR, MTT*, No. 4.
11. Cherepanov, G.P. 1966. Nekotorye voprosy razrusheniya khrupkikh porod pri szhatii (Some aspects of fracture of brittle rocks under compression). In: *Problemy Mekhaniki Gornykh Porod.* Nauka, Alma-Ata.
12. Mossakovskii, V.I., P.A. Zagubizhenko and P.E. Berkovich. 1965. Napryazhennoe sostoyanie ploskosti, oslablennoi lomanoi treshchinoi (Stressed state of plane weakened by broken crack). In: *Kontsentratsiya Napryazhenii*, No. 1, Naukova Dumka, Kiev.
13. Mossakovskii, V.I. and P.E. Berkovich. 1968. Odna zadacha teorii khrupkogo razrusheniya (One facet of the theory of brittle fracture). *Prikladanya Mekhanika*, **4**, No. 4, Naukova Dumka, Kiev.
14. Dudukalenko, V.V. and N.B. Romalis. 1973. O napravlenni rosta treshchiny v usloviyakh ploskogo napryazhennogo sostoyaniya (Direction of crack growth under planar stressed state). *Izv. AN SSSR, MTT*, No. 2.
15. Stavrogin, A.N. 1969. Issledovanie predel'nykh sostoyanii i deformatsii gornykh porod (Studies of limiting states and deformation of rocks). *Izv. AN SSSR, Fizika Zemli*, No. 12.
16. Brace, W.F. and E.G. Bombolakis. 1963. A note on brittle crack growth in compression. *J. Geophys. Res.*, **68**, No. 12.
17. Schoiz, C.H., L.R. Sykes and I.P. Aggarwal. 1973. A physical basis for earthquake prediction. *Science*, **181**.
18. Anderson, D.L. and I.H. Whitcomb. 1973. The dilatancy-diffusion model of earthquake prediction. In: Proc. Conf. on Tectonic Problems of San Andreas Fault System. Standford Univ. Publ. Geol. Sci., Vol. 13.
19. Muskhelishvili, N.I. 1966. Nekotorye osnovnye zadachi matematicheskoi teorii uprugosti (Some Major Facets of the Mathematical Theory of Elasticity). Nauka, Moscow.
20. Cook, T.S. and F. Erdogan. 1972. Stress in bonded materials with a crack perpendicular to the interface. *J. Eng. Sci.*, **10**.
21. Kostrov, B.V. and R. Dmowska. 1973. A shearing crack in a semispace under plane strain conditions. *Arch. Mech. Stosowanej*, **25**, 3.
22. Mossakovskii, V.I. and M.T. Rubka. 1965. Popytka postroeniya teorii prochnosti dlya khrupkikh materialov, osnovannoi na e'nergeticheskikh soobrazheniyakh Griffitsa (An attempt to frame a theory of strength for brittle materials on the basis of Griffith's energy concepts). *PMM*, **29**.

UDC 550.34.01.013

Basis of Statistical Theory of Preparation of Earthquake Focus

V.I. Myachkin and O.D. Voevoda

The paper reviews experimental and theoretical data on fracturing processes in heterogeneous media. It is shown that investigation of the conditions of propagation of an isolated fault in a randomly heterogeneous medium is among the essential approaches to formulation of a theory of earthquake preparation. It is possible to compute the distribution of intervals of unstable fault growth and of the corresponding average characteristics.

It is now common knowledge that the process of crack (fracture) growth is a major factor in rock burst. One of the major facets of seismology, namely the physics of the earthquake focus, is indeed the physics of fracture of large rock masses in the environment of earth's interior [1]. Consequently the specific features of fracture growth in real solid bodies hold great interest for seismologists.

Historically, complete success has been achieved in studies of the strength and stability of various engineering installations. However, although fractures are studied both in engineering and in seismology, there are basic differences between these two disciplines. While in engineering the start of rapid fracture spread generally causes complete destruction of components, in an earthquake the fracture stops inside the earth's crust. Therefore, in addition to the circumstances of the inception of rapid fracture spread it is necessary to study the circumstances of fracture arrest. It is also significant that a large number of diverse earthquakes [2] occurs in a completely heterogeneous medium within a limited area. Hence, as distinct from engineering, focal mechanics demands a study of the growth of a large number of fractures in a heterogeneous medium. Evidently such a study involves statistical methods. Also, while formulating the theory of earthquake preparation there is naturally an attempt to make use of the results and techniques of continuous medium mechanics. In view of this certain versions of the statistical description of the fracture process and their applicability to the study of earthquake preparation, are discussed below.

STATISTICAL DESCRIPTION OF FRACTURING

The application of statistical methods to the strength problem is based on the fact that a real solid body is a statistical assemblage of some primary elements possessing varied physico-mechanical properties and defect characteristics. Each of these elements is responsible in a definite measure for the strength of the body as a whole. In rocks the primary elements are individual crystals, including the surface of contact and embryonic microcracks, etc. [3]. These heterogeneities of the rock structure bear random characteristics, inviting the application of statistical methods of study. This implies that the laws of distribution of defects and their interaction must be known.

The theory of scale effect [4] explains the difference in the strength of specimens of different sizes prepared from the same material. The probability P of the material fracturing under some stress σ is the basic concept of this theory. For a homogeneous stressed state this probability is expressed by formula [1]:

$$P(\sigma) = 1 - \exp\left[- V \left(\frac{\sigma}{\sigma_0} \right)^m \right], \tag{1}$$

where V is the strained volume; m and σ_0 are some constants, σ_0 implying the limiting stress for the primary element of the body.

Despite the fact that the theory of scale effect explains the difference in the strength of specimens of different sizes, the origins of failure (fracture) are explicitly ignored in this theory. The approach is faulty because the strength of the primary structural element depends not only on the properties of the material but also on the type of stressed state influencing the primary defects. In fact, where the primary defect is a microcrack, its critical stress depends on the properties of the material (e.g. specific surface energy γ), as well as on the size and orientation of the microcrack. Consequently, each type of stressed state demands a knowledge of the corresponding density of strength distribution of primary defects.

The statistical theory of limiting equilibrium [2, 3], where fractures and the laws of probability of distribution of their geometrical parameters (size, orientation, etc.) are introduced in explicit form, does not suffer from these drawbacks. According to this theory growth of even one crack (failure of the primary element) may cause complete failure of the body (weak link hypothesis). Therefore only stresses that do not develop any crack are absolutely safe. The maximum stress at which cracks do not develop is called the limiting stress for a given body. It should be emphasized here that the limiting stress is not synonymous with the stress that causes total failure of the body. The probability of failure of a body of volume V under a stress P_1 can be expressed as [5]:

$$F_v(P_1) = 1 - [1 - F_1(P_1)]^{N \frac{V}{V_0}}, \tag{2}$$

where N is the average number of primary fractures in volume V_0; $F_1(P_1)$ is the distribution of limiting stress for a primary defect.

The condition of limiting equilibrium for a plate bearing a system of noninteracting cracks of random orientation and length was obtained in [6]. A graph of limiting states was constructed that tallied well with the experimental results. It is also significant that the scale effect dependent on the number of fractures in volume V and the type of stressed state were explained within the framework of the statistical theory of limiting equilibrium.

Notwithstanding the marked successes of statistical theories of scale effect and limiting equilibrium, these theories do not describe the process of fracture growth in a heterogeneous medium. In fact, the theory of scale effect takes the heterogeneity of the medium into account but explicitly ignores the initiators of the failure, i.e. the fractures. The limiting equilibrium theory involves fracture distribution but leaves the distribution of the specific surface energy (strength) of the material out of its purview. Thus failure starts as a result of the unsteady growth of one of the most dangerously oriented fractures. This implies that the statistical theory of limiting equilibrium describes the failure process at the last stage of total failure of the body. The preparation of this failure, in which a multitude of fractures participate, is not covered by this theory.

An earlier attempt at statistical description of the failure process was perhaps made in [7]. The basic underlying idea of this work is that the failure process is irreversible at all stages. In fact, since the failure process consists of the development and healing of fractures, irreversible growth and merger of fractures or irreversible healing, instrumental in restoring the continuity of the material, occur at various stages of this process.

The following model of failure of solid bodies was adopted in [7]. Microcracks, which may grow, merge heal up or collapse, originate in the body throughout the period of stress at the points of stress concentration. The stress operating in the body is not generally equal to that applied, i.e. the stress builds up significantly near the tops of large cracks and relaxes near their planes. Macrofracture, causing total failure of the body, appears as a consequence of such processes. Each crack of the system is described by its state λ (state denotes any parameter describing the crack) at the instant of time t. Where the state of the crack changes with time, this change is described by some trajectory $\lambda(t)$ in the space of the state. The growth, healing and merger of fractures comprise a mechanism that selects one of the probable trajectories.

The whole set of fractures is described by their density of distribution in accordance with the states $f(t, \lambda) \geqslant 0$, here $f(t, \lambda)\, d\lambda = dF(t, \lambda)$ being the number of fractures in the state range λ, $\lambda + d\lambda$ at the instant of time t. In the straining process the number of fractures in the state range will go on changing with their appearance, merger, and healing. This change per unit

time can be expressed as:

$$\frac{d}{dt}[dF(\lambda, t)] = dG_1(\lambda, t) - dC_2(\lambda, t) + dQ_1(\lambda, t) - dQ_2(\lambda, t) + dP_1(\lambda, t) - dP_2(\lambda, t) + dM_1(\lambda, t) - dM_2(\lambda, t), \quad (3)$$

where dG_1 and dG_2 are the number of cracks attaining the state λ and relieved of this state; dQ_1 and dQ_2 are the number of cracks attaining the state λ as a result of growth and relieved of this state; dP_1 and dP_2 are the number of cracks attaining the state λ as a result of merger and relieved of this state; dM_1 and dM_2 are the number of fractures arrested due to heterogeneities of the medium.

In a sense, equation (3) is an equation of the continuity of the number of cracks in a particular state i.e., this or an identical equation can describe the process of development of many fractures, destroying the body.

Equation (3), hereinafter called a kinetic equation, can be rewritten in terms of the respective densities of distribution as

$$\frac{df}{df} = \frac{\partial t}{\partial t} + \frac{d\lambda}{dt}\frac{\partial \lambda}{\partial \lambda} = (g_1 - g_2) + (q_1 - q_2) + (p_1 - p_2) + (m_1 - m_2), \quad (4)$$

where $d\lambda/dt = V$ is the rate of change of state.

The work [4] introduces the concept that the transition of a fracture from one state to another occurs with what is called a transition probability. Equation (4), rewritten using the transition probability, appears to be formally analogous to Boltzmann's gas kinetics equation. Thus the solution of equation (4) should describe the evolution of the density of distribution f with time, implying that a description of all parameters of the failure process in question will be obtained. Unfortunately, equation (4) in its general form has not been solved. To derive a solution some simplifications were introduced in [4], not all of which are physically substantiated.

The whole multiscalar fracture array is broken into three types: microfracture (m), macrofracture (M) and correlated microfracture (c). Merger of microfractures gives rise to a macrofracture. Near the end of this macrofracture correlated microfractures start which, upon merger with the macrofracture, increase the length of the latter and bring about the collapse of the body. Regrettably, their very formal approach to the process of fracture development prevented the authors of [7] from obtaining notably rigorous physical results. Such an approach should be considered promising and applicable in principle to the study of focus preparation because it reflects the real phenomena in nature.

In view of the foregoing it is necessary to choose a course that would allow an analysis of certain aspects of earthquake preparation. That is, what is required is a description of the process that would take into account the presence of a larger number of fractures distributed in a randomly heteroge-

neous medium. For this it is necessary that the laws of fracture growth be considered not from any *a priori* premises but as the direct consequences of fracture physics. Evidently statistical description of a multitude of fractures should begin from an analysis of the growth of a single fracture in a randomly heterogeneous medium.

In this paper we attempt probabilistic description of the behavior of a single crack spreading in such a medium. It was assumed that the fracture does not heal and can spread only in its initial direction. Also, among all the types of rock heterogeneity only strength heterogeneity, i.e. the dependence of the specific surface energy γ on the coordinates of points in the medium, was considered.

CONDITION OF FAILURE OF HETEROGENEOUS MEDIUM

It is known from fracture mechanics [1, 8] that a fracture attains its critical equilibrium when following equation is valid:

$$\gamma = G, \tag{5}$$

where γ is the specific surface energy of the material and G is the crack-moving force.

Equation (5) is called the local failure criterion as referred to the end of the crack. Precisely because of its local character the equation is particularly suitable for analyzing the process of failure of a heterogeneous medium.

For an isolated crack of ideally brittle fracture in an infinite plate the crack-moving force is determined [6] by formula:

$$G = ak^2 = a\sigma^2 x \sin^2 \alpha, \tag{6}$$

where a is a coefficient dependent on the modulus of elasticity; k is the coefficient of stress intensity at the end of the crack; σ is the magnitude of the homogeneous stress field at infinity; α is the angle between the fracture plane and the direction of the applied stresses.

For a crack subjected to nonplanar straining, $a = \pi/4 \cdot \mu$. For a crack subjected to homogeneous tension $a = \pi\,(1-\nu^2)/2E$, where μ is the shear modulus, ν is Poisson's ratio and E is Young's modulus. If the medium is homogeneous (γ = constant) and equation (5) is fulfilled, the fracture will become unstable ($d\sigma/dx < 0$) and will spread dynamically at a fixed level of applied stress. In such a case the fracture will increase in length up to infinity —a fact contradictory to actually observed fractures. The fracture is arrested when (5) does not hold good, i.e. when G becomes less than γ. This implies that the fracture is stopped when G diminishes or the strength of the medium γ increases, but the increase in strength is also a consequence of the heterogeneity of the medium.

To characterize the variation of γ relative to G, i.e. to differentiate the points of inception and arrest of the fracture, we will introduce the relations

between the derivatives $\gamma' = d\gamma/dx$ and $G' = dG/dx$. Then the circumstances of inception and arrest of the fracture can be written as:

$$G(\sigma_1 x_i) = \gamma(x_i), \qquad G'(\sigma_1 x_i) > \gamma'(x_i),$$
$$G(\sigma_1 x_i) = \gamma(x_i), \qquad G'(\sigma_1 x) < \gamma'(x_i). \tag{7}$$

Thus the fracture starts at a value of the stresses σ at which the slope of G becomes steeper than the slope of γ at a point of the medium where the end of the fracture is located. The same holds good for the arrest of a fracture too.

It is evident from the foregoing that the heterogeneity of the medium has a profound influence on the process of fracture growth. The strength heterogeneity of the medium is primarily responsible for the arrest of the fracture. This implies that phenomena conforming more to those observed in nature can be analyzed by rejecting the homogeneity hypothesis.

FRACTURE GROWTH IN RANDOMLY HETEROGENEOUS MEDIUM

As noted above, the heterogeneity of real materials is of a statistical nature. The specific surface energy γ comprises a scalar random field and has a random value for each of the arguments x.

The random field $\gamma(x)$ at a point can be described by the common density of distribution $W(\gamma_i \gamma') \geqslant 0$ of the random values of γ and γ' at that point. The quantity

$$P = W(\gamma_i = G_1, \gamma')\, \Delta\gamma\, \Delta\gamma' \tag{8}$$

states the probability that a point x is critical. This means that at this point $G \leqslant \gamma_i \leqslant G + \Delta\gamma$, and $\gamma_i' \leqslant \gamma' \leqslant \gamma_i' + \Delta\gamma'$. It can be readily shown that the intersection of $\gamma(x)$ and G in the interval $\Delta\gamma$ corresponds to their intersection in the interval Δx. When Δx is quite small, so that not more than one intersection is possible, $\Delta\gamma$ and Δx are related as

$$\Delta\gamma = |\gamma_i' - G|\, \Delta x_1, \tag{9}$$

where $G' = a\sigma^2$.

Putting (9) in (8), we get the probability of finding the critical point in an interval Δx as

$$P = W(\gamma_i = G_1 \gamma_i')\, |\gamma_i' - a\sigma^2|\, \Delta\gamma'\, \Delta\gamma_i. \tag{10}$$

Integrating (10) over all possible values of $\gamma' < a\sigma^2$ we find the probability of inception of the dynamic spread of a fracture at a point x to be

$$P_i(\sigma) = \int_0^{a\sigma^2} W(\gamma_i = G_1 \gamma_i')/\gamma_i' - a\sigma^2/d\gamma_i'\, dx. \tag{11}$$

The expression for the probability of arrest of the fracture at a point x_i is obtained analogously as

$$P_2(\sigma) = \int_{a\sigma^2}^{\infty} W(\gamma_i = G_1 \gamma_i') |\gamma_i' - a\sigma^2| d\gamma_i' dx. \tag{12}$$

As is evident from expressions (11) and (12), the probabilities of inception and arrest of a fracture depend largely on the nature of the heterogeneity of the medium and the level of the operating stresses σ. Let us point out that these expressions are formally analogous to the formulas for the probability of the random process overshooting a certain level [10]. The implications of a homogeneous medium are obvious from (11) and (12). In reality $\gamma = \gamma_0 = \text{constant}$. In that case

$$W(\gamma_i = G_1 \gamma_i') = \delta(G - \gamma_0)\, \delta(\gamma' = 0),$$

where $\delta(x)$ is the Dirac function.

Substituting (10)* in (11) and (12) and integrating with reference to x, we derive

$$P_1 = \int_0^{\infty} \delta(G - \gamma_0)\, dG \int_{-\infty}^{a\sigma^2} \delta(\gamma' = 0)\, d\gamma' = \begin{cases} 1 \text{ when } \sigma > 0 \\ 0 \text{ when } \sigma = 0, \end{cases} \tag{13}$$

$$P_2 = \int_0^{\infty} \delta(G - \gamma_0)\, dG \int_{a\sigma^2}^{\infty} \delta(\gamma' = 0)\, d\gamma' = \begin{cases} 1 \text{ when } \sigma = 0 \\ 0 \text{ when } \sigma > 0. \end{cases} \tag{14}$$

It follows that with the probability 1 the fracture will begin to spread dynamically under any stress other than nil at a point of the medium where $G = \gamma_0$. The probability of arrest of the fracture at $\sigma > 0$ is nil. The fracture is arrested only when the applied stress is withdrawn.

Let us see how the fracture spreads in these circumstances. Let the initial fracture end at the point x_0 (see Figure). Further spread of the fracture is possible only when σ attains a value at which $G_0 = \gamma_0$. When $G_0' > \gamma_0'$, at point x_0 the fracture will lose its stability and spread dynamically in the interval l up to the point x_1, where it stops. Further movement of the fracture is subject to an increase in the stress σ^*. In the interval $a = x_0' - x_1$ the fracture advances steadily. At some value of $G_0^{(1)}$ the fracture at point x_0 will again lose stability and spread dynamically right up to the next strength barrier. Thus in a heterogeneous medium the fracture propagates spasmodically, and the length l of the instability intervals depends on the nature of the heterogeneity and the level of the operating stresses.

*Equation number changed in the context of the text—General Editor.

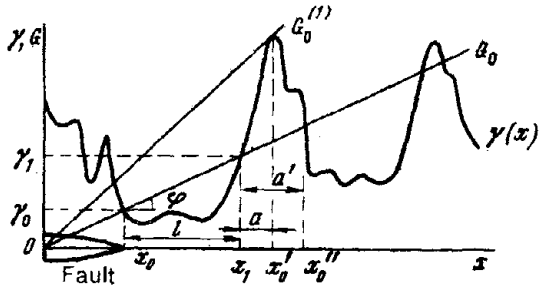

Growth of fracture in randomly heterogeneous medium:
$\gamma(x)$ is one of the probable realizations of a random strength field; x_0 is the initial half-length of a fracture; G_0 is the crack-moving force; x_1 is the point of fracture arrest; $l = x_1 - x_0$ is the interval of dynamic fracture growth, and a is the interval of steady fracture growth.

DISTRIBUTION OF INTERVALS OF UNSTEADY FRACTURE GROWTH IN RANDOMLY HETEROGENEOUS MEDIUM

Let us consider a fracture with the initial half-length x_0 (see Figure). At some value of the operating stress σ the fracture will lose stability and spread dynamically up to the point $x_1 > x_0$, where it will stop. Let us denote by P the probability of the fracture stopping $P(\gamma, \gamma', x_1, \sigma)$. The variation of this probability can be visualized as follows:

$$P = (\gamma, \gamma', x_1 + \Delta x_1 \sigma) = P(\gamma, \gamma', x_1, \sigma)\, Q_1(\gamma, \gamma', x_1, \sigma), \qquad (15)$$

where Q is the probability of dynamic fracture growth in the interval x_1, $x + \Delta x$ provided the fracture moved dynamically in the interval x_0, x.

The provisional probability Q can be expressed through the probability of an additional event as follows:

$$Q_1(\gamma, \gamma', x_1, \sigma) = 1 - Q_2(\gamma, \gamma', x_1, \sigma), \qquad (16)$$

where

$$Q_2(\gamma, \gamma', x_1, \sigma) = q_2'(\gamma, \gamma', x_1, \sigma)\, \Delta x \qquad (17)$$

is the probability of the fracture stopping at the point x_1 provided the fracture moved dynamically up to this point.

Putting (17) in (16) and then in (15), and passing on to the limit $\Delta x \to 0$, we get the following equation for the probability P:

$$\frac{dP}{dx} = -Pq_2. \qquad (18)$$

The solution of this equation takes the form

$$P(\gamma,\ \gamma',\ x_1,\ \sigma) = \theta(\gamma' - a\sigma^2)\ \exp\left\{-\int_0^{\infty} q_2(\gamma, \gamma',\ x_1,\ \sigma)\ dx\right\}, \qquad (19)$$

where the factor before the exponential is the Heavyside unit function expressed as:

$$\theta(\gamma' - a\,\sigma^2) = \begin{cases} 1 \text{ when } G = \gamma \text{ and } \gamma' > a\sigma^2 \\ 0 \text{ when } G = \gamma \text{ and } \gamma' < a\sigma^2. \end{cases} \qquad (20)$$

The factor takes into account the probability of arrest of the fracture at a point x where $\gamma' > a\,\sigma^2$. Let us note that (18) is formally analogous to the equation for the probability of illumination of a point x on a rough surface by a ray of light reflected at an angle φ from this surface at a point x_0 [9].

To express the probability P of the fracture stopping through the parameters of the medium and of the fracture, q_2 should be expressed in explicit form. For this purpose let us analyze the events A and B. Event A includes the condition that the fracture stops at a point $x_0 < x' < \bar{x}_1$. Let the probability of this event be denoted by $P(A)$. Let us denote by $P(B)$ the probability of event B, which is such that in the interval x_0, x the fracture moves dynamically as far as point x.

From the known formula we get

$$P(A/B) = \frac{P(AB)}{P(B)}, \qquad (21)$$

where $P(A/B)$ is the probability of the fracture stopping at a point x, provided the fracture moved dynamically up to this point. Comparing (17) and (21), we get

$$q_2(\gamma,\ \gamma',\ x_1,\ \sigma)\ \Delta x = P(A/B). \qquad (22)$$

The probability $P(B)$ can be regarded as the probability that at each point of the interval $l = x - x_0$ of the unsteady fracture growth $\gamma(x) < \gamma_0 + x\,a\,\sigma^2$. This probability can be expressed by the continuous integral

$$P(B) = \lim_{\substack{\Delta x \to 0 \\ N \to \infty}} \prod_{n=1}^{N} \int_0^{\gamma_0 + n\Delta x a\sigma^2} \int_{-\infty}^{\infty} W_{2N+2}(\gamma_0,\ \gamma_0' \ldots \gamma_N,\ \gamma_N')\ d\gamma_n\, d\gamma_n', \qquad (23)$$

where W_{2N+2} is the combined density of distribution of random values of γ and γ' at the points $x_0\ \Delta x_j\, 2\,\Delta x \ldots N\,\Delta x$; N is the integral part of the ratio $x/\Delta x$.

For the probability $P(A)$ of the fracture stopping we get from (12)

$$P(A) = \int_{a\sigma^2}^{\infty} (\gamma' - a\sigma^2)\ W(\gamma_1 = \gamma_0 + l\,a\sigma^2,\ \gamma')\, d\gamma'. \qquad (24)$$

From (23) and (24) we get the expression for $P_1(AB)$

$$P(AB) = \lim_{\substack{\Delta x \to 0 \\ N \to \infty}} \prod_{n=1}^{N} \int_0^{\gamma_0 + n\Delta x a\sigma^2} \int_{-\infty}^{\infty} \int_{a\sigma^2}^{\infty} (\gamma'_N - a\sigma^2)\, W_{2N+4}(\gamma_0, \gamma'_0 \ldots \gamma_N$$

$$= \gamma_0 + xa\sigma^2, \gamma'_N)\, d\gamma_n\, d\gamma'_n\, d\gamma'_N. \tag{25}$$

Putting (23) and (25) in (21) and then in (19) we get the expression for the probability of the fracture stopping at point x as

$$P(\gamma, \gamma', x, \sigma) = \theta(\gamma' - a\sigma^2) \exp - \int_0^{\infty} \left[\lim_{\substack{\Delta x \to 0 \\ N \to \infty}} \prod_{n=1}^{N} \int_0^{\gamma_0 + n\Delta x a\sigma^2} \int_{-\infty}^{\infty} W_{2N+2}\, d\gamma_n\, d\gamma'_n \right]^{-1}$$

$$\left[\lim_{\substack{\Delta x \to 0 \\ N \to \infty}} \prod_{n=1}^{N} \int_0^{\gamma_0 + n\Delta x a\sigma^2} \int_{-\infty}^{\infty} \int_{a\sigma^2}^{\infty} (\gamma'_N - a\sigma^2)\, W_{2N+4}\, d\gamma_n\, d\gamma'_n\, d\gamma'_N \right] dx \Big\}. \tag{26}$$

This expression, in principle, enables us to find the probability of the fracture stopping at a point x in a medium. In such a case no limits are imposed on the size of the initial fracture, the level of operating stresses, or the nature of the heterogeneity of the medium.

To simplify the integrals in (26), let us introduce the characteristic parameters of the medium $\bar{\gamma}$ and $\bar{\gamma}_1$—the average values of γ and γ'. Analyzing these values, we get

$$\bar{\gamma} = r\,\bar{\gamma}_1, \tag{27}$$

where r is the radius of correlation, i.e. some characteristic segment of the axis x, averaging of which surfaces to get the average value of γ with the desired accuracy. Using the failure condition (5), we get

$$\bar{\gamma} = a\sigma^2 \bar{x}, \tag{28}$$

where $\bar{x}$ is the average size of the critical fracture.

From (27) and (28) we get the ratio of the characteristic parameters of the medium with the operating stress and the average fracture size

$$\frac{r}{x} = \frac{a\sigma^2}{\bar{\gamma}_1}. \tag{29}$$

Let us now consider the limiting cases of (15)

$$\begin{aligned} &r \ll \bar{x},\ \sigma_2 \gg \sigma_{\bar{x}},\ a\sigma^2 \ll \bar{\gamma}', \\ &r \approx \bar{x},\ \sigma_2 \approx \sigma_{\bar{x}},\ a\sigma^2 \approx \bar{\gamma}', \\ &r \gg \bar{x},\ \sigma_2 \ll \sigma_{\bar{x}},\ a\sigma^2 \gg \bar{\gamma}'. \end{aligned} \tag{30}$$

where $\sigma_2 = \sqrt{\bar{\gamma}/ar}$, $\sigma_{\bar{x}} = \sqrt{\bar{\gamma}/a\bar{x}}$ are the limiting stresses for fractures of sizes r and $\bar{x}$, respectively. The relations (30) define the failure process in a hete-

rogeneous medium. In fact, when r is the size of an "elementary" fracture, the first case represents a microfracture located in a sharply heterogeneous medium. The second case is transitional and represents a fracture whose size is comparable with the scale of heterogeneity of r. A microfracture in a smoothly heterogeneous medium corresponds to the third case.

Thus it is imperative to decide the type of case when analyzing the failure process in a heterogeneous medium. A similar question has to be answered when clarifying the concept "continuity" of the medium. It was stated in [5], that the failure of a continuous medium should be regarded as the failure of the particular structural element of the material that is depicted as a continuous medium at the corresponding level of macroscopicity, i.e. as the formation of fractures whose size exceeds that of the particles of the material considered as elementary. In fracture mechanics the size of the terminal part of the fracture is customarily regarded as elementary. Only two cases are probable here: the size of the fracture is much greater than or is comparable with the size of the terminal part. Macro- and microfractures correspond to these cases.

In this paper continuity was conceded from the start. Since the model of an ideally brittle fracture is here considered, the macroscopicity of the fracture in respect of the size of the terminal region is recognized automatically. However, since the fracture grows in a heterogeneous medium there is another level of description of macroscopicity, namely, the correlation of fracture size and the characteristic scale of heterogeneities of the medium. Thus the two levels—size of the terminal region and characteristic scale of heterogeneities of the medium—should be strictly distinguished when describing the process of failure of a heterogeneous medium. There is an additional parameter, $\nu = a\sigma^2/\bar{\gamma}'$, characterizing the extent of heterogeneity of the medium.

It may be pointed out that the need to consider the correlation between the scale of heterogeneity and the size of the fracture in any analysis of the processes of failure of real materials was indicated as early as 1956 [10].

MACROFRACTURES IN SHARPLY HETEROGENEOUS MEDIUM

Let us consider the first case of equation (30), which corresponds to the macrofracture $r \ll \bar{x}$ located in a medium with the sharp heterogeneities $\nu \ll 1$. For simplicity we assume that $\gamma(x)$ represents a statistically homogeneous random field. Since $r \ll \bar{x}$, the correlation of starting and stopping points of the fracture can be ignored. Further, the homogeneity condition [9] implies that the values of γ and γ' at the same point of the medium are unrelated. Under these assumptions the densities W in the integrand in (26) separate into the products of the densities of distribution of γ and γ' at each

point. Taking this into account, we get the following asymptotic expression for the probability of the fracture stopping:

$$P(\gamma, \gamma', x_1, \sigma) = \theta(\gamma' - a\sigma^2) \exp\left\{-F(\sigma) \int_0^\infty W(\gamma_1 = \gamma_0 + l a\sigma^2)\, dl\right\}, \tag{31}$$

where

$$F(\sigma) = \int_{a\sigma^2}^{\infty} (\gamma' - a\sigma^2)\ W(\gamma')\, d\gamma'. \tag{32}$$

Putting the new variable $\gamma_1 - \gamma_0 = l a\sigma^2$, in the integral (31), we get

$$P(\gamma', l, \sigma) = \theta(\gamma' - a\sigma^2)\ \exp\left\{-\frac{F(\sigma)}{a\sigma^2} \int_0^{la\sigma^2} W(\gamma_1 - \gamma_0)\, d(\gamma_1 - \gamma_0)\right\}. \tag{33}$$

Equation (33) gives the distribution of integrals of unsteady fracture growth in a randomly heterogeneous medium. Differentiating the function $P(\gamma', l, \sigma)$ with respect to l, we can find the density of distribution $P(\gamma', l, \sigma)$ of unsteady fracture growth intervals at a given value of σ. Knowing the density of distribution $P(\gamma', l, \sigma)$ the characteristics of the failure process in question, e.g. the average value of l, can be found from the known equations of probability theory as follows:

$$\bar{l} = \int_0^{L_{\max}} l p(\gamma', l, \sigma)\, dl. \tag{34}$$

The most probable value of l can be derived from the external condition of the density of probability $P(\gamma', l, \sigma)$ by the expression

$$\frac{dp(\gamma', l, \sigma)}{dl} = 0. \tag{35}$$

It is readily seen that the distribution function $P(\gamma', l, \sigma)$ and the statistical characteristics of a fracture are dependent on the distribution of strength heterogeneity and the level of operating stresses.

REFERENCES

1. Kostrov, B.V. 1972. Mekhanika ochaga tektonicheskogo zemletryaseniya (Mechanics of Tectonic Earthquake Focus). Author's abstract of Doctoral thesis, IFZ, AN SSSR, Moscow.
2. Riznichenko, Yu.V. 1966. Problemy fiziki zemletryasenii (Problems of earthquake physics). *Izv. AN SSSR, Fiziki Zemli*, No. 2.

The generalized correlation of the period of appearance of forerunners ΔT_{an} (time interval between start of forerunners recording and the earthquake) and the seismic earthquake energy E (straight line 1 in the Figure) was shown in [14] to be:

$$\log \Delta T_{an}\,(\text{year}) = \delta \log E(J) - \xi, \tag{1}$$

where $\delta = 0.48$ and $\xi = 7$. (Earthquake forerunners are anomalies in the time-dependent course of the physico-mechanical characteristics of matter in the focal zone of an incipient earthquake. The anomalies are indicators of partial failure of rocks in the focal zone [14].) Let us transform (1) as

$$\frac{\Delta T_1}{\Delta T_2} = \left(\frac{E_1}{E_2}\right)^{\delta}, \tag{2}$$

where E_1 and E_2 are two different random values of seismic energy; ΔT_1 and ΔT_2 are the corresponding periods of appearance of forerunners (hereinafter the subscript 'an' is dropped from the notation ΔT_{an} for brevity). Seismic energy, as was shown in [15], can be expressed by the stress-drop $\Delta\sigma$, which is equal to the difference between the inital (σ_i) and final (σ_f) stresses in the area of the failure, as given by

$$\Delta\sigma = \sigma_i - \sigma_f, \tag{3}$$

and the seismic moment M_0, as given by

$$E = \frac{\Delta\sigma}{2\mu} M_0, \tag{4}$$

where μ is the shear modulus.

Since it is uncertain whether the released stress $\Delta\sigma$ is constant for earthquakes of different energies or differs according to the classes of earthquake energy, we will make the simplest assumption, i.e. we will assume that $\Delta\sigma_1 \neq \Delta\sigma_2$ for the above two earthquake energy values. Then from (2) and (4) we get

$$\frac{\Delta T_1}{\Delta T_2} = \left(\frac{\Delta\sigma_1 M_{01}}{\Delta\sigma_2 M_{02}}\right)^{\delta}. \tag{5}$$

The seismic moment can be expressed through the earthquake energy, making use of the Brune-Aki graph [16] depicting the relative dependence of the seismic moment M_0 on the energy E. Analysis of M_0 and E-values for different earthquakes by the method of least squares, as shown in this graph, allowed derivation of the empirical formula:

$$M_0\,(\text{J}\cdot\text{cm}) = 10^{8.66} E^{1.17}\,(\text{J}). \tag{6}$$

From (2), (5) and (6) we get

$$\frac{\Delta T_1}{\Delta T_2} = \left(\frac{E_1}{E_2}\right)^{\delta} = \left(\frac{\Delta\sigma_1}{\Delta\sigma_2}\right)^{-5.9\delta} = \left(\frac{\Delta\sigma_1}{\Delta\sigma_2}\right)^{-n} \tag{7}$$

where $n = 5.9\delta$.

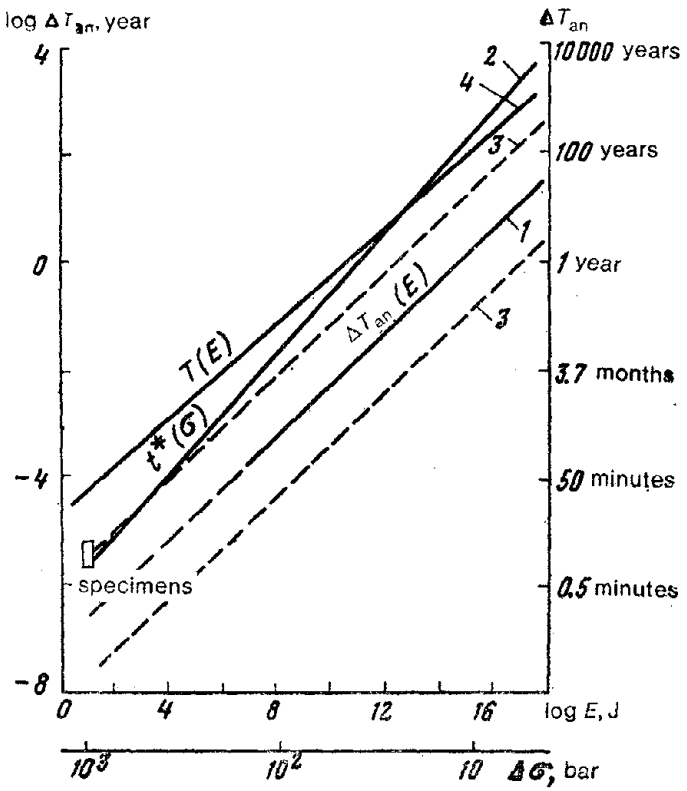

Fatigue of rock masses in earthquake focal zones:

1—From observations of earthquake forerunners [14]; 2—Fatigue of Maxwell body calculated by equation given in [4]; 3—Standard deviation for log ΔT_{an}; 4—Recurrence periods of earthquakes in Kurile-Kamchatka area [29].

The tangent of the angle of inclination of the average graph of earthquake forerunners has the value $\delta = 0.48$ [14]. Then $n = 2.84$, i.e. $T_{an} \sim \Delta\sigma^{-2.84}$.

An equation of the type (7) correlating ΔT_{an} and $\Delta\sigma$ can be obtained by different means, using the dependence of the earthquake energy E on the failure area S. For this purpose we will substitute in (4) the seismic moment M_0 in accordance with its definition in [17] in terms of the displacement jump a, failure area S and shear modulus μ:

$$M_0 = \mu a S \tag{8}$$

and the expression for a [15]:

$$a = c \frac{\Delta\sigma}{\mu} S^{1/2}, \tag{9}$$

where c is a dimensionless characteristic of the focus varying within the range 0.2–0.4 [15]. Consequently, we have

$$E = \frac{c}{2\mu} \Delta\sigma^2 S^{3/2}. \tag{10}$$

It is not difficult to get the function $S(E)$ by further transformation using the data of [18] on the correlation of the focal area and the earthquake energy. After simple transformations we get from [18]:

$$S^{3/2} = AE^{1.4} \tag{11}$$

where A is a constant. Further, by eliminating $S^{3/2}$ from (10) with the help of (11) we get from (2)

$$\frac{\Delta T_1}{\Delta T_2} = \left(\frac{E_1}{E_2}\right)^{\delta} = \left(\frac{\Delta\sigma_1}{\Delta\sigma_2}\right)^{-5\delta} = \left(\frac{\Delta\sigma_1}{\Delta\sigma_2}\right)^{-n}. \tag{12}$$

Then $n = 2.40$, i.e. $\Delta T_{an} \sim \Delta\sigma^{-\sigma^{-2.40}}$.

Lastly, the third probable means of ascertaining the function $\Delta T_{an}(\Delta\sigma)$ also gives ΔT_{an} as the inverse exponential function of $\Delta\sigma$. In fact, putting (9) in (8), we get the expression for the seismic moment M_0 through $\Delta\sigma$ and S [15] as:

$$M_0 = c\,\Delta\sigma\, S^{3/2}. \tag{13}$$

Further, substituting M_0 from (6) and $S^{3/2}$ from (11) in (13), we get from (2)

$$\frac{\Delta T_1}{\Delta T_2} = \left(\frac{E_1}{E_2}\right)^{\delta} = \left(\frac{\Delta\sigma_1}{\Delta\sigma_2}\right)^{-4.35\delta} = \left(\frac{\Delta\sigma_1}{\Delta\sigma_2}\right)^{-n}. \tag{14}$$

Then $n = 2.09$, i.e. $\Delta T_{an} \sim \Delta\sigma^{2.09}$

Thus all the methods of determining the function $\Delta T_{an}(\Delta\sigma)$ proposed above give the inverse exponential function of the type of (7) with the average exponent under stress relation $n \cong 2.4$, i.e.

$$\frac{\Delta T_1}{\Delta T_2} = \left(\frac{E_1}{E_2}\right)^{\delta} = \left(\frac{\Delta\sigma_1}{\Delta\sigma_2}\right)^{-5.03\delta} = \left(\frac{\Delta\sigma_1}{\Delta\sigma_2}\right)^{-2.4}. \tag{15}$$

Regarding equations (7), (12), (14) and (15) obtained above, it should be pointed out that they were deduced on the assumption that the shear modulus μ and the coefficient c from (9), dependent [15] on the shape of the failure area in the focus, have constant values for earthquakes of different energies. While the assumed constancy of μ distorts the function $\Delta T_{an}(\Delta\sigma)$ insignificantly because of the small variation in the modulus of elasticity, the second assumption that c = constant for different E, perhaps calls for proof, despite the small variation ($c = 0.2$–0.4) known [15] for this coefficient. Such proof seems to be provided by the close exponential values under relaxed stresses in (7) and (12) derived by two independent methods. The first does

not assume the constant shape of the failure areas of earthquake foci of different energies, whereas the second accepts this assumption.

The time interval ΔT_{an} characterizes the period of earthquake preparation, i.e. the period of irreversible growth of a crack system preparing the major fracture [14]. The relaxed stress $\Delta\sigma$ in the earthquake focus, as shown in [15], characterizes the magnitude of stresses for rock bursting. Therefore, the relation (15) should be regarded as an equation for fatigue of rock masses in earthquake focal zones in exponential form. An equation for fatigue of similar form has been obtained for elastoviscous bodies in several theoretical and experimental studies [3, 4, 19, 20]. It is interesting that equation (15) agrees with the conclusion drawn in [15] that the stress drop $\Delta\sigma$ in the focus may be greater for weak or less for strong earthquakes. Thus, (7), (12) and (14), deduced from (1) by three independent methods, enabled us to establish the correlation between the disruptive stresses and the period of earthquake warnings (the periods of earthquake preparation in the above sense). Moreover, these equations support the idea that the observed [14, 21–24] increase in the warning period with the rise in earthquake energy [eq. (1)] is the result of fatigue of the rock masses in the focal zone, i.e. the graph of earthquake forerunners [14] is based on the fatigue equation.

The result obtained helps to explain the high correlation coefficient ($r = 0.91$) for the major feature (prolonged forerunners) of the graph of earthquake forerunner (straight line I in the Figure) constructed for forerunners in different parts of the world [14]. It also helps to explain the much narrower divergence of ΔT_{an}-values (and correspondingly higher correlation factor) in the graphs plotted for forerunners in different regions [21–24]. On the other hand, the higher factor of correlation between ΔT_{an} and E in graphs of earthquake forerunners for different regions may substantiate to some extent the result derived here, namely the detection of the functional nature of $\Delta T_{an}(E)$ on the basis of fatigue phenomenon.

From this standpoint it is interesting to see how far the observed function $\Delta T_{an}(E)$ corresponds to the theoretical correlation of the failure time t^* (the interval between the instant of stress application and the instant of failure) and the operating stress σ. As an example of such a correlation we will take the fatigue equation for a Maxwell body given in [4]. This equation, written as an equation of failure time, takes the following form:

$$\frac{t_1^*}{t_2^*} = \left(\frac{\sigma_1}{\sigma_2}\right)^4, \tag{16}$$

resembling equation (15) obtained above for the ratio of the times of appearance of earthquake forerunners ΔT_1 and ΔT_2 for the energies E_1 and E_2.

Equation (16) was derived by solving the problem of quasistatic crack expansion (under a constant stress far below the ultimate resistance) in an elastoviscous Maxwell medium to some critical length l^* at which the crack

begins to propagate dynamically and sudden failure takes place. The choice of (16) as a theoretical correlation of failure time and applied stress for comparison with the observational data [with eq. (1)] was dictated by the following considerations:

First, the process of crack growth under stresses is considered explicitly in the fatigue theory developed in [4]. It is, if not essential, at least highly desirable for comparison of the results of any fatigue theory with the observational data of earthquake forerunners since they themselves appear due to the developing disruption of the continuity of the earth's material [14].

Second, formula (16), as noted above, is a fatigue equation for an elastoviscous Maxwell body. Hence it describes the phenomenon of fatigue of a rheological medium, whose major properties correspond to the rheological properties of rocks in earthquake focal zones [10]. Lastly, formula (16) relates to stresses far below the ultimate resistance and in this context corresponds to a case realizable in the focal zone during earthquake preparation [10, 25].

To relate the theoretical function $t^*(\sigma)$ with the observed function $\Delta T_{an}(E)$ it is necessary to know the correlation between disruptive stresses (or, as noted above, the correlation of stresses released after failure [15]) and the seismic energy released upon rock failure. The values of disruptive stresses in earthquakes and their relation with the seismic energy have so far been inadequately studied. All that is known is that in the magnitude range $M \cong 6$–8 ($K = \log E \cong 14$–17) the values of stresses released upon failure lie in the range 1–100 bar without showing any regularity [26]. It is also known that the shear stresses relaxed upon failure have values of the order of 10^3 bar for rock specimens tested at high confining pressures and temperatures and that the seismic energies of failure of the specimens responding to these values are of the order of 10 J [27, 28].

If in accordance with the data cited above, we accept that the relieved stress $\Delta\sigma_{av} \cong 10$ bar corresponds to the seismic energy $E = 10^{15.3}$ J ($M_{av} = 7$) and the relieved stress 10^3 bar corresponds to the energy 10 J, we get the following relation between the disruptive (relieved) stresses and the seismic energy:

$$\Delta\sigma^{-7}\,(\text{bar}) \cong 10^{-22}\,(\text{bar/J})\,E\,(\text{J}). \tag{17}$$

This relation unifies phenomena of different scales (failure of specimens and earthquakes). This fact on the one hand raises some doubts as to the validity of (17) but on the other permits us to obtain the correlative function $\Delta\sigma(E)$. In fact, the correlative function of (17) derived from observational data suggests that the decrease in relieved stress $\Delta\sigma$ by about half an order corresponds to an increase in seismic energy E by three orders [the same thing follows from the semiempirical equation (15) deduced by another method]. This explains why the function $\Delta\sigma(E)$ cannot be ascertained from the above data of [26]. The $\Delta\sigma$ values, diverging by two orders and corre-

sponding to a seismic energy (E) variation range of three orders, cover the variation of the relieved stresses $\Delta\sigma$ occurring in this range by half an order. But the wide difference in the failure energy of specimens and earthquakes permits us to circumvent this problem because the statistical divergence of $\Delta\sigma$ surpasses it in a wide range of variation of E values which corresponds to the variation of $\Delta\sigma$ values.

Equation (17) allows deduction of a semiempirical relation between the failure time t^* and the seismic energy E on the basis of the theoretical formula (16)

$$\log t^* \text{ (year)} = 0.56 \log E \text{ (J)} - 6.06. \qquad (18)$$

Average values [27, 28] of failure time (from the instant of stress application to the instant of total failure) as well as of disrupting (relieved) stresses were used as preliminary data (reference point) to derive (18) for specimens of different rocks subjected to high confining pressures and temperatures. These data (10^2 sec and 10^3 bar) are denoted in the Figure by a rectangle. The data computed by (18) are shown in the Figure by straight line 2.

Comparative evaluation of observed (straight line 1) and theoretical (straight line 2) data shows that, true to the definition (the instant of stress application to the instant of failure), the theoretical failure time t^* involved in the seismic process characterizes the total time for which the tectonic forces responsible for earthquakes operate in the focal zone, i.e. the time t^* seems to characterize the period of recurrence of earthquakes in this focal zone. The observed time ΔT_{an}, on the other hand, seems to characterize for this focal zone the time from the beginning of predominance of weakening over strengthening of rocks until the earthquake [14]. It therefore seems to constitute only part of the total time for which the tectonic forces responsible for the earthquake operate in this zone.

Consequently it can be assumed that $t^* > \Delta T_{an}$. This assumption agrees with the values of t^* and ΔT_{an} given in the Figure For $K = 1$ (specimens), $t^* \cong 100$ sec and exceeds $\Delta T_{an} = 10$ sec [obtained by extrapolating eq. (1) for forerunners to the failure energy range of specimens] by one order. This conforms with the data on failure time and the time of anomalous behavior of various physico-mechanical properties of rock specimens [27, 28]. For $K = 6$, $t^* \cong 18$ hr and $\Delta T_{an} = 0.6$ hr; for $K = 12$, $t^* \cong 4.5$ years and $\Delta T_{an} \cong 0.7$ month; for $K \cong 15$, $t^* \cong 220$ years and $\Delta T_{an} \cong 1.5$ years; for $K = 17$, $t^* \cong 2700$ years and $\Delta T_{an} \cong 14$ years.

Thus t^* is one order higher than ΔT_{an} in the small seismic energy range and rises progressively to two orders higher in the case of the severest catastrophes. These values of the failure time t^* do not warrant excessive reliance in view of a certain ambiguity in the failure stress values used in calculations. Also, the conditions of theoretical solution of the problem of quasistatic crack growth [4] diverge from the conditions of fracture growth in the focal

zones. Yet it is certainly interesting to collate the theoretical values of t^* for the recurrence of earthquake with the observed values.

In the Figure curve 4 represents the average data of [29] calculated by the formula:

$$\log T(\text{year}) = 0.45 \log E(\text{J}) - 4.676, \tag{19}$$

obtained from the formula given in this work for the frequency of earthquake recurrence. (The choice of area was dictated by the fact that most of ΔT_{an} values [14] pertain to this area.) Let us cite some figures for comparison of t^* values. For $K = 6$, $T \cong 3.5$ days; for $K = 12$, $T \cong 5.3$ years; for $K = 15$, $T \cong 120$ years; for $K = 17$, $T \cong 940$ years.

Let us round off the comparison of the observed function $\Delta T_{an}(E)$ with the theoretical function $t^*(\sigma)$ [4] used for ascertaining the time of failure in the seismic process. The main conclusion emerging from this comparison is that despite the divergence of the conditions of theoretical solution of the problem of quasistatic crack growth (fixed size of embryonic crack, omission of crack interaction, constant uniaxial tensile stress, etc. [4]) from the conditions of fracture growth in earthquake focal zones, the nature of the function $t^*(\sigma)$ (straight line 2 in the Figure) broadly conforms to the nature of the function $\Delta T_{an}(E)$ (straight line 1 in Figure). In the light of the correlation of ΔT_{an} and $\Delta\sigma$ derived in this paper [eq. (15)] this conclusion should be regarded as confirmation of the probability of a functional correlation between ΔT_{an} and E based on fatigue considered in the differential derivation (see above) of such correlations.

The quantitative comparison of the functions $t^*(\sigma)$ and $\Delta T_{an}(E)$, i.e. the comparison of t^* and ΔT_{an}, is of a hypothetical nature in view of the above remarks about the reliability of determination of the failure time t^* from (18). But it should be noted that the agreement between the calculated failure time t^* and the periods of earthquake recurrence T in the wide range of energy classes $K \cong 9$–15 is satisfactory for $K < 9$ and $K > 15$ (see the Figure and the above values of t^* and T). Also, the theoretical failure time t^* is significantly lower (by 1–2 orders) than the time of appearance of earthquake forerunners ΔT_{an} in the whole range of seismic energies. This leads us to expect, besides similarity of the nature of the function $T(E)$, $t^*(\sigma)$ and $\Delta T_{an}(E)$ (see the Figure), a correct approach to the computation of the periods of earthquake recurrence and the appearance of forerunners based on the theory of fatigue of elastoviscous materials.

The authors thank B.V. Kostrov for valuable advice and comments.

REFERENCES

1. Zhurkov, S.N. and T.P. Sanfirova. 1960. Izuchenie vremennoi i temperaturnoi zavisimosti prochnosti (Study of dependence of strength on time

and temperature). *FTT*, **2**, No. 6.
2. Rabotnov, Yu.N. 1959. O mechanizme dlitel'nogo razrusheniya (Mechanism of the endurance limit). In: *Voprosy Prochnosti Materialov i Konstruktsii*. Izd-vo AN SSSR, Moscow.
3. Kachanov, L.M. 1960. O vremeni razrusheniya v usloviyakh polzuchesti (Time of creep failure). *Izv. AN SSSR, OTN. Mekhanika i Mashinostroenie*, No. 5.
4. Kostrov, B.V., L.V. Nikitin and L.M. Flitman. 1970. Rasprostranenie treshchin v uprugovyazkikh telakh (Crack propagation in elastoviscous bodies). *Izv. AN SSSR, Fizika Zemli*, No. 7.
5. Cherepanov, G.P. 1967. O rasprostranenii treshchin v sploshnoi srede (Crack propagation in a continuous medium). *PMM*, **31**, No. 3.
6. Barenblatt, G.I., V.M. Entov and R.L. Salganik. 1966. O kinetike rasprostraneniya treshchin (Kinetics of crack propagation). *Inzh. Zh. MTT*, pts. 1 and 2, Nos. 5 and 6.
7. Kachanov, L.M. 1961. K kinetike rosta treshchin (Kinetics of crack growth). *PMM*, **25**, No. 3.
8. Averbakh, B.L. 1973. Nekotorye fizicheskie aspekty razrusheniya (Some physical aspects of failure). In: *Razrushenie*, Vol. 1, Mir, Moscow.
9. Riznichenko, Yu.V. 1965. O seismicheskom techenii gornykh mass (Seismic flow of rock masses). In: *Dinamika Zemoni*, Nauka, Moscow.
10. Zubkov, S.I. 1969. O raschete reologicheskimi metodami vremennogo khoda napryazhenii v ochagovykh zonakh zemletryasenii (Rheological methods of computing time-dependent course of stresses in earthquake focal zones). *Izv. AN SSSR, Fizika Zemli*, No. 4.
11. Riznichenko, Yu.V. 1968. Energeticheskaya model' seismicheskogo rezhima (Seismic energy model). *Izv. AN SSSR, Fizika Zemli*, No. 5.
12. Nason, R.D. 1973. Fault creep and earthquakes on the San Andreas fault. Proc. Conf. on Tectonic Problems of the San Andreas Fault Systems. Stanford Univ. Publ., **13**.
13. Takada, M. 1965. On the ground deformation and phenomena forerunning natural disasters. *Bull. Disaster Prevention Res. Inst.*, **14**, No. 3.
14. Myachkin, V.I. and S.I. Zubkov. 1973. Svodnyi grafik predvestnikov zemletryasenii (Average graph of earthquake forerunners). *Izv. AN SSSR, Fizika Zemli*, No. 6.
15. Kostrov, B.V. 1972. Mekhanika ochaga tektonicheskogo zemletryaseniya (Mechanics of Tectonic Earthquake Focus). Author's abstract of Doctoral thesis. *IFZ AN SSSR*, Moscow.
16. Aki, K. 1972. Earthquake mechanism. *Tectonophysics*, **13**, Nos. 1–4.
17. Aki, K. 1966. Generation and propagation of G-waves from the Niigata earthquake of June 16, 1964. *Bull. Earthquake Res. Inst. Tokyo Univ.*, **44**, No. 2.

18. Shebalin, N.V. 1969. Makroseismicheskoe pole i ochag sil'nogo zemletryaseniya (Macroseismic Field and Focus of Strong Earthquakes). Author's abstract of Doctoral thesis, *IFZ AN SSSR*, Moscow.
19. Ivanov, V.S. et al. 1965. Rol' dislokatsii v uprochnenii i razrushenii metallov (Role of Dislocation in Hardening and Failure of Metals). Nauka, Moscow.
20. Hoff, N. 1953. Creep and fracture. *J. Appl. Mech.*, **20**, No. 1.
21. Rikhitake, T. 1969. An approach to prediction of magnitude and occurrence time of earthquakes. *Tectonophysics*, **8**, No. 2.
22. Semenov, A.N. 1969. Izmenenie otnosheniya vremen probega poperechnikh i prodol'nykh voln pered sil'nymi zemletryaseniyami (Variation in the ratio of travel times of transverse and longitudinal waves before strong earthquakes). *Izv. AN SSSR, Fizika Zemli*, No. 4.
23. Keilis-Borok, V.I. and L.N. Malinovskaya. 1966. Ob odnoi zakonomernosti v vozniknovenii sil'nykh zemletryasenii (On a feature of strong earthquakes). In: *Seismicheskie Metody Issledovanii*, Nauka, Moscow.
24. Aggarwal, I.P. et al. 1973. *Nature*, **241**, No. 5385.
25. Magnitskii, V.A. 1965. Vnutrennee stroenie i fizika zemli (Internal Structure and Physics of the Earth). Nedra, Moscow.
26. Chinnery, M.A. 1969. Theoretical fault models. *Publ. Dominion Obs.*, **37**, N. 7.
27. Griggs, D.T., F.J. Turner and H.C. Heard. 1960. Deformation of rocks at 500–800°C. Rock Deformation (A symposium). *The Mem. Geol. Soc. of America*, **79**.
28. Tomashevskaya, I.S. and Ya.N. Khamidullin. 1972. Predvestniki razrusheniya obraztsov gornykh porod (Failure forerunners of rock specimens). *Izv. AN SSSR, Fizika Zemli*, No. 5.
29. Fedotov, S.A. 1967. O seismicheskom tsikle, vozmozhnosti kolichestvennogo seismicheskogo raionirovaniya i dolgosrochnom seismicheskom prognoze (The seismic cycle, scope for quantitative seismic zoning, and long-term seismic forecasting). In: *Seismicheskoe Raionirovanie Territorii SSSR*, Nauka, Moscow.

II. Laboratory Studies on Fracture

Preceding page blank

by choosing the appropriate thermodynamic conditions.

Heard [3] conducted fundamental studies of types of failure in limestone specimens under varied thermodynamic conditions. Higher hydrostatic pressures in experiments involving additional compression and tension increase the plasticity (Fig. 2a, b). The same happens at higher temperatures (Fig. 3). The composition of rock has little bearing on the failure mechanism at

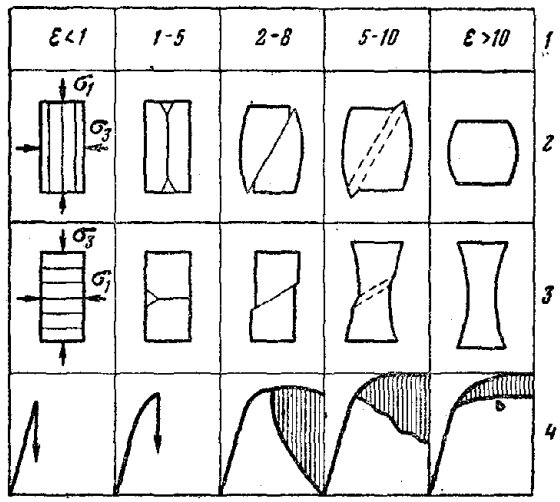

Fig. 1. Diagrammatic representation of specimen failure in compression (2) and tension (3) experiments; typical values of relative deformation before failure (1) and stress-strain graph (4) [2] are shown.

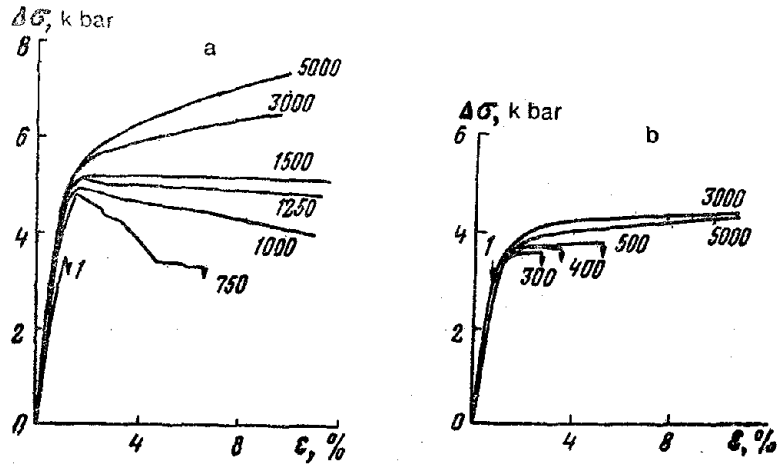

Fig. 2. Stress-strain graph for limestone subjected to confining pressure at 25°C (a) and 400°C (b) [3]. Numbers on curves indicate confining pressure.

higher thermodynamic parameters, as is noticeable from a comparison of the above characteristics of limestone and the behavior of, for instance, granite and basalt (Fig. 4a, b) [4].

The behavior of rock in relative compression or tension tests under confining pressure is qualitatively identical but differs quantitatively in that in compression experiments the transition from brittle fracture to plastic flow occurs at much lower temperatures and pressures (Fig. 5). This means that under terrestrial conditions the same rock may pass from plastic flow to brittle fracture and vice versa, depending on the type of stressed state.

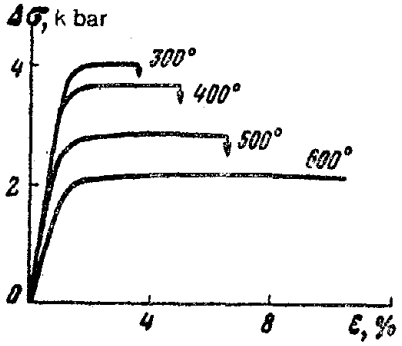

Fig. 3. Stress-strain graph for limestone subjected to confining pressure of 400 bar at different temperatures [3].

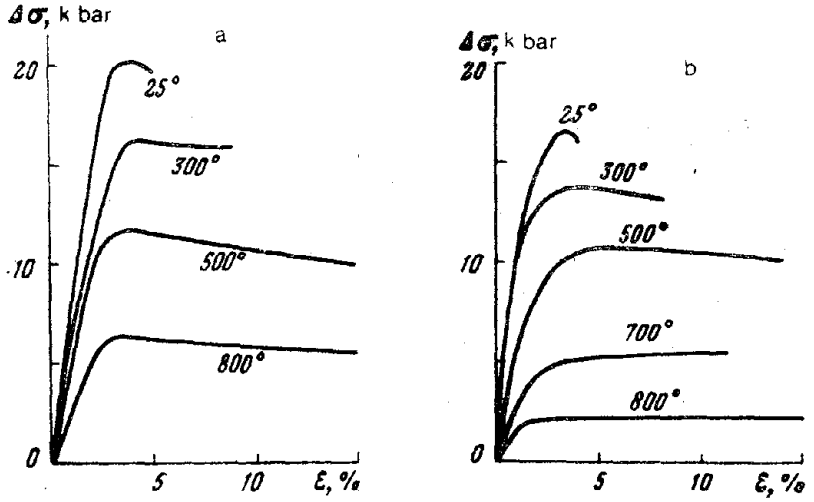

Fig. 4. Stress-strain curves for granite (a) and basalt (b) in compression experiments at confining pressure of 5 kbar and at different temperatures [4].

On the basis of studies of rock strength at various transitional stresses Mogi constructed stress-strain curves showing that specimens strained plastically under confining compression and, in addition, pressed uniaxially ($\sigma_3 = \sigma_2 < \sigma_1$) pass into the brittle fracture stage when $\sigma_3 < \sigma_2 < \sigma_1$ (Fig. 6) [5].

Intrapore pressure exercises a great influence on the strength of rock and the type of failure. This is obvious from the widely divergent results obtained in the testing of specimens protected or unprotected by a shell from penetration of liquid that creates hydrostatic pressure [6, 7]. For uniform straining of shell-jacketed and unjacketed specimen much higher differential pressures have to be applied in the first case; moreover, in this case the specimen will attain the stage of uniform flow at lower confining pressures.

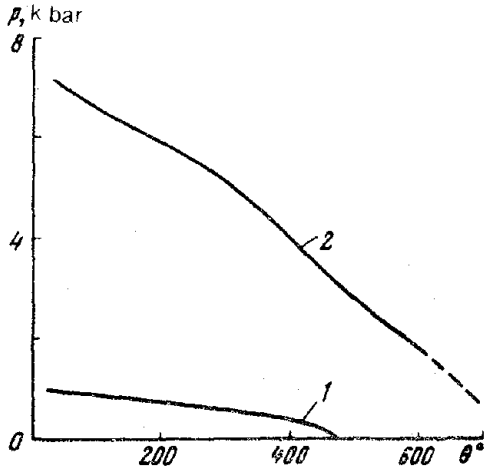

Fig. 5. Boundaries of transition from brittle fracture (below) to plastic flow (above) in compression (1) and tension (2) experiments with confining pressure and temperature [3].

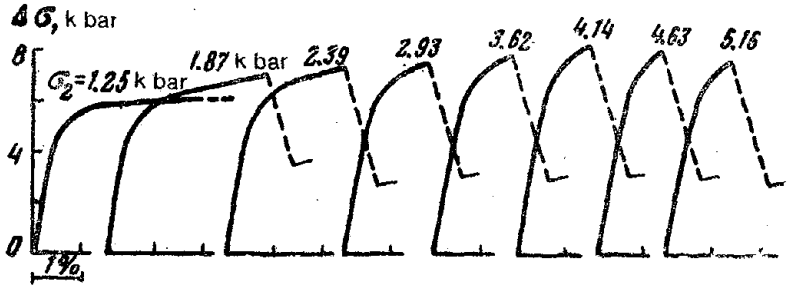

Fig. 6. Stress-strain graph depending on the value of intermediate stress σ_2 in experiments on triaxial compression $\sigma_3 \leqslant \sigma_2 < \sigma_1$ ($\sigma_2 = 1.25$ kbar).

The effect of intrapore pressure on the straining properties of rocks was studied quantitatively under controlled intrapore pressures. Liquid or gas was injected under the shell of the specimen placed in a high-pressure chamber. The rise of internal pressure in this case renders the rocks highly brittle [3], as is evident from Fig. 7a. Let us point out that there is no basic difference between the effects of intrapore liquid or gas if quantitative effects and physico-chemical interaction of the fluid and the rock skeleton are ignored.

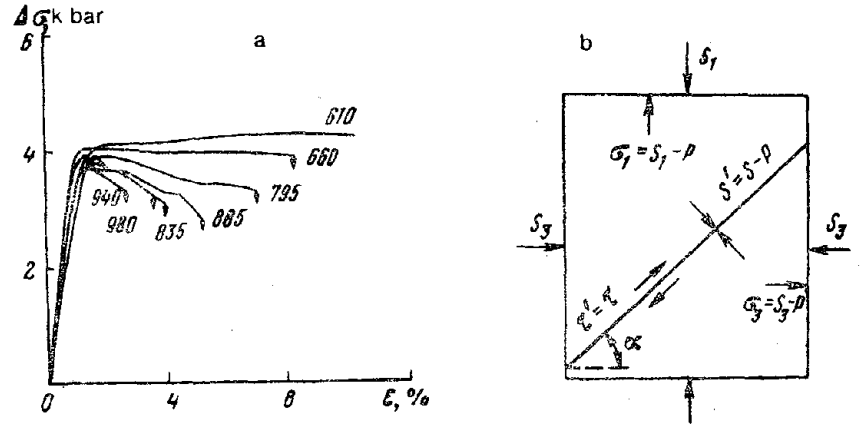

Fig. 7. Effect of intrapore pressure on failure type:
a—Stress-strain graph; numbers on each curve indicate intrapore water pressure [3]; b—Diagram of mechanical action of intrapore pressure [8].

Computation of the stress operating on the specimen enabled the authors of [8] to establish (Fig. 7b) that the intrapore pressure P reduces the normal stresses in the probable failure area

$$S' = \frac{(S_1 - p) \cdot (S_3 - p)}{2} + \frac{(S_1 - p) - (S_3 - p)}{2} \cos 2a = S - p$$

and does not affect the tangential stresses

$$\tau' = \frac{(S_1 - p) - (S_3 - p)}{2} \sin 2a = \tau,$$

thereby facilitating shear brittle fracture. In this case factors of crack formation in the earth are not determined by compressive lithostatic pressure but by what is called the effective pressure, comprising the difference in lithostatic and intrapore pressures. In particular, we obtain the modified Coulomb-Mohr law

$$\tau_{\text{eff}} = \tau_0 + (p_{\text{lith.}} - p_{\text{intrapore}}) \cdot \tan \varphi,$$

where $\tan \varphi$ is the coefficient of internal friction.

Brace showed [9] that the law of effective stress is valid for rocks only

when the average strain rate is not less than 10^{-7} 1/sec in view of the phenomenon of dilatancy hardening, which we touch upon below.

Thus the accumulated experience of laboratory rock fracturing shows that under the pressures and temperatures obtaining in the earth's interior the specimens develop upon shearing either a solitary crack or a crack array (shear zone). By shear crack we mean the main crack formed in compression tests. However, so far there does not seem to be any proof that tensile cracks do not precede shear failure. The resistance of rocks to tensile fracture is much less than the shear strength, and since heterogeneity of the rock facilitates the formation of local areas of relative tension it is quite probable that tensile microcracks may form even under high hydrostatic pressure.

A.N. Stavrogin [10] proposed a model of a main shear crack (Fig. 8). The crack consists of the tensile elements b oriented close to the axis of maximum compression and of the shear areas a inclined to this axis at 45°. The length of the tensile elements b diminishes with an increase in the confining pressure $p = \sigma_2 = \sigma_3$, thereby increasing the angle of inclination of the main crack and the number of possible shear planes (i.e. decreasing the distances between them). In the limiting case pure shear fracture can arise under high confining pressures, and the question arises what this limit is.

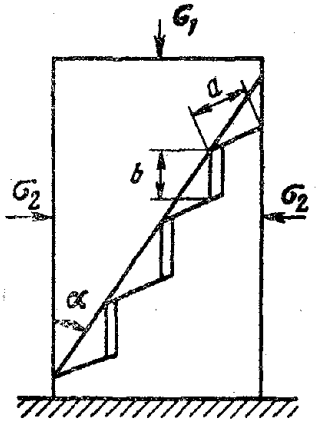

Fig. 8. Model of main shear crack:
a—Shear elements; b—Tensile elements [10].

Wawersik and Brace [11] carried out experimental studies on the orientation of microcracks appearing at various stages of straining of granite and diabase specimens. It was found (Fig. 9) that at a maximum confining pressure of 1.5 kbar the number of cracks oriented close to the axis of maximum compression, i.e. cracks containing tensile elements, is still quite high.

The measurements were made at the straining stage of the specimen that

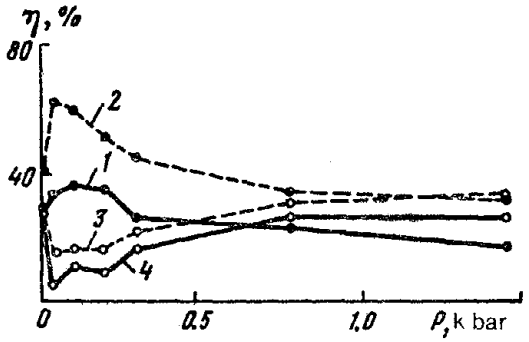

Fig. 9. Distribution of cracks oriented to compression axis at angles $< 5°$ (1), $< 10°$ (2), $> 30°$ (3), $> 35°$ (4), in specimen under varying external pressures [11].

marked the start of formation of main microcracks. N.M. Osipenko fractured rocks (granodiorites, basalts, dolerites) step-by-step in uniaxial compression [12], analyzed the fractured surface microscopically and correlated these data with the coefficients of stress intensity obtained. He showed that the transverse dimensions of the steps corresponded in order of value to typical structural and textural elements of the rocks.

The kind of failure of rock specimens under uniaxial and confining compression was studied by Rummel [13] in limestone specimens. Microscopic analysis suggests that under confining pressures up to 140 atm the longitudinal cracks diminish in number. They are replaced by shear cracks by slipping along inclined grain edges, and by intragrain slipping. In the pressure range 140–210 atm the sample suffers brittle fracture, yielding shear microcracks, while at pressures above 210 atm the fracture was quasiplastic, i.e. the shear macrocrack was replaced by a multitude of slip areas.

Granted that a macrocrack results from interaction of numerous cracks, their growth and merger, let us discuss the study of solitary cracks and their interaction in greater detail.

According to Griffith's theory, brittle materials fail because they always contain initial defects like grain edges, various inclusions, embryonic cracks, etc. Griffith developed his theory initially with reference to tensile cracks that appear in the field of uniaxial tensile stresses. Later he extended it to the biaxial stressed state, including uniaxial and biaxial compression.

There is a distinct difference between the growth of tensile cracks under tension and under compression. When the sample is stretched the tensile crack spreads right up to the boundary of the sample (provided it does not encounter a strength barrier on the way). Tensile cracks may stabilize under compression. This aspect has been studied most comprehensively with reference to initial inclined cracks at the end of which tensile cracks form at

some angle to the orientation of the initial crack.

The stress field around this crack has been studied in detail theoretically by V.V. Panasyuk [14] and Kobayashi et al. [15]. It has been studied experimentally by Duda [16], Hoek and Bieniawski [17] and D.N. Osokina and N.Yu. Tsvetkova [18] using the photoelastic method, by O.G. Shamina et al. [19] and L. Vaniek et al. [20] using the shading method, and by Kobayashi [15] using the "moiré-fringe" method.

In all these studies the crack was modeled as a narrow slit whose sides were free or pressed together. The results of studies of cracks with free sides by various methods do not contradict one another. In Fig. 10 we cite from [17] the pattern of interference bands (lines of equal tangential stresses) around a slit incised in a glass plate placed under uniaxial compression. A similar pattern of colored interference bands in Araldite was observed by Duda, who called it "butterfly's body". It is noteworthy that he observed a characteristic skew-symmetric stress field in the case of an open slit and of a slit incised to a depth of nine-tenths of the thickness of the model, so that the sides remained interlinked.

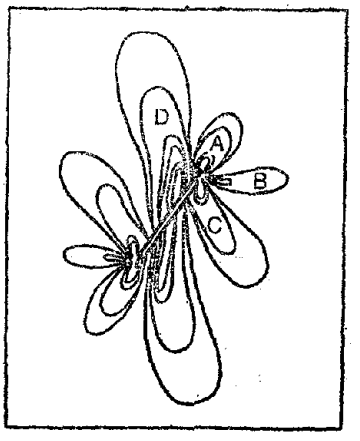

Fig. 10. Pattern of interference bands around slit with free sides.

The maximum tangential stress pattern for closed slits in plates of gelatinous material is shown in Fig. 11 [18]. The stress field appears to be completely symmetric. Apparently the contact between the sides of the slit is much stronger in this case than in Duda's experiments, and this is responsible for the difference in the stress pattern.

However, in both cases the maximum concentration of tangential stresses is observed at points of the medium lying on the extension of the crack, and at points close to the top of the crack.

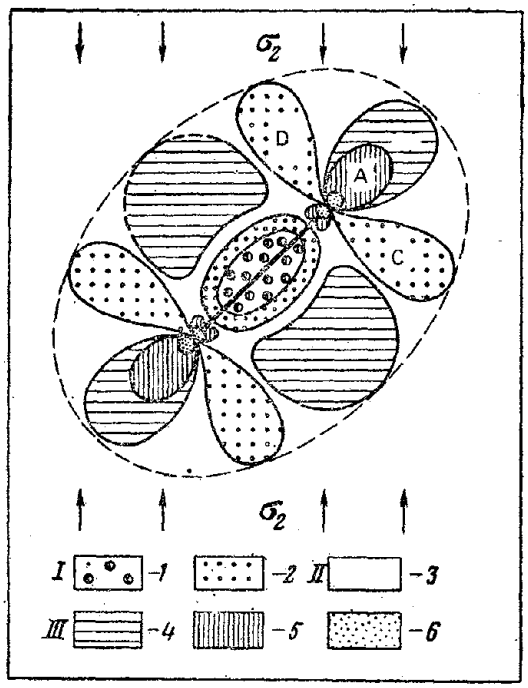

Fig. 11. Pattern of interference bands around slit with linked sides:
I—τ_{max} position: 1—strong; 2—medium; II—3—τ_{max} unchanged;
III—higher τ_{max}: 4—weak; 5—medium; 6—strong.

Considering that the maximum tangential stress is the difference between two principal stresses and taking the distribution of mean stresses around the slit [19] into account, the pattern depicted in Fig. 10 may be interpreted as follows: In the A, B and C regions the compressive stress exceeds the tensile, but in the D region the tensile stress exceeds the compressive.

The failure of real materials containing initial cracks with free sides is governed by the observed stress maxima. In paraffin and alabaster specimens tested under uniaxial compression [21] shear cracks were observed in the A, B and C regions and tensile cracks in the D region. In the A region the shear crack spread toward the initial crack (slit), in the B region horizontally, in conformity with the trajectory of shear stresses, and in the C region initially almost at right angles to the orientation of the original crack, thereafter following a course approximating the direction of maximal tangential stresses in the specimen (45° relative to the compression axis). The horizontal shear cracks appeared at random. The cracks appeared in the A region under rapid stress, but in the B region under slow stress when a large area of plastic deformations was created.

Studying the aftershocks of the Mongolian earthquake, Duda [16] noticed that from a certain instant of time the aftershocks began to appear roughly at an angle 40° relative to the direction of fracture in the main shock. He attributes this to the stress field around the main fracture playing the part of a stress concentrator like the slit in laboratory experiment.

Free-sided fractures are improbable in the natural environments of the earth's interior. But what stress pattern the friction between the two sides will assume is difficult to suggest, i.e. the magnitude of the friction is unknown. As regards tensile cracks, which appear at the ends of the open slit under tensile stresses (Fig. 10, D region), they are really oriented at an angle of 90° relative to the slit—a fact observed by many workers [14, 17–19, 21–25].

The maximal tangential stress pattern (Fig. 11) is interpreted as follows: compression is prevalent in the A and C regions, tension in the D region. The shear cracks in the A and C regions for this case are known to us, and tensile cracks in the C region are described in [12, 17, 18]. Depending on the magnitude of the friction between the sides tensile cracks are formed at an angle of nearly 70° to the slit.

As they spread the tensile cracks formed at the top of a free or closed slit bend and become parallel to the compression axis. A marked increase in stress is needed for them to develop further [14, 23].

Some echelons of preliminary cracks in glass lying at some angle to the direction of compression were studied in [17, 22–25]. It may be concluded from these studies that even though the stresses at the apexes of a preliminary crack in the echelon are higher than the stresses at the apexes of a solitary crack, they do not affect the spread of the cracks formed, i.e. the tensile cracks formed at the apexes of the adjacent preliminary cracks do not interact.

This is valid, however, for the initial growth stage of tensile cracks. In certain echelons the preliminary cracks may merge upon further pressure when they are close to one another (they are fractions of their length apart). This aspect is studied elaborately in [24, 25].

The concentration coefficient K of tensile stresses at the apexes of parallel cracks forming a system oriented toward the compression axis of the specimen at different angles was determined by the photoelastic method. The value of K changes from K_0 at the apex of a solitary crack to several times K_0, depending on the relative disposition of the crack.

In his studies on the growth of tensile cracks triggered by preliminary cracks forming various systems with fairly high K, Bombolakis proved that the critical inclination of preliminary cracks relative to the compression axis is 45° [24]. Two stages were distinguished in the growth of tensile cracks. In the first stage they grow in a direction normal to the preliminary cracks and do not merge with the latter. In the second stage the tensile cracks curve out and merge together. It is notable that in O.G. Shamina and S.A.

Strizhkov's experiments cracks grew in an identical way in epoxy resin specimens (the material generally used for photoelastic models), but this phenomenon was not observed (see p. 92) in alabaster specimens. The reason seems to be that the physico-mechanical properties of materials used for photoelastic studies differ from those of a real medium.

During compression tests of pegmatite specimens Bombolakis [25] noticed that in conformity with model studies echelons of embryonic cracks having fairly high K values are activized. Curiously, individual embryonic microcracks were united in the process by means of alternating tensile and shear elements.

On the basis of experimental findings on the behavior of cracks under compression, Brace and Bombolakis [22, 23, 28] formulated their fundamental thesis: a brittle shear macrocrack cannot originate from a single embryonic crack because a tensile crack is formed on stretching the specimen. A specific echelon of preliminary cracks lying along a line inclined to the direction of compression is essential. For this the crack separation should not be more than several crack lengths. This conclusion is supported by theoretical calculation of the conditions of crack interaction [14, 26, 27].

An example of an echelon of preliminary and tensile cracks formed in a stressed glass plate, which Brace [28] considers as typical and similar to the crack system observed in rocks, is given in Fig. 12.

Interestingly, the ultimate stress essential for formation of shear macrocracks in glass is much higher than the stress required for preliminary crack

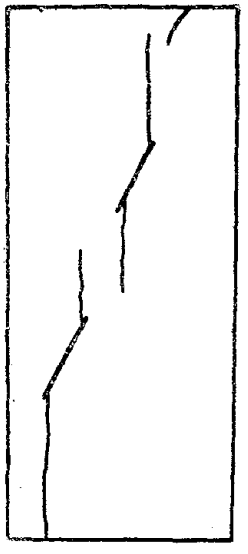

Fig. 12. Example of echelon of preliminary (bold line) and tensile (thin line) cracks formed in glass plate under stress.

growth, whereas these stresses are roughly the same in rocks. The authors attribute this to the probable rupture of joints between tensile cracks developed from the apexes of contiguous embryonic cracks.

The formation of tensile cracks triggered in rock specimens by a stress concentrator in the form of a round hole bored perpendicular to the axis of compression is studied in [13, 29–31].

The tensile cracks appeared at the points of tensile stress concentration and spread a short distance in a direction parallel to the compression axis before stabilizing. To induce further growth of the crack it was necessary to increase the stress markedly.

The development of these cracks was studied elaborately by F. Rummel [13] on limestone and marble specimens. These experiments are of great interest because they were conducted at a fixed strain rate using a special servo-controlled testing machine. It was possible to adjust the strain rate both along the stress axis and in the transverse direction. During the experiment crack development was observed under the microscope, so that all the stages could be studied systematically.

It was found that secondary cracks, which initially spread at an angle of 45° and later became parallel to the stress axis begin to appear near the hole after tensile crack stabilizes. However, neither stress nor microscopic crack analysis allowed the author to determine unambiguously the type of crack that is oriented at an angle of 45°. Most probably they are shear cracks, at the ends of which tensile cracks appear as described above.

As the stress along the planes of secondary cracks increases, shearing takes place and shear macrocracks are formed.

When applying laboratory data to tectonic processes occurring in the earth, the wide difference in time scales has to be reckoned with. The time factor has a direct bearing on rock strength, as was shown by S.N. Zhurkov [32, 33] on the basis of kinetic concepts. For a wide range of materials loads, and temperatures, he proposed the following simple formula relating durability of material and stress:

$$\tau = A e^{\frac{U-a\sigma}{kT}},$$

where U is the activation energy of failure; k is the Boltzmann's constant; T is the temperature; A and a are parameters of the material. The universality of this law was demonstrated for rocks too [34].

The data in [34] help to establish (Fig. 13) that the time until the specimen fails remains constant only when the differential and confining pressures change in a definite proportion. This means that a unitary time scale for earthquake preparation at different depths of the earth is not to be thought of.

The well-established monotonous fall in failure loads with diminishing

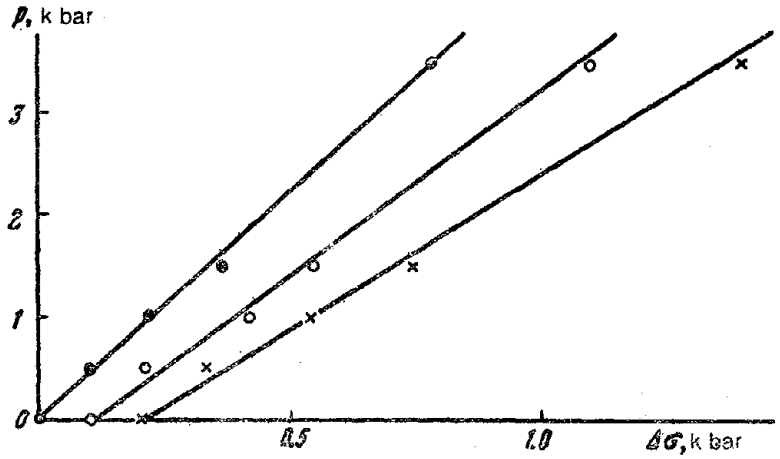

Fig. 13. Correlation of confining and differential pressures with same specimen failure time τ = const; three straight lines correspond to three different values of τ.

strain rate is a consequence of fatigue strength [9, 35, 36]. Interestingly, this correlation seemed very weak at the lower limit of the strain rate (about 10^{-10} 1/sec) attained under laboratory conditions [36].

The effect of fatigue strength may manifest itself in time-dependent fracturing, which in an inhomogeneous brittle material is observed as creep during strain measurements under natural and laboratory conditions [37–41]. Three stages of creep are observed in laboratory tests [42, 43], the last of which culminates in failure of the specimen (Fig. 14). The strain is proportional to the logarithm of the time at stage I (best studied) and to the time at stage II. It is shown in [43] that the laws of strain variation at creep stages I and II can be derived from simple statistical concepts of the failure of a heterogeneous material involving the law of fatigue strength, the statistical strength distribution in the specimen and the increase with time of the length of microcracks.

Creep stage III has been little studied and inadequately elaborated simply because of experimental difficulties arising from the unavoidable effect of the testing machine on the failure process.

As shown in [44], the strain is found to be accelerated by crack interaction at the last, prefailure microcrack growth stage (at about 95% of the failure stress), called the dynamic fracture stage.

The expansion with time of the volume of the specimen during creep under constant stress is closely linked with dilatancy, usually studied at a constant strain rate. Expansion of heterogeneous materials accompanied by changes in shape is also noted by Bridgman [45] in metals and has been studied elaborately for rocks by Brace and Stavrogin [46, 47].

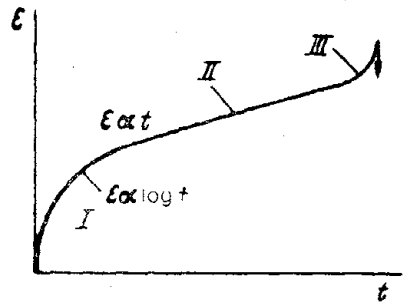

Fig. 14. Sketch diagram of rock straining in creep.

In some recent studies [48, 49] dilatancy is considered decisive for explaining earthquake forerunners. It is believed that tensile microcracks appear in the earthquake preparation zone. These initially facilitate consolidation of the rocks owing to a drop in the intrapore water pressure and later cause the earthquake after restoration of this pressure to the normal level.

The universality of such an approach to earthquake preparation and forerunners appears doubtful. First of all there is a difference of several orders between the size of the microcracks formed due to dilatancy and the size of the faults that cause earthquakes; confirmation of the direct link between them presupposes the occurrence of dilatancy in a large area.

It is shown in [47] that the volume of the specimen increases steeply only at a definite ratio of the principal stresses (Fig. 15):

$$c = \frac{\sigma_{\min}}{\sigma_{\max}} = (0.2-0.4).$$

Simultaneous prevalence of such conditions over a large area of the earth, particularly at different depths, is improbable. Dilatancy hardening, suggested in [50], is difficult to explain when the dilatancy develops gradually, because such hardening occurs in rocks only at high strain rates [9].

As is evident from Fig. 16, at the strain rate $\epsilon < 10^{-7}$ 1/sec, typical of the tectonic processes in the earth, dilatancy hardening does not develop because the solutions present in the rock fill the parts of the increased volume, while the intrapore pressure remains constant. Apparently dilatancy may play a notable part at a definite earthquake preparation stage. This involves the growth of microjointing in various localities of the earth's crust, which, in turn, promotes the gradual growth of large cracks.

The general pattern of crack formation in laboratory experiments was furnished by Brace [9] (Fig. 17). A stage of microcrack growth deviating from Hooke's law is reached after the elastic behavior of the specimen. After attaining the critical failure stress the microcracks begin to grow intensely

under diminishing stress. If the specimen does not suffer complete collapse the strength may increase upon subsequent straining along the existing fracture due to friction.

Detailed study of the area of diminishing strength just before the main crack forms is of special interest for physics of earthquake. Commonly the specimen is crushed rapidly due to the dynamic impact of the press, rendering the laboratory findings on this stage inapplicable to natural conditions. But the authors of [11] succeeded in showing that the failure process can

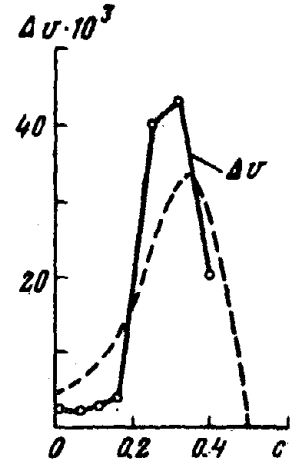

Fig. 15. Volume change with type of stressed state in two specimens of marble.

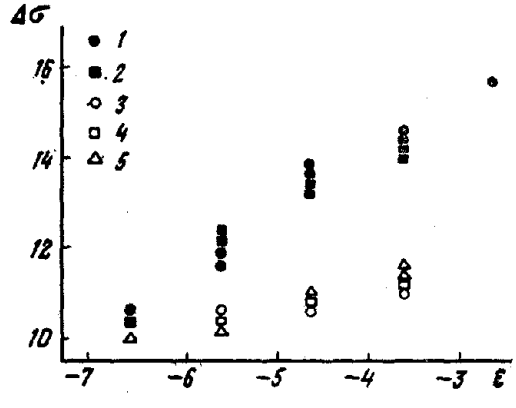

Fig. 16. Granite strength as function of strain rate at confining pressure 3.1 kbar and pore pressure 1.6 kbar with pore pressure of:
1—Water; 2—Acetone, saturated; 3—By water; 4—By acetone; 5—Dry [9].

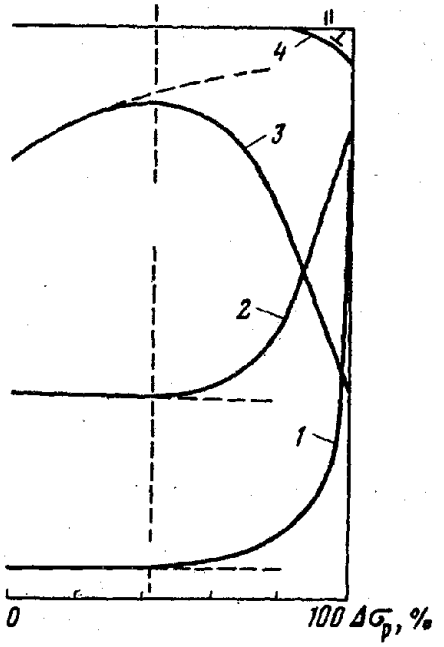

Fig. 20. Average graph of variation in number of microcracks (1), volume (2), electrical resistance (3), and elastic wave velocity (4) for rocks fractured at load σ_p.

It was found that anomalous changes in the majority of parameters begin at loads exceeding one-half the failure loads. The course of the curves depends little on the confining pressure, provided all the graphs are standardized with reference to the differential stress, representing the difference between the maximum compressive load and the confining pressure.

Studying the longitudinal wave velocity along the length ($V_p^{\parallel}$) and breadth ($V_p^{\perp}$) of the specimen, Rummel [29] noticed that at the initial stage of the experiment $V_p^{\perp}$ diminishes faster than $V_p^{\parallel}$. This is attributable to the preeminent development at this stage of tensile cracks parallel to the axis of maximum compression. The diminution occurs gradually, indicating, in the author's view, the continuity of the failure process. In [52–54] special attention is given to microcrack recording. This brought to light the phenomenon of microcrack concentration in a narrow zone at loads exceeding 95% of the failure loads.

An interesting microcrack growth sequence is noticed in [53], devoted to the study of buckling failure. By the time a crack developed the microseismic activity of the neighboring crack ceased altogether. In studying microcrack formation it was found that the lower frequencies increase in the

specimen before failure [55], and the slope of the recurrence curve diminishes [56].

Before concluding this review of experimental studies we must mention the suggestion that the typical phenomenon of failure by rapid sliding, involving friction along the prepared fracture, is the probable mechanism of earthquakes [57, 58]. At a high strain rate blocks of rock may pass from stable-sliding along the fault to stick-slip accompanied by stress jump. A small plastic minerals content, low porosity, high effective pressure, and small thickness of the crackforming zone are the factors that contribute to stick-slip. A higher temperature facilitates stable-sliding. Water may play a dual role by interacting chemically with the solid phase, weakening the rock and promoting stable-sliding, or enhancing brittleness at higher interstitial water pressure, giving rise to unstable shoves. In our view stick-slip can hardly be expected in natural environments as referred to earthquakes. In the earth fracture growth involves ripping open the end of the fracture. In laboratory conditions the properties of such fractures were studied by displacing one block of rock relative to another serving as a whole body.

The foregoing brings us to the general question whether laboratory results can be applied to the earth. The results obtained certainly provide qualitative descriptions of the phenomena peculiar to large rock masses. And there is an identity between changes in the properties of specimens before failure and earthquake forerunners [59]. But the situation changes when attempts are made to use laboratory experimental results for quantitative study of processes occurring in the earth.

The problem of physical modeling for the case in question may perhaps consist in creating models physically simulating the earthquake focal zone. This problem remains practically unsolved to date. Three factors are necessary for creation of such a model: knowledge of the basic parameters of the original, computation of the model on the basis of similarity theory, and practical realization of the model.

In a first approximation the behavior of the material in the focal zone can be described by a rheological equation involving at least strain, strain rate and gradient, stress, stress rate and gradient, and temperature:

$$\Phi\left(\epsilon, \frac{\partial \epsilon}{\partial t}; \frac{\partial \epsilon}{\partial n}, \sigma, \frac{\partial \sigma}{\partial t}, \frac{\partial \sigma}{\partial n}; \theta\right) = 0. \tag{1}$$

If a certain physical process in nature is described by the equation

$$y = \varphi(x_i) \tag{2}$$

and in the model by

$$y' = \varphi'(x_i'), \tag{3}$$

then the physical processes in nature and in the model will be similar when $y' = \beta\gamma$; $x' = a_i x_i$ where β and a are similarity factors [60, 61]. Writing

$\gamma = \beta\varphi\,(x_i'/a_i)$ and comparing (2) and (3), we get the condition of similarity. While computing the model it is possible to neglect the temperature and gradients along this direction considering the processes as isothermic. Then, confining ourselves to mechanical similarity (leaving aside electrical, magnetic, chemical and other processes in the earth), we have to satisfy simultaneously the conditions $\epsilon' = \gamma\epsilon$, $\sigma = \beta\sigma$, $t' = \tau t$ and add to this the geometric criteria $(x', y', z_i') = a\,(x, y, z)$. Using the results of [60] it can be proved that for modeling the Hooke body it is necessary to satisfy the unique criterion of equality of Poisson's ratios for the model and nature, which are equal to the ratios of the Young and shear moduli, as given by

$$E' = \beta/\gamma E;\quad \mu' = \beta/\gamma\mu.$$

For a more complex rheological body it would also be necessary to observe the similarity criterion for the viscosity coefficient

$$\eta' = \beta/\gamma\tau\eta. \tag{4}$$

To sustain the similarity in the crack-forming processes (most fascinating for physics of earthquake) it would be necessary to satisfy the equation for dynamic similarity involving the force of inertia

$$\tau = \alpha\sqrt{\delta\frac{\gamma}{\beta}}, \tag{5}$$

$$\xi' = \beta/\alpha\xi, \tag{6}$$

where δ is the density constant and ξ is the bulk density. Of course, it is also desirable to satisfy the similarity conditions on the fracture boundaries, taking locking and friction into account.

Evaluating the results of the experiments described above, we must state with regret that the similarity theory was not adhered to in any of these studies. Let us refer to the modeling of the phenomena occurring in time. A specific feature of the laboratory experiments required that the experiments should not last more than a few hours or days. This means that the time constant $\tau \approx 10^{-5}$. In order to adhere to the similarity theory for large displacements the strain constant should be 1 and the possibility of realizing high pressure does not allow us to obtain $\beta \gg 1$.

We find from equation (4) that the viscosity coefficient η' of the model should be many times lower than the viscosity coefficient of the original. On the other hand, it follows from the dynamic similarity equation (6) that the geometric constant is also of the order of 10^{-5}, i.e. the material should be very finely dispersed. Thus we arrive at the conclusion that rocks in laboratory experiments cannot serve as models of natural conditions. From this viewpoint it is preferable to use model materials [62]. The above analysis shows that it is impossible to model all the characteristics of earthquake preparation in one experiment. However, attempts can be made to study various

aspects of the process systematically.

Reviewing the experiments on the failure of materials under diverse thermodynamic conditions, a program was chalked out at the IFZ to study the characteristics of the earthquake preparation involving: (a) preparation of solitary tensile and shear cracks, (b) interaction of two tensile and shear cracks, (c) zones of crack concentration, avalanchelike acceleration of crack formation, and main fault formation.

Measurements were made in a variety of rocks and synthetic materials at different stressed states. A complex of mechanical and electrical parameters was studied in the course of the experiments. The major task of the first stage of the studies was to realize controlled internal failure. Some of the results obtained are listed below [63–65]; they can be utilized to substantiate the hypothesis of earthquake preparation, to explain forerunners and to develop prediction techniques.

REFERENCES

1. Sb. Bor'ba s Vnezapnyami Vybrosami Uglya i Gaza v Shakhtakh (Collection: Combating Sudden Blowouts of Coal and Gas in Mines). *Tr. Geofiz. In-ta,* No. 34 (161), 1956.
2. Griggs, D. and J. Handin. 1960. Observations on fracture and hypothesis of earthquakes. *Rock Deformation*, No. 4.
3. Heard, H.C. 1960. Transition from brittle fracture to ductile flow in Solenhofene limestone as a function of temperature, confining pressure and interstitial fluid pressure. *Rock Deformation,* No. 4.
4. Griggs, D.T. et al. 1960. Deformation of rocks at 500° to 800°C. *Rock Deformation*, No. 4.
5. Mogi, K. 1971. Effect of the triaxial stress system on the failure of dolomite and limestone. *Tectonophysics*, **11**.
6. Griggs, D. 1936. Deformation of rocks under high confining pressure. *J. Geol.*, **44**.
7. Handin, J. 1953. An application of high pressure in geophysics. In: Experimental Rock Deformation, *Trans. Amer. Soc. Mech. Engrs.*, **75**.
8. Hubbert, M.K. and W.W. Rubey. 1959. Role of fluid pressure in mechanics of overthrust faulting. *Bull. Geol. Soc. America*, **70**.
9. Brace, W.F. 1971. Micromechanics in rock systems. *Structure, Solid Mechanics and Engg. Design.*
10. Stavrogin, A.N. 1968. Analiz eksperimental'nykh rezul'tatov po deformatsii i razrusheniya gornykh porod (Analysis of experimental results on rock straining and fracturing). In: *Sb. Gornoe, Davlenie Sdvizhenie Gornykh Porod i Metodika Marksheiderskikh Rabot*, VINITI, Moscow.

11. Wawersik, W.R. and W.F. Brace. 1971. Postfailure behavior of granite and a diabase. *Rock Mechanics*, **3**.
12. Osipenko, N.M. 1971. Nekotorye voprosy mekhaniki razrusheniya treshchinovatykh gornykh porod (Some aspects of the failure mechanics of fractured rocks). Author's abstract of Doctoral thesis. IFZ, Moscow.
13. Rummel, F. and C. Fairhrust. 1970. Determination of postfailure behavior of brittle rock using a servocontrolled testing machine. *Rock Mechanics*, **2**, 189.
14. Panasyuk, V.V. 1968. Predel'noe ravnovesie khrupkikh tel s treshchinami (Limiting Equilibrium of Cracked Brittle Bodies). Naukova Dumka, Kiev.
15. Kobayashi, A.S., W.Z. Engstrom and B.R. Simon. 1964. Crack-opening displacements and normal strains in centrally notched plates. *Exper. Mech.*, April.
16. Duda, S.Y. 1965. The stress around a fault according to a photoelastic model experiment. *Geophys. J. Roy. Astron. Soc.*, **9**, No. 4.
17. Hoek, E. and Z.T. Bieniawski. 1965. Brittle fracture propagation in rock under compression. *J. Fracture Mech.*, **1**, No. 3.
18. Sb. Predvestniki Zemletryasenii (Collection: Earthquake Forerunners). VINITI, Moscow, 1973.
19. Shamina, O.G., A.A. Pavlov and Yu.V. Kopnichev. 1973. Issledovanie protsessa podgotovki treshchin (Study of the crack preparation process). *Izv. AN SSSR, Fizika Zemli*, No. 8.
20. Vaniek, L., K. Klima, Ya. Kozak and O. Shamina. 1973. Izuchenie shliren-metodom uprugikh voln, prokhodyashchikh cherez oblasti kontsentratsii napryazhenii (Study of elastic waves passing through areas of stress concentration of Schlieren photography). *Dokl. AN SSSR*, **210**, No. 2.
21. Shamina, O. 1972. Laboratory investigation of process of crack preparation. Report at Meeting ECK, Brashov.
22. Brace, W.F. and E.G. Bombolakis. 1963. A note on brittle crack growth in compression. *J. Geophys. Res.*, **68**, No. 12.
23. Bombolakis, E.G. 1964. Photoelastic investigation on brittle crack growth within a field of uniaxial compression. *Tectonophysics*, **1**, No. 4.
24. Bombolakis, E.G. 1968. Photoelastic study of initial stages of brittle fracture in compression. *Tectonophysics*, **6**, No. 6.
25. Bombolakis, E.G. 1973. Study of the brittle fracture process under uniaxial compression. *Tectonophysics*, **18**.
26. Finkel', V.M. 1970. Fizika razrusheniya (Fracture physics). Metallurgiya, Moscow.
27. Jokobori, T. and M. Ichikawa, 1964. Elastic solid with an infinite low of collinear cracks and the fracture criterion. *J. Phys. Soc. Japan*, **19**, 2341.

28. Brace, W.F. and J.D. Byerlee. 1967. Recent experimental studies of brittle fracture of rocks. In: *Failure and Breakage of Rock*, New York.
29. Rummel, F. 1972. Bruchausbreitung in Kalksteinproben. *Veröffentl. Inst. Bodenmech. und Felsmech. Univ. Fricleriana in Karlsruhe*, H. 55.
30. Brace, W.F. and J.B. Walsh. 1962. Some direct measurements of the surface energy of quartz and orthoclase. *Amer. Mineralogist*, **47**, 1111.
31. Hoek, E. 1963. The application of experimental mechanics to the study of rock stress problems encountered in deep level mining in South Africa. Proc. Internat. Congrs. Exper. Mech., New York.
32. Zhurkov, S.N. and B.N. Narzullaev. 1953. Vremennaya zavisimost' prochnosti tverdykh tel (Time-dependence of solid body strength). *ZhTF*, **23**, 10.
33. Zhurkov, S.N. 1968. Kineticheskaya kontseptsiya prochnosti, tverdykh tel (Kinetic concept of solid body strength). *Vestn. AN SSSR*, No. 3.
34. Tomashevskaya, I.S. and Ya.N. Khamidullin. 1972. Vozmozhnost' predskazaniya momenta razrusheniya obraztsov gornykh porod na osnove fluktuatsionnogo mekhanizma rosta treshchin (Scope for prediction of failure time of rock specimens on basis of fluctuational mechanism of rock growth). *Dokl. AN SSSR*, **207**, No. 3.
35. Pavlova, N.A. and A.A. Shreiner. 1968. Vliyanie skorosti deformirovaniya na protsess deformatsii i razrusheniya gornykh porod v usloviyakh ob'emno-napryazhennogo sostoyaniya (Effect of strain rate on rock strain and fracture under three-dimensionally stressed state). In: *Fiziko-Mekhanicheskie Svoistva Gornykh Porod Verkhnei Chasti Zemnoi Kory*, Nauka, Moscow.
36. Stavrogin, A.N. and E.D. Pevzner. 1971. Fizikomekhanicheskie svoistva gornykh porod pri dinamicheskikh nagruzkakh v usloviyakh slozhnykh napryazhennykh sostoyanii (Physicomechanical properties of rock loaded dynamically under complex stressed states). In: *Fizicheskie Svoistva Gornykh Porod pri Vysokikh Termodinamicheskikh Parametrakh.* Naukova Dumka, Kiev.
37. Mott, N.F. and G.R.N. Nabarro. 1948. Dislocation theory and transient creep. *Report on Strength of Solids*, London.
38. Matsuchima, S. 1960. On the flow fracture of igneous rocks. *Bull. Disaster Prevent. Res. Inst. Kyoto Univ.*, **36**, 2.
39. Robertson, E.C. 1960. Creep in Solenhofen limestone. *Mem. Geol. Soc. America*, **79**, 227.
40. Erzhanov, Zh.S. 1965. Teoriya polzuchesti gornykh porod i ee prilozheniya (Creep theory of rocks and its application). *Gornoe Davlenie, Sb.*, 59, Leningrad.
41. Tocher, D. 1960. Creep on the San Andreas fault, creep rate and related measurements at Vineyard, California. *Bull. Seismol. Soc., America*, **50**.

42. Robertson, E.C. 1964. Viscoelasticity of rocks. *State of Stress in the Earth Crust*, No. 4.
43. Scholz, C.H. 1968. Mechanism of creep in brittle rock. *J. Geophys. Res.*, **73**, 10.
44. Scholz, C.H. 1968. Microfracturing and the inelastic deformation of rock in compression. *J. Geophys. Res.*, **73**, 4.
45. Bridgman, P. 1955. Issledovanie bol'shkikh plasticheskikh deformatsii i razryva (Study of Large Plastic Deformations and Faults). IL, Moscow.
46. Brace, W.F. 1964. Brittle fracture of rocks. *State of Stress in the Earth Crust*, No. 4.
47. Stavrogin, A.N. 1968. Deformatsiya i prochnost' gornykh porod (Staining and strength of rocks). In: *Sb. Gornoe Dovlenie, Sdvizhenie Gornykh Porod i Metodika Marksheiderskikh Rabot*, VINITI, Moscow.
48. Nur, A. 1972. Dilatancy, pore fluids and premonitory variations of s/p travel times. *Bull. Seismol. Soc. America*, **62**, 5.
49. Scholz, C.H., L.R. Sykes and Y.P. Aggarwal. 1973. A physical basis for earthquake prediction. *Science*, **181**.
50. Frank, F.C. 1965. On dilatancy in relation to seismic sources. *Rev. Geophys.*, **3**, 4.
51. Tomashevskaya, I.S. and G.A. Sobolev. 1969. Odnovremennye issledovaniya mekhanicheskikh i elektricheskikh yavlenii, soprovozhdayushchikh protsessy razrusheniya obraztsov gornykh porod pri slozhnom napryazhennom sostoyanii (Simultaneous study of mechanical and electrical phenomena accompanying processes of fracture of rock specimens under complex stressed state). In: *Sb. Fizika Gornykh Porod i Protsessov. Tr. MGI*, Moscow.
52. Mogi, K. 1962. Study of the elastic shocks caused by the fracture of heterogeneous materials and its relation to earthquake phenomena. *Bull. Earthquake Res. Inst. Univ. Tokyo*, **40**, 125.
53. Mogi, K. 1968. Source locations of elastic shocks in the fracturing process in rocks. *Bull. Seismol. Soc., Japan.* **46**, 5.
54. Scholz, C.H. 1968. Experimental study of the fracturing process in brittle rock. *J. Geophys. Res.*, **73**, 4.
55. Shamina, O.G. 1966. Uprugie impul'sy pri razrushenii gornykh porod (Elastic impulses in rock fracturing). *Izv. AN SSSR, Ser. Geofiz.*, No. 5.
56. Vinogradov, S.D. 1964. Akusticheskie nablyudeniya protsessov razrusheniya gornykh porod (Acoustic Observation of the Processes of Rock Fracture). Nauka, Moscow.
57. Brace, W.F. and J.D. Byerlee. 1966. Stick-slip as a mechanism for earthquakes. *Science*, **153**.
58. Brace, W.F. 1972. Laboratory studies of stick-slip and their application to earthquakes. *Tectonophysics*, **14** (3, 4).

59. Sobolev, G.A. 1973. Perspektivy operativnogo prognoza zemletryasenii po elektrotellurichеskim nablyudeniyam (Prospects of routine earthquake prediction from electrotelluric observations). In: *Sb. Predvestniki Zemletryasenii*. VINITI, Moscow.
60. Nazarov, A.G. 1965. O mekhanicheskom podobii tverdykh deformiruemykh tel (Mechanical Similarity of Solid Deformable Bodies). Izd-vo AN ArmSSR, Erevan.
61. Sedov, L.I. 1970. Mekhanika sploshnoi sredy (Mechanics of Continuous Medium). Nauka, Moscow.
62. Gzovskii, M.V. 1963. Osnovnye voprosy tektonofizika i tektonik Baidzhansaiskogo antiklinoriya (Fundamentals of Tectonophysics and the Tectonics of the Baidzhansai Anticlinorium). Vol. 2, Izd-vo AN SSSR, Moscow.
63. Shamina, O.G., A.A. Pavlov, S.A. Strizhkov and Yu.F. Kopnichev. Ultrazukovoe prozvuchivanie oblasti podgotovki odinochnoi makrotreshchiny (Ultrasonic sounding of region of preparation of solitary macrocrack). This collection, p. 92.
64. Stakhovskaya, Z.I. and A.V. Kol'tsov. Issledovanie vliyaniya kvaziplasticheskogo techniya na skorost' prodol'nykh voln organicheskom stekle pri dvukhosnom szhatii (Effect of quasiplastic flow on longitudinal wave velocity in organic glass under biaxial compression). This collection, p. 120.
65. Tomashevskaya, I.S. Izmenenie razlichnykh fizicheskikh parametrov v protsesse deformatsii i razrusheniya obraztsov gornykh porod (Change of various physical parameters during straining and fracturing of rock specimens). This collection, p. 134.

UDC 550.314

Ultrasonic Sounding of Region of Preparation of Solitary Macrocrack

O.G. Shamina, A.A. Pavlov, S.A. Strizhkov and Yu.F. Kopnichev

The authors studied the amplitude and velocity pattern of ultrasonic waves propagating through the region of microcracking prior to formation of the main crack in specimens of synthetic materials under pressure. This paper reports characteristic changes of longitudinal and transverse waves before shear and tensile crack formation in brittle and plastic materials. The characteristics observed can be used for predicting the faulting time.

INTRODUCTION

Study of the process preparatory to disruption of the medium directly involves one of the fundamental problems of seismology, namely the physics of the focus and the prediction of the time of earthquake occurrence. Seismologists usually assumed that tectonic earthquakes are a consequence of the rupture of material in the earth's interior under the impact of accumulated elastic stresses. In this context laboratory studies of the mechanism of crack formation as a model of the rupture process in the focus acquired basic significance in the study of earthquake physics.

At the moment we are not equipped with adequate information on the parameters of the medium and the nature of the forces in play to comment on the model of the earthquake focus observing the similarity conditions.

In line with current concepts, acquired from a study of failure mechanics and the voluminous experimental material bearing on the behavior of various geophysical fields before and after strong earthquakes, the process of rupture of the medium at the focus can be broadly conceived as follows: The first stage involves a rise in elastic stresses in the focal region and the appearance of isolated faults at the points of maximum stress concentration. The second stage involves growth of these faults, slowly at the beginning, but rapidly, like an avalanche [1], later when the number and size of the faults increase so much that they begin to interact and merge. Merger of small faults leads to the formation of one or several large faults and to the relief of stresses in the surrounding region [2]. The relief of stress from the minor faults faci-

litates their healing, so that the strain is concentrated in a narrow zone [3]. This results in the growth of a main fault and initiation of the earthquake.

It is clear from the foregoing that in laboratory studies of material failure attention should be focused on the preparation and growth of a lone crack as well as on crack interaction. In this context what is of interest is not the total failure of the specimen but the faults that arise therein in the loading process when the specimen still retains its bearing capacity and so can be considered as large, and free from the effect of inertia of the press.

AIM OF THE STUDY

To study ruptures in a specimen and to interpret observational data confidently it is imperative to know in advance where these ruptures will occur or to "provoke" rupture at a desired point. Combining direct observations of the rupture zone and studies by other methods, in particular geophysical, it should not only be possible to acquire a correct understanding of how the rupture develops, what role the stressed state of the medium takes, and what the properties of the medium and the nature of the macro- and microfractures are. It should also be possible to create in reality the physical basis for interpreting field observations and developing methods of earthquake prediction.

Experimental studies in the failure of materials are conducted widely within the framework of the applied problems of failure mechanics. Two directions are dominant, namely study of the growth of a solitary crack and determination of the strength characteristics of the material. We will leave the second direction aside because it involves in the main total destruction of the specimen and determination of the nature of the destructive load. We are concerned with the growth of individual crack. Much success has been achieved in this area with reference to failure mechanics. The latest techniques are used, e.g. high-speed filming of the surface of opaque or transparent specimens using photoelastic techniques, fractography, implanting electric lines in the surface of the specimen to determine the speed of cracks, modulation of the fractured surface by ultrasonic shear waves, etc.

The maximum speed of crack propagation V_{cr}, which is generally lower than or equal to the velocity of Rayleigh waves, has been determined for many materials. It has been shown that V_{cr} is a function of the stressed state and may rise or fall with crack propagation. The shape and size of the plastic zone has been determined. The interrelation of critical crack length and load has been ascertained. Certain concrete systems of interacting cracks have been analyzed. An excellent review of the contemporary studies of the failure mechanism is to be found in the book by V.M. Finkel' [4].

Despite the great success achieved in the field of failure mechanics seismologists need more detailed information on rupture. Information is needed

on the physical nature of rupture in materials with different properties of rock masses than to those of metals and polymers on which crack growth is commonly studied in mechanics. Also needed is information on the appearance and growth of fracture under compression and in a complex stressed state. In order to solve the applied problems of mechanics various attempts have been made to study the growth of cracks under uniaxial tension. It is necessary to study the radiation of elastic waves by rupture.

This article is based on experimental study of rupture preparation. Therefore we will refrain here from dealing with the emanation of elastic energy through growing rupture and the techniques of failure study based on recording the elastic impulses arising during crack formation. Let us note, however, that there is an extensive literature on the latter question [5–7] and that the emanation of elastic waves by cracks is described in [8–9].

Little has been done so far in the domain of experimental study of rupture preparation from the premises of focus physics. Essentially this study has been conducted for rock specimens by I.S. Tomashevskaya (this collection) and the American seismologists Brace [10], Byerlee [11] and Scholz [7]. These studies are reviewed by G.A. Sobolev and O.G. Shamina in an article in this collection. Photoelastic studies of the circumstances of fracture formation are reviewed in the same article.

METHOD OF STUDYING PREPARATION OF A SOLITARY CRACK

We conducted experimental studies in the preparation of a solitary crack (main fault) with specimens of synthetic materials subjected to uniaxial compression. The preparation zone was transmitted by ultrasonic waves, since in seismology the focal zones are transmitted by elastic waves generated by weak earthquakes or ruptures [12, 13]. The results were compared with the stress pattern right at the theoretically computed site of the future rupture and also obtained by the shading and photoelastic methods in transparent specimens.

The seismologic transmission technique is based on the well-known fact that the passage of elastic waves through a medium depends on the stressed state of the medium. This dependence was used for experimental determination of the stressed state of rocks in specimens and in the massif [14], but the "integral effect" of the passage of elastic waves through the entire volume to be disrupted was studied in all cases. It was shown that in the compressed volume of rock the velocity and amplitude of elastic waves in the direction of compression grow with the pressure initially, but then diminish as the failure point is approached. Theoretical studies showed that the velocity and amplitudes of elastic waves increase due to pore closure and the increased rigidity of the rock skeleton under pressure. The reduction in

elastic wave velocity and amplitude just before failure may be attributed to the appearance of microfractures. It would seem that analogous phenomena should accompany the preparation of a solitary crack.

It is noteworthy that attainment of breaking stress throughout the medium is not imperative for the appearance of fracture in part of the medium. When there is sufficient concentration of stress at the edge of some heterogeneity the continuity of the material is broken and the fracture continues to grow until it reaches a region of stresses too low for it to grow any farther or encounters a strength barrier in its path. When the dimensions of the region of stress concentration are comparable with the length of the propagating waves the nature of the wave pattern is influenced not only by the passage of the waves through the region itself but also by the diffraction in the region as in a heterogeneous inclusion.

We realized the concentration of stresses creating a solitary crack at a predetermined point of the specimen by artificially incorporating in the specimen one or two open slits differing in relative disposition.

Experiments were conducted with prism- or plate-shaped specimens. For $100 \times 100 \times (15–20)$ mm^3 plates the slit was 10–15 mm long and 0.2 mm wide. All slits were oriented at 45° to the direction of pressure.

The stress applied to the specimen, the total strain in the specimen, and the ultrasonic waves propagating through the crack preparation region were recorded automatically during the experiments. The apparatus assembly is described in detail in [15].

The point where a crack may develop on the surface of the specimen was coated with an electric conducting layer to study the microcrack forming process and the time of origin of macrofracture. The variation in the electrical conductivity of the layer upon crack formation was recorded automatically throughout the experiment.

INITIATION OF SOLITARY MACROCRACK BY ONE SLIT

Different types of gashes are widely used in testing specimens for mechanical failure. We proceeded along the well-known lines of introducing a slit in the specimen to concentrate the stresses.

Stresses around the slit in a plane specimen subjected to tensile stress have been described in detail by V.V. Panasyuk [16]. Considering that within the elastic limit a change in the sign of applied stresses yields only a change in the sign of stresses and strains at the point in question, we should be able to use V.V. Panasyuk's data for our purpose. It follows from these data, in particular, that when compressive stress is applied to the specimen tensile stresses develop at the tips of the slit. Under these stresses tensile cracks may grow normal to the slit orientation if the periphery of the crack is free from friction or, if there is friction, is at some angle.

Our theoretical analysis of stress trajectories showed that horizontal shear stresses should develop at the tips of the slit.

It should be noted that all theoretical calculations were made for perfectly elastic infinite plates and an infinitely narrow slit or gash. Experimental studies are needed to clarify how far the solutions obtained are applicable to a finite specimen, a slit of finite thickness, and the occurrence of friction at the boundary of bearing surfaces of the specimen.

Tests were conducted essentially by photoelastic technique [17, 2]. We conducted similar studies by the shading technique [15] (see also [18]). The experimental data are quite consistent with the theoretical pattern of stress distribution.

Hereinafter we will refer repeatedly to the pattern of stresses around the slit. Therefore, for clarity we give (Fig. 1) a diagram of stresses contours at the slit drawn by V.V. Pavlov and N.E. Trushina on the basis of measurements by the polarization technique.

Experimental studies of tensile crack formation due to stress concentration at the tips of the slit in brittle materials are described in [16, 19, 20]. The results obtained corroborate the theoretical conclusion regarding the probability of formation of tensile cracks and the mode of propagation.

Shear cracks might also be expected to appear in plastic materials. Our studies support this presumption [2, 15, 21]. They were conducted with specimens of different materials chosen so that the failure of relatively homogeneous (alabaster and hyposulfite), amorphous and crystalline (sealing wax and plaster of Paris), and relatively plastic (sealing wax and Plexiglas) specimens could be compared.

Photographs of fractured specimens are shown in Fig. 2. The specimens

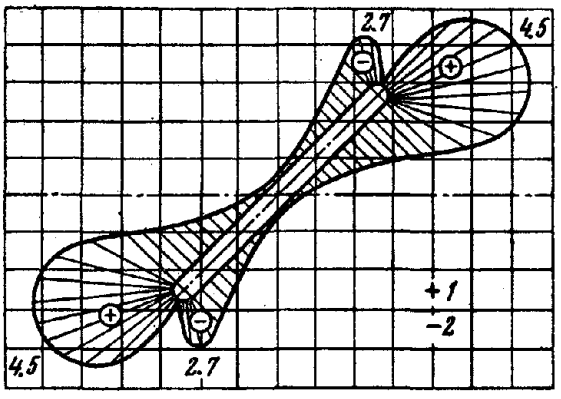

Fig. 1. Diagram of stress contours:
1—Compression; 2—Tension.

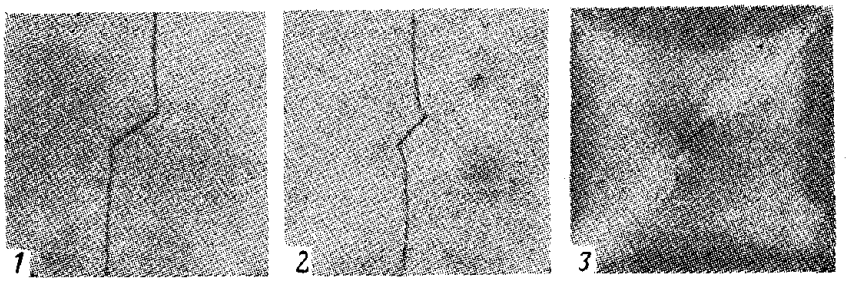

Fig. 2. Photographs of fractured specimens of different materials:
1—Hyposulfite; 2—Alabaster; 3—Paraffin.
Slit is open in (2) and (3); sides of slit are rigidly linked in (1).

were specially stressed to total failure to prove that the crack was the only macrocrack responsible for the failure of the specimen.

Stable shear cracks developed only in paraffin specimens. They were also observed in plaster of Paris and alabaster when the specimen was cubic and not a plate, but they were unstable.

Shear cracks appeared in paraffin specimens whether they were cubes or plates. The crack would begin to spread from the end of the slit horizontally but would soon curve and then develop diagonally. Such crack behavior is quite understandable, since the stress concentration brought about by the slit decreases very fast with distance, and subsequently "global" stresses begin to operate in the specimen. As is known, the maximum tangential stresses in a specimen subjected to uniaxial compression are oriented at 45° to the direction of compression.

Tensile cracks were observed in all the specimens tested. Depending on whether the slit was open or closed the cracks began to propagate normal to the slit or at 70°. Sometimes this was accompanied by the appearance of horizontal shears, but this was unpredictable.

A concentrator of a different type was needed to observe the appearance of stable shear cracks in brittle specimens. According to the conclusions in [19] based on experimental studies, a stable shear crack cannot be created in brittle materials by only one defect; it is necessary to introduce an "echelon" of embryonic cracks. To clarify the nature of this echelon in real materials we studied the interaction of two slits oriented differently.

INITIATION OF SOLITARY MACROCRACK BY INTERACTION OF TWO SLITS

Theoretical solution of the problem of crack interaction involves analysis of equilibrium of a medium containing a few or many definitely disposed

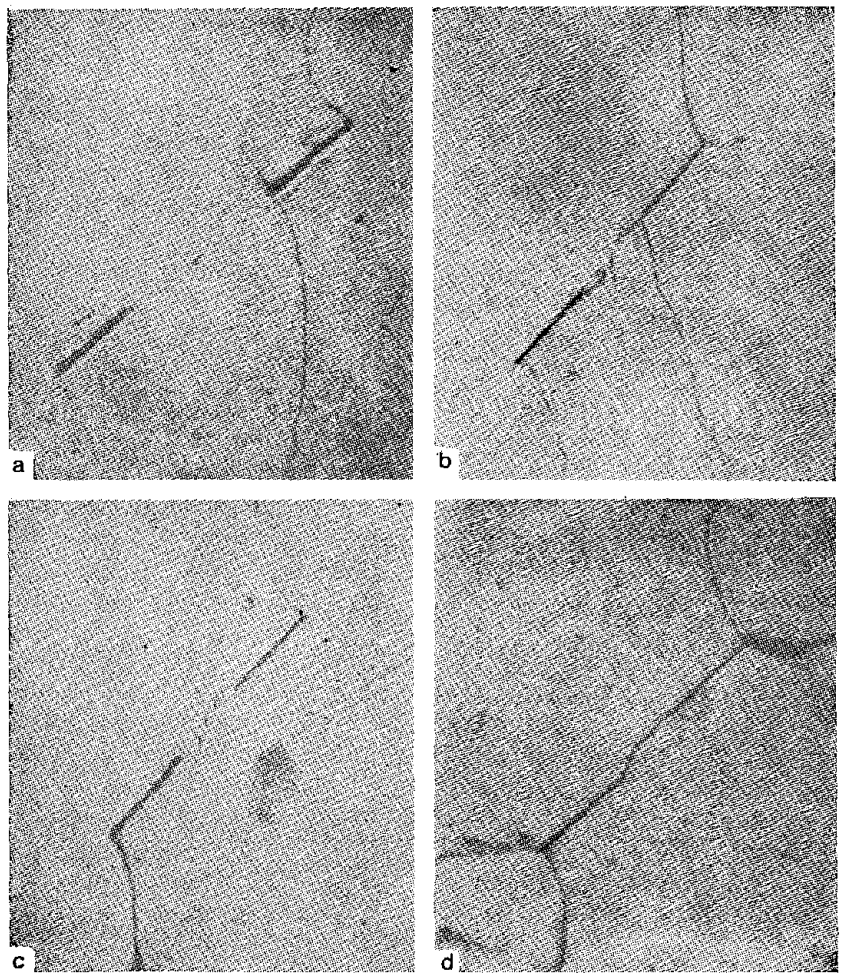

Fig. 4. Photographs of fractured alabaster specimen bearing diagonal slits:
a—$a/l = 2$; b, c, d—$a/l = 1$.

centration at the apexes of cracks of different crack arrays. It was shown that the concentration coefficient may be the same as in the case of a single slit or surpass it several times, depending on the mutual disposition of cracks.

Horizontal shear stresses build up at the ends of slits lying at the same level when the slits are placed as in *d* and *g*. Consequently steadier growth of horizontal shear cracks is to be expected than is observed in experiments with one slit. Photographs of fractured specimens are shown in Fig. 6.

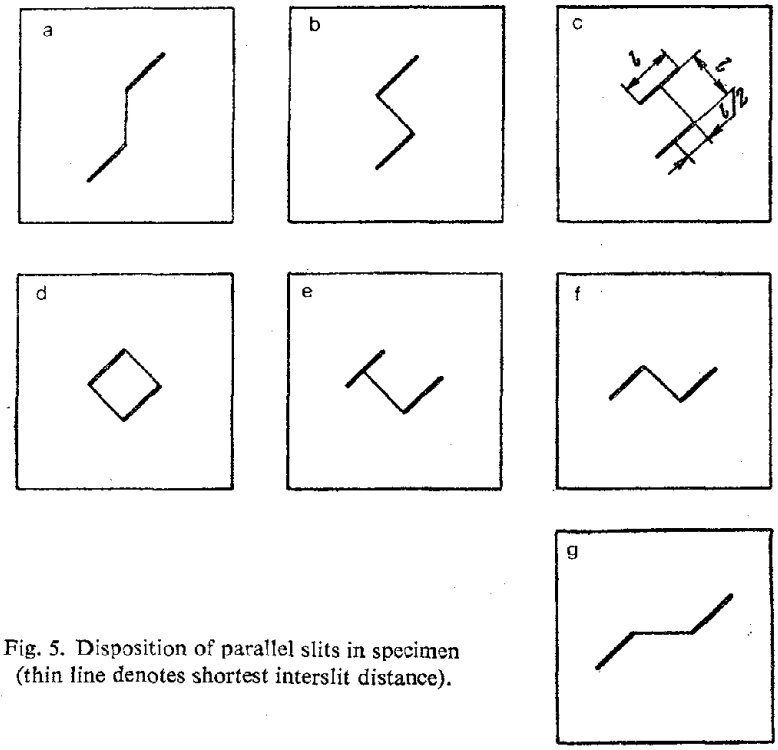

Fig. 5. Disposition of parallel slits in specimen (thin line denotes shortest interslit distance).

Experiments showed that *a*, *b*, *c*, and *e* type slit arrays help to generate tensile cracks in the region of interaction. The *d* array, as expected, also facilitates tensile crack formation, but it also gives rise to two shear cracks propagating from the ends of the slit to the lateral edges of the specimen.

The *g* array initiates shear cracks. The *f* array does not cause fracture in the region of interaction, being a kind of boundary between the arrays producing steady tensile cracks and the arrays yielding shear crack.

It should be added that, as in the case of a solitary slit, the tensile cracks propagated in all cases from the outer ends of the slits. The variation in the electrical conductivity of the coating at the inner and outer ends of the slits suggests that the preparation of the "interacting cracks" began earlier than that of the outer tensile cracks, so that the latter did not affect the stressed state in the region of interaction during the preparation.

ULTRASONIC MEASUREMENTS

Ultrasonic waves passing through the region of the fracture crack were

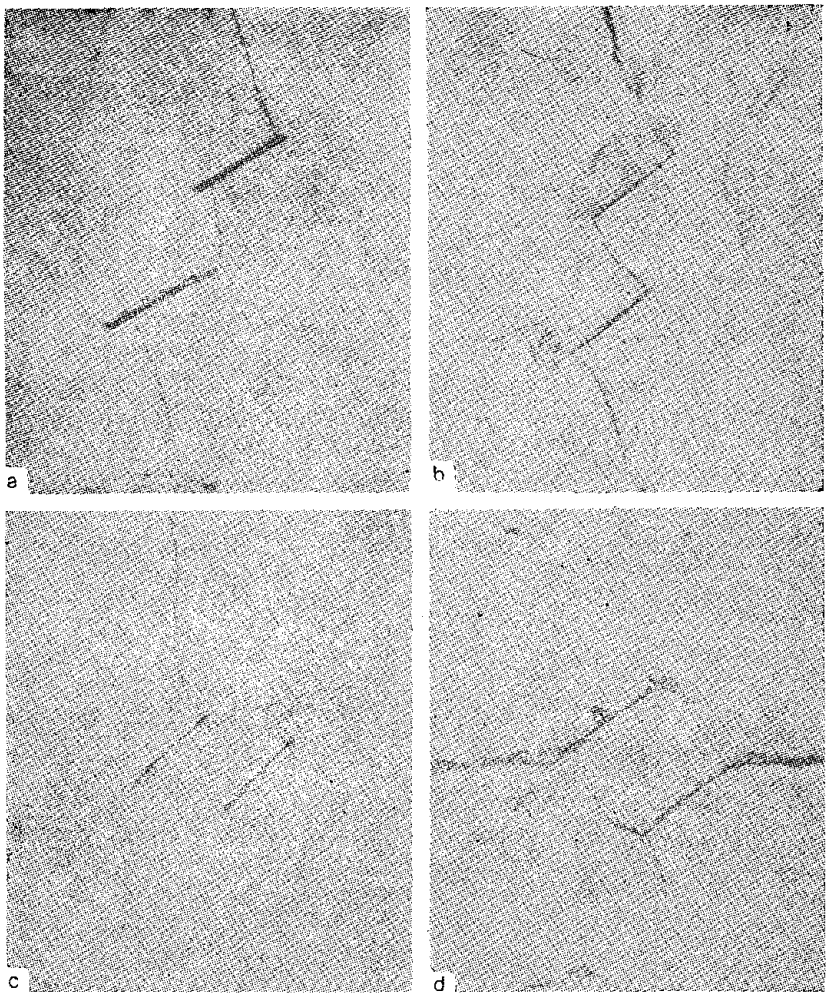

recorded continuously throughout loading of the specimen. For this purpose a special movie camera was used to film the signal from an oscilloscope screen at a speed of one frame a second.

The amplitude and arrival time of longitudinal P and transverse S waves generated by appropriately polarizing piezoceramic transducers were studied. So that the P and S waves should be recorded simultaneously without the interference of surface waves, the transducers were placed on opposite edges of the specimen. The tests were conducted in the 300–400 kHz range. The arrival time of the first or second crest of the P and S waves was measured

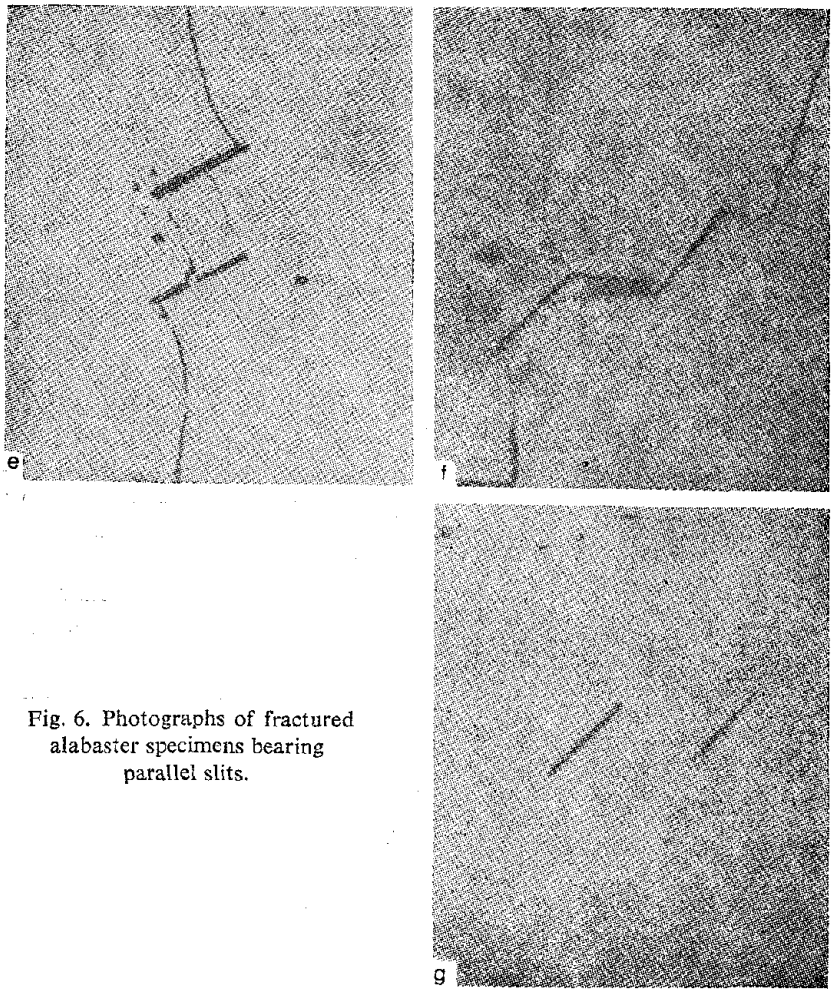

Fig. 6. Photographs of fractured alabaster specimens bearing parallel slits.

from seismograms because the accuracy of phase time measurements is far greater than the accuracy of measurements of the first arrival time. The maximum error in time recording is 0.1 μ sec and P and S wave arrival times of 14–26 μ sec and 22–43 μ sec respectively.

The fluctuation in amplitudes was measured between the first and second peaks. For proper contact between the transducers and the specimen the former were fastened to the surface of the specimen with spring clips. The error in amplitude measurement was actually determined from the thickness of the line of seismogram, so that it was dependent on the amplitude. The relative error in amplitude measurement during the experiment ranged from 1 to 10%.

The seismogram (Fig. 7) obtained for a specimen where diagonal shear crack was initiated gives an idea of the wave pattern observed in our experiments.

To ascertain the influence of the variation in the properties of the specimen under pressure on wave propagation in the specimen, measurements were made first in a flawless specimen (without slits) with the transducers arranged similarly. In certain cases the waves passing through and bypassing the region of crack preparation were recorded simultaneously.

The data on the macrocrack preparation region (initiated in our experiments in a variety of materials using a single slit) made clear by P waves is elaborated in [2, 15, 21]. Characteristic changes in P wave amplitude, e.g. a steep drop (40–50%) before formation of the main tensile crack in the specimen, were observed for all brittle materials studied. A slight (1–3%) increase in travel time was also noticed. Highly homogeneous material, such as hyposulfite subjected to evacuation when fused, is an exception.

Premonitory symptoms of tensile crack formation were not noticeable in plastic materials like paraffin or sealing wax. Possibly, owing to the lower viscosity of the material the microcracks supposed to be formed during macrocrack preparation were immediately "filled" again.

The shear crack in paraffin was preceded by a steep but fairly monotonic drop ($\sim$ 50%) in P wave amplitude and a sharp ($\sim$ 10%) rise in the arrival time of the P wave before the initiation of rupture.

The experiments described below were conducted on alabaster specimens

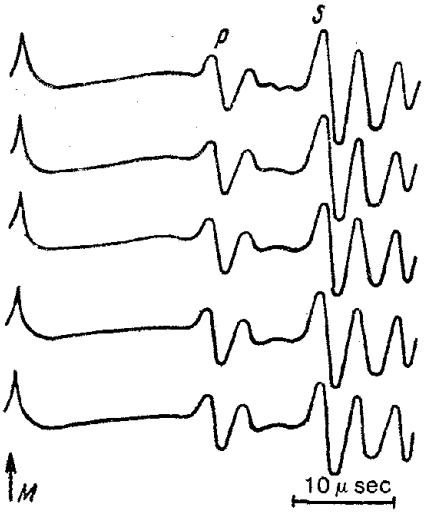

Fig. 7. Seismogram obtained during diagonal shear crack formation (M is instant of emanation).

in which the process of tensile and shear crack preparation initiated by pre-existing flaw systems were studied. The influence of the variation in the properties of the material under pressure on the characteristics of elastic waves was studied in experiments with flawless specimens. The specimens were brought to complete failure, which was noted in the creep curve or in the fall of the stress-strain curve. When the microcrack-forming process begins is difficult to say, because in a flawless quasihomogeneous specimen it initially has a random nature. According to A.Ya. Dubovik's data, the microcrack formation in concretes is noticeable at 30% of the failure load (50% of the load at which visible cracks appear) [25].

Tensile crack. The characteristic variations in the amplitude and travel time of longitudinal waves during the preparation of a tensile crack initiated by a solitary slit and by slit arrays under continuous loading are shown in Fig. 8. Experiments were chosen in which the stress-strain relationship broadly obeys the same law.

The thin arrow in the figure denotes the instant of time at which the electrical conductivity of the coasting begins to change in small jumps, i.e. at which the microcrack-forming process begins at the coated point on the end of the slit. The short, bold arrows correspond to the beginning of continuous intensive change in conductivity, the larger ones to completion of this change, indicating total rupture of the coating. This instant we take as the point of completion of macrocrack-formation.

We find that depending on the method of inducing them, the appearance of tensile cracks is preceded by a steep (over 50%) fall in the amplitude and a sharp (6% on the average) rise in the arrival time of P waves. Let us note that the variation of time is about 1%, and of amplitude of P waves, of the order of 20%, when a flawless specimen fails.

It is striking that rupture of the conducting coating upon formation of the tensile crack in the region of interaction of two slits takes place when the amplitude of the longitudinal wave A_P drops almost to zero. A_P is quite high (50% of the initial value) at the instant of rupture of the coating resulting from tensile crack formation initiated by a solitary slit. Apparently tensile macrocrack formation is more difficult in the case of interaction of two slits than with just one slit. Probably this event is preceded by a more severe disruption of the medium than is demanded for a tensile crack initiated by stress concentration at the end of one slit.

Experiments with specimens of synthetic materials and rocks show that the premonitory symptoms of failure [2, 21] last longer if the load applied is slower. Analogous results were obtained in the experiments here described. With slower loading of the specimen the process of crack preparation is prolonged and the rupture under greater load occurs later. The arrival time of elastic waves before actual rupture also increases at a slower rate.

It is worth nothing that the variation in the loading rate at the initial

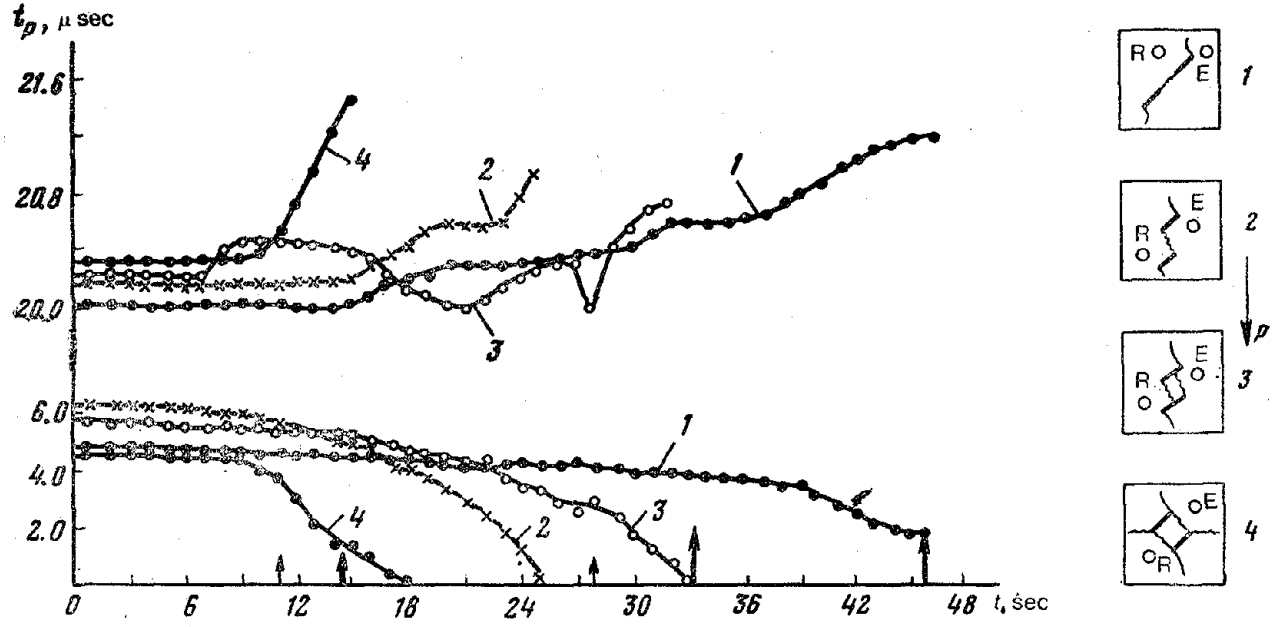

Fig. 8. Results of P wave transmission through variously initiated (1-4) tensile crack preparation regions: E—Emanating source; R—Receiver.

stage (within the small range employed in our experiments) affects only the instant of solitary crack formation. General failure of the specimens, however, occurred almost at the same load and same deformation of the specimens.

If the specimen was not brought to the condition of total failure the cracks closed and could not be traced visually after the load was withdrawn. Experiments involving cyclic loading of specimens with a single crevice [2, 21] showed that at the beginning of microcrack formation A_P and t_P partially regained their initial value after unloading, i.e. the microcracks partially healed. The macrocrack forming process can be checked if it does not reach the avalanche stage. A characteristic feature of the avalanche stage is that A_P falls continuously and t_P rises even after withdrawal of the load.

Apparently, under continuous loading the rapid uninterrupted change in the electrical conductivity of the coating also corresponds to this avalanche-like microcrack-forming stage. Total rupture of the coating showed that the avalanchelike process culminated in macrocrack formation.

To determine the approximate space in which the microcrack formation progressed, several specimens were sounded vertically. Changes in the amplitude of the first arrival (of waves) in the neighborhood of the crevice as compared to those observed in the unfractured part of the specimen allowed us to delineate the region of microcrack formation. It was found that in the plane of the plate it is about 1.5 cm from each side of a crack about 3 cm long.

Expressed in ultrasonic wavelengths, the total width of the microcrack-forming region is (3–4) λ.

Studies have shown that during tensile crack preparation the transverse waves behave like longitudinal waves. Fig. 9 gives the measurements of the amplitude A_S and arrival time t_S of transverse waves when tensile cracks appear in the region of interaction of two slits and when the cracks are initiated by a solitary slit. The load was applied at the same rate in the two experiments. The specimen failed in 48 sec in the first experiment and in 61 sec in the second.

A sharp decrease in A_S and increase in t_S before rupture are observed in both experiments (t_S increases by about 4% on the average, and A_S diminishes by more than 60%). Further, t_S, like t_P, does not increase monotonously; before the actual rupture t_S increases at a slower rate and in certain cases even begins to fall. Likewise A_S does not always fall continuously, and in several cases local maxima are noticeable. These resemble those seen in the graph (Fig. 10), which gives the experimental data on simultaneous recording of P and S waves passing through the preparatory region of a tensile crack triggered by an isolated slit.

As is evident from Fig. 10, t_S and t_P cease to increase as A_P and A_S fall by 18 sec. t_P and t_S are found to diminish for some time and then rise again

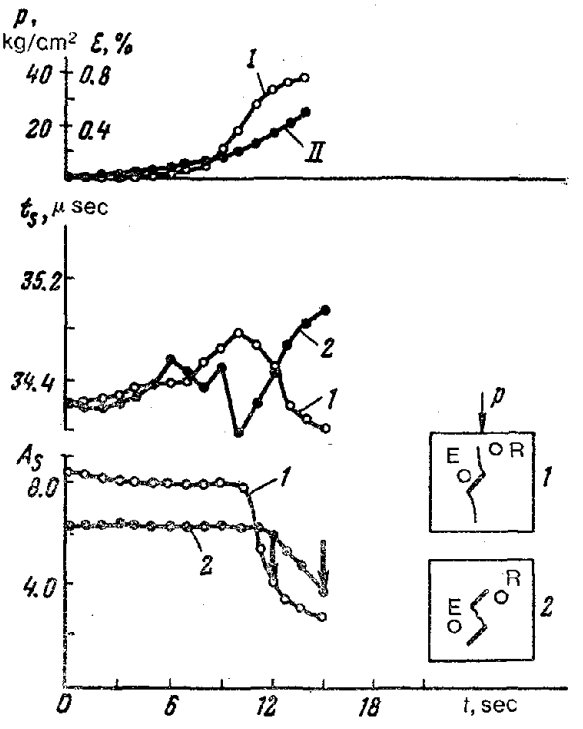

Fig. 9. Results of S wave transmission through region of preparation of tensile cracks triggered by various means (1 and 2):
Numbers (Figs. 9-12, 14) show variation of stress and strain with time.
I—ϵ; II—p.

until the next fall of amplitude by 28 sec. As in the previous event, a few seconds after A_P and A_S fall t_P and t_S are found to diminish. The next increment of t_P and t_S exceeds the preceding one and is linked with the rupture leading to general failure.

This behavior of the arrival time of elastic waves in the process of rupture preparation can be interpreted as follows: As is known, rupture occurs due to relaxation of contiguous regions of the medium and, consequently, withdrawal of stresses from finer cracks. This causes the minor cracks to heal partially or completely. The medium becomes more monolithic and the elastic wave velocity, which diminished with increasing microcracks, increases again. The experimentally established slower decrease of t_P and t_S as compared to the fall of A_P and A_S caused by fracture is natural, because time is required for the cracks to heal.

Why the amplitude of elastic waves does not increase with the reduction of travel time is a question yet to be answered. It was expected that the heal-

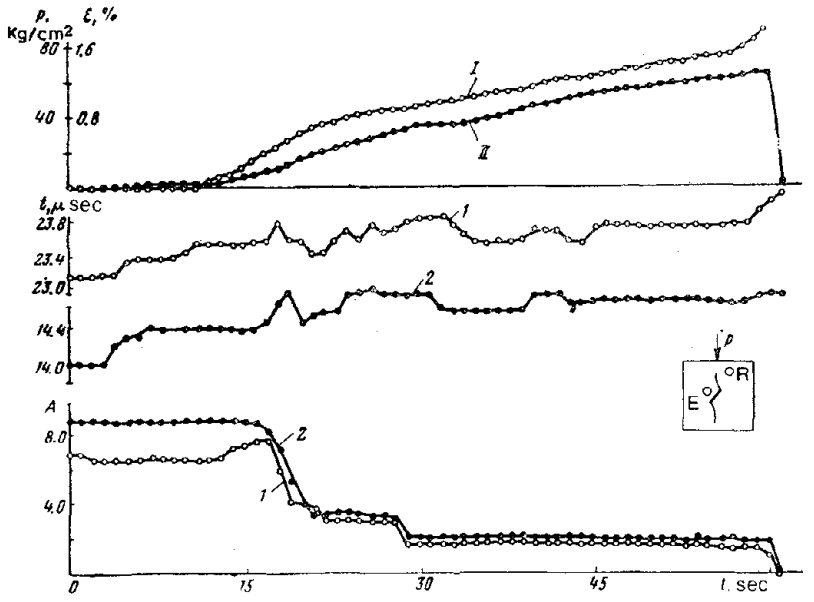

Fig. 10. Results of ultrasonic wave transmission through tensile crack preparation region:
Waves: 1—*S*; 2—*P*.

ing, had it occurred, would reduce loss of elastic energy in the microcracks. But in reality the amplitude merely ceases to fall, without showing any marked increase.

Probably, in "healing" the crack sides come closer together, but the locking between them is not restored, so that, as before, the cracks play the part of minor inclusion in which the energy of the elastic waves is dissipated.

Shear crack. Our studies of shear crack preparation in paraffin specimens are described in detail in [2] and [21]. Collation of the data on translucence and direct observations at the site of shear crack formation suggested that the change in the amplitude and arrival time of *P* and *S* waves in the process of rupture preparation is induced by shear and tensile microcrack formation and plastic flow. This region, indicated by clouding of the paraffin, is wider, the slower the increase in load. In the event of very rapid loading it is almost drawn toward the crack itself, and then the shear and tensile cracks become clearly visible (Fig. 2, specimen 3). The period during which a sharp increase in arrival time and then a steep fall in amplitude are observed is also reduced with rapid loading. Measurements of A_P and t_P during cyclic loading showed that, as in the case of rupture, healing of microcracks occurs during unloading. The failure process can be arrested provided it does not reach the avalanche stage.

In alabaster specimens both diagonal and horizontal shear cracks consisted of elements of shear and tensile ruptures which could be visually discerned. This characteristic of shear macrocracks seems to be common to both plastic and brittle materials, including rocks, which exhibited analogous phenomena in F. Rummel's experiments (oral communication).

Divergence might be expected in the behavior of P and S waves during macrocrack preparation because the relative number of shear and tensile cracks might vary from specimen to specimen. However, experiments with paraffin specimens in which steady changes of A_P and t_P were noticed before rupture suggested the existence of analogous premonitory symptoms for S waves too.

Let us take the diagonal shear crack. In experiments with specimens where a diagonal shear crack was produced the amplitudes of P and S waves began to fall slowly long before fracture, as in experiments with paraffin. Most probably this is due to changes in the properties, i.e. due to random microfracturing of the specimen material under pressure.

The decay of amplitude was hastened with the initiation of microfracturing in the preparation region, as evidenced by a change in the electrical conductivity of the coating. It was again retarded before actual rupture. Local maxima are noticeable in the A_S curves in Fig. 11.

The range of amplitude variation from the instant of loading to the instant of macrofracture was 20–60% for A_P and 30–60% for A_S. Variation of A_S was generally more marked than that of A_P, but individually the amplitudes were not characterized by steady variations of the type seen in Fig. 11 and premonitory of rupture initiation.

The arrival time of P and S waves began to increase markedly during microfracturing. As in tensile microcrack preparation, the decay of amplitude was accompanied by reduction of t_P and t_S. As the moment approached, t_P and t_S registered sudden increases and then fell, indicating rupture initiation. On an average t_P rose by 3–4% and t_S by 4%.

Steady variations in wave amplitude were not observed if there was shear crack formation as well. Rise and fall of A_P were noticeable during the experiment. In certain cases A_P remained almost unaltered.

The amplitude of S waves behaved differently. In all experiments, with rare exceptions, A_S was found to fall (by 20% on an average) before rupture and to rise sharply (by 30%) at the rupture point. Generally, rise of A_S coincided with the period of pronounced change in the electrical conductivity of the coating due, we believe, to the avalanche stage of microfracture. In experiments lasting about 1 min the time before fracture during which fall of A_S occurred was 6–8 sec on the average.

The P and S wave arrival times increased just before rupture and this was generally preceded by a marked reduction in t_P and t_S. Time variation was generally 3–4%.

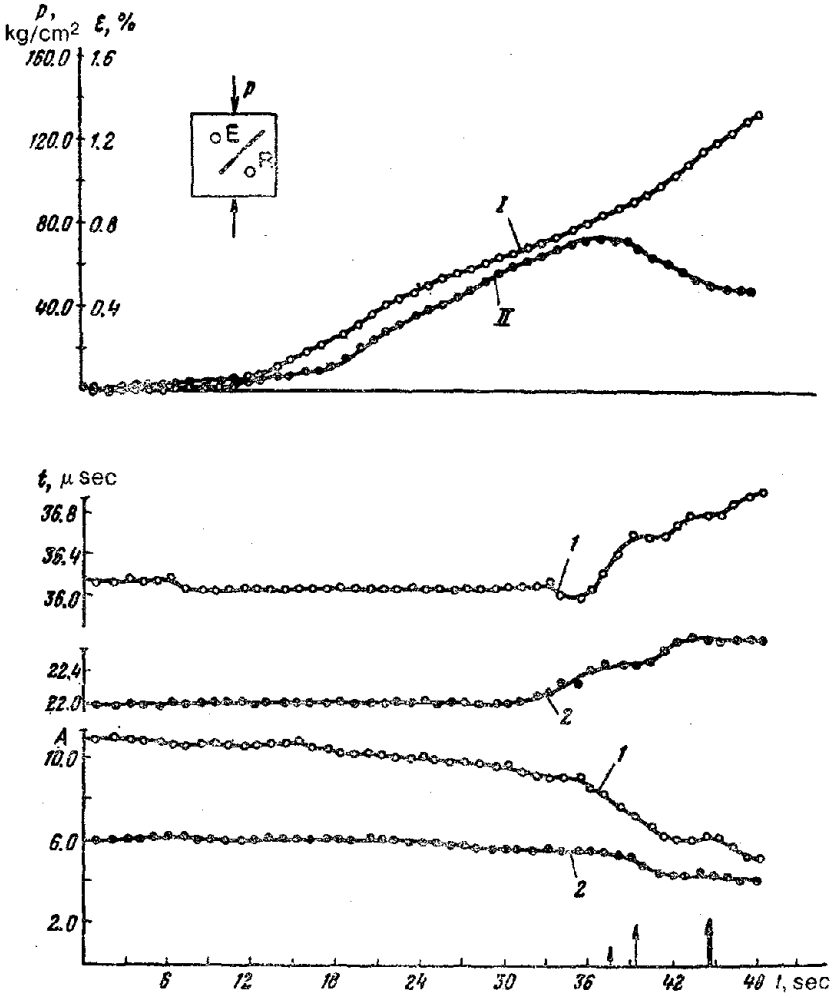

Fig. 11. Results of ultrasonic wave transmission through region of diagonal shear crack preparation:
Waves: 1—*S*; 2—*P*.

Typical experimental results for horizontal shear cracks are given in Fig. 12.

Collation of experimental data on diagonal and horizontal shear cracks shows that the *P* and *S* wave arrival times can be utilized to predict the fracture time. The amplitude of *S* waves submits to characteristic changes only in horizontal shear cracking. The amplitude of *P* waves does not show changes that could be used for prediction purposes.

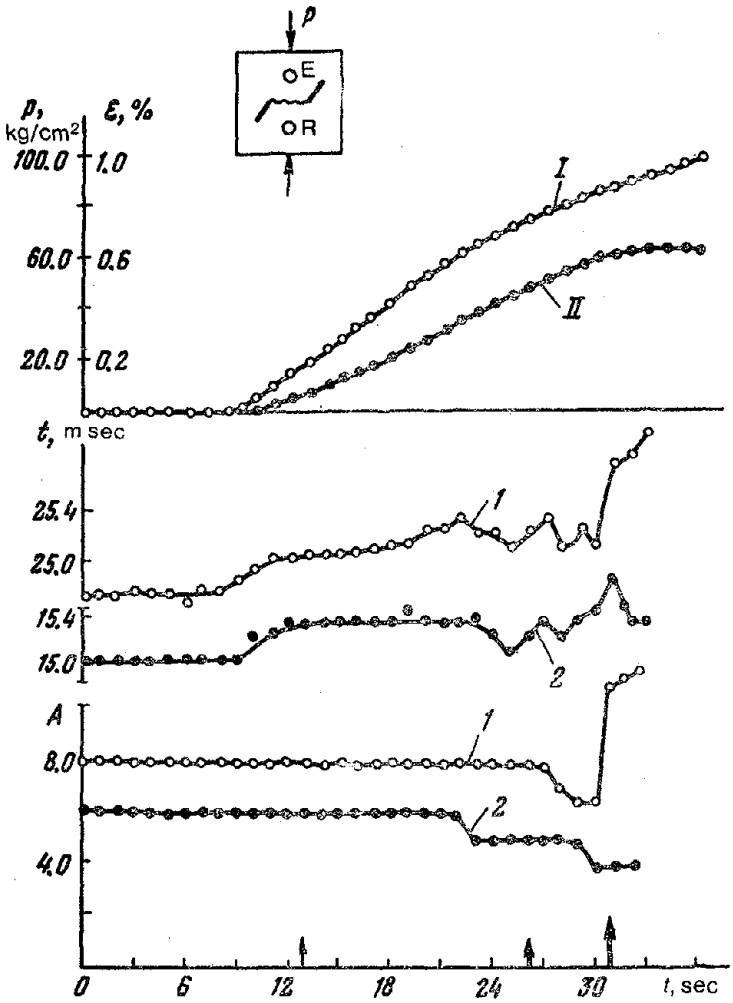

Fig. 12. Results of ultrasonic wave transmission through region of horizontal shear crack preparation:

Waves: 1—*S*; 2—*P*.

This conclusion differs from that prompted by the study of shear macrocrack preparation in paraffin specimens. However, as indicated above, shear cracking in paraffin specimens was preceded by pronounced plastic deformation and disintegration, which together profoundly changed the properties of the material. In the brittle alabaster specimen, on the other hand, plastic deformation did not occur in the process of shear crack preparation and only minor shear and tensile cracks were formed.

Besides mechanical contact, forces of molecular locking continue to operate between the sides of a shear crack, so that the normal displacement vector does not show a sharp jump between the sides. This seems to be the reason why P waves do not reveal such cracks. Propagating through a tensile crack, P waves invariably lose part of their energy because in tensile fracture the sides of the crack are free from locking forces. As a result the normal displacement between them should abruptly increase.

Thus, depending on the role taken by tensile cracks in the process of macroscopic shear fracture preparation, the amplitude of P waves may decay or remain almost unaltered and even increase due to consolidation of the specimen material.

The results of concurrent observation of P waves passing through the region of tensile (omitting shear elements) and the region of shear (including both shear and tensile elements) macrocrack preparation are presented in Fig. 13. The measurements are schematically shown in the figure.

As regards the S wave, both tensile and shear cracks are boundaries at which the tangential displacement component in the wave becomes discontinuous. Therefore, when microfracture begins prior to the shear macrocrack, A_S should diminish independently of the type of microcracks formed. In

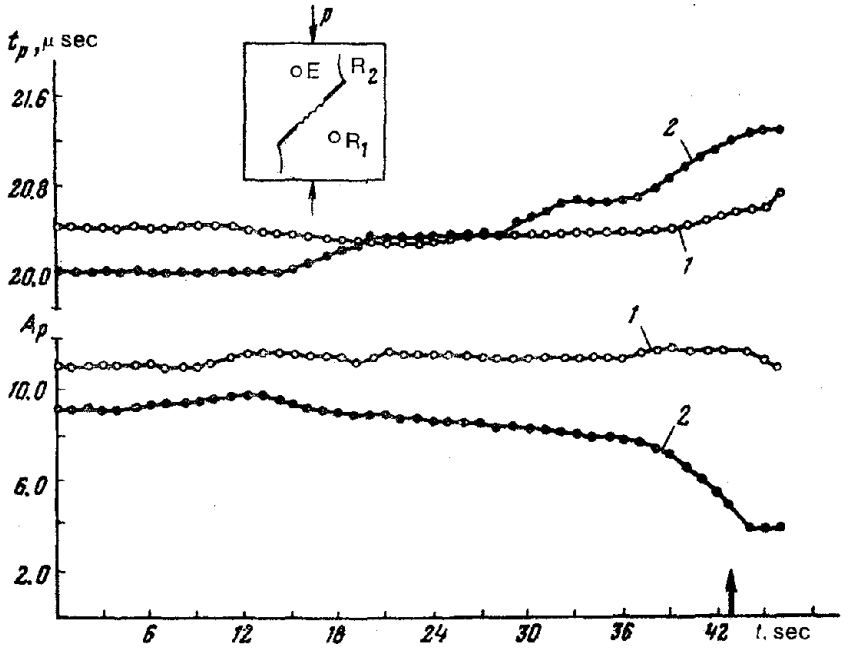

Fig. 13. Results of concurrent passage of P waves through shear (1) and tensile (2) crack preparation region.

physical interpretation of V_P/V_S variations is ambiguous. One of the most probable reasons is crack formation [1]. It was therefore fascinating to collate the regularities that we had observed in the variations of elastic wave characteristics caused by crack formation before macrofaulting with field measurements.

The graphs constructed for the t_S/t_P and A_P/A_S ratios are given in Fig. 15. The graph of V_P/V_S change before a strong earthquake based on [27] is given at the top for reference.

The t_S/t_P and A_P/A_S graphs are similar for tensile and "free" shear crack preparation. A general fall in the t_S/t_P and a rise in the A_P/A_S ratio is noticeable. But these graphs differ from the t_S/t_P and A_P/A_S graphs for shear crack formation inside the specimen.

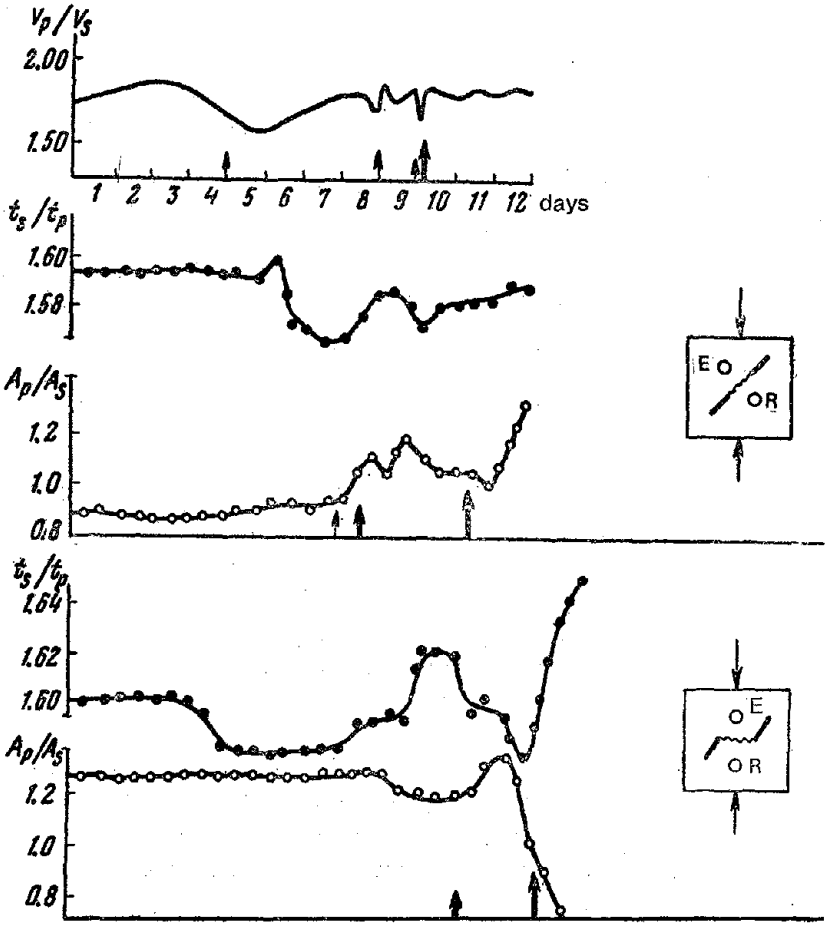

The t_S/t_P and A_P/A_S curves for "internal" shear crack have minima and maxima. The minimum on the t_S/t_P curve and the maximum on the A_P/A_S curve precede diagonal fracturing. The fracturing event arrives at a higher t_S/t_P and a lower A_P/A_S ratio. The whole period of t_S/t_P and A_P/A_S variation through minimum, maximum, minimum precedes horizontal shear cracking. The fracture occurs in the third phase.

Collation of the results obtained with the field observations made leads us to suggest that of all the microcracks investigated the preparation of internal shear cracks induces changes of t_S/t_P that are most akin to those observed before earthquake initiation.

The observed characteristics of elastic waves passing through the region of tensile and shear macrocrack preparation coupled with the observations

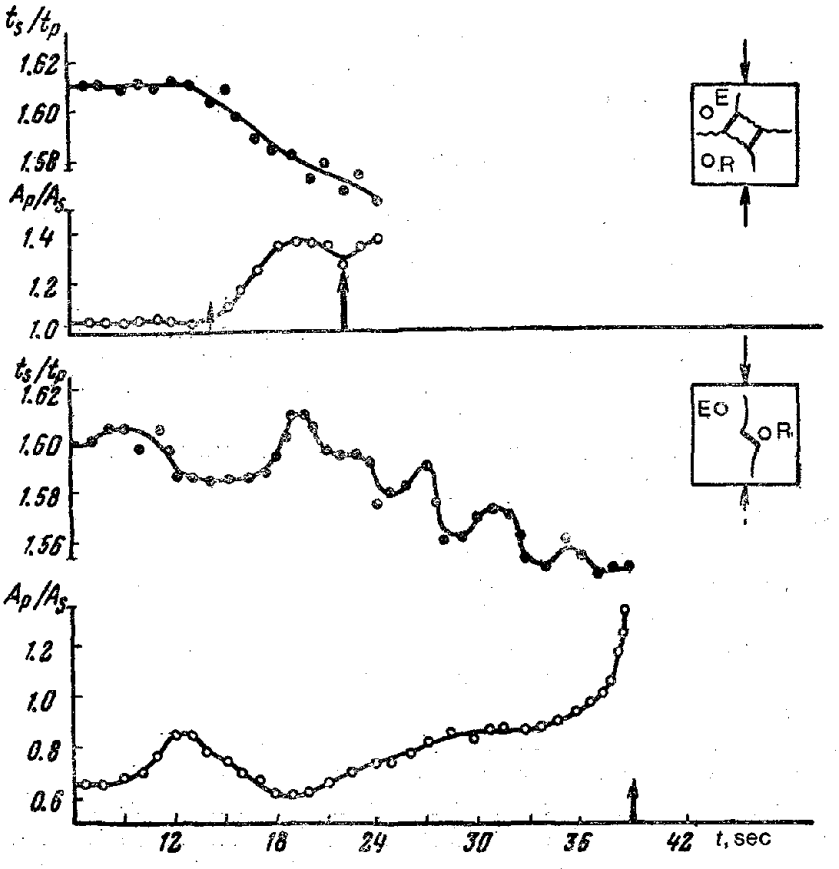

Fig. 15. Variation in t_S/t_P and A_P/A_S ratios before fracturing and variation in V_P/V_S before strong earthquakes [27].

in the region itself give an idea of the regularities of the microcrack-forming process preceding macrofracture which does not contradict the general physical concepts developed in this monograph.

The similar pattern of longitudinal and transverse wave velocity ratios obtained in laboratory and field studies suggests that seismic earthquake forerunners can be explained by crack formation.

REFERENCES

1. Myachkin, V.I. et al. 1972. The study of variations in geophysical fields near focal zones of Kamchatka forerunning of strong earthquakes. *Tectonophysics*, **14**, No. 3/4.
2. *Sb. Predvestniki Zemletryasenii* (Collection: Earthquake Forerunners). VINITI, Moscow, 1973.
3. Belousov, V.V. and K.I. Kuznetsov. 1948. K voprosu o fizicheskikh uslovyakh obrazovaniya tektonicheskikh razryvov (Physical circumstances of tectonic faulting). *Izv. AN SSSR, Ser. Geogr. i. Geofiz.*, **13**, No. 6.
4. Finkel', V.M. 1970. Fizika razrusheniya (Fracture Physics). Metallurgiya, Moscow.
5. Vinogradov, S.D. 1964. Akusticheskie nablyudeniya protsessa razrusheniya gornykh porod (Acoustic Observations of Rock Fracture). Nauka, Moscow.
6. Mogi, K. 1968. Source location of elastic shocks in the fracturing process in rocks. *Bull. Earthquake Res. Inst. Univ. Tokyo*, **46**, pt. 5.
7. Scholz, C.H. 1968. Microfractures, aftershocks and seismicity. *Bull. Seismol. Soc. America*, **58**, No. 3.
8. Savage, J.C. and L. Mansinha. 1963. Radiation from a tensile fracture. *J. Geophys. Res.*, **68**, No. 23.
9. Savage, J.C. 1967. Spectra of *S*-wave radiated from bilateral fracture. *Bull. Seismol. Soc. America*, **57**, No. 1.
10. Brace, W.F. and J.D. Byerlee. 1966. Stick-slip as a mechanism for earthquakes. *Science*, **153**, No. 3739, 990.
11. Byerlee, J.D. 1968. Stick-slip, stable sliding and earthquakes—effect of rock type, pressure, strain rate and stiffness. *J. Geophys. Res.*, **73**, No. 18.
12. Kondratenko, A.M. and I.L. Nersesov. 1962. Nekotorye resul'taty izucheniya izmeneniya skorostei prodol'nykh voln i otnosheniya skorostei prodol'nykh i poperechnykh voln v ochagovoi zone (Some results of study of longitudinal wave velocity variation and longitudinal and transverse velocity ratios in the focal zone). *Tr. IFZ AN SSSR*, No. 25 (192), p. 130.

13. Fedotov, S.A. et al. 1970. Investigation of earthquake prediction in Kamchatka. *Tectonophysics*, **9**, No. 2/3, 249.
14. Riznicheko, Yu.V. et al. 1956. Seismoakusticheskie metody izucheniya napryazhennogo sostoyaniya gornykh porod na obraztsakh i v massive (Seismoacoustic methods of stressed state study in rock specimens and massifs). *Tr. Geofiz. In-ta*, No. 34.
15. Shamina, O.G., A.A. Pavlov and Yu.F. Konnichev. 1973. Issledovanie protsessa podgotovki treshchiny (Study of the crack preparation process). *Izv. AN SSSR, Fizika Zemli*, No. 8.
16. Panasyuk, V.V. 1968. Predel'noe ravnovesei khrupkikh tel s treshchinami (Limiting Equilibrium of Fractured Brittle Bodies). Naukova Dumka, Kiev.
17. Siwerin Duda, J. 1965. The stress around a fault according to a photoelastic model experiment. *Geophys. J. Roy. Astron. Soc.*, **9**, No. 4.
18. Vaniek, L., K. Klima, Ya. Kazak and O. Shamina. 1973. Izuchenie shliren-metodom uprugikh voln, prokhodyashchikh cherez oblasti kontsentratsii napryazhenii (Study of elastic waves passing through the region of stress concentration by Schlieren photography). *DAN*, 210, No. 2.
19. Brace, W.F. and E.G. Bombolakis. 1963. A note on brittle crack growth in compression. *J. Geophys. Res.*, **68**, No. 12.
20. Bombolakis, E.G. 1965. Photoelastic investigation of brittle crack growth within a field of uniaxial compression. *Tectonophysics*, **1**, No. 4.
21. Shamina, O.G. and A.A. Pavlov. 1974. Issledovaniya podgotovki treshchin otryva i skola (Study of tensile and shear crack preparation). *Izv. AN SSSR, Fizika Zemli*, No. 2.
22. Yokobori, T. and M. Ichikawa. 1964. Elastic solid with an infinite row of collinear cracks and the fracture criterion. *J. Phys. Soc. Japan*, **19**, 2341.
23. Bombolakis, E.G. 1968. Photoelastic study of initial stages of brittle fracture in compression. *Tectonophysics*, **6**, No. 6.
24. Bombolakis, E.G. 1973. Study of the brittle fracture process under uniaxial compression. *Tectonophysics*, **18**, No. 3/4, 261.
25. Dubovik, A.Ya. 1971. Razrabotka i primenenii akusticheskogo spektral'nogo metoda dlya ispytaniya betonov, ispol'zuemykh v gidrotekhnicheskom stroitel'stve (Development and Application of the Acoustic Spectral Method for Testing Concretes Used in Hydroengineering Construction). Author's abstract of Doctoral thesis, Leningrad.
26. Semenov, A.N. 1969. Izmenenie otnosheniya vremen probega poperechnykh i prodol'nykh voln pered sil'nymi zemletryaseniyami (Variation in the ratio of travel times of transverse and longitudinal waves before strong earthquakes). *Izv. AN SSSR, Fizika Zemli*, No. 4.
27. Aggarwal, J.P. et al. 1973. Premonitory seismic velocity changes correlate with earthquakes. *Nature*, **241**, No. 5385.

UDC 539.37

Effect of Quasiplastic Flow on Longitudinal Wave Velocity in Organic Glass under Biaxial Compression

Z.I. Stakhovskaya and A.V. Kol'tsov

The paper discusses the variation in elastic wave velocities in specimens strained until failure under biaxial compression. Internal fracture of specimens and stable areas of diminishing longitudinal wave velocities were noticed before failure of the sample.

In the process of crustal straining rocks occur in a complex stressed state. Zones are created where stresses mount until rupture and the appearance of quasiplastic zones. However, the variation in stresses and dislocations occurring inside the earth's crust is impossible to observe under natural conditions.

This paper describes laboratory attempts to create a complex stressed state in which fracture can occur only at fixed sites. In the usual types of experiment the stress field is uniform throughout the volume of the specimen or changes analogously in many directions, making it impossible to predict the site and direction of the future fracture. Testing of materials under biaxial compression as proposed by Bridgman [1] seemed to suit our purpose best.

Let us briefly discuss the experimental technique. We used a machine consisting of a solid mandrel (*1*) and a piston (*2*) of alloy steel subsequently submitted to thermal treatment (Fig. 1). The mandrel and the piston were provided with holes at the bottom to place ultrasonic sensors (*3*) to measure ultrasonic wave velocities. The specimen (*4*) was tightly fixed in the mandrel. This was necessary for pressure to develop in one of the horizontal directions as well when vertical pressure was applied. Two faces of the specimen were free. With this loading procedure, in the event of friction the faces adjoining the mandrel occur in a complex stressed state, while straining produces two cruciform sliding zones (Fig. 2). These zones appear under a relatively small load.

Organic glass was used as the model material, for it is quite homogeneous, transparent, and highly deformable. The last property was very important for our experiments because in less deformable materials sufficient horizontal

stress did not build up with increased vertical loading of the specimen, i.e. factually the biaxial stressed state was not produced. Crack formation in the experiment was recorded on an S-1-33 oscillograph. Not all cracks were recorded on the oscillograph, however. The transparency of the specimens allowed additional, visual observation of their internal state.

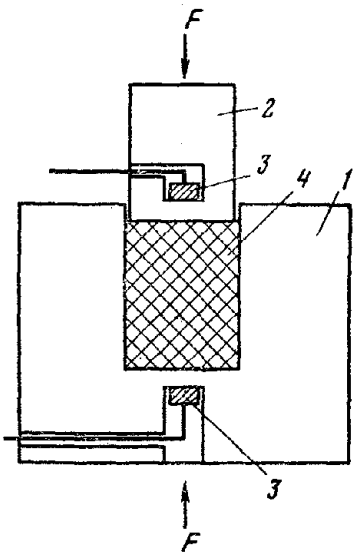

Fig. 1. Sketch diagram of biaxial compression machine.

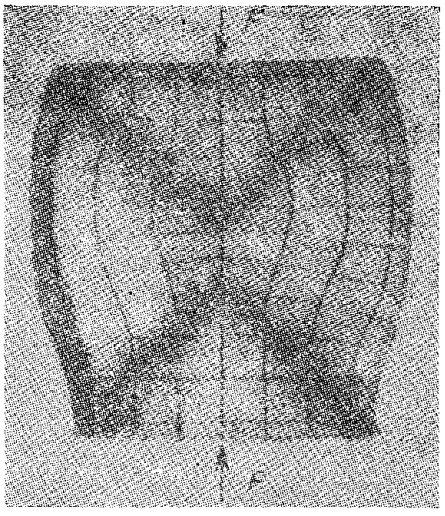

Fig. 2. Photograph of unfractured specimen after testing.

The specimens prepared were 5.4 cm in height and 4.6 cm (size of the mandrel) $\times$ 3.5 cm^2 in cross section.

TsTS-19 ceramic sensors of 1.8 MHz frequency placed in special casings which reduced the frequency a little were used to measure ultrasonic waves and record microcracks.

The strain was measured during the experiment with the help of a strain meter consisting of rings fitted with strain gages [2]. The strain gages were constructed on the principle of a Wheatstone bridge, whose imbalance was recorded during the experiment by a loop oscillograph. The strain meters were initially calibrated with reference to an indicator. The strain was measured to an accuracy of 0.02 mm and the travel times of ultrasonic waves to an accuracy of 0.5%.

The experiments were carried out under slow loading for 1 to 2 hr. This was necessary in order to be able to prolong all the processes occurring in the specimen and to halt the experiment as soon as visible cracks appeared.

Before the experiment the specimen was tightly fitted to the mandrel *1* (Fig. 1) and then a 0.5 $\times$ 0.5 cm^2 grid was painted on the lateral face. The specimen was placed in the mandrel and subjected to vertical pressure. The deformation of the specimen, longitudinal wave velocities, and crack formation were recorded simultaneously. Three sensors like those used for ultrasonic wave measurement were placed in the mandrel at different distances from the specimen to record waves radiating from the cracks. The closest sensor acted as the starter of the apparatus functioning under set conditions, while the other two recorded the arrival of the waves from the cracks formed. The sensors were very sensitive; they responded to the ultrasonic wave radiations and so to the longitudinal wave velocity V_P. The microcracks were recorded by turn.

During the experiment the specimen increased in cross section, the area of the cross section being smaller at the base and near the piston than in the middle. Fig. 2 is a photograph of an unfractured specimen after the experiment. The deformation of the specimen can be seen from the displacement of the cross lines. The sliding cross appearing in the loading experiment is also shown in this figure.

Several correlations noted in the tests are shown in Figs. 3 and 4. Curve 3 (Fig. 3) derives from the differentiation of curve 2. The correlation of ultrasonic wave velocities and load for specimens 15 (curve 1) and 14 (curve 2) is shown in Fig. 4.

As can be seen from the graphs in Fig. 3, the stress F on the specimen at first rose almost uniformly, but at a slower rate starting from 18 t. It should be noted that constant speed of movement of the press plates was maintained during loading of the specimen, but the resistance of the specimen to different stresses varied, producing a flexion on the curve. The deformation of the specimen Δl under such loading increased almost evenly up to

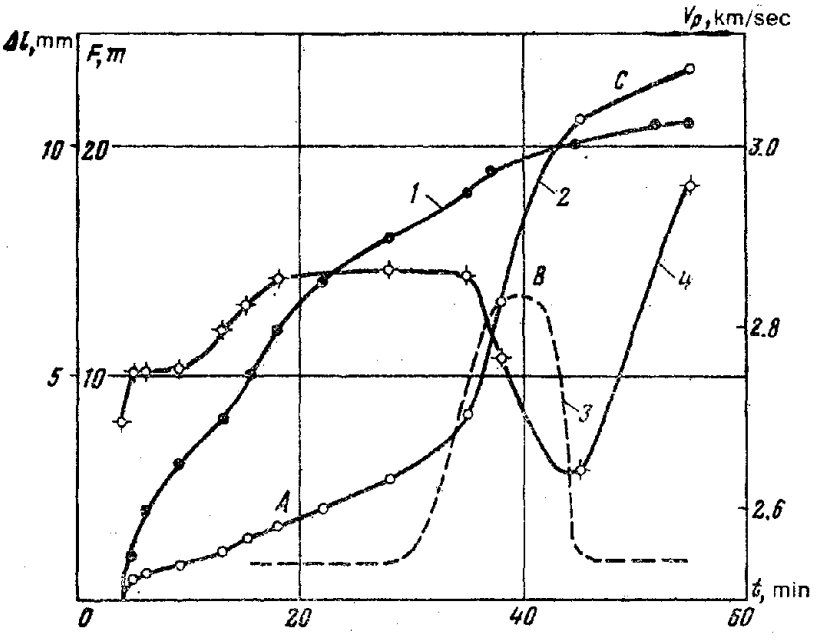

Fig. 3. Applied stress F (1), specimen deformation (2), strain rate (3), and longitudinal wave velocity V_P (4) as functions of duration of experiment for specimen 14.

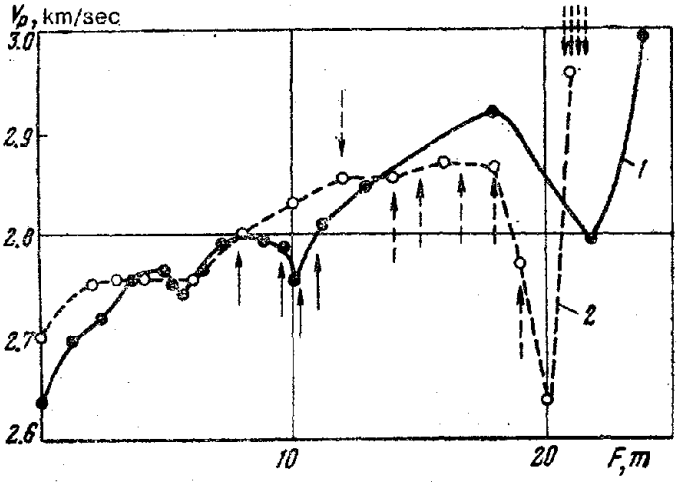

Fig. 4. Longitudinal wave velocity V_P as function of stress for specimens 15 (1) and 14 (2). Arrows show moments of recorded signals from cracks.

a load of 16 t (Fig. 3, segment A of curve 2), steeply (segment B) thereafter, but sluggishly beyond 20 t of the force (segment C). Cracks as shown in Fig. 4, were recorded in the course of the experiment. A swarm of cracks was recorded at a stress of 21 t. The variation in strain rate is well depicted by curve 2 (Fig. 3).

In segment B (Fig. 3, curve 2) the transverse section of the specimen increased rapidly toward the free space. Curve 3 has a maximum in this segment. If the transverse expansion of the specimen is considered inelastic in this segment, the specimen should expand transversely commensurate with its vertical contraction, i.e. by roughly 0.6 cm, resulting in a 17% increase in area. This in turn should reduce the stress operating inside the specimen. The stress drop cannot be assessed from the available graphs because with the increasing load throughout segment B, the specimen deformed differently at different points, and the quasiplastic deformation varied in the volume of the specimen.

As can be seen from Figs. 3 and 4, a steep fall in elastic wave velocities accompanied by crack formation with pronounced quasiplastic flow occurred under loads ranging from 17 to 18 t. The stress mounted slowly in this segment right up to failure. The specimens collapsed suddenly as the loading rate was increased. Under loads of 21–24 t the transverse section of the specimen increased, while the velocity V_P rose to a higher level. Comparison of curves 4 and 3 (Fig. 3) shows that the maximum of curve 3 almost coincides with the minimum of curve 4, i.e. the fall in the velocity V_P seems to be related to the rate of quasiplastic flow in the specimen. The slight noncorrespondence between the maximum and the minimum can perhaps be attributed to the measuring points being too few. This was also true of the lower load ranges 3–6 t and 10–11 t, where the elastic wave velocities were also found to fall. These data do not permit differentiation of the influence of plasticity and jointing on longitudinal wave velocity.

The experiments were interrupted at different stages of loading, as shown in Figs. 2 and 5. For instance, specimen 14 (Fig. 2) was not fractured, specimen 18 (Fig. 5a) was stressed to the initial stage of fracture, and specimen 15 (Fig. 5b) was stressed to complete failure. Fracture occurred at a very high rate, generally along the sliding cross, i.e. along the line of maximum tangential stresses, as is evident from Fig. 5b.

Thus, for organic glass specimens taken as models for the study of local fracture of materials the major findings are as follows:

1. Definite stable segments characterized by reduced elastic wave velocities were found on the elastic wave velocity V_P versus load F curve. These segments correspond to accelerated quasiplastic flow in the specimen.

2. The segments of reduced elastic wave velocities are replaced by higher velocities before failure.

3. Fracture begins inside the specimen.

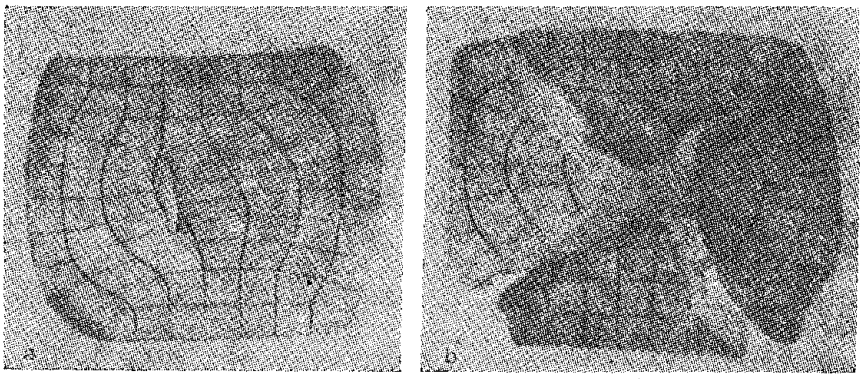

Fig. 5. Fracture stages:
a—Initial (specimen 18); b—Total failure (specimen 15).

4. Fracture of specimens in biaxial compression can perhaps be likened to some extent to the phenomena occurring in the earth's crust during earthquakes.

The writers express their deep gratitude to G.A. Sobolev for his help in conducting the experiments and interpreting the results.

REFERENCES

1. Bridgman, P.V. 1955. Issledovanie bol'shikh plasticheskikh deformatsii i razryva (Study of High Plastic Deformations and of Rupture). IL, Moscow.
2. Stakhovskaya, Z.I. 1960. Primenenie tenzometrov soprotivleniya dlya izmerenii usilii i deformatsii pri vysokikh davleniyakh (Use of resistance tensometers for measuring stresses and strains under high pressures). In: *Probory i Tekhnika Eksperimenta*, No. 1.

UDC 550.34.05.016

Study of Fracture Processes in Specimens under Unilateral Compression

S.D. Vinogradov

This paper provides data obtained on elastic impulses arising from straining and fracturing of specimens over a wide range of strain rates. The intensity of the seismic process is a function of the strain rate. Impulse distribution with time has a common shape before formation of the main fault.

INTRODUCTION

Fracture processes in specimens and elastic impulses arising therefrom are being studied in the USSR, Japan and the USA. Certain common features of seismic energy release in fracture have been investigated [1–11]. It was found, in particular, that the energywise impulse number distribution has a shape akin to earthquake recurrence distribution [1, 2, 4]. This explained how the slope of recurrence graphs changes with changes of parameters. It was found that the slope changes with the approach of fracture, which was confirmed by observations in mines (before mine shock) and by detailed studies of seismic regimes before strong earthquakes [2, 9]. The majority of the experiments were conducted at loads increasing at a constant stress or strain rate. The range of strain rates was rather narrow, being generally limited by the capacity of the press. The number and distribution of impulses with time varied a little with the type of fracture, but in all cases the number of impulses was found to increase before ultimate failure of the specimen.

Some general findings from a long series of experiments on the fracture of specimens of the same material in the wide range of strain rates $10^{-3} - 10^{-9}$ sec^{-1} [3, 12–14] are elucidated in this paper. The experiments were conducted under unilateral compression. An ordinary hydraulic press was used for tests conducted at $10^{-3} - 10^{-6}$ sec^{-1} strain rates, and a spring press was used to attain a strain rate of 10^{-9} sec^{-1} in experiments conducted under constant load. The specimens were prepared from cement and stone chips, mostly small (2–3 mm), but large (25–30 mm) in a few cases. The cement-chip weight ratio was kept at 1:1 in all cases. The specimens were $10 \times 10 \times 10$ cm cubes

or $7\times7\times14$ cm parallelopipeds (in experiments under constant load). A series of six to eight tests was conducted for each strain rate and the results were averaged.

STRAIN RATE

Experiments under constant load [14] achieved slow strain rates comparable with those attained under natural conditions. Analysis of strain records showed that straining of specimens was a process of quasiviscous flow at a constant strain rate. Nonlinearity was noted only at the beginning of the experiment immediately after loading, and the strain rate remained constant almost to the very end. The average magnitude of straining of all specimens fell in the range 0.1–0.5 mm, so that the load remained practically the same. The average strain rate was 1.2×10^{-9} sec^{-1} for specimens containing large chips and 10^{-9} sec^{-1} for specimens containing small chips. As the load was 150–160 kgf/cm^2, it was possible to determine the effective viscosity, which was 10^{17} poise. The relaxation period was found to be 2×10^6 sec.

To compare these rates with the strain rates attained in seismic regions under natural conditions we will use the principal similarity criterion for strain processes, namely the product of strain rate $\dot{\epsilon}$ and relaxation period τ of the material. In our case

$$\dot{\epsilon}\cdot\tau \approx 10^{-9}\cdot 2\cdot 10^6 = 2\cdot 10^{-3}.$$

Data on strain rates in different seismic regions show that they lie roughly in the range $10^{-11}-10^{-13}$ sec^{-1}, i.e. about 2–4 orders less than those found in our experiments. However, considering that the relaxation period of the crustal material is 2–5 orders in excess of what was obtained in our experiments, the order of the product $\dot{\epsilon}\tau$ obtained in our experiments seems to be almost the same as in seismic regions. Thus the straining conditions, at least the strain rates, in our experiments were comparable to those obtaining in natural conditions.

SEISMIC ENERGY RELEASE IN STRAINING AND FRACTURING OF SPECIMENS

Recording of elastic impulses arising from cracks formed in the process of specimen straining and determination of the energy of each impulse allowed estimation of the total seismic energy released during the experiment as well as the average magnitude of energy released in unit time. Knowledge of the stress, strain, and the elastic properties of the material allowed computation of the elastic energy stored in the specimen as well as the average force straining the specimen. Thus it was possible to evaluate the energy of the process of different strain rates.

Special reference should be made to the experiments under constant load. These experiments were necessary to obtain low strain rates that could not be attained with the usual hydraulic presses. Throughout the experiment, from the beginning to total failure, the specimen was under constant load: 80–85% of the failure load. Strain records during the tests showed that the strain rate remained constant over prolonged periods. In fact, the specimen was strained and fractured under quasiviscous flow states at a constant level of stored elastic energy. This energy merely redistributed itself inside the specimen due to crack formation and stress redistribution.

Estimate of the total seismic energy released in the process of specimen straining showed that this value does not vary much with variation in the strain rate. For instance, with the strain rate changing from 10^{-3} to 10^{-9} sec^{-1} (by 6 orders) the seismic energy dropped by 90 times in the case of specimens containing large chips and by 50 times in the case of specimens containing a large proportion of fine chips.

The average magnitude of the seismic energy released in unit time varies much more steeply. The variation with strain rate of seismic energy released in unit time is shown in Fig. 1. It can be seen that the correlation does not change in nature over the entire range of strain rates. It can be said that the time-rated seismic energy is an excellent indicator of the rate of the straining process.

Determination of the absolute energy of each impulse allowed computation of the total seismic energy. The average energy of the seismic process $\overline{dE}/dt$ was calculated by dividing the total seismic energy by the duration of

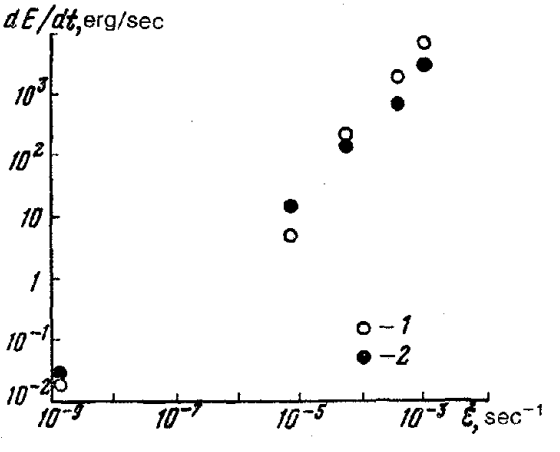

Fig. 1. Seismic energy released in unit time as function of strain rate:
1—Large chips; 2—Small chips.

the experiment in seconds. For specimens containing large and small chips it was 0.04–0.05 erg/sec in experiments conducted under constant load. The energy w spent in straining can be readily calculated provided the load and the dislocation rate are known. On an average it is 150 erg/sec for specimens containing large chips and 117 erg/sec for specimens containing small chips. The values computed are tabulated below:

	Load, T	Dislocation rate, cm/sec	w, erg/sec	dE/dt, erg/sec	$dE/dt : w$
Chips					
Large	7	1.9×10^{-8}	150	0.045	3×10^{-4}
Small	8	1.4×10^{-8}	117	0.050	4×10^{-4}

Thus the seismic to straining energy ratio is of the order of one-hundredth of 1 percent. The factor obtained pertains to the whole process rather than to some isolated seismic event. Therefore this factor, indicating that the seismic energy is some hundredths of 1 percent of the energy consumed in straining, pertains to prolonged processes and can be used for evaluating the "regional" energy balance.

ELASTIC IMPULSE DISTRIBUTION WITH TIME IN STRAINING AND FRACTURING OF SPECIMENS

Impulse distribution with time reflects the progress of specimen fracture. This process is a function of strain rates and properties of the deformable material, in particular its heterogeneity.

Data are cited in [4, 10, 11–18] on the time-dependent distribution of elastic impulses arising from straining and fracture of rock specimens at a high strain rate. The experiments did not last more than 2–2.5 hr. In all cases the authors noted an increased number of impulses just before fracture of the specimen. Comparison of time-dependent impulse distribution in our experiments with varying strain rates showed that the distribution varies with the strain rate. This apart, heterogeneity of the material also has an influence.

In the experiments conducted at a high rate (10^{-3} sec^{-1}) of straining of specimens containing small chips a large proportion of the impulses is concentrated at the end. Up to 50% of the total impulses is accounted for by 10% of the test time. Impulse distribution becomes more uniform with a drop in the strain rate (to 10^{-6} sec^{-1}). In experiments under constant load (strain rate 10^{-9} sec^{-1}) it acquires specific features.

Figure 2a shows an example of the sequence of impulses with time in an experiment under constant load. Fig. 2b gives the record of strain (displacement of the press plates) in the same experiment. A large number of impulses are observed at the beginning of the experiment after the load is applied.

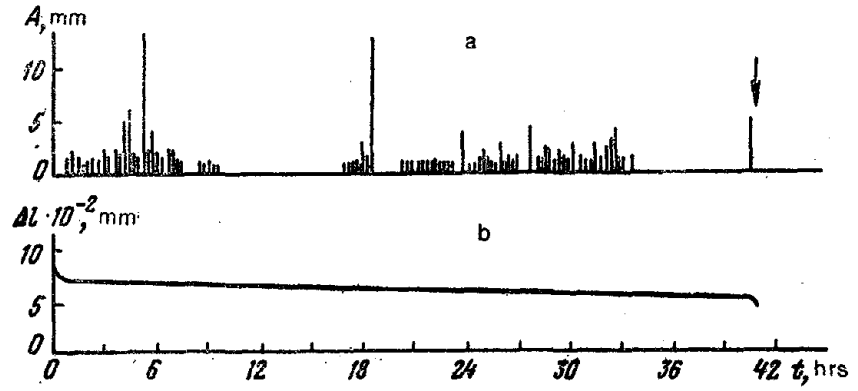

Fig 2. Sequence of elastic impulses and strain rates in experiment under constant load:

Specimen containing small chips: a—Sequence of elastic impulses with time; b—Absolute longitudinal straining of specimen.

In the middle phase they are distributed more or less evenly. A lull, i.e. absence of impulses for some time, is observed in all experiments just before fracture.

Impulse distribution with time during straining and fracturing of specimens containing large chips has the same shape. Of course, in the middle of the experiment the impulses in this case constitute one or two more compact groups, but a lull is observed before fracture of the specimen in all cases.

Time distribution of elastic impulses created in the course of straining and fracturing of the specimen can be compared (of course only qualitatively) with the time distribution of local ruptures in rocks during preparation of the main fault in an earthquake. Under mining conditions this is the volume of rock where the mine shock occurs; in seismic regions it is the focal region of strong earthquakes.

Observations in coalmines of the Kizel basin revealed [17] that impulses diminish in number just before the mine shock, which occurs in a state of relative lull. Impulse distributions before mine shocks were recorded in detail at the Anna mine (Czechoslovakia) [18]. Two mine shocks, one of them quite powerful, were recorded in the region of observations. A period of lull was noted before the shocks in both cases. For instance, the strong mine shock of February 21, 1962, occurred in a state of lull lasting about 1 hr.

A similar phenomenon of lull is observed before earthquakes [19]. As an example, we checked the variation in seismicity with time before four earthquakes that occurred in the Gissaro-Kokshaal fault zone. For this purpose regions were chosen that were delimited by the principal aftershocks of

the Garm earthquakes on April 20, 1941 ($M = 6.5$), the Khait earthquake on June 10, 1949 ($M = 7.6$), and two Ulugchat earthquakes on April 15, 1955 ($K = 16$) and August 29, 1963 ($K = 16$).

A review of the seismicity in these regions revealed that the lull before the Garm earthquake lasted from May, 1940 to April, 1941. Not a single earthquake ($K \geqslant 12$) occurred for about a year.

Before the stronger Khait earthquake the lull lasted from August, 1944 to July, 1949. No earthquake ($K = 12$) occurred during the period.

A somewhat similar phenomenon was observed before the Ulugchat earthquake. Not a single earthquake ($K \geqslant 10$) occurred before the April 15, 1955 earthquake from 1952 to April, 1955. Only two foreshocks of $K = 11$ were recorded just before the earthquake. A prolonged period of lull was also noted before the August 29, 1963 earthquake. After July, 1961 only one earthquake occurred in March, 1963 ($K = 11$).

So we see that the temporal pattern of main fault preparation in specimens submitted to quasiviscous flow is qualitatively similar to the fault preparation in natural environments. A time gap in which no new faults appear is noted in the limited volume of the deformable material before formation of the main fault. This lull period is noticed before fracturing of specimens, before mine shocks and before earthquakes. Examination of the straining behavior of the specimens during this period (Fig. 2b) shows that the strain rate does not change markedly. Essentially plastic deformation occurs during this period without macroscopic fractures, facilitating closure and partial healing of pre-existing cracks. This in turn implies that the material whose properties altered on account of crack formation has its properties restored to some extent and tends to regain its original state. This explains, in particular, the baylike form of the change in the V_P/V_S ratio before earthquakes [20, 21].

CONCLUSION

Study of fracturing processes in specimens of heterogeneous materials revealed that the intensity of seismic processes definable by seismic energies released in unit time markedly depends on the strain rate, i.e. on the force applied to the material and expended on its straining. This dependence manifests itself in identical form over a wide range of strain rates.

Examination of elastic impulse distribution with time during specimen straining under quasistatic flow conditions enabled us to identify the general regularity in crack formation during main fault preparation. Occurrence of quasiplastic deformation for some period before the appearance of the main fault is a characteristic feature of this regularity.

Laboratory studies are therefore helpful in understanding the physical nature of the seismic process.

REFERENCES

1. Vinogradov, S.D. 1959. O raspredelenii chisla impulsov po energii pri razrushenii gornykh porod (Impulse distribution with energy in rock fracture). *Izv. AN SSSR, Ser. Geofiz.*, No. 12.
2. Vinogradov, S.D. 1964. Akusticheskie nablyudeniya protsessov razrusheniya gornykh porod (Acoustic Observation of Rock Fracture Processes). Nauka, Moscow.
3. Vinogradov, S.D. and K.M. Mirzoev. 1969. Sb. Vliyanie neodnorodnosti materiala na grafiki povtoryaemosti upryugikh impulsov pri razrushenii obraztsov (Collection: Effect of Heterogeneity of Material on Recurrence Graphs of Elastic Impulses in Specimen Fracturing). Donish, Dushanbe.
4. Mogi, K. 1962. Study of elastic shocks caused by the fracture of heterogeneous materials and its relation to the earthquake phenomena. *Bull. Earthquake Res. Inst. Univ.*, Tokyo, **40**, 1.
5. Mogi, K. 1963. The fracture of the semi-infinite body caused by an inner stress origin and its relation to the earthquake phenomena. *Bull. Earthquake Res. Inst. Univ.*, Tokyo, **41**, 3.
6. Mogi, K. 1967. Earthquakes and fracture. *Tectonophysics*, **5**, No. 1.
7. Scholz, C.H. 1968. The frequency-magnitude relation of microfracturing in rocks and its relation to earthquakes. *Bull. Seismol. Soc. America*, **58**, No. 1.
8. Scholz, C.H. 1968. Experimental study of the fracturing process in brittle rocks. *J. Geophys. Res.*, **73**, No. 4.
9. Mamadaliev, Yu.A. 1964. Ob issledovanii parametrov seismicheskogo rezhima vo vremeni i v prostranstve (Study of seismic regime parameters in time and space). Sb. *Voprosy Regional'noi Seismichnosti Srednei Azii*. Ilim, Frunze.
10. Mogi, K. 1968. Source location of elastic shocks in the fracturing process in rocks. *Bull. Earthquake Res. Inst. Univ.*, Tokyo, 46, pt. 5.
11. Tomashevskaya, I.S. and Ya.N. Khamidullin. 1972. Predvestniki razrusheniya obraztsov gornykh porod (Fracturing forerunners of rock specimens). *Izv. AN SSSR, Fizika Zemli*, No. 5.
12. Vinogradov, S D. and K.M. Mirzoev. 1969. O vliyanii formy i razmerov vklyuchenii na raspredelenie chisla razryvov po energii (Influence of shape and size of inclusions of energywise distribution of faults). Sb. *Seismicheskii Rezhim Tadzhikistana*, Donish, Dushanbe.
13. Vinogradov, S.D. and K.M. Mirzoev. 1970. Ob energii uprugikh impul'sov pri razrushenii obraztsov iz neodnorodnykh materialov (Energy of elastic impulses in fracturing of specimens of heterogeneous materials). *Izv. AN SSSR, Fizika Zemli*, No. 1.
14. Vinogradov, S.D., K.M. Mirzoev and N.G. Solmov. 1973, Seismiches-

kaya energiya pri razrushenii obraztsov pod postoyannoi nagruzkoi (Seismic energy in specimen fracturing under constant load). *Izv. AN SSSR, Fizika Zemli*, No. 3.

15. Antsyferov, M.S., N.G. Antsyferova and Ya.Ya. Kogan. 1971. Seismoakysticheskie issledovaniya i problema prognoza dinamicheskikh yavlenii (Seismic Studies and the Problem of Predicting Dynamic Phenomena). Nauka, Moscow.
16. Shamina, O.G. 1956. Uprugie impulsy pri razrushenii obraztsov gornykh porod (Elastic impulses in fracturing of rock specimens). *Izv. AN SSSR, Ser. Geofiz.*, No. 5.
17. Vinogradov, S.D. 1957. Akustichcskie nablyudeniya v shakhtakh Kizelevskogo ugol'nogo basseina (Acoustic observations in mines of Kizel coal basin). *Izv. AN SSSR, Ser. Geofiz.*, No. 6.
18. Vinogradov, S.D. 1963. Akusticheskie issledovaniya protsessov razrusheniya gornykh porod v shakhte "Anna", Chekhoslovkiya (Acoustic studies of fracturing processes in rocks in the Anna mine Czechoslovakia). *Izv. AN SSSR, Ser. Geofiz.*, No. 4.
19. Kelleher, J., L. Sykes and J. Oliver. 1973. Possible criteria for predicting earthquake locations and their application to major plate boundaries of the Pacific and the Carribean. *J. Geophys. Res.*, **78**, No. 14.
20. Nersesov, I.L., A.I. Semenov and I.G. Simbireva. 1971. Prostrastvenno-vremennoe raspredelenie vremen progaga poperechnykh i prodol'nykh voln v Garmaskom raione (Space-time distribution of travel times of transverse and longitudinal waves in the Garm region). Sb. *Eksperimental'naya Seismologiya*, Nauka, Moscow.
21. Aggarwal, J.P. et al. 1973. *Nature*, **241**, No. 5385.

UDC 552.1-539.4

Change of Various Physical Parameters during Straining and Fracturing of Rock Specimens

I.S. Tomashevskaya

Experimental results are reported on the variation of some physical parameters in the process of straining of dry and water-saturated rock specimens in complex stressed state with residual strains. The specimens were studied with the help of thin sections prepared from specimens strained to different degrees.

Study of specimens of rock enables us to follow the trend of change in physical parameters under controlled external and internal factors and stresses. We will try to explain the probable mechanisms of preparation of natural phenomena, e.g. earthquakes, by comparing these data with the data derived under field conditions in seismically active regions. At the present stage of development of physics of earthquake focus more and more time is being devoted to laboratory studies of the parameters observed in field conditions.

Experiments were undertaken in the High Pressure Laboratory of the IFZ, Academy of Sciences, USSR to study a set of parameters of rock specimens. The physical characteristics chosen were analogous in that elastic wave velocities, seismoacoustic impulse distribution, electrical resistance, longitudinal and transverse deformations, etc. were studied in polygons to ascertain the earthquake forerunners. These characteristics were studied in the process of specimen straining by uniaxial compression under varying confining pressures.

The question arises whether it is better to study different rocks or to take varieties of rock or other materials such that they satisfy to some extent the various conditions of modeling, i.e. they should be fine-grained, fairly plastic, etc.

The fracturing and straining mechanisms of fine and coarse-grained, rocks are different, so it is necessary to know under what conditions and at what grain size the various straining and fracturing mechanisms will develop. For instance, in most sedimentary rocks strain and rupture occur due to slipping of cement and jointing, not in the strong grains but at grain boundaries or in the cement [1].

In fine-grained ceramics where the grains are not likely to have many flaws the strains generally occur at grain boundaries. In igneous rock composed of a variety of polycrystals local fractures appear not at grain boundaries but inside the grains, where the flaws are reoriented in individual crystals. As a result cracks appear inside the grains and often stop at the boundaries. Strain studies under natural conditions show that the grains themselves are strained, and cracks appear and grow inside the grains. Therefore it is necessary to know how the set of parameters will behave in the straining process when different mechanisms come into play.

Experiments were conducted in a high-pressure device [2] where the specimen could be subjected to as much as 10 kbar confining pressure and to additional uniaxial compression as high as 50 t. The rock specimens were cylinders 20 mm in diameter and 50–60 mm in length or $50 \times 20 \times 20$ mm^3 blocks. The specimens were isolated from the pressure-transmitting medium. All parameters, except elastic wave velocities, were recorded continuously throughout the experiment with the help of an N-700 oscillograph. The travel time of elastic waves was photographed discretely from the screen of a recording instrument, while the time of photographing was correlated by special markers with the general pattern of variations of all values.

Let us see how the various parameters change with different straining mechanisms. The straining mechanisms were studied by comparing thin sections prepared from strained specimens after withdrawal of load with sections of rock rendered strain-free in the laboratory.

Elastic wave velocities. Studies of longitudinal wave velocities along and perpendicular to the direction of differential loading [3, 4, 9] revealed that when the load is applied axially under different hydrostatic conditions the longitudinal wave velocity rises initially but begins to fall later due to fracturing. Variation in V_P diminishes sharply (quite smoothly in the case of fine-grained, but steeply in the case of coarser materials) as the confining pressure increases. In our experiments two types of variations of transverse wave velocity V_S were noted in the process of straining of air-dried specimens under uniaxial compression. When specimens of brittle rocks, e.g. granite, are strained, V_S initially remains unchanged. But starting with 30–70% of the failure load V_S begins to fall at a rate dependent on the way the future main fault develops relative to the orientation of the piezotransducers.

Figure 1 shows how V_S changes in specimens of granite varieties and crystalline schist. But if the specimens are strained plastically before fracturing a totally different V_S variation pattern is obtained. In the elastically strained region V_S remains unchanged or changes negligibly, but as soon as the specimen begins to undergo plastic deformation V_S increases, falling again before or during fracture.

The V_S variations in marble, dolomite and clay shale specimens are shown in Fig. 2. The specimens ultimately fractured brittly, but they suffered

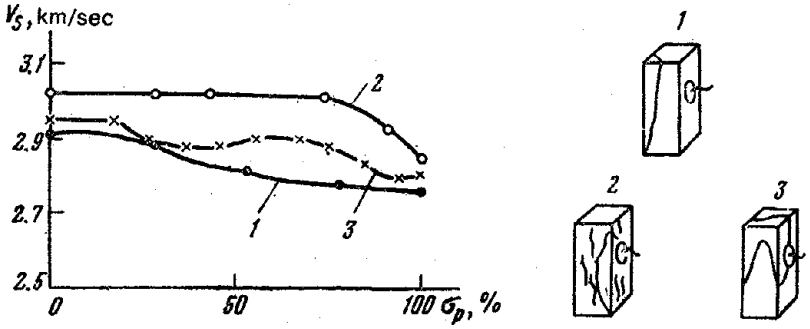

Fig. 1. Variation in V_S during specimen loading:
1—Crystalline schist; 2 and 3—Granites. Above—orientation of piezotransducers and cracks in each specimen.

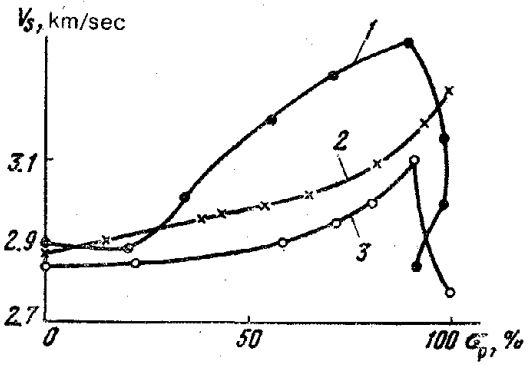

Fig. 2. Variation in V_S during loading of plastic rocks:
1—Marble; 2—Dolomite; 3—Clay shale.

plastic deformation before fracture, as is noticeable in thin sections.

In the straining process the V_P/V_S ratio does not remain constant. It changes in accordance with the fact that V_P and V_S do not change proportionally but according to their own individual laws.

Figure 3 shows how the V_P/V_S ratio varies in the most brittle of the rocks examined—granite (1)—and in the most plastic rock examined—marble (2). An indistinct minimum in a region bearing 30% of the fracture load and a subsequent rise in the V_P/V_S ratio are observed in granite. In marble a sharp change in the V_P/V_S ratio occurs during plastic deformation. It may be suggested that the V_P/V_S ratio falls as long as the rock is undergoing plastic deformation but rises as soon as cracks, i.e. brittle fractures, appear.

According to V.A. Dubrovskii [5] transverse wave velocities increase during plastic deformation because in the process dislocations or very small

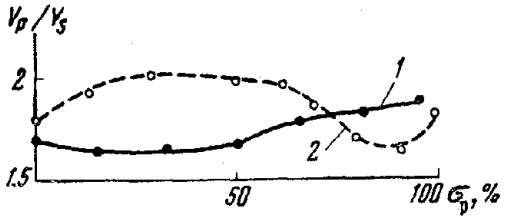

Fig. 3. V_p/V_S versus percent of fracture load:
1—Granite; 2—Marble.

fractures accumulate in the rock in numbers that temporarily hinder the development of large fractures, so that the rock is consolidated (like the cold-working process in metals).

The amplitude change of the first longitudinal waves in the straining process is shown in [3]. Transverse wave amplitude changes not only because of internal processes but also because of variations in the mode of contact between the sensor and the specimen in the straining process. Therefore the measured amplitude values will not reflect the processes occurring right in the specimen of rock.

Strength characteristics. What are the external and internal factors responsible for altering the strength characteristics of rocks? Where is sudden brittle or gradual fracturing to be expected? To answer these questions tests were run with rock specimens of the same composition but bearing varying residual strains inherited under natural conditions; with specimens where two different rocks were in natural contact; with air-dried and water-saturated specimens; and with specimens of the same rock but strained at different rates. Examples of change of strength under hydrostatic pressure are cited in Table 1. The "contact" specimens were cut from a single block where granite and xenolith were in natural contact. Specimens were cut from contacting rocks far from the point of contact as well as from rocks where the contact passed almost through the middle. All the specimens were oriented with their long axis perpendicular to the line of contact. It was found that under atmospheric pressure the "contact" specimens on the average had the same strength as the stronger of the contact rocks. On enhancement of the confining pressure to 1 kbar, which corresponds to a crustal depth of 3–4 km, the average strength characteristics varied, almost doubling in granite and xenolith and remaining almost unchanged in "contact" specimens.

Strength increase with the pressure is less in rock specimens subjected to marked natural straining than in fresh rocks whose thin sections exhibit no sign of residual strains. Data on two granites collected from Kamchatka are cited in Table 1 as examples. In tests under a confining pressure of 1.5 kbar the strength of fresh granite almost quadrupled, but that of granite subjected to initial straining only doubled.

Table 1. Variation in strength (σ, kbar)* of rock specimens with increase in confining pressures (p, kbar)

Description of rocks	σ_0 at p_{atm}	p	σ_p	$\sigma_p - \sigma_0$
Effect of contact				
Granite, highly fractured	1.34		3.1	1.76
Xenolith-hornfels	1.92	1	4.35	2.43
Specimens of granite and xenolith in contact	2.02		1.9	Nil
Effect of pre-existing strains				
Granite, fresh	1.27		5.04	3.77
Granite deformed plastically in natural conditions	1.72	1.5	3.29	1.57
Effect of recrystallization of rocks in solid state				
Granite, fresh	1.27	1.5	5.04	3.77
Granitogneiss	0.7		3.19	2.5

*Values given in the Table are averages from 4-5 tests under identical conditions.

Endurance limits and solid-state rock recrystallization diminish analogously. The effect of water-saturation finds expression in a reduction in the specimen's strength relative to the strength of air-dried specimens and in alteration of the fracture characteristics. For instance, air-dried doleritic basalt specimens suffered brittle fracture at pressures ranging from 1 atm to 5.5 kbar (in the pressure range p_{atm}—1.9 kbar, P—1.5–4.3 kbar and p—5–11.4 kbar). Thin sections hardly exhibited any fracture preparation, whereas in water-saturated specimens fractures accumulated in the process of specimen straining, so that abrupt fracture (in the pressure ranges p_{atm}—1.9 kbar, P—1.5–3.5 kbar and $p = 5$–5.6 kbar) with liberation of much energy was ruled out. Along the fault the specimens had a wide zone of crushed material.

Strain rate. The duration of stress is taken into account in experiments on endurance limit or in experiments featuring varying stress or strain rates. It plays a significant part in determination of the strength characteristics of rocks. Both prefracture time and strength change substantially in all these experiments. In our tests the rate of additional axial stress applied to the specimen was maintained constant. As examples, the results for fresh granite under varied confining pressures are cited in Fig. 4 and for four varieties of rock under a confining pressure of 1.5 kbar in Fig. 5. The experimentally obtained points are averaged by drawing straight lines through them. Consequently they are described within the range of strain rates investigated by the Zhurkov equation modified for variable stresses [6].

There are data to show that a different straining mechanism almost entirely independent of time operates in regions under weak stresses or slow straining [7, 8]. Moreover, this dependence may weaken due to stress release.

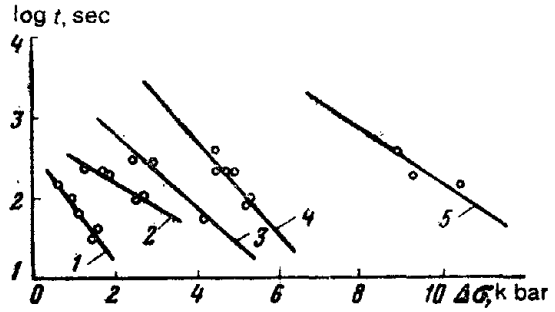

Fig. 4. Prefracture time t as function of maximum differential stress $\Delta\sigma$ under different confining pressures for granite specimens:
1—p_{atm}; 2—p = 0.5 kbar; 3—1 kbar; 4—1.5 kbar; 5—3.5 kbar.

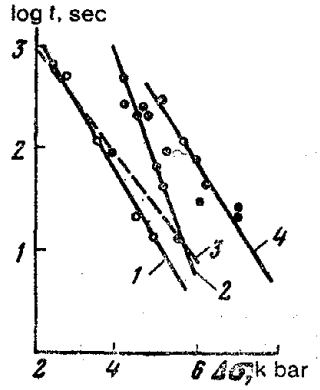

Fig. 5. Prefracture time t as function of maximum differential stress $\Delta\sigma$ for different rocks tested at p = 1.5 kbar:
1—Granodiorite; 2—Granite; 3—Altered gabbro;
4—Plagiogranite-porphyry.

Seismo-acoustic impulse distribution. The nature of elastic impulses generated in the process of straining of rock specimens to some extent reflects the type of main fracture in the offing. For instance, "contact" specimens have, so to speak, two regions of stress drop and two corresponding impulse groups clearly separated in time (Fig. 6). Also, the time gap separating these impulse groups clearly depends on the magnitude of the confining pressure. If under atmospheric pressure these two groups followed each other almost without any interruption, then a time interval without impulses was

observed at a pressure of 1 kbar. But the specimens withstood greater uniaxial stress than before the appearance of the first group of impulses. Irregular strain variations (Fig. 6) were observed simultaneously with the impulse groups, suggesting that the first impulse group resulted from fracture in the granite component of the specimens, while the second was associated with development of the main fault.

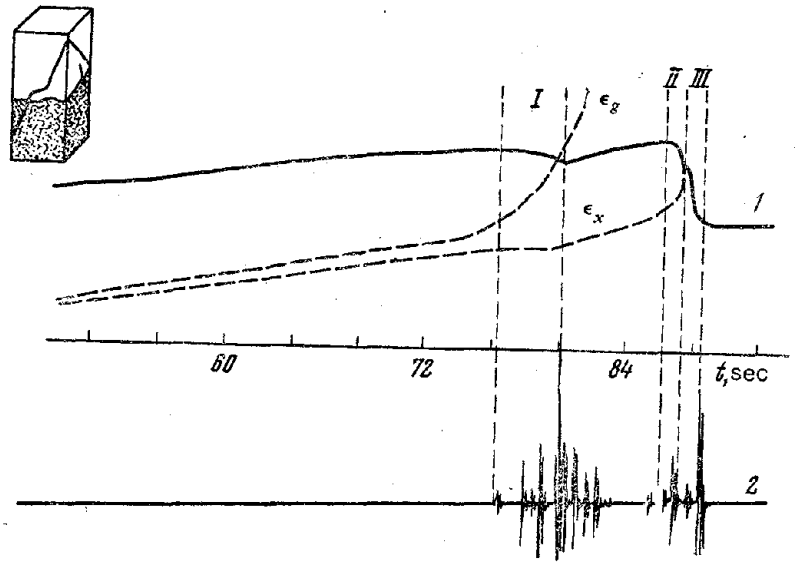

Fig. 6. Seismo-acoustic impulse distribution with time and variation of strain and differential stress in "contact" specimens tested at $p = 1$ kbar:
I, II, III—Regions of stress drop; 1—differential stress; 2—impulse; ϵ_g—strain in granite; ϵ_x—strain in xenolith. Orientation of macrocracks is shown schematically, top left.

The stress drop and relative amplitudes of seismo-acoustic impulses during straining of "contact" specimens by uniaxial compression under 1.5 kbar confining pressure (Fig. 6) are given below:

	I	II	III
Stress drop, kbar	0.42	0.65	1.65
Duration of stress drop, sec	3.7	0.8	0.8
Ratio of maximum impulse amplitude in each region to maximum impulse amplitude in region I	1	0.32	0.71
Number of impulses accompanying stress drop	5	2	2
Ratio of total amplitude of impulses recorded during stress drop to maximum impulse amplitude in region I	1.87	0.41	0.83

The macrocracks usually noticeable in such specimens were of the type shown in Fig. 6, with one main crack and one or more inclined cracks in the granite component of the specimens terminating at the granite-xenolith boundary. Microscopic examination revealed an array of cracks in the granite component, terminating at the granite-xenolith boundary.

Such large and clearly defined impulse groups were not observed in granite or xenolith specimens. In granite specimens fractured with a wide crushed zone isolated impulses were recorded even under increased confining pressure. After application of additional uniaxial stress impulses were recorded almost continuously. They had small amplitudes which, however, increased rapidly before fracturing. The initial uniaxial stress drop was accompanied by a maximum impulse amplitude 10–15 times in excess of the impulse amplitude under stresses remote from the fracture. The process of stress drop was accompanied by impulses of steeply falling amplitudes.

Xenolith specimens fractured by shearing, and the process of axial stress increase was accompanied by a small number of isolated impulses with a relatively wide time gap. Finally, a cluster of impulses whose maximum amplitude surpassed all previous impulses tenfold appeared with rupture of the specimen.

Clearly different patterns of seismo-acoustic impulse accumulation were obtained under equal straining of fresh rock and compositionally analogous specimens strained markedly in natural conditions. Fresh rocks show a tendency to accumulate potential energy in large amounts, and the release of this energy to a notable extent in the form of local brittle fracture is rare. In rocks bearing pre-existing residual strains the energy dissipates in the straining process on account of a large number of local fractures. The specimens rupture gradually with a steady fall of differential stresses. Impulse swarms with a wide time gap and a maximum amplitude generally preceding somewhat the initial fall of maximum endurance stress are recorded.

Higher confining pressure alters the impulse distribution pattern even when the fracturing is almost of the same type. For instance, in air-dried fresh granite specimens the number of impulses prior to fracturing decreases with increasing pressure. At $p = 3.5$ kbar either no impulse was observed right up to fracture or one or two impulses were recorded in certain cases under stresses equal to 75–80% of the fracture stress. The amplitude of such impulses matches the amplitude of the impulse accompanying fracture.

Water-saturation of the specimens alters the nature of the fracture as well as the time-dependent impulse distribution pattern with regard to both amplitude and frequency. Other conditions remaining the same, the impulses recorded in the straining process in water-saturated rock outnumbered those in air-dried specimens. But they have one-third or one-fourth the relative amplitude, the number of low-frequency impulses being smaller. Tests were run with specimens of a variety of rocks of widely varying porosity. It was

found that in fracturing the rock material is crushed more when the amount of water required for saturation of the specimen is greater.

Strain. Local ruptures may restore, if only temporarily or partially, the equilibrium lost locally due to stress variation in the specimen. And this process is least affected by the loading apparatus. The choice of measuring techniques is very important for such observations. For instance, the relationship between impulse generation and strain variation could not be ascertained while recording longitudinal and transverse strains with strain gages that measure the separation of two points. But when the strains were measured by resistor elements attached directly to the specimen's surface and by recording the actual strain on the lateral surface of the specimen [4] the relationship between impulse generation and strain variation became quite clear, particularly for impulses of relatively high amplitude.

Very fine-grained varieties of rock (basalts, diabases, etc.) and coarse-grained rocks very strongly altered by various secondary processes so that they represented, so to speak, a homogeneous mass (gabbro from Kamchatka, plagiogranite porphyry from Tashkent, etc.) fractured brittly almost in one plane in the range of confining pressures used. Their strain curves were linear almost until fracture and anomalous areas of strain variation were small. Moreover, for such rocks V_P changes negligibly; the fall of V_P begins at 95–97% of the failure load. It amounts to a few unit percent and diminishes progressively with increasing confining pressure.

Local fractures and the region of main fault preparation are often better expressed in strain-time curves for rocks with grain sizes of up to 5–7 mm and, what is more important, sharp grain boundaries (of granites, granodiorites, granite gneisses, etc.). The regions of local fracture preparation are separated practically distinctly in "contact" specimens. Increasing rapidly after the passage of an elastic impulse or a group of impulses, strain growth seems to abate before the appearance of local fracture (Fig. 6).

The longest time intervals of anomalous changes in the set of parameters are observed in the case of rock specimens bearing under natural conditions significant residual strains, cracks and other defects not healed by various secondary processes. These anomalous changes are great in absolute terms even at fairly high confining pressures and are augmented with a decreasing rate of differential loading. Examples of relative changes in the set of parameters before fracturing are cited in Table 2.

Thus these studies and the data reported by other workers on the change of various parameters in the straining process, particularly in the region adjoining the fracture, show that the pattern of parameter change and of fracture preparation depends on the mineralogical composition of the rocks, their origin, the grain size, the presence or lack of various residual strains, and the degree of relief from these strains through various secondary processes. Systematic study of the changes in the set of physical parameters in the pro-

Table 2. Relative changes of longitudinal wave velocity V_P, electrical resistance ρ, and time interval of anomalous phenomena for various rocks

Rocks	p, kbar	σ, kg/cm²·sec	$\Delta V/V_P$, %	$\Delta\rho/\rho$, %	$\Delta t/t$, %
Gabbro, very strongly	1.6	74	2.5	1.6	7.3
altered	1.9	8	8.8	2.1	19.4
Granite, fresh	1.5	42	5.0	1.5	8.0
	1.5	3	7.1	4.0	13.8
Granite, gneiss	1.3	43	9.3	3.2	8.3
	1.3	9	15.0	4.8	18.7

cess of rock straining plus careful micrographic studies are necessary for an understanding of the role of each of these factors.

REFERENCES

1. Pavlova, N.N. et al. 1970. Eksperimental'nyi metod izucheniya vozniknoveniya, razvitiya i vzaimodeistviya mikrotreshchin v gornykh porodakh pri napryazhennom sostoyanii szhatiya (An experimental method of studying crack origin, growth and interaction in rocks strained by compression). *Neftegazovaya Geologiya i Geofizika*, No. 7.
2. Volarovich, M.P., D.B. Balashov, I.S. Tomashevskaya and V.A. Pavlogradskii. 1963. Izuchenie vliyaniya odnoosnogo szhatya na skorosti uprugikh voln v obraztsakh gornykh porod v usloviyakh vysokogo gidrostatischeskogo davleniya (Study of the effect of uniaxial compression on elastic wave velocity in rock specimens under high hydrostatic pressure). *Izv. AN SSSR, Ser. Geofiz.*, No. 8.
3. Tomashevskaya, I.S. 1970. Nekotorya resul'taty laboratornykh izmerenii svoistv gornykh porod pri slozhnom napryazhennom sostoyanii (Some data on laboratory determinations of rock properties and complex stressed state). Sb. *Fizicheskie Osnovaniya Poiskov Metodov Prognoza Zemletryasenii*, Nauka, Moscow.
4. Tomashevskaya, I.S. and Ya.N. Khamidullin. 1972. Predvestniki razrusheniya obraztsov gornykh porod (Forerunners of fracture of rock specimens). *Izv. AN SSSR, Fizika Zemli*, No. 5.
5. Dubrovskii, V.A. and V.L. Lan'kov. 1972. Ob otnoshenii amplitude P_{sr}-i P-voln (On the P_{av}/P_{wave} amplitude ratio). *Izv. AN SSSR, Fizika Zemli*, No. 6.
6. Tomashevskaya, I.S. and Ya.N. Khamidullin. 1972. Vozmozhnost' predskazaniya momenta razrusheniya obraztsov gornykh porod na osnove

fluktuatsionnogo mekhanizma rosta treshchin (Scope for predicting the time of fracture of rock specimens basing on the fluctuation mechanism of crack growth). *Dokl. AN SSSR*, **207**, No. 3.

7. Stavrogin, A.N. and E.D. Pevzner. 1972. Metody i resultaty issledovanii svoistv gornykh porod pri izmenenii skorosti deformirovaniya i vidov napryazhennogo sostoyaniya (Methods and results of studying rock properties with change of strain rate and type of stressed state). *Gornoe Davlenie i Gornye Udary*, Vol. 35, VNIMI, Leningrad.
8. Vinogradov, S.D., K.M. Mirzoev and N.G. Salomov. 1973. Seismicheskaya energiya pri razrushenii obraztsov pod postoyannoi nagruzkoi (Seismic energy in rock fracture under constant load). *Izv. AN SSSR, Fizika Zemli*, No. 3.
9. Matsushima, S. 1960. Variation of the elastic wave velocities of rocks in the process of deformation under high pressure. *Bull. Disaster Prevent. Res. Inst. Kyoto Univ.*, **32**.

UDC 552.1.537

Effect of Dehydration on Physical Properties of Rock Specimens at High Pressures and Temperatures

E.I. Parkhomenko and A.T. Bondarenko

The paper reports the effect of dehydration on strain, strength and the electrical characteristics of serpentinized ultrabasic and other rocks. The probability of redistribution of stresses and creation of anomalous zones as a result of dehydration are indicated.

According to modern concepts the crust and the upper mantle are the most dynamically active parts of the earth where complex physical, physicochemical and other processes of transformation of matter proceed constantly [1, 2]. As a result not only the composition, structure and physical properties of the rocks suffer changes but redistribution of mechanical stresses may also occur due to expansion or contraction of the volume of the rock. In the first instance widespread rock metamorphism, of which hydration and dehydration of certain rock-forming minerals are a partial manifestation, should be referred to such processes. Both processes induce a greater change in the volume of the rock than does polymorphism. Not only density but a host of other mechanical properties of matter: elastic parameters, plasticity, and strength characteristics—change during these processes. It is a matter of urgency to examine the probable scale of occurrence of these processes in the earth's crust and to gather experimental data on the effect of hydration and dehydration on various physical properties of minerals and rocks. This holds interest not only for physics of earthquake focus but also for the formulation of working hypotheses on the probable nature of the propagating strata in the earth's crust [3, 4]. This might well shed light on the origin of the poorly-propagating strata, which occur at similar depths.

SALIENT INFORMATION ON MINERAL DEHYDRATION

Dehydration obviously occurs only in rocks containing minerals of which water of crystallization or constitution is a constituent. The water of crystallization present in the crystal lattice of the minerals as H_2O molecules is generally removed as the minerals or the rocks are heated up to, and rarely

beyond, 300°C. Constitutional or hydroxyl water is formed from the OH^- and H^+ ions introduced into the crystal lattice of the minerals. In such minerals the water is synthesized at temperatures ranging from 300°C to 1300°C.

Minerals containing water of crystallization in fairly large concentrations (approximately 15–50%) are most widespread in the crustal sedimentary strata. Many of these minerals, e.g. soda, gypsum, mirabilite, scorodite, natroborocalcite, calamine, talc, pyrophyllite, etc., form huge deposits. Besides, kaolin, dickite and several other clay minerals containing water of constitution in fairly high proportion (~15%) are also widespread in the sedimentary strata. Only hydroxyl-bearing minerals are typical of metamorphic and igneous rocks. Minerals of the amphibole, mica, serpentine, and chlorite group belong to this type of rock-forming minerals. Rocks formed of these minerals (amphibolites, gneisses, diabases, etc.) are distributed regionally and are the most probable representatives of the "granite" and "basalt" strata. But it should be noted that in the crust of weathering of basic igneous rocks montmorillonite and natrolite are formed; these contain water of crystallization and constitution up to 24%.

The chemically bound water diminishes progressively with advancing metamorphism. The lower stability limit of amphiboles in regionally metamorphosed basic rocks corresponds to 400–430°C under vapor pressure $p_{H_2O} = 1$–7 kbar. The upper limit corresponds to 590–650° and $p_{H_2O} = 6.5$ kbar in basic rocks and to $t = 700$–1150°C and $p_{H_2O} = 15$–20 kbar in ultrabasic rocks [5–7].

EFFECT OF DEHYDRATION ON PHYSICAL PROPERTIES OF ROCKS AND MINERALS

The kinetics of hydration and the changes in the physical properties of minerals and rocks in the hydration process were not studied under laboratory conditions in view of the technical difficulty involved. Experimental study of the reverse process, i.e. dehydration, was undertaken essentially to clarify its thermal characteristics and incidentally to reveal the pattern of change in physical properties [8–12].

Data on the variable electrical and strength characteristics are now available for several rocks. Copious experimental data on the electrical properties of rocks and minerals show that electrical parameters are sensitive indicators of physico-chemical processes under severe thermodynamic conditions. In view of this, alongside the available published data on the changes in rock strength upon dehydration we will discuss experimental results on the electrical conductivity and on the dielectric constant of minerals and rocks containing bound constitutional water.

Serpentinized ultrabasic rocks and serpentinites are quite widespread in

many areas of the earth's crust, the fault zones in particular [6]. The origin of the Mid-Atlantic Graben and the current uplift of the Colorado Plateau are associated with the serpentinization process accompanying the hydration phenomenon [13].

The extent of serpentinization of ultrabasic rock assemblages exercises a marked influence on the velocity of elastic wave propagation, strength characteristics, density, electrical and other properties [8–11]. For instance, the difference in the velocities of longitudinal waves between unaltered and totally serpentinized olivinites is about 2500 m sec^{-1} i.e. the velocity diminishes from 7.3 to 5.3 km/sec. Correspondingly, the density falls from 3.2 to 2.4 g/cm^3. The pattern of change in electrical conductivity and dielectric constant with an increasing proportion of serpentine-group minerals in the rock is determined essentially by the quantitative proportion of bi- and trivalent iron oxides, and when the latter occur as ore mineral, by the structural and textural features of the mineral.

Serpentinized rocks exhibit a wide range of electrical parameters which may markedly influence the geophysical fields of the earth's crust.

Study of the electrical conductivity and dielectric constant ϵ of ultrabasic rocks serpentinized to varying extents reveals that dehydration gives rise to anomalous changes in these parameters (Fig. 1). Disruption of the linear log σ versus $1/T$ relationship, indicating irregular change of σ, is observed at temperatures corresponding to the dehydration process. In that case the higher the water content of the rocks, the wider the temperature range of the anomaly. The temperature-dielectric constant curves generally show maxima.

The strength characteristics of serpentinized rocks at high pressures and temperatures were studied by Releigh and Paterson [8]. It was shown that at room temperature (20°C) increased strength and plasticity, change of failure morphology (from brittle to plastic), and a reduced coefficient of internal friction are observed with increased confining pressure. These features change markedly as the temperature climbs to 600°C. It was also found that the compressive strength of antigorite-chrysotilic and chrysotile-lizarditic serpentinite diminishes sharply in their dehydration temperature range. For instance, while the strength reduction of antigorite-chrysotilic serpentine is just 35% in the temperature range 25–500°C, it is 90% in the narrow temperature range 500–700°C, and is characterized by brittle fracture. The behavior of the other serpentine (chrysotile-lizarditic) is similar but the strength drops steeply at lower temperature—specifically in the range 300–500°C.

A higher temperature of initial strength loss is noticed with rising hydrostatic pressure. The duration of heating, on the other hand, has the opposite influence, i.e. the initial sharp loss of strength is at a lower temperature upon prolonged heating. As the duration changes from 0.5 to 7.0 hr the ultimate temperature of strength retention falls from 550–600°C to 500°C. The following mechanism is proposed for strength reduction on dehydration: first, a

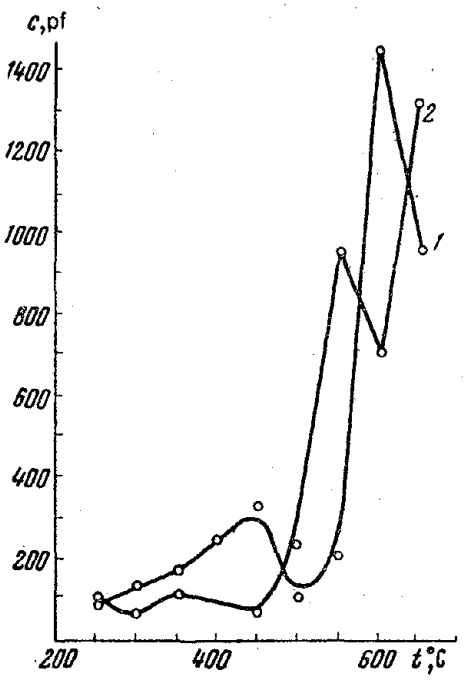

Fig. 1. Dielectric constant (capacitance) of serpentinized ultrabasic rock as function of temperature:
1—p = 1 kbar; 2—p = 20 kbar.

rise in pore water pressure and, second, loss of intergrain cohesive power due to the formation of new pores and diffusion of water through grain boundaries.

Experimental data obtained by N.I. Pavlova and A.A. Fomin [14] on the influence of the anomalously high pore pressure of kerosene on the ultimate strength of limestone and sandstone showed that the ultimate strength falls by 10–15% at a constant effective pressure of 200 kgf/cm² and at a pore pressure of nonpolar liquid reaching 200 kgf/cm².

The above effect should be much more pronounced under electrolyte action and high temperatures. However, aside from strength drop due to increased pore pressure, structural change of the solid phase upon dehydration also seems to be important.

The experimental data on gypsum are discussed in [9]. The strength of gypsum is comparable with the strength of serpentinites at their dehydration temperatures and falls steeply at high hydrostatic pressures.

Despite the pressure of about 4% water in soda and magnesic amphiboles our experimental data showed that upon dehydration σ changes irregularly with rising temperature. Moreover, the rectilinear segment of the log σ =

$f(1/T)$ curve after amphibole dehydration corresponds to low activation energy, apparently showing low amphibole strength. The nature of the anomalous region of electrical conductivity changes with rising temperature in amphiboles with high iron content. In this case segments of spasmodic increase of σ, say for actinolite-bearing chlorite and epidote, are noticeable on $\log \sigma = f(1/T)$ curves in a narrow temperature range (Fig. 2).

Chlorites are in no way less important in this respect. They are widespread among low-temperature metamorphic, metasomatic, and veined structures and are the most typical minerals of the green schist facies. Chlorites

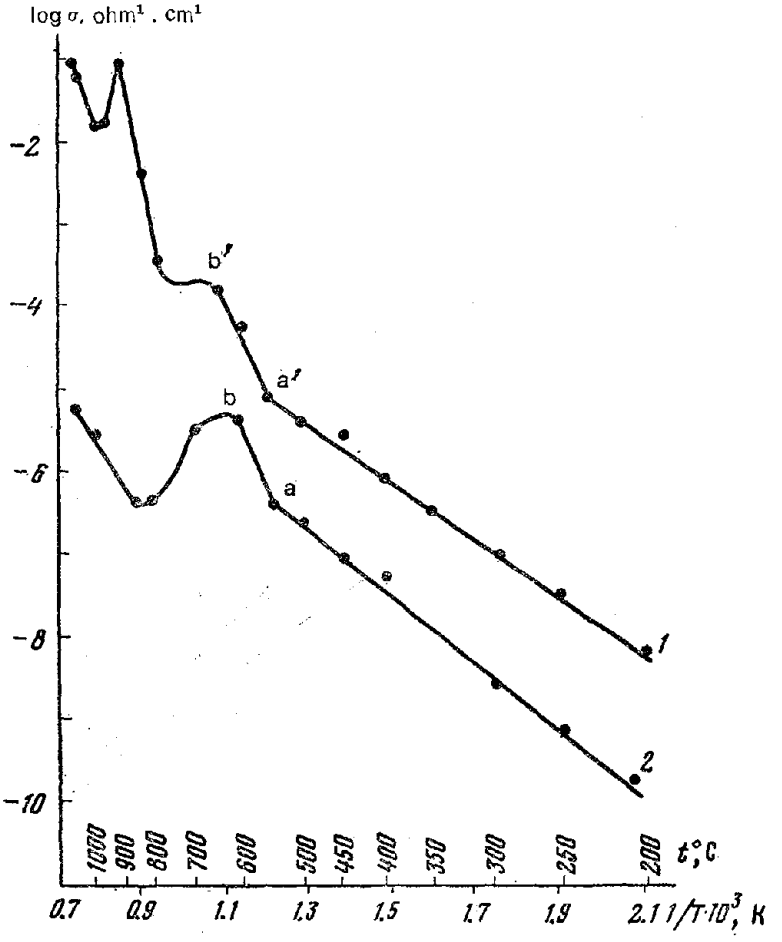

Fig. 2. Steep change in electrical conductivity of actinolite (1) and hornblende (2) (segment a-b) upon dehydration of minerals by heating.

contain higher proportions of constitutional water (9–14%) than do amphiboles and chemically unstable iron oxides ranging in total content from 5 to 55%. Since chlorites, with their high electrical conductivity, are minerals that determine the electrical properties of rocks, it is natural that the electrical properties of rocks and the nature of the dehydration process will change markedly with their concentration and electrical parameters.

We studied a variety of metamorphic rocks composed of magnesium and ferruginous chlorites. The most typical example of change with rising temperature in the electrical conductivity of rocks bearing ferruginous chlorites is chloritized gneiss. It consists of 46% plagioclase, 31.9% quartz and 22% chlorite.

The experimental data cited in Fig. 3 show that the linear relationship of $\log \sigma$ and $1/T$ is disturbed in the temperature ranges 450–600°C and 780–900°C. The electrical conductivity hardly changes at these temperatures as a consequence of the dehydration process. This fact is confirmed quite well

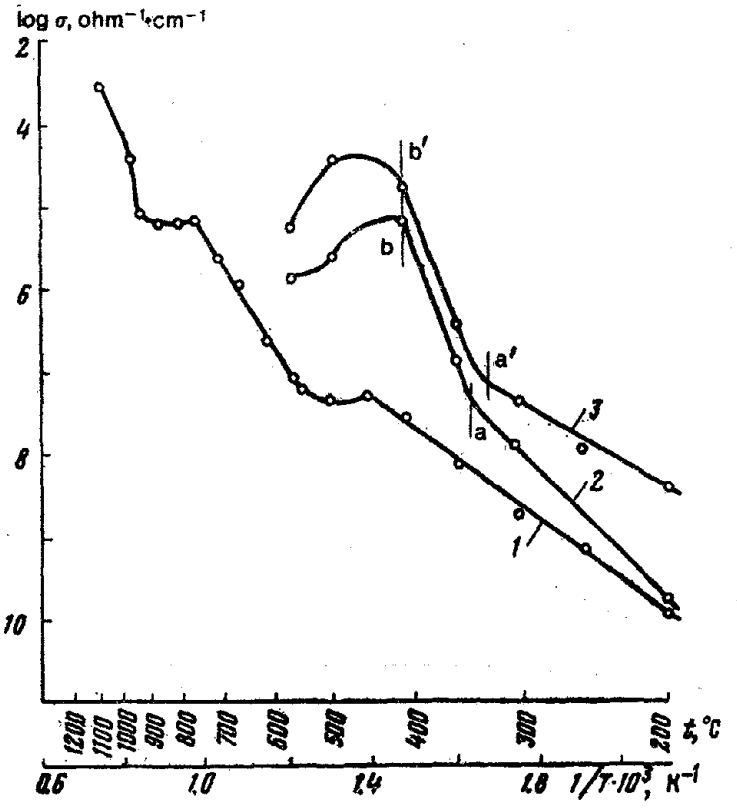

Fig. 3. Change of $\sigma = f(p, t)$ of chloritized gneiss upon dehydration: 1—p_{atm}; 2—p = 0.5 kbar; 3—ϵ = 6 kbar; a-b—Activated section.

by thermal analysis. The two endothermic peaks in the ranges 500–650°C and 750–850°C appeared due to the removal of constitutional water from the crystal lattice of chlorites.

Study of the effect of pressure on the nature of the dehydration process is of maximum interest for physics of earthquake focus. Almost all of the more common minerals of the amphibole group: serpentine, natrolite, brucite—a large number of serpentinized ultrabasic rocks, serpentinites, chlorite, and amphibole-bearing rocks were studied at high pressures and temperatures. Intensification of dehydration under increased quasihydrostatic pressure is a common feature of all these geologic bodies. That shear stresses, which are known to reduce the thermodynamic parameters of polymorphic transitions markedly, develop in addition to normal stresses in the specimen being tested seems to be a fact of much significance.

Let us cite some examples to illustrate the effect of high pressure on the behavior of electrical parameters during rock dehydration. As is evident from Fig. 4, the break in the $\log \sigma = f(1/T)$ curve for serpentinized dunite shifts appreciably toward lower temperatures at a pressure of 20 kbar, indicating a fall in dehydration temperature in our experimental conditions. Comparison of the temperature ranges corresponding to a sharp drop in strength and to a steep rise in electrical conductivity for two rocks of comparable mineralogical composition shows that they are in fair agreement (Fig. 4).

At dehydration temperatures the dielectric constant ϵ exhibits a maximum which also shifts toward higher temperatures under pressure (Fig. 1).

The steeper growth of σ and ϵ with mounting pressure at dehydration

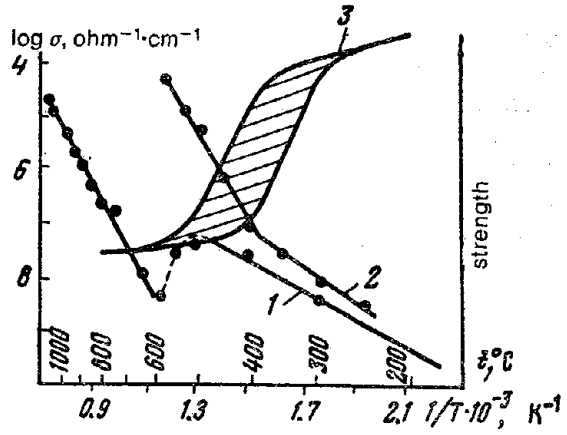

Fig. 4. Electrical conductivity of serpentinized dunite as function of temperature at different pressures:
1—p_{atm}; 2—p = 20 kbar; 3—Variation in strength of serpentinized peridotites at 5 kbar.

temperatures is a fascinating finding. In the pressure range 1–20 kbar the electrical conductivity may increase by two orders and the dielectric constant by 5 or 6 times (Fig. 5). At higher temperatures ($t = 600°C$) the electrical conductivity and dielectric constant increase negligibly with rising pressure.

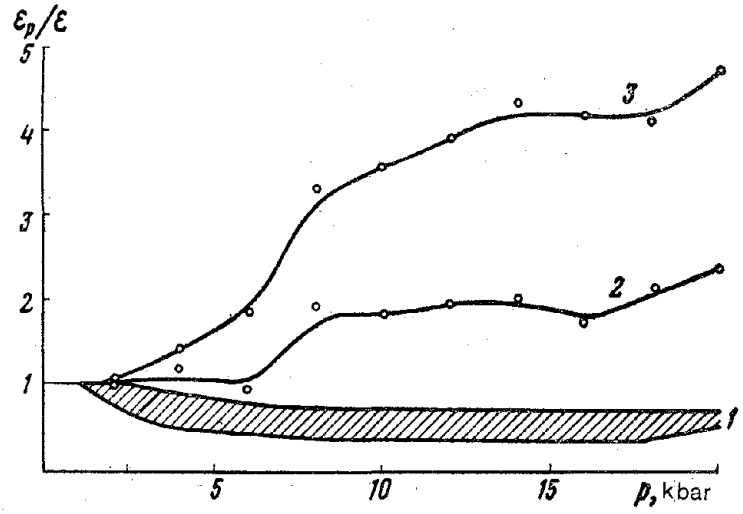

Fig. 5. Relative dielectric constant as function of pressure at different temperatures, °C:
1—300, 400, 600; 2—500; 3—550.

Despite its different mineralogical composition, chloritized gneiss exhibits an analogous change in electrical conductivity. It is obvious from Fig. 6 that at 500°C the electrical conductivity rises by one order when the specimen is loaded to 5 kbar and by two orders when loaded to 7 kbar. The electric conductivity rises much less at the culminating stage of the dehydration process. Besides, appreciable lowering of isotherm is noted at 550°C toward lower electrical conductivity. This suggests that a new phase with different electrical and physical properties forms after removal of the complex OH^- ion from the crystal lattice. But it should be noted that these anomalies of σ are more poorly manifest in magnesic chlorite-bearing rocks than in ferruginous chlorite-bearing rocks.

Apart from the experimental data supporting substantial changes in electrical conductivity, dielectric constant, strength, deformability, fracture morphology and density, it was shown by studies on $Mg_2SO_4 \cdot 7H_2O$ that appreciable volume contraction and increase in the coefficient of internal friction occur upon dehydration [15]. There is no doubt that the elastic properties of minerals and rocks also change significantly in this process.

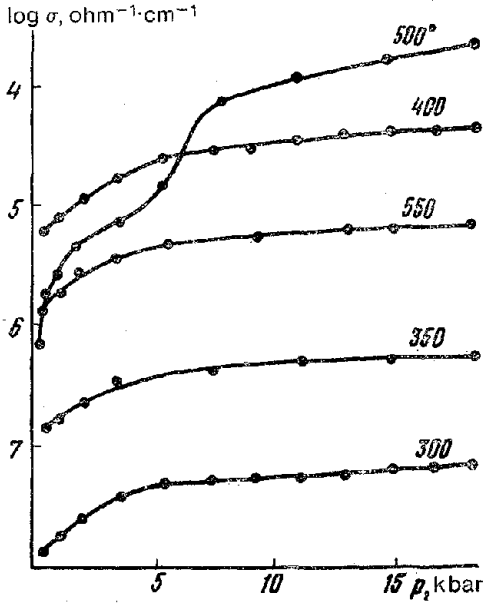

Fig. 6. $\sigma = f(p, t)$ of chloritized gneiss.

CONCLUSION

The probable occurrence of amphibole rocks even in the upper mantle has been indicated. On the basis of experimental data on the stability of green schist minerals Terner and Ferhugen [16] suggested that the temperature of this facies ranges from 300°C to 500°C at the pressures $p_{H_2O} = 3$–8 kbar, i.e. it may occur at the bottom of the earth's crust. It has been shown that dehydration may take place at a constant temperature. With rising temperature the rate of this process v increases exponentially in accordance with the formula

$$v = \frac{kT}{h} \exp(\Delta g/RT),$$

where T is the temperature, K; k is the Boltzmann's constant; h is Planck's constant; Δg is the free energy; R is the gas constant. Consequently, even a slight rise in temperature will markedly accelerate the process. Since dehydration is accompanied by heat absorption and appreciable volume contraction, occurrence of hydroxyl-bearing minerals in the crust and upper mantle of the earth may provide a probable source of redistribution of mechanical stresses. On the other hand, heat is released in the reverse (hydration) process, creating additional stresses of the thermal type. Moreover, in contrast

to dehydration, hydration is accompanied by substantial volumetric expansion, for instance, of the order of 30% or more upon serpentinization of ultrabasic rocks.

Thus the formation of rock modifications, resulting in lower density but higher volume in the upper crust, may stimulate uplift and swelling of the overlying strata and create areas of higher mechanical stresses in the lower strata. It is not unlikely that the growth of salt diapirs is related to the process of hydration of certain minerals codeposited with rock salt. The dehydration process, on the other hand, should cause reverse tectonic movements, i.e. should cause settling of the corresponding crustal areas, obviously with concomitant redistribution of mechanical stresses. Zones of lower strength are formed in certain rock volumes upon culmination of the dehydration process. Consequently, regions of probable rupture develop upon uniform stress distribution. These regions should appear along the anomalies of various geophysical fields—electrical, seismic and gravitational.

Study of the dynamics of dehydration under increased pressure enables us to visualize the following picture: The dehydration process may start developing at a rate directly dependent on the rate of pressure increase, provided the pressure, rising at a fixed rate, begins to act on a rock volume at temperatures approaching its dehydration temperature. This follows from the experimental data on the electrical conductivity of rocks under mounting pressure at constant temperature. It also follows from the premise that the reaction is accelerated under pressure if the matter occupies a volume smaller than its original volume. Intensification of dehydration, in turn, will be accompanied concurrently by strength reduction and stress redistribution, leading to rupture at some instant of time.

Thus the most general review of rock hydration and dehydration as referred to physics of earthquake focus indicates the probable interrelationship of these phenomena. Special laboratory experiments and theoretical studies based on them are needed for further development of the ideas advanced in this paper.

REFERENCES

1. Subbotin, S.N., G.L. Naumchik and I.Sh. Rakhimov. 1968. Mentiya zemli i tektogenez (The Mantle of the Earth and Tectogenesis). Naukova Dumka, Kiev.
2. Belousov, V.V. 1966. Zemnaya kora i verkhnyaya mantiya materialov (The Crust and the Upper Mantle Materials of the Earth). Nauka, Moscow.
3. Berdichevskii, M.N. et al. 1969. Anomaliya elektroprovodnosti zemnoi kory v Yakutii (Anomaly of electrical conductivity of the crust in

Yakutii). *Izv. AN SSSR, Fizika Zemli*, No. 10.

4. Berdichevskii, M.N. et al. 1973. Elektroprovodnost' verkhnei mantii i provodyashchie sloi v kore i v verkhnei mantii (Electrical conductivity of the upper mantle and conducting strata in the crust and upper mantle). Sb. *Stroenie Zemnoi Kory i Verkhnei Mantii Morei i Okeanov.* Nauka, Moscow.
5. Marks, V. 1972. Sb. K voprosu o pole ustoichvosti paragenezov s amfibolami (Collection: Stability Field of Parageneses with Amphiboles). Inst. Geol. i Geokhim. Ural'skogo Nauchn. Tsentra. AN SSSR.
6. Mushnin, I.B. and V.A. Brevilepal. 1972. Pirokseny rannemezozoiskoi shchelochno-gabbroidnoi formatsii Yuzhnogo Tyan'-Shanya v Ssvyazi s nekotorymi vorposami petrogenezisa (Pyroxenes of the Southern Tien Shan Early Mesozoic alkali-gabbroid formation with reference to certain aspects of petrogenesis). *Izv. AN Tadzh SSR, Otd. Fizikomat. i Geologokhim. Nauk*, 3 (45).
7. Solov'ev, T.N., V.A. Molchanov and Ya.S. Genshaft. 1973. Eksperimental'nye dannye po ustoichivosti gidroksilosoder-zhashchikh mineralov v mantii zemli (Experimental data on the stability of hydroxyl-bearing minerals in the mantle). *IX Vses. Soveshch. po Eksperimental'noi i Tekhnicheskoi Petrografii, Tezisy Dokladov (Irkutsk, 5–8 Iyulya 1973 g). Irkutsk, Izd. In-ta Geokhim. SO AN SSSR.*
8. Releigh, C.B. and M.S. Paterson. 1965. Experimental deformation of serpentinite and its tectonic implications. *J. Geophys. Res.*, **70**, No. 16.
9. Heard, H.C. and W.W. Rubey. 1963. Possible tectonic significance of gypsum to anhydrite plus water (abstract). *Geol. Soc. America Spec. Paper*, **76**, 77.
10. Parkhomenko, E.I., B.P. Belikov and Z. Dvorzhak. 1973. Vliyanie serpentinizatsii na uprugie i elektricheskie gornykh porod (Effect of serpentinization on elastic and electrical properties of rocks). *Izv. AN SSSR, Fizika Zemli*, No. 8.
11. Bodarenko, A.T. 1973. Vliyanie protsessov degidratatsii porod i meneralov pri vysokikh davleniyakh i temperaturakh v svyazi s anomal'nymi ob"-emami v zemnoi kore (Effect of dehydration on electrical conductivity of metamorphic rocks and mineral assemblages at high pressures and temperatures with reference to anomalous spaces in the crust). *Dokl. AN SSSR*, **208**, No. 5.
12. Moskaleva, S.V. 1970. O vozmozhnoi prirode poverkhnosti Mokhorovichicha (Probable nature of the Mohorivicic discontinuity). Sb. *Problemy Stroeniya Zemnoi Kory i Verkhnei Mantii.* No. 7, Nauka, Moscow.
13. Hess, H.H. 1957. Serpentinity, crogenez i epeirogenez (Serpentinites, crogenesis and epeirogenesis). Sb. *Zemnaya Kora*, IL, Moscow.
14. Pavlova, N.I. and A.A. Fomin. 1973. Vliyanie anomal'no plastovykh

davlenii na protsess deformatsii i razrusheniya gornykh porod (Effect of anomalous bed pressures on the straining process in rock fracture). *Tezisy Dokladov Vses. Nauchnotekhn. Konf. "Razrushenie Gornykh Porod pri Burenii Skvazhin"*. ONTI Bash NIPI Neft', Ufa.

15. Lifshits, L.D. and Yu.N. Ryabinin. 1970. O vozmozhnom uchastki fazovykh prevrashchenii pri protsessakh v ochage zemletryasenii (Probable contribution of phase transitions in processes occurring in the earthquake focus). Sb. *Fizicheskie Osnovaniya Poiskov Metodov Prognoza Zemletryasenii*. Nauka, Moscow.
16. Terner, F.J. and J. Ferhugen. 1961. Petrologiya izverzhennykh i metamorficheskikh porod (Petrology of Igneous and Metamorphic Rocks). IL, Moscow.

UDC 537.226

Triboelectrification and Triboluminescence of Minerals during Straining and Fracturing

E.I. Parkhomenko and Yu.N. Martyshev

The paper reviews published data on triboelectrification and triboluminescence of various kinds of matter in the straining and fracturing process. It is shown experimentally that these effects are more intense in piezoelectric minerals than in nonpiezoelectric ones.

Changes in the earth's electromagnetic field and luminescence are among the diverse phenomena observed before and during earthquakes [1–7]. Substantial statistical data have been reported by several researchers in support of the perturbation of the earth's electric field and luminescence caused by seismic activity.

Various changes in the earth's electromagnetic field during seismic activity were also reported in [2–7], published in the past decade. A definite time-dependent connection between these anomalies and earthquakes of the energy class above 11 and with focal depths of 25–30 km was noted in several cases [3]. The most interesting and authentic data on luminescence phenomena were published in [6, 7] and collected by I.V. Anan'in (Table 1).

Analysis and review of the published data support the following conclusions:

1. Not all earthquakes are preceded or accompanied by a change in the electric field or by luminescence.

2. Such phenomena are essentially recorded during perceptible earthquakes (magnitude greater than 4).

3. The most intense changes in the electromagnetic field and in luminescence occur in the epicentral region. The observed perturbations of the electromagnetic field and of luminescence phenomena are very varied in nature and occur at different times from the start of the earthquake.

It is believed that accumulation of information on the correlation of seismic data with electromagnetic and luminescence phenomena coupled with laboratory studies on rock and mineral specimens may contribute much to the understanding of the processes involved in earthquakes.

Since the experimental data now available are limited, we studied luminescence and electrification of minerals and rocks in the process of straining

Table 1. Parameters of earthquake focus and characteristics of luminescence phenomena

Region, site of earthquake, date	Magnitude	Focus depth, km	Focus spread, km	Nature of luminescence	Location relative to epicenter and time of luminescence
Sakhalin coast, Okha, June 7, 1953	5¼	15	7	Bright light-colored spot against background of deep lead-colored clouds	Above epicenter during earthquake
Sakhalin coast, Moneron, 1971	7.2	10-30	60	Bright air luminescence over water	Above epicenter
Kamchatka, Ust'-Kamchatskoe, December 5, 1971	7.7	50	100	Glowing of hood of rubber tired tractor	More than 100 km away from epicenter (village Krutoberegovo) at start of earthquake
Caucasus, Kasumken, April 20, 1966	5.5	10-20	10	Shining cloud of ellipsoid shape	Above epicenter
Caucasus, Dagestan, 1970	6.6	10-30	35	Corona discharge type of luminescence	Above epicenter
Carpathia, 1940	7¼-7½	150	60-100	Diverse luminescence phenomena; full or partial luminescence of sky, soil, hills, telegraphic and electric transmission lines, sparks, etc. mainly of red tint	Over area of 300×500 km² in epicentral region

Central Asia, Brichmullin (Chatkal), Oct. 24, 1959	$5\frac{3}{4}$	15	12	Luminescence of hill slopes and surrounding localities with bluish flame	Above epicenter
Central Asia, Tashkent, 1966	5.0	8-10	5	(a) Flash of fire	Above epicenter a few seconds before earthquake
				(b) Whitish-pink scattered light (according to nearby villagers)	
				(c) Spontaneous glowing of gaslight mantle	Above epicenter several hours before earthquake

and fracturing. It will therefore be expedient first to analyze the available data on electrification and luminescence phenomena in straining and rupturing of crystals of various kinds of matter.

TRIBOLUMINESCENCE OF CRYSTALLINE MATTER

Until the 1930s studies in triboluminescence of organic and inorganic matter were of a qualitative nature and were directed toward identification and classification of matter capable of glowing in the fracturing process.

Since the 1930s visual observations have been replaced, thanks to the development of experimental techniques and physical methods, by analysis of luminescence spectra, allowing a deeper understanding of the nature of the phenomenon. It was found that lines corresponding to nitrogen are mostly present in the luminescence spectra of sugar, rock salt and several other crystals [8].

The photoelectric luminescence recording technique revealed varying durations of the luminescence of various kinds of matter and fading of the luminescence with diminishing fracturing load and rising temperature [9]. Occurrence of luminescence before fracturing is indicated in [10, 11].

Studies in the tribo- and photoluminescence of manganese-bearing zinc sulfide crystals in a thermal field led Lenard, et al. [9] to the conclusion that luminescence centers responsible for photoluminescence are excited during fracture of ZnS crystals. Luminescence of mica, quartz, gypsum, KCl, and NaCl was studied in [12–14]. Feeble luminescence is observed on exfoliation of mica in air in the dark owing to the discharge occurring between cleavage planes [13]. The gas does not ionize under high vacuum due to negligible concentration of its molecules but the glass becomes fluorescent, as in cathode-ray tubes.

The authors of [14] observed luminescence and electron emission in fracturing of quartz, gypsum and tourmaline. Luminescence and electron emission in rapid crystallization of mirabilite, $Na_2SO_4 \cdot 10H_2O$, caused by rupture due to loss of water of crystallization were studied in [15].

Studies in the luminescence kinetics of alkali halide crystals showed that photoemission occurs as isolated photo impulses of varied intensity, of which wide fluctuations in amplitude are a characteristic feature [16, 17]. An increased strain rate stimulates increased frequency and amplitude of photo impulses. Impulses of regular form, which have a steep front limited by the time of increase of the recording system (10 sec), and more gradual fall, are observed mostly in fracture of LiF, NaCl, KCl, NaF and CsI crystals.

Several peculiarities are noted in the luminescence spectrum. For instance, the structure of the LiF spectrum is characterized by a set of several bands, whereas the luminescence spectrum itself is identical with the spectrum of the electric discharge in air under atmospheric pressure. The number of

flashes of light in the process of rupture of this crystal diminishes with rising temperature and concentration of impurities.

It was proved for the series of halide crystals that the luminescence in the air caused by rupture consists essentially of the emission of excited nitrogen molecules of the air. The intensity of luminescence of alkali halides of the NaCl structure devoid of special inclusions increases with increasing mechanical strength.

The luminescence spectrum produced upon rupture of Mn-admixed Na_2ZnGeO_4 crystal showed coincidence of mixima of tribo- and photoluminescence.

Thus two groups of crystalline substances differing in the nature of their luminescence have so far been identified. Nitrogen bands have the largest share of the luminescence spectra of some crystals, whereas characteristic bands indicating luminescence of the crystal itself dominate in the luminescence spectra of others. In most cases the crystals of the second group are luminophores containing an activator and possessing photo- and electroluminescence properties. In this context it was found that the photo- and triboluminescence spectra of crystals exhibiting photoluminescence are similar. The data on the kinetics of the luminescence process also suggest that gas-discharge emission in the surrounding atmosphere occurs in the former case and emission from excited luminescence centers in the crystal in the latter.

A characteristic feature of both groups of crystals is that part of the mechanical perturbation energy is transformed into light energy. The mechanism of electric field generation, subsequent perturbation and emission of light is dependent on the physical properties of individual objects and may vary. It should be noted that the maximum intensity of luminescence is observed in air and the minimum in carbon dioxide [18].

TRIBOELECTRIFICATION IN THE PROCESS OF STRAINING AND FRACTURING OF IONIC CRYSTALS

This phenomenon was first noticed by A.V. Stepanov in 1933 during plastic deformation of rock salt. The effect of straining conditions and various factors—impurities, irradiation, temperature, and electric field—on the kind of electrification of ionic crystals in plastic deformation was subsequently studied in [16–20].

Detailed recent studies of the triboelectrification of ionic crystals in the straining and rupturing process yielded new data on the electrification and luminescence phenomena [16, 17].

It appears that the charge on the surface of an LiF crystal strained under uniaxial compression originates at the elastic deformation stage. The potential difference rises smoothly with increasing strain and generally attains its

maximum in the plastic deformation stage. The potential difference diminishes on further straining and the charge on the surface may be reversed. At the rupturing stage the fluctuations of elastic impulses increase, but the change in surface charge lacks well-expressed regularity. At the stage of final rupture the amplitude of potential fluctuations falls and the surface charge disappears.

Charge generation on the surface of the crystal at the elastic deformation stage can be attributed to rupture from the points of locking of pre-existing weakly locked dislocations in crystal and their movement in the friction planes. The increase in surface charge with progressive formation is a consequence of the increased number of dislocations moving in the same sliding plane and direction. The maximum charge is generated at the plastic deformation stage due to vigorous movement and proliferation of dislocations in the initial sliding planes. As shown in [18], sharp deflections of the curve toward an increased signal are attributable to the passage of sliding bands through the entire specimen, whereas the deflections toward a reduced signal are attributable to the creation of new sliding bands.

Elastic impulses increase in number at stresses in excess of the ultimate strength when brittle fracture of the specimens begins with the formation of cracks essentially along their planes [12]. Further fracture is accompanied by fewer impulses, but control of the fracture process is rendered difficult because the specimens are covered with crack arrays.

Comparison of the patterns of change in the triboelectrification and triboluminescence of LiF show that the surface charge changes abruptly at the instant of flashes of light, and luminescence appears only at the brittle fracture stage yielding cracks.

No correspondence between the impulse amplitudes of potentials on the electrodes and the amplitudes of flashes of light is observed in the rupture of crystals under uniaxial compression, but a correlation seems to obtain between these parameters in rupture under concentrated load.

Study of the thermal effect on the triboelectrification and triboluminescence of LiF crystals showed that as the temperature rises above 20°C there occurs an increase in surface charge, a reduction in number of impulses of electric signals with decreasing amplitude and a fall in the intensity of growing.

On the basis of the results obtained, the observed phenomena can be explained as follows: At the instant of crack formation, coinciding with the flash of light, there occurs an outburst of dislocations in regions under highly concentrated mechanical stresses, producing cracks that reach the surface. As a result, the surface charge shoots up and the amplitude and polarity of the potential impulse become dependent on the number of mobile dislocations and the direction of their movement relative to the measuring electrode.

Gas-discharge luminescence accompanying the rupture of alkali crystals indicates the creation of high-voltage electric fields. The voltage field neces-

sary for gas discharge in air under atmospheric pressure was estimated to be $\sim 10^5$ V/cm [21]. This value is quite realistic for the voltage field near freshly formed surface of LiF crystals.

EXPERIMENTAL DATA ON TRIBOLUMINESCENCE AND TRIBOELECTRIFICATION OF CERTAIN MINERALS

Experiments on the triboelectrification and triboluminescence of minerals and rocks were conducted by a procedure described in [17]. The apparatus used permitted simultaneous recording of the salient features of these phenomena in the process of straining and fracturing of specimens under uniaxial compression. The specimens were prepared in the shape of prisms 4×4 mm in cross section and 8 mm in height. Aquadag electrodes were inserted into two opposite lateral faces. An electrometric amplifier automatically recording the potential of the measuring electrode on an electronic potentiometer was used to study the electrification process. The luminescence was recorded with the help of a photomultiplier and an oscillograph.

Results of a semiquantitative nature (Table 2) were obtained in the first stage of the study. It should be emphasized that not all the materials investigated exhibited electrification and luminescence. Wherever these phenomena manifest themselves, their nature is largely analogous to the triboelectrification and triboluminescence of alkali halide crystals. Analysis of the behavior of the potential of the measuring electrode indicates that in general the surface charge of the specimen increases steadily at the initial stage of straining and attains its maximum value just short of the fracturing strain of the material. Thereafter the curve shows deflections due to crack formation upon failure. The cracking generally occurs with audible reports. Decrease in the charge and its disappearance are typical features of the final stage of the fracture process.

As already stated above, the triboelectrification of alkali halide crystals in plastic deformation is a consequence of the movement of charged dislocation. The nature of the electrification at the deformation stage preceding rupture of the minerals we tested remains an open question. There is no dispute, however, that the voltage impulses at the time of rupture of the materials that coincide temporally with crack formation and luminescence, result from the charges appearing on freshly-formed surfaces.

These phenomena in minerals of the alkali halide type can perhaps be regarded as due to electrical discharge processes occurring on freshly-created surfaces. This means that a high-intensity electrical field is created in the course of crack formation and propagation.

Luminescence of minerals is observed only at the stage of rupture of the specimens as monetary flashes of light of varying intensity. To understand the mechanism of the phenomenon, the kinetic and spectral composition of

Table 2. Comparative characteristics of triboelectrification and triboluminescence of several minerals and rocks

Mineral or rock	Electrification in relative units	Luminescence
Limestone	0	Absent
Anhydrite	0	Absent
Fluorite	8	Intensity medium
Hornblende	4	Weak
Microcline	4	Intensity medium
Granodiorite	0	Absent
Marble	0	Absent
Cancrenite	20	Strong
Natrolite-1*	10	Strong
Natrolite-2*	6	Strong
Spodumene	2	Weak
Albite	1	Weak

*Specimens differing in orientation.

the emission should be studied for a variety of objects.

As is evident from Table 2 the electric and luminescence intensities are interrelated. Further, it should be noted that both these phenomena are intensified with accelerated deformation.

CONCLUSION

It is now well known that the seismic phenomena observed on the earth's surface are manifestations of the rupture of the interior. Vast areas of cataclased rocks near faults bear evidence of crack formation. The growth pattern of these cracks is dependent on the rate of application of mechanical stress and the strain characteristics of the medium. Besides, electrification and luminescence of various crystalline substances, including many minerals and rocks, in the process of straining and fracturing are experimentally established facts.

Thus the change in the atmospheric potential gradient and the luminescence noticeable during strong earthquakes do not contradict laboratory results. The only difference to be noted is that under laboratory conditions the luminescence is an effect of gas-discharge from freshly-created crack surface with a potential of the order of 10^6 V/cm, whereas under natural conditions it apparently results from high electric field intensities caused by ionization of atmospheric nitrogen and oxygen.

It follows that the records of electric fields and the data on photophenomena during earthquakes provide additional information on the processes occurring in the earthquake focus. Besides observations on the behavior of the earth's electric field, it is necessary to collect detailed information on the place and time of earthquake occurrences and on the duration and nature of photophenomena and to develop laboratory experiments on electrification and luminescence of geological structures under mechanical stresses.

REFERENCES

1. Parkhomenko, E.I. 1968. Yavleniya elektrizatsii v gornykh pronodakh (Electrification Phenomena in Rocks). Nauka, Moscow.
2. Sb. Predskazanie Zemletryasenii (Collection: Earthquake Prediction). Mir, Moscow, 1968.
3. Sb. Fizicheskie Osnovaniya Poiskov Metodov Prognoza Zemletryasenii (Collection: Physical Basis of Search for Methods of Earthquake Prediction). Nauka, Moscow, 1970.
4. Sobolev, G.A. et al. Izuchenie mekhaniko-elektricheskikh yavlenii v seismoaktivnom raione (Study of mechanoelectric records in a seismic region). This collection, p. 196.
5. Barsukov, O.M. and O.N. Sorokin. 1973. Izmenenie kazhushchegosya soprotivleniya gornykh porod v Garmskom seismoaktivnom raione (Study of apparent resistance of rocks in the seismoactive region). *Izv. AN SSSR, Fizika Zemli*, No. 10.
6. Ulomov, V.I. 1971. Svetovye effekty i elektricheskie yavleniya, soprovozhdayushchie zemletryaseniya (Photoeffects and electric phenomena accompanying earthquakes). Sb. *Tashkentskoe Zemletryasenie, 26 Aprelya 1966 g.*, Tashkent, FAN.
7. Tserfas, K.E. 1971. Yavleniya atmosfernogo elektrichestva, predshestvuyushchie zemletryaseniyam (Atmospheric electric phenomena preceding earthquakes). Sb. *Tashkentskoe Zemletryasenie, 26 Aprelya 1966 g.*, Tashkent, FAN.
8. Longchamlon, H. 1925. Recherches experimentales sur les phenomenes de triboluminescence et de cristalloluminescence. *Bull. Soc. Franc. Mineral*, **48**, 130.
9. Lenard, P., F. Schmidt and R. Tomaschek. 1928. *Handbuch, Exp. für die experimentelle Physik.*, Bd. 23, p. 976.
10. Chudacek, I. 1967. The kinetics of the triboluminescence of zinc sulfide. *J. Physik.*, **17**, 34.
11. Chudacek, I. 1965. Periodic triboluminescence of zinc sulfide. *J. Physik.*, **15**, 359.

UDC 550.34.05.16

Apparatus and Method of Study for Sounding Earthquake Focus Zones

V.I. Myachkin, N.A. Dolbilkina, O.A. Maksimov, A.M. Paleonov and V.B. Preobrazhenskii

The paper reports technique and apparatus for field studies in prospecting of the earthquake focus zone near the east coast of Kamchatka during 1966–1972.

Regular observation of time-variations in the characteristics of detonation-generated elastic waves propagating through earthquake focus zones—a phenomenon known as seismic prospecting—was first made in early 60s in Soviet Central Asia under the guidance of I.L. Nersesov and a little later near the east coast of Kamchatka [1, 2], in the USA [3] and in Japan [4].

Studies in the prospecting of earthquake focus zones to ascertain the variations in their parameters in the earthquake preparation process should logically be carried out in areas of intense seismic activity. The Kurile-Kamchatka seismic zone is one such region in the Soviet Union.

Kamchatka is covered by a developed network of regional seismic stations enabling collation of the results obtained on current seismicity. The epicentral zone of crustal earthquakes passes through the ocean along the Kamchatka coast. Therefore an appropriate observational technique was adopted: the seismic stations were located on the coast and detonations were carried out in the ocean quite far from the coast (as much as 150 km). One major requisite of such an observation system is temporally constant location of the detonation points and seismic stations. The detonation points were determined with the help of a "coordinator" radionavigational system to an accuracy of $\pm$ 50 m [5].

The apparatus assembly ensured recording of detonation-generated seismic waves at the coastal stations, recording of shock waves and the actual instant of detonation on the ship, and a unified service transmitting time signals and the time of detonation to the coastal seismic stations (Fig. 1).

The apparatus assembly of the coastal seismic station consisted of VEGIK type pendulums, PSL-30/60 amplifiers and an N-700 oscillograph with M 001-1 ($f_0 = 120$ Hz) galvanometers. To widen the amplifier range in the low

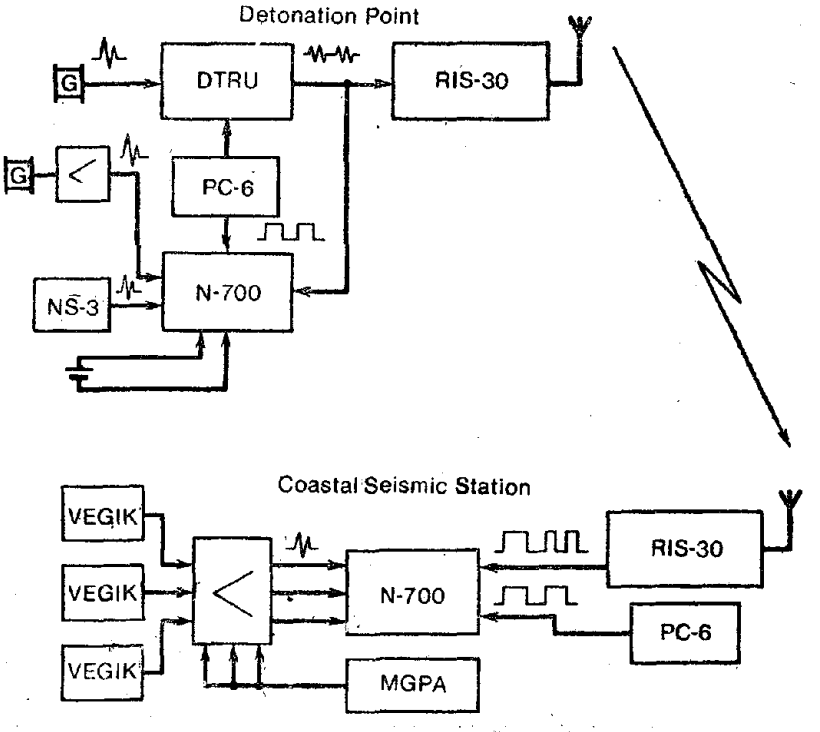

Fig. 1. Block diagram of apparatus assembly at detonation point and coastal seismic stations.

frequency range the junction capacitances in the PSL-30/60 amplifier were increased and the transformer outlet was replaced by an RC [4]. The amplifiers were fitted to 6-channel anode and filament voltage control units. Portable MGPA generators were used to calibrate the amplifiers in the course of operation. The amplifiers were calibrated at the end of each recording cycle. An ROC panel* was used to record pendulum constants and control the polarity and magnification of the entire recording track.

The coastal seismic stations recorded the three-component (Z, H_1 and H_2) seismic waves, the second marks of the PC-6 chronometer, the detonation time, and the signals of the unified time service. Recording of pendulum constants, calibration and recording of amplifiers and galvanometers, and computation of magnification curves were done every year during the field season.

The magnification of recording channels at the central seismic station A is graphically depicted in Fig. 2. The magnification is regulated in steps. The maximum magnification at 10 Hz frequency is 300,000.

*ROC panel—Recording and operation control panel.

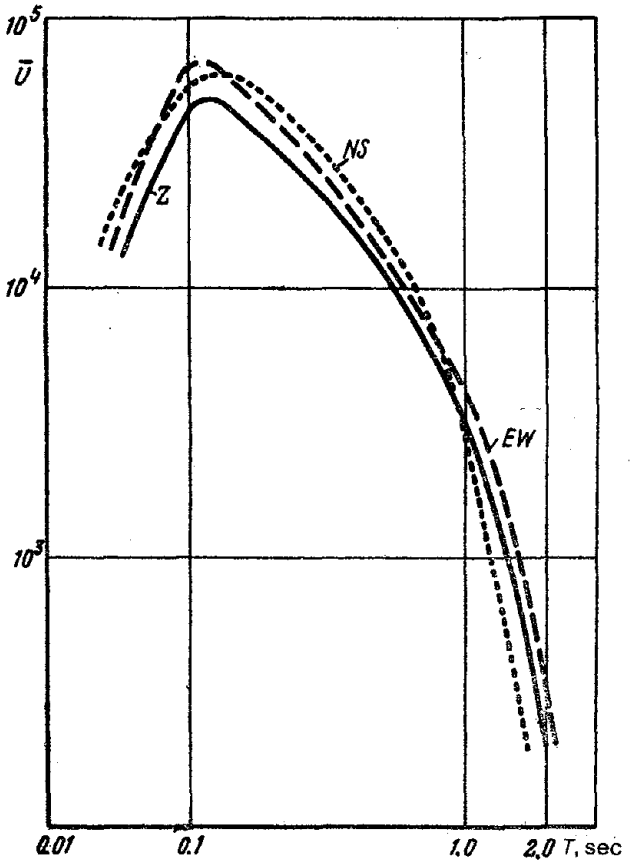

Fig. 2. Curves showing magnification of recording channels at station A.

RIS-30 type radio transmitters transmitted the detonation time and the time signals and maintained communications between the ship and the coastal seismic stations.

The detonation-generated shock waves were recorded by an N-700 oscillograph on two channels. The first, the galvanometric (NS-3 pendulum, M001-1 galvanometer, $\bar{V}$-50) channel, was meant for energy and form control of the detonation impulse. The second channel (hydrophone, amplifier, M001-2 galvanometer), the higher-frequency one, recorded reflections from the bottom which allowed the depth of the sea at the detonation point to be determined. The signal from the hydrophone amplifier reached the detonation time recording unit (DTRU), which produced the detonation time and time signals transmitted to the radio receiving station. These signals were

transmitted at 1250 Hz carrier frequency. The DTRU had a flip-flop circuit, a carrier-frequency generator and a quartz clock with 1 and 0.1 sec divisions. All signals transmitted to the radio receiving station were recorded on an N-700 oscillograph. The true detonation time was recorded concurrently. For this purpose a wire loop containing a small battery fastened to the detonator and connected with one of the galvanometers of the oscillograph was paid out from a special windlass [6, 7].

The detonator exploded at a depth of 90 m. Large standard detonators weighing 135 kg were dropped from the ship cruising at a speed of 15–18 knots. Two-way radiocommunication was maintained between the ship and the coastal seismic stations. The time signals were transmitted from the ship by radio for 3 min before detonation. The transmission of time signals was halted as soon as the detonation occurred and recording was started at the coastal seismic stations. Thereafter, as the shock waves generated by the detonation reached the ship, the signal of the detonation time was generated by the hydrophone impulse for 1.8 sec after which time signal transmission was resumed. The recording was continued for 2 min at the coastal seismic stations and for 10–15 sec on the ship.

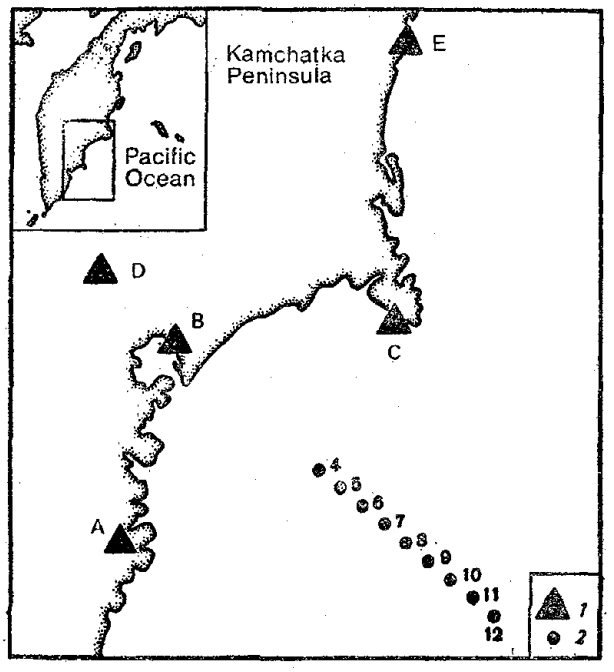

Fig. 3. Sketch map showing location of coastal seismic stations (1) and detonation points (2).

The relative location of the detonation points and coastal seismic stations (Fig. 3) ensured translucence of the focal zone in Avacha Bay in three different directions. The distance of the detonation points from the coastal seismic stations varied from 69 to 221 km, so that various layers of the crust from the upper strata to the mantle could be prospected. The observation system enabled recording of detonation-generated seismic waves propagating through the earthquake focus zone longitudinally (coastal stations C and E) and transversely (coastal stations B and D). If necessary the observation system could be widened by carrying out detonations at additional points where reference detonations were conducted in 1967–1968.

REFERENCES

1. Fedotov, S.A. et al. 1970. Investigation on earthquake prediction in Kamchatka. *Tectonophysics*, No. 9.
2. Myachkin, V.I. et al. 1972. The study of variations in geophysical fields near focal zones of Kamchatka. *Tectonophysics*, **14**.
3. Eisler, J. 1969. Investigation of a method for determining striae accumulation at depth. *Bull. Seismol. Soc. America*, **59**, No. 1.
4. Iizuka, S. 1971. Measurements on the time variations of seismic wave velocities by explosion-seismic method. Report of the CCEP, **6**.
5. Konovalov, V.V. and L.I. Kuznetsova. 1962. Sudovye radionavigatsionye ustroistva (Radionavigational Devices in Ships). Morskoi Transport, Moscow.
6. Sb. Razvedochnaya i Promyslovaya Geofizika (Collection: Exploration and Industrial Geophysics). No. 23, VNII Geofizika, Moscow, 1958.
7. Maksimov, O.A., V.I. Myachkin and V.B. Preobrazhenskii. 1969. Otmetka momenta vzryva pri seismicheskikh rabotakh na more (Recording of Detonation Time during Seismic Work at Sea). *Tr. IFZ*, No. 5, Nauka, Moscow.

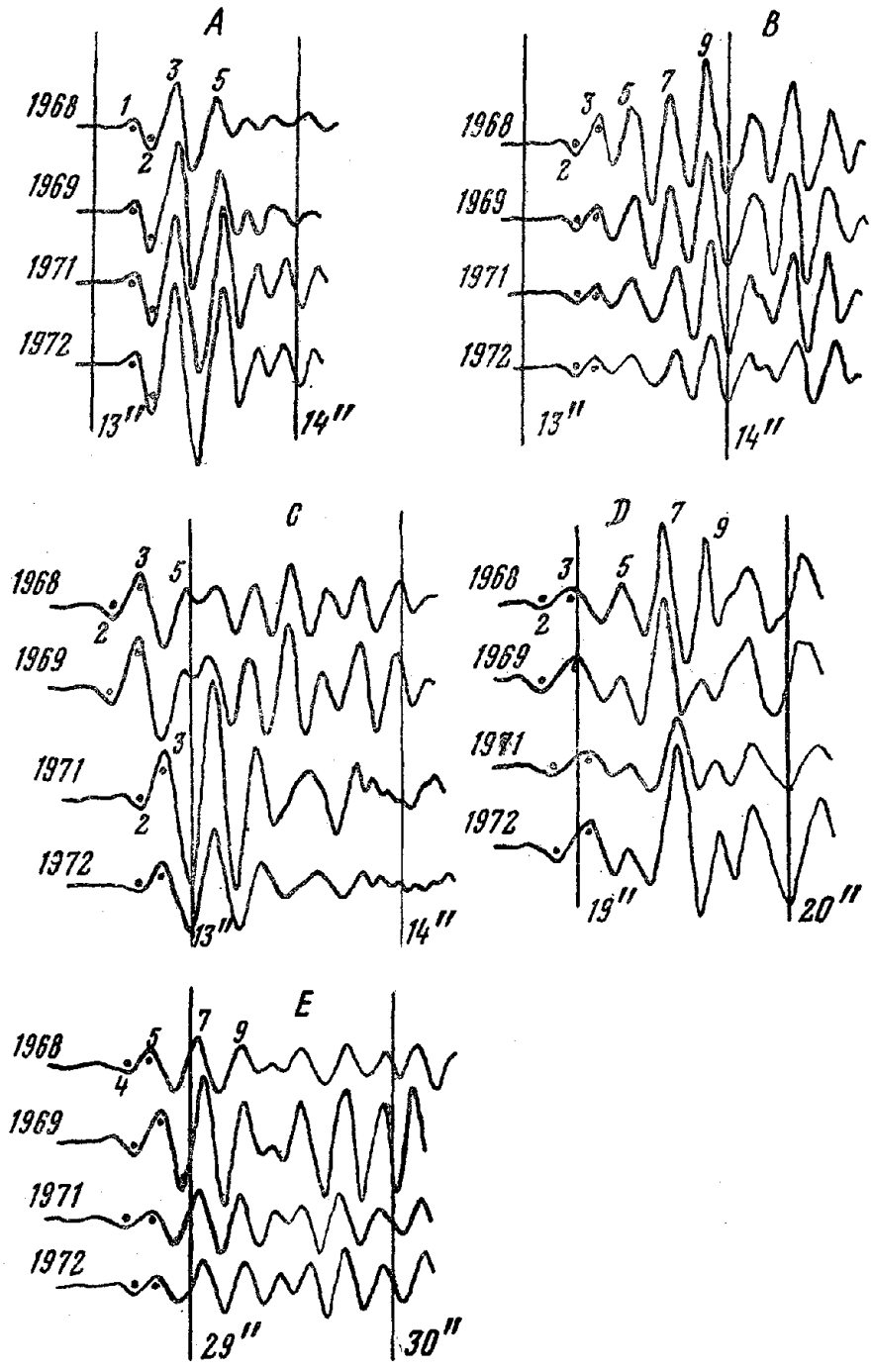

Fig. 1. Specimen seismograms obtained at stations A, B, C, D and E.

apparatus. But if replacement of the apparatus was unavoidable due to some fault, this was placed on record, so that any phase changes occurring thereafter could be easily detected and averted. Constancy of the characteristics of the apparatus assembly at a station was ensured in the field by recording the constants.

Replacement of coordinate plotting boards could shift the detonation points by as much as 50 m. In the worst case the systematic time shift did not exceed 0.01 sec when the distance in the direction of the receiving station increased (or decreased) by 50 m, provided that the wave traversed the whole of this additional path at an average velocity of 5 km/sec. Use of the same hard plotting board since 1969 precluded this type of systematic error.

The random error in determination of the time of wave travel from the detonation point to the station is the sum of random error in measurement of the time of wave travel from the hydrophone to the seismograph and random error in determination of the correction:

$$dt = dt_i + d(\delta t).$$

The random error in the measurement of dt_i can be expressed as

$$dt_i = \sqrt{(dt_i)_1^2 + (dt_i)_2^2 + (dt_i)_3^2},$$

where $(dt_i)_1$ is the error in seismographic measurements; $(dt_i)_2$ is the error in time determination due to scatter of detonations with depth; and $(dt_i)_3$ is the error in time determination due to scatter of detonations at the point relative to the theoretical detonation point.

1. The error in $(dt_i)_1$ measurements does not exceed $\pm$ 0.01 sec (recording speed $\sim$ 40 mm/sec, observed frequency $f \sim$ 5 Hz). This result was checked by repeated measurements of the same phase by different interpreters. The measurement scatter always fell within $\pm$ 0.01 sec.

2. The distribution of detonation depths h for all the years of observations was studied to derive the value of $(dt_i)_2$. As shown in Fig. 2a, it has a vividly expressed asymmetry. However, the detonation time, on which alone the detonation depth would seem to depend, is distributed according to the normal law (Fig. 2b). Special study of the causes of the observed h-distribution features showed that depth variations were due not only to detonator faults but also to the initial conditions of the detonator drop. Further, orientation of the cylindrical detonators with respect to the surface of the sea made a big difference to the depth of detonation. Ignorance of this factor was responsible during 1966–1969 for wide depthwise scatter of detonators.

As is evident from the figure the maximum number of detonations was in the depth range 75–100 m which may cause a time variation $(dt_i)_2$ of $\pm$ 0.015 sec for the first-arriving waves.

3. Error in the position of the ship at the theoretical detonation point strongly affects the results of measurements. The accuracy of coordinate

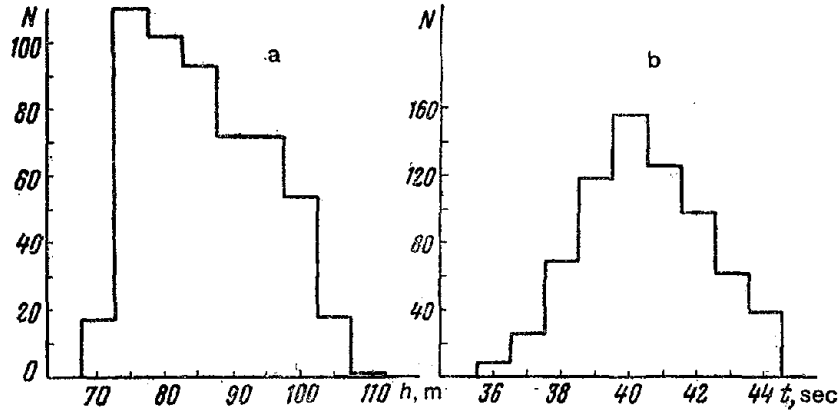

Fig. 2. Histograms of (a) detonation depth h and (b) time of detonator triggering t_b during 1966-1972.

determination at sea is $\pm$ 50 m provided the whole coordinating system in the PRD 4–8 functions reliably. However, to this error is added unavoidable error in detonator dropping due to objective and subjective circumstances of detonation (operator's personal error, delay of command aboard ship, wind, current, roughness of the sea, etc.). This error was determined from the data on the coordinator function for three "typically excellent" arrivals, results of which are given in Fig. 3. It is evident from the figure that $|\Delta r| =$ (0–50) m, the average being $\overline{|\Delta r|} = 30$ m, accounts for 94% of the detonations. The average value is taken as reliable. Thus the total error in detonator drop should not exceed $\pm$ 80 m and $(dt_i)_3$ should be $\pm$ 0.016 sec. Errors in excess of $\pm$ 100 m are considered gross and the corresponding measurements are discarded.

Thus the random error in seismographic measurement of wave travel time, comprising the sum of the individual random errors $(dt_i)_1$, $(dt_i)_2$ and $(dt_i)_3$, in accordance with the estimates given above is $\pm$ 0.025 sec.

Let us now determine the accuracy of calculation of the correction factor δt. The calculation is made in accordance with the scheme given in Fig. 4 as follows:

$$\delta t = \frac{\sqrt{h^2 + (V_{sh}\, t_b + a^2)}}{V_S},$$

where h is the detonation depth; V_{sh} is the speed of the ship at the detonation time; t_b is the interval from when the detonator enters the water until the shock waves reach the ship; a is the distance from the stern of the apparatuses recording the shock waves on the ship; V_S is the velocity of sound in water.

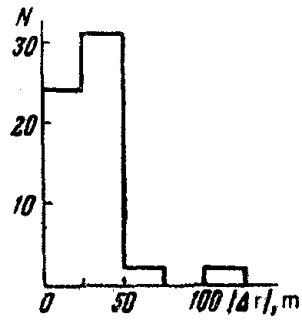

Fig. 3. Distribution of absolute departures $|\Delta r|$, m of points of detonator submergence from theoretical for July 26 and Sept. 21-22, 1972.

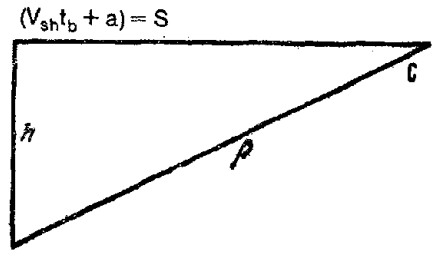

Fig. 4. Scheme for calculation of δt (sh—ship).

The known correlation of the times of first pulsation of gas bubbles formed by underwater detonations and the depth for detonators of constant power is used for the measurement of the detonation depth h [4]. The pulsation time is determined from the recordings of the apparatus assembly on the ship with an accuracy better than $\pm$ 0.010 sec, allowing determination of the detonation depth to an accuracy of $\pm$ 5 m.

The average ship's speed at the time of the detonation is determined from the log to an accuracy of $\pm$ 5%. The time t_b is measured with a stop watch with an error of $\pm$ 0.05% and the distance a with an error of $\pm$ 1 m. The velocity of sound in the upper water body may vary from season to season to the extent of $\pm$ 1%. Differentiating the expression for δt determination and including the cumulative error of its individual terms, we find the error $d(\delta t)$ to be $\pm$ 0.015 sec.

The true correction factor δt_{tr} determined to an accuracy of $\pm$ 0.005 sec was recorded in 1966 and 1972 on the ship for several detonations. In all 22 tests were performed to show that the average absolute value of $\overline{|\delta t_{tr} - \delta t_{theo}|} = 0.01$ sec. These experiments confirmed the correctness of the $d(\delta t)$ error value obtained above.

The error $d(\delta t)$ should be added to the random error in seismographic determination of dt_i so that we finally find $dt = \pm 0.04$ sec. In the worst case the maximum possible error of dt can be ± 0.06 sec when all the random errors with the same sign are summed. A major error is generally due to error in stationing the ship at the fixed point. In the region in question there is no more accurate system of ship stationing at sea, and random error can be reduced only by increasing the number of observations. Therefore the detonations were carried out as far as possible in series repeated on different days of the season.

Observations revealed that the average standard deviation of time S for a series of three to five detonations does not exceed ± 0.03 sec. Thus $S(n = 3\text{–}5)$ for the detonations at the PRD 4 during 1966–1969 was distributed at stations A, B and C as follows:

< 0.01 sec	4
from 0.01 to 0.02 sec	9
from 0.02 to 0.03 sec	9
from 0.03 to 0.04 sec	1
$\geqslant 0.04$ sec	0.

The maximum possible error of a single observation diminished $\sqrt{n}$ times with an increased number of observations, supporting the random pattern of the above errors.

The random error in wave arrival time differences Δt at two stations lying on the same azimuth are obtained by summing the random errors in t-values determined seismographically at the two stations as

$$d(\Delta t) = dt_1 + dt_2,$$

where 1 and 2 are the station numbers.

The errors in detonation coordinates and depths affect the measurements at the stations identically. Therefore, on the face of it the error $d(\Delta t)$ comprises only the errors in measuring operations, and thus in the worst case $d(\Delta t) = \pm 0.02$ sec for a single measurement. However, Δt is an unknown function of the velocity and path of elastic waves. It is to be expected that slight variances near the PRD would cause marked changes in Δt if there were pronounced local heterogeneities at the detonation point or in the path of the elastic wave propagation. Therefore the constancy of the Δt values should be checked. For this purpose special series of detonations were carried out in 1968, 1971 and 1972 with predetermined scatter of coordinates near PRD 4, 6 and 8. The experiments revealed that the difference in the time of wave travel transverse to the focal zone $\Delta t_\perp$ depends very little on the error in detonation coordinate and depth. With $\Delta r \leqslant \pm 350$ m in different directions from the theoretical point and with the depth varying within ± 15 m the difference $\Delta t_\perp$ varied within $\leqslant \pm 0.01$ sec.

The difference $\Delta t_\parallel$ in the same experiments was dependent on the PRD

locations and Δr values. The results of Δt measurements are given in Table 1.

It is evident that near the PRD 4 and 6 $\Delta t_{\parallel}$ varies very widely with the error in the detonation coordinates. This is perhaps attributable to the difference in the structure of the upper crustal strata in somewhat different azimuthal directions. Thus the divergence of the azimuths from PRD 4 at stations E and C is 30°. At PRD 8 it drops to 10° and the epicentral error there hardly affects $\Delta t_{\parallel}$.

Table 1

PRD	$\Delta r < 100$	$100 \leqslant \Delta r < 200$	$200 \leqslant \Delta r < 300$
4	± 0.01	± 0.015	± 0.035
6	– 0.01 –	– 0.015 –	– 0.035 –
8	– 0.01 –	± 0.01	± 0.01

Summing up, it can be said that by appropriate choice of data (taking the results in Table 1 for $\Delta t_{\parallel}$ into account) the difference Δt can be measured three times as accurately as the wave travel time t. For this purpose a large number of measurements are used because even the "gross" errors $100 \leqslant \Delta r < 300$ m are not discarded. This, of course, raises the reliability of statistical estimates of Δt as compared to the same estimates of t.

Results of observations. Let us consider the pattern of Δt measurements with time in two perpendicular directions: parallel and transverse to the focal zone.

Figure 5 shows the average seasonal values of $\Delta t_{\perp} = t_D - t_B$ (Fig. 5a) and $\Delta t_{\parallel} = t_E - t_C$ (Fig. 5b). The $\Delta t_{\parallel}$ values obtained from the detonations at PRD 6 were ignored because the waves generated by a detonation at this point damp strongly while propagating toward station C and are very rarely distinguishable from the background noise. A 90% confidence time is assigned in Fig. 5 to each value of $\Delta t_{\perp}$ and $\Delta t_{\parallel}$.

The variation in differential parameters with a probability not lower than 0.9 is significant. The behavior patterns of $\Delta t_{\perp}$ and $\Delta t_{\parallel}$ differ. For instance, while transverse to the focal zone the differential parameter rises at PRD 4 and 6 from 1968 through 1969 and at PRD 8 from 1969–1970 through 1971, parallel to it the parameter either remains unaltered (PRD 4) or declines systematically (PRD 8). Admission of variation in Δt entails recognition of time variation, even if it cannot be proved statistically.

Let us now consider the variations in the average seasonal values of absolute wave travel times at station B (transverse to the zone, Fig. 6a) and C (parallel to the zone, Fig. 6b). The confidence times in Fig. 6 were of the same significance.

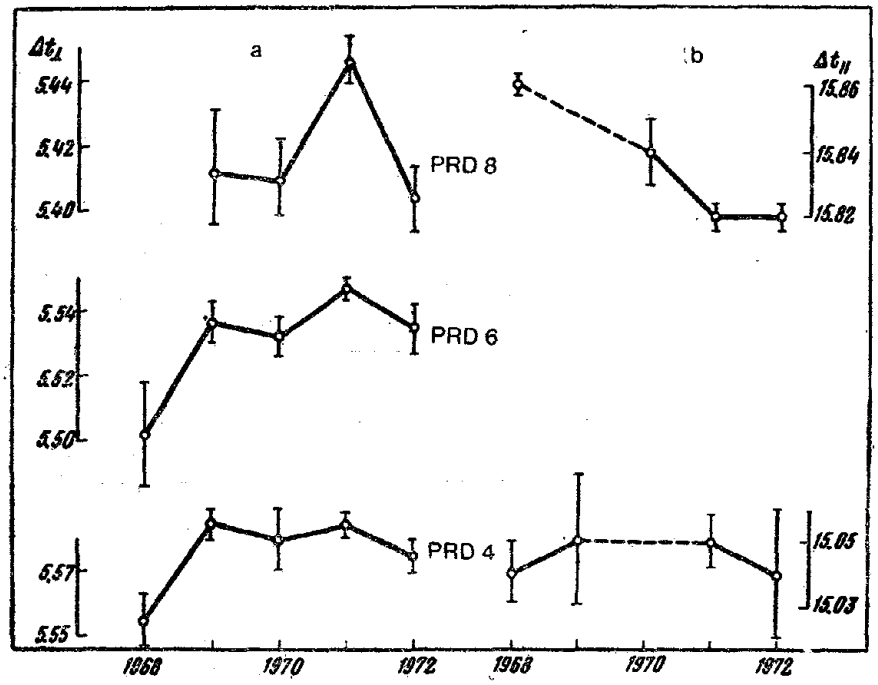

Fig. 5. Variations in average values of differential parameters:
a—Transverse to focal zone, $\Delta t_{\perp}$; b—Parallel
to focal zone, $\Delta t_{\parallel}$.

The wave travel time t_B was found to increase in a direction transverse to the focal zone. The rise in the differential parameter $\Delta t_{\perp}$ was caused by the relatively steeper increase in the travel time at station D. These variations are not related to the zone of elastic wave origin since the increase in t_B and t_D would be identical and simultaneous if they were. They are also unrelated to the elastic wave recording zone, for then they should differ for t_B and t_D in detonations at the three points. It can therefore be suggested that the place of time anomaly lies in the deeper crust. The waves recorded at both stations, as stated above, transverse their major path at depths of ~ 10 km. Unquestionably, however, the first-arrival waves recorded at station D come from relatively deeper areas than those recorded at station B. The rise of t_D pre-eminently at PRD 4 and 6 and of t_B at PRD 8 in 1968–1969 suggests that t varies within a relatively narrow depth range. By 1971 the anomalous region of higher t values had widened and embraced deeper areas at PRD 8 (station D).

In a direction parallel to the focal zone the behavior of t_C is quite different, depending on the location of the detonation point. The time t_C did

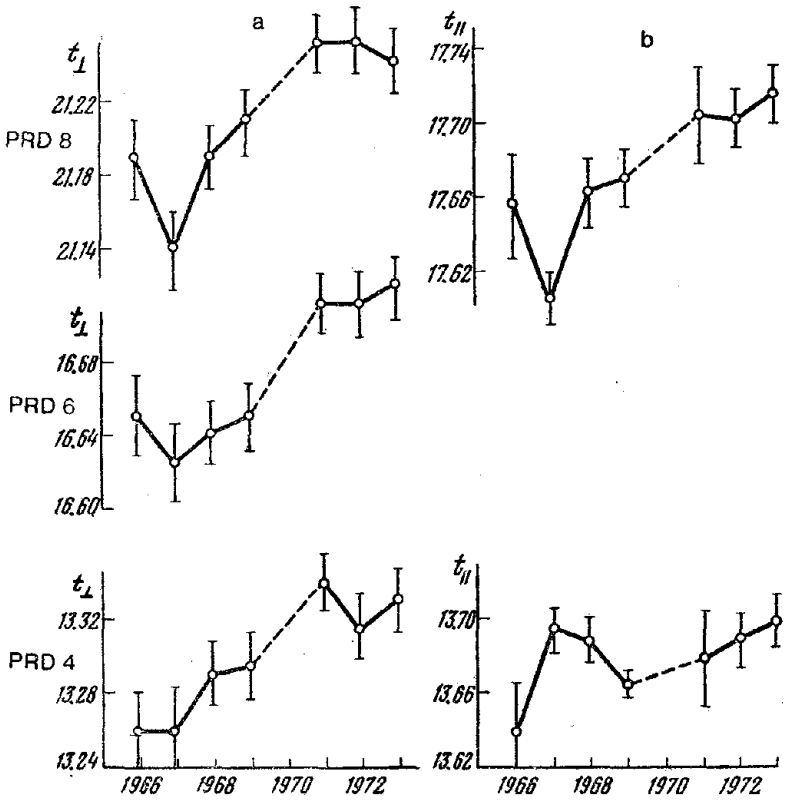

Fig. 6. Variations in average wave travel times:
a—At station B, $t_\perp$; b—At station C, $t_\parallel$.

not vary noticeably in the PRD 4 routes (station C) during 1968–1972. The differential parameter $\Delta_\parallel$ did not vary either, indicating that the travel time t_E also remained constant during this period at station E recording waves through the deepest zones. On the contrary, the time t_C increased continuously from 1968 through 1971 in the PRD 8 route (Station C). This explains the decrease in the differential parameter $\Delta t_\parallel$ during these years. The time t_E remained unchanged in this case.

Thus the travel time of waves penetrating to depths $H \lesssim 10$ or more than 20–30 km was not found to vary appreciably in a direction parallel to the focal zone during 1966–1972. The anomalous region here seems to embrace intermediate to depths of $\sim$10–20 km.

Simultaneously with the inrcease in wave travel times t_B, t_C and t_D, the wave travel times were also found to increase in one more direction at station A. The variations in t_A are shown in Fig. 7. A distinct t_A maximum for 1971 is a typical feature of all the curves.

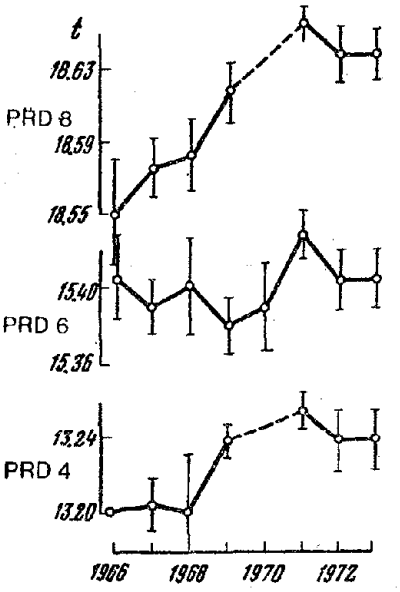

Fig. 7. Variations of average wave travel times at station A.

Collection of the measurements reveals that at least at certain periods the abyssal processes develop unevenly in time and space. Sharper variations transverse to the focal zone are typical for 1968–1971, perhaps due to stress variations essentially in definite directions.

Table 2 shows the maximum average seasonal travel time variations during the observation period with reference to 1971. The constancy of velocity in water and the upper layers of the sedimentary strata was considered in the computation.

The variations in elastic wave velocities in an extensive zone stretching linearly not less than 100 km and localized in deeper crustal strata seem to be related to the preparation of the strong earthquake that occurred during

Table 2. Maximum variation of $\frac{\Delta t}{t}$ (%) $\approx \frac{\Delta V}{V}$ % in different directions

PRD	Station			
	A	B	C	D
4	0.55	0.85	0.40	0.65
6	0.40	0.70	—	0.65
8	0.80	0.65	0.75	0.45

the November 24, 1971 expedition observations. (The epicenter was Avacha Bay in a region lying between PRD 4–6 and station C, $M = 7.2$ and depth $H = 100$ km.) The fault did not reach the surface and is estimated from the spread of the aftershock zone of over 50 km [5]. It is significant that the maximum travel times noted before the earthquake persist in subsequent years at a comparable level. This fact can be interpreted as restoration of the normal velocity field before earthquake initiation. The anomalous field for earthquake with $M = 7.2$ [6, 7] may persist for about 10 years. Therefore it is not improbable that by the time we started our observations in 1966 the velocities under the Avacha Bay floor were already highly variable and we recorded the second half of the forerunner bay.

A 0.4–0.8% variation in elastic wave velocities roughly corresponds to a horizontal stress drop by 50–100 kgf/cm^2.

The variations in wave travel time differences at stations B and D are shown in Fig. 8. It is evident that marked momentary fluctuations correlatable in time with the variations in electrotelluric currents [8] occurred just before the November 24, 1971 earthquake. Proximate analysis at the end of the season in 1972 showed steep fall in the wave travel times t_B and t_D at stations B and D as well as in the difference $\Delta t = t_D - t_B$.

A.M. Paleonov and R.P. Solov'eva predicted a strong earthquake in the area of observations in December, 1972 and informed the IFZ accordingly. Indeed, an earthquake of $M = 6.0$–6.5 occurred in this area on December 25, 1972.

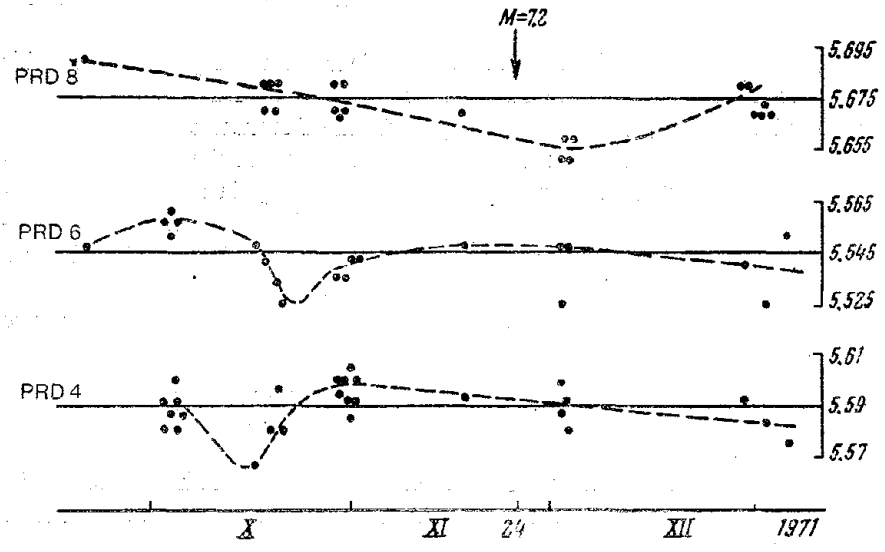

Fig. 8. Variation in wave travel time of $\Delta t_\perp$ in 1971.

CONCLUSION

1. Representative data allowing determination of variations in the kinematic parameters of elastic waves with time were obtained by seismic sounding of the crust under Avacha Bay during 1966–1972.

2. A region stretching not less than 100 km where wave travel times increased by 0.40–0.80% by 1971 was identified at crustal depths of 10–20 km under Avacha Bay.

3. The variation pattern of wave travel times during 1966–1972 and the size and duration of the region of variations do not contradict the view correlating the formation of this region with the preparation of the November 24, 1971 Petropavlovsk earthquake.

4. Temporary fluctuations of travel times were noted just before the November 24, 1971 earthquake.

REFERENCES

1. Myachkin, V.I. et al. Apparatura i metodika rabot po prosvechivaniyu ochagovykh zon zemletrysenii (Apparatus and method of study for sounding earthquake focus zones). This collection, p. 169.
2. Tulina, Yu.V., S.M. Zverev and G.A. Karsil'shchikova. 1972. Zemnaya kora i verkhnyaya mantiya v oblasti fokal'noi zony u Vostochnoi Kamchatki (Crust and upper mantle of the earth in eastern Kamchatka focal zone). Sb. *Seismicheskie Svoistva Granitsy Mokhorovichicha.* Nauka, Moscow.
3. Myachkin, V.I. et al. 1972. The study of variations in geophysical fields near focal zones of Kamchatka. *Tectonophysics*, **19**, 2.
4. Kaul, R. 1953. Podvodnye vzryvy (Submarine Detonations). IL, Moscow.
5. Gusev, A.A. and L.S. Shumilina. 1974. Makroseismicheskii effekt Petropavlovskogo zemletryaseniya 25 Noyabrya 1971 goda na territorii Kamchatskoi oblasti (Macroseismic effect of the November 25, 1971 Petropavlovsk earthquake in the Kamchatka area). Sb. *Sil'nye Kamchatskie Zemletryaseniya 1971 Goda.* Nauka, Vladivostok.
6. Rikitake, T. 1969. Approach to prediction of magnitude and occurrence time of earthquake. *Tectonophysics*, **9**, 2.
7. Myachkin, V.I. and S.I. Zubkov. 1973. Svodnyi grafik predvestnikov zemletryasenii (Average graph of earthquake precursors). *Izv. AN SSSR, Fizika Zemli*, No. 6.
8. Sobolev, G.A. et al. Izuchenie mekhanoelektricheskikh yavlenii v seismoaktivonom raione (Study of mechanoelectric records in a seismic region). This collection, p. 196.

UDC 550.34.05.134

Numerical Modeling of Propagation of Seismic Rays through Earthquake Focus Zones

G.S. Kushnir and V.I. Myachkin

The paper reports the possibility of computer estimation of rays propagating through local inhomogeneities simulating earthquake focus zones. It is shown that in such models the rays and hodographs are deformed and bear anomalous features. The ranges of variation of apparent longitudinal wave velocities in the anomalous areas of the hodographs are consistent with the results of field experiments.

Much attention is being paid nowadays to the study of focus zones traversed by elastic waves generated by detonations and natural earthquakes whose foci are located in the anomalous zones of imminent earthquakes [1–4].

The results of field experiments depend on several factors, e.g. the structure of the medium in the area in question, the size, shape, and physical properties of the focus of the imminent earthquake, the observation system adopted, etc.

With the present state of seismology it is impossible to determine accurately the variation ranges of seismic wave velocities and amplitudes in earthquake preparation zones because the estimates of variations of the stressed state of the medium are rather conflicting. Rough estimates show that with a stress variation of the order of 10 mn/m^2 at depths of 5–15 km the velocity is likely to vary by 1–2% and the amplitude by 10–30% [5].

When the factors affecting observational data are many it is logically desirable to have an idea of the ones whose nature can be studied in detail on models. This aspect has been dealt with in many studies, like [6] on the physical modeling of the earthquake focus. However, the resolving capacity of this method is limited. For instance, introduction of the source into the model without spoiling it is difficult. Only certain special models of the focal zone, viz. a tensile crack, and inclusions with rigid boundaries can be created in experiments with specimens; study of each wave in a clean form is impossible; and so on. Thus, not only is the class of useful models limited, but certain subtle effects arising from elastic wave propagation through the focal zone model become inaccessible.

Mathematical modeling of elastic wave propagation through the medium is free from these inadequacies. Mathematical modeling has been the subject of extensive studies involving various modifications of algorithms and programs permitting numerical determination of rays and hodographs in complex heterogeneous media [7–9]. A detailed bibliography is given in [10].

An algorithm and an algorithm-based program allowing numerical determination of rays and hodographs in random three-dimensional heterogeneous media are described in [9]. In this program the model is represented by data on velocities at the nodal points of a three-dimensional orthogonal grid, and the velocity data for the intervening points are derived by interpolation. This representation in the models of the medium increases the computation time two to threefold, but compared to analytical description is better for analyzing real sections and models with local inhomogeneities.

Having an apparatus for analysis at their disposal, the authors proceeded to study the simplest model. This can tackle quite a wide range of probable situations.

This study analyzes a single-layer model I with a downward (X_3-coordinate) constant velocity gradient of 0.03 sec^{-1} and a surface velocity $C = 5.5$ km/sec. The choice of a single-layer model simplifies analysis because the number of different types of waves reaching the surface and hindering analysis of the effect of inhomogeneity on elastic wave propagation increases in multilayer models.

In model I representing a rectangular block with the linear dimensions $X_1 = 240$ km, $X_2 = 80.0$ km and $X_3 = 30.0$ km the local inhomogeneity simulating the focal zone of an earthquake is introduced along the coordinates X_1 and X_3. The maximum velocity increment found at the center of the inhomogeneity is 1.7%. The inhomogeneity is an elliptical cylinder whose generatrix is parallel to the X_2 axis. The axis of the cylinder lies on a line passing through the points P_1 (50.0, 0.0, 10.0) and P_2 (50.0, 80.0, 10.0) (Fig. 1). The semiaxes of the ellipse are $b_1 = 6.0$ km (along the X_1 axis) and $b_3 = 8.0$ km (along the X_3 axis). The inhomogeneity has no fixed boundaries and the velocities therein fall steadily to the velocity in the surrounding medium, i.e. they represent smooth differentiable functions.

The velocity profile for models I and II containing the inhomogeneity is shown in Fig. 2.

So far as these authors are aware, this is the first time such modeling has been done, and analysis of similar models is not available. In view of this, the linear dimensions of the model and the inhomogeneity were chosen so that data could be obtained for collation with the data from prospecting of focal zones of earthquakes obtained by the IFZ on the Kamchatka coast. At the same time the analysis was programed so that by altering the step on the network along each axis of the coordinates the linear dimensions of the model could be altered and different alternatives of the relative disposition

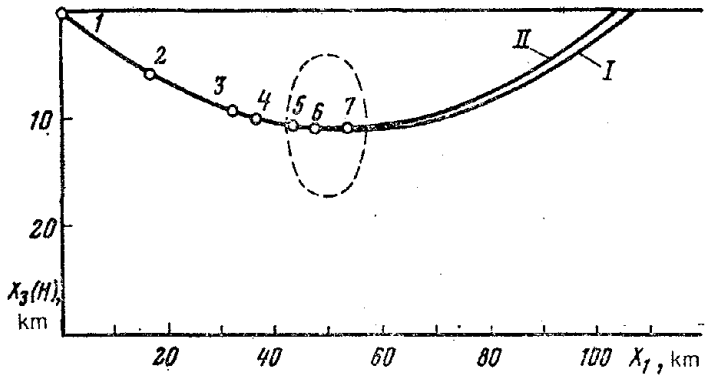

Fig. 1 Section of models along X_1 axis:
I and II—Rays passing through point on surface in models I and II, respectively. Sources lying on one ray in model II are denoted by circles and numerals. Inhomogeneity contours are shown tentatively.

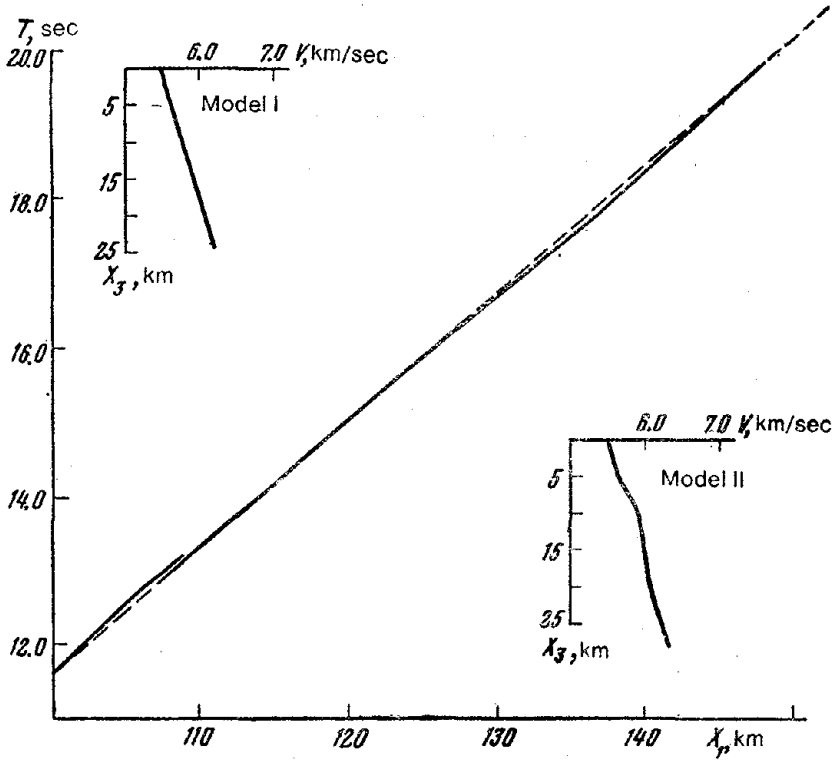

Fig. 2. Sections of hodographs constructed for source 1:
Broken line represents hodograph in model I; continuous line, that in model II.

of the inhomogeneous zone, the coordinates of sources and points of ray reception could be analyzed.

To analyze the models the source was placed on the surface of point 1 with the coordinates $X_1 = 0.0$ km, $X_2 = 40.0$ km and $X_3 = 0.0$ km, and the rays and hodographs for models I and II were computed by a program presented in [9]. After analysis of these rays a ray was constructed that corresponded to the point a on the hodograph for model II (Fig. 3), i.e. to the point of maximum regression of the hodograph, and six more sources were set on this ray. Sources 5–7 lie inside the inhomogeneity, source 5 being almost at its edge and 7 beyond its center. The rays were computed and the hodographs constructed (sections shown in Figs. 2 and 3) for all these sources.

From a comparison of the hodographs constructed for models I and II it is evident that in model II they are appreciably deformed. They show local

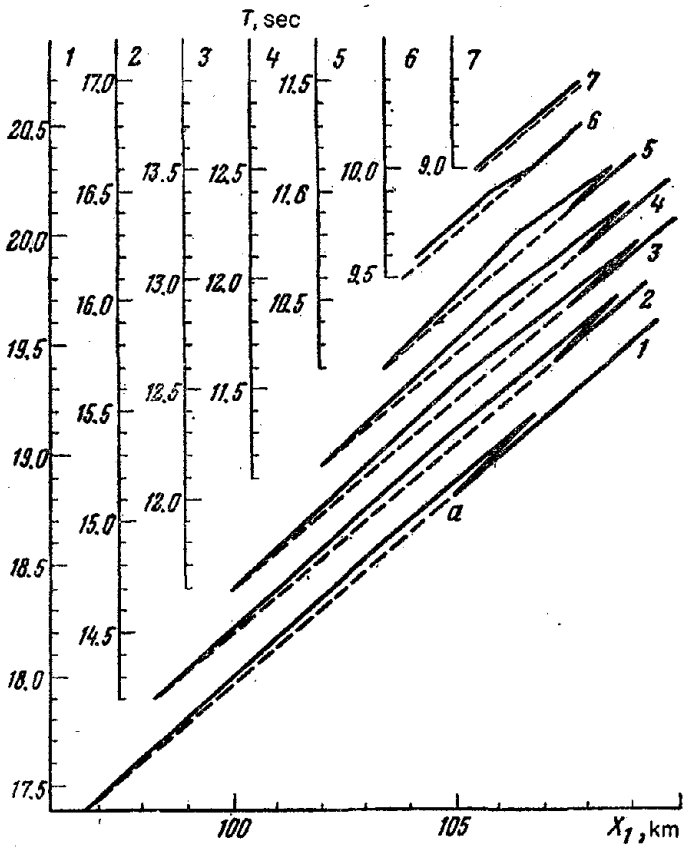

Fig. 3. Hodographs constructed for sources 1-7.

maxima and minima, and cusps whose location on the hodographs depends on the relative disposition of the source, and inhomogeneities. The divergence of the hodographs widens as the source approaches the inhomogeneity. In the process the length of the anomalous sections and the regression loop in the hodographs are reduced. In the case of source 7, the hodographs constructed for the models I and II coincide (within computational errors) throughout the length. This is because the rays in model II pass through the inhomogeneous zone where the velocity undergoes negligible change (about 0.1%).

Let us consider the hodographs in the loop region obtained for model II. For sources 1–6, in the anomalous region they are "hump-shaped" with a prominent local maximum (Fig. 3). The apparent wave propagation velocities measured from the "ascending" and "descending" sections of the hodographs differ materially for each of the sources (see Table).

Table

Hodograph section for analysis	Source				
	1	2	3	4	5
"Ascending"	5.570	5.520	5.500	5.400	5.100
"Descending"	5.780	6.130	6.370	6.670	6.770
Model I	5.760	5.870	5.920	5.940	5.960

The table shows that for sources 1–5 the difference in apparent velocities measured from various sections of the corresponding hodographs in models I and II ranges from $\pm$ 0.5 to $\pm$ 14.0%.

The variability of apparent seismic wave velocities at distances where anomalous distortion of the hodographs occurs conforms to the field data obtained, for instance in [4].

Let us consider in greater detail the sections of the hodographs bearing the regression loop (Fig. 3). As the trajectories of the rays approach the inhomogeneity center, around which the inhomogeneity gradient increases at the fastest rate, the rays progressively bend upward from their trajectories at the same angle of departure in the "smooth" model. Near the center of the inhomogeneity the rays travel on the average 0.03–0.06 sec faster than along the corresponding distance in the "smooth" model I. However, up to and beyond the inhomogeneity the rays traverse a longer distance than at the same points on the surface of the "smooth" model. Thus the effect of "acceleration" of the rays in the inhomogeneity is so to speak compensated by lengthening of their trajectory. They reach the surface of the model much later. The closer the trajectories of the rays come to the center of the inhomogeneity the greater their deflection on leaving the inhomogeneity, and in

the latter part of their trajectories the rays travel to the surface at high angles. The difference in the arrival times of the rays at the surface in models I and II is narrowed down. Yet their travel time in model II exceeds the time of ray propagation in the smooth model I.

The hodograph constructed for model II is deformed like a "hump" having a local maximum. After the inhomogeneity center is traversed by the rays the variation in the velocity gradient in the inhomogeneity acquires a different character, i.e. it becomes less than in the smooth model, and the lower half of the inhomogeneity deflects the rays downward. There appears a regression loop in the hodograph. With decreasing distance between the source and the inhomogeneity the length of the regression loop in the hodograph decreases and the time jump therein increases.

Let us compare the anomalies, i.e. the effect of hodograph deviation Δt in models I and II, with the location of the corresponding sources and the inhomogeneity. To have a very clear idea let us take the maximum deviations, which correspond to the bonding point, i.e. to the local maximum, in the hodographs of a model containing an inhomogeneity. It is evident from the graph (Fig. 4) that the maximum deviations are obtained for a source placed at the margin of the inhomogeneity.

The correlation between the magnitude of the effect and the increase in the distance up to the model of the focal zone can be used to explain the

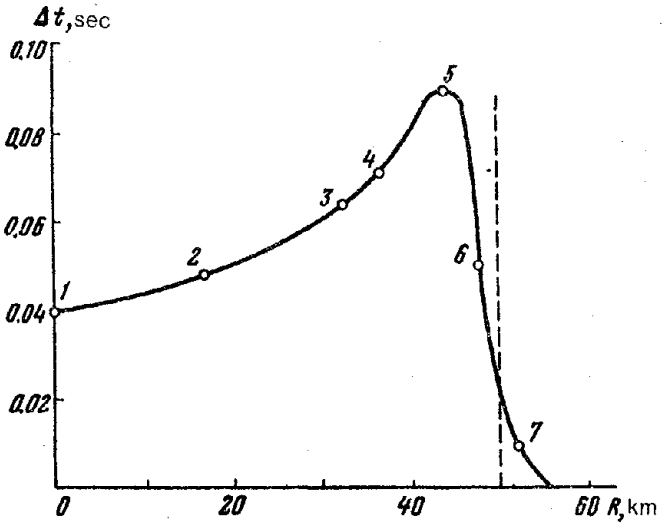

Fig. 4. Maximum divergence of hodographs in models I and II as function of relative disposition of sources and inhomogeneity:
Sources are denoted by circles and numerals, center of inhomogeneity by broken line.

effect of variation of the velocity ratio V_P/V_S and to delineate the zone where changes in the physical properties of the medium occur.

It is noteworthy that anomalous distortions occur even for rays propagating in the lower half of the inhomogeneity. The hodographs obtained for source 3 are cited in Fig. 2. However, since the variation in the velocity gradient is not as sharp in the lower half of the inhomogeneity as in the upper, the effect is less pronounced and the divergence of the hodographs does not exceed $\Delta t = 0.03$ sec in time. The distortion is noticeable on a large section of the hodograph. The ray propagation time in the inhomogeneity model is less than the propagation time of the rays reaching the same points on the surface of a "smooth" model.

Thus as a result of analysis, the effect of anomalous distortions of rays and hodographs are obtained for the model that takes into account the inhomogeneity in the shape of an elliptical cylinder with a maximum addition of velocity of 1.7% on its axis. The anomaly effect in the hodographs is pronounced and is much in excess of experimental error.

Ray and hodograph distortion is observed on the surface for preset disposition of sources and inhomogeneity at definite distances. Hence, in real field experiments in the prospecting of earthquake focus zones the results partly depend on the observation system adopted.

The experimental data on the prospecting of earthquake focus zones by detonations carried out by the IFZ on the Kamchatka coast are cited in [1]. The rising trend of absolute travel time t_r observed at some stations and the mounting difference of elastic wave travel times Δt at stations B and D during 1968–1971 are noteworthy. It is believed that changes in the mean values of t and Δt by 1971 were stimulated by the preparation of the earthquake that occurred on Sep. 24, 1971 near the Kamchatka coast. Assuming that travel times varied uniformly throughout the observation zone and that ray lengths remained unaltered, the authors of the paper found that the seismic wave velocity fell on an average by 0.3%. Let us analyze these data in the light of the results obtained in this paper.

It follows from Fig. 3 that a rise in absolute wave travel times may occur when the reception points are located at distances where "hump-shaped" distortions are observed in the hodographs. Consequently a simultaneous rise in absolute wave travel times t and average travel time differences Δt for a pair of stations is realizable provided the stations lie at distances where the rays yielding the "ascending" part of the hodograph are received.

Thus, granting that stresses increased in the part of the medium through which seismic waves with anomalous arrival times propagated and that the form of the anomalous zone was close to the inhomogeneous zone investigated, it may be suggested that the seismic wave propagation velocities increased in the anomalous zone. The data cited in the table and in Fig. 4 show that for sources lying near the inhomogeneity a slight change in coordi-

nates appreciably affects ray and hodograph distortion. For instance, sources 5 and 6 differ according to the X_1 coordinate by 4 km and the difference in the maximum divergence of their hodographs is twofold (Fig. 4). Thus when using data obtained with nonfixed seismic wave sources, as was done in [2, 4], the difference between the seismic wave arrival times recorded at two stations should be treated with definite caution.

Finally, the following conclusions can be drawn:

1. Computerized modeling in principle allows assessment on the surface of the effect of a local inhomogeneity simulating the earthquake focus zone under preparation, on the seismic waves propagating through it.

2. Given the structure of the medium in the area in question this modeling permits us to assess the scope of different observation systems and to select the best.

3. The hodograph alters in a complicated way and has an extended section of travel time fall due to the increased length of the rays. In the process this effect of time change may greatly surpass in magnitude the effect arising from the increase in velocity in the inhomogeneous zone, and the net change may have a different sign to that of the latter.

4. Numerical modeling confirms once more that at least for the study of focal zones 10 km across the profile observation system may permit reliable determination of the variations in elastic wave velocity and the signs of velocity increase in the developing focus zone. The shape and size of the zone of inhomogeneity and the magnitude of the velocity increase in the inhomogeneity can be determined to a first approximation.

5. The method evolved allows investigation of a wide class of physical models of inhomogeneities developing with time and more efficacious identification of earthquake precursors by seismic methods.

REFERENCES

1. Myachkin, V.I. and N.A. Dolbikina. 1973. Seismicheskoe "Prosvechivanie" ochagovykh zon (Seismic "sounding" of focus zones). Sb. *Predvestniki Zemletryasenii. Tr. IFZ AN SSSR*, VINITI, Moscow.
2. Nersesov, I.L. et al. 1973. Vozmozhnosti prognozirovaniya zemletryasenii na primere Garmskogo raiona Tadzhikskoi SSR (Scope of earthquake prediction with reference to the Garm region of the Tadzhik SSR). Sb. *Predvestniki Zemletryasenii. Tr. IFZ AN SSSR*, VINITI, Moscow.
3. Eisler, J. 1969. Investigation of a method for determining stress accumulation at depth. *Bull. Seismol. Soc. Amer.*, **59**, No. 1.
4. Stewart, G.S. 1973. Prediction of the Pt. Mugu earthquake by two methods. Proc. Conf. on Tectonic Problems San Andreas Faults System, Standford Univ. Press, **XIII**.

5. Tomashevskaya, I.S. 1970. Nekotorye rezul'taty laboratornykh izmerenii svoistv gornykh porod pri slozhnom napryazhennom sostoyanii (Some laboratory determinations of rocks in complex stressed state). Sb. *Fizicheskie Osnovaniya Poiskov Metodov Prognoza Zemletryasenii*. Nauka, Moscow.
6. Shamina, O.G. 1972. Model investigations of inclusions in medium. *Z. Geophys.*, **38**.
7. Oblogina, T.I. and Yu.A. Burmakov. 1971. Seismicheskie luchi i godografy v trekhmernoneodnorodnykh sredakh (Seismic rays and hodographs in three-dimensional heterogeneous media). *Izv. AN SSSR, Fizika Zemli*, No. 1.
8. Belonosova, A.V., S.S. Tadzhmukhamedova and A.S. Alekseev. 1967. K raschetu godografov i geometricheskogo rackhozhdeniya luchii v odnorodnykh sredakh (Computation of hodographs and geometric divergence of rays in homogeneous media). Sb. *Nekotorye Metody i Algorithmy Interpretatsii Geofizicheskikh Dannykh*, Nauka, Moscow.
9. Kushnir, G.A. and F.N. Pruchkina. 1974. Chislennoe opredelenie luchei i godografov v trekhmernykh neodnorodnykh sredakh (Numerical determination of rays and hodographs in three-dimensional heterogeneous media). Sb. *Vychislitel'naya Seismologiya*, No. 7, Nauka, Moscow.
10. Cerveny, V. 1972. Theory of elastic wave propagation in inhomogeneous media. *Z. Geophys.*, 38.

UDC 550.343.2

Study of Mechanoelectric Records in a Seismic Region

G.A. Sobolev, V.N. Bogaevskii, R.A. Lementueva, N.I. Mugunov and A.A. Khromov

The paper describes the prerequisites for the detection of electrical earthquake warning signals, the results of theoretical and laboratory studies, and the apparatus and techniques of field observations. It examines the strong earthquake warning signals recorded at Kamchatka and their computer analysis for prediction of earthquake occurrence times.

Preparation of strong earthquakes manifests itself in progressive fracture accompanied by variation in strain rates and stressed states in various areas of seismoactive regions. It is sensible to expect that emf will be generated in the earthquake preparation zone by natural mechanoelectric transducers.

NATURAL MECHANOELECTRIC TRANSDUCERS

It was suggested in [1] that piezo-, seismo- and triboelectric phenomena and electric potentials generated by deformed natural double electric layers and cracking should precede earthquakes. Nor can generation of charges in the earth due to movement of dislocations upon rock deformation be ruled out. Some of these mechanoelectric effects were studied quantitatively in laboratories and fields and some were merely identified.

The piezoelectricity of rocks was studied essentially under mechanical loads of variable signs during geophysical surveys. It was found that during the passage of elastic waves the electric signals recorded do not exceed a few tens of microvolts a meter [2].

The ratio of secondary energy generated by piezoelectric phenomena to the primary energy of elastic waves can be derived from the thermodynamic equation

$$\frac{\xi_{\text{piezo}}}{\xi_{\text{elastic}}} = \frac{\sum_{k}^{3}\sum_{m}^{3}\eta_{km}E_{km}E_{k}E_{m}}{\sum_{i}^{6}\sum_{j}^{6}c_{ij}\epsilon_{i}\epsilon_{j}},$$

where E, η, c and ϵ are respectively the electric field intensity, dielectric susceptibility, elastic constant, and elastic deformation.

Using equations of the type $E_k = \frac{1}{\eta_{ki}} e_{ki}\, \epsilon_i$, where e is the piezoelectric constant and expressing the parameters by numerical values characteristic, for example, of quartz-bearing piezoelectric rocks of the granite type, viz. $\eta \approx 0.6$, $e = 10^3$, and $c = 9 \times 10^{11}$ in CGSE units, we get

$$\frac{\xi_{\text{piezo}}}{\xi_{\text{elastic}}} = \frac{1}{\eta_{km}} \frac{e_{mi}\, e_{kj}}{c_{ij}} \approx 2 \cdot 10^{-6}.$$

With such a low effectiveness natural piezoelectric transducers are unlikely to show strong electric fields of a piezoelectric nature prior to earthquake. The scope of electric current generation in quasistationary processes in particular is not clear because the current density of bound charges is proportional to the rate of change of elastic stress or strain $j = \dot{\sigma} = \dot{\epsilon}$. However, our experiments consisting of recording electric current and stress during withdrawal of load from quartz-bearing rock specimens under the press demonstrated that current density to a maximum of 10 μa/m^2 can be obtained from unit surface of the specimen at an electric field intensity of as much as 4 mV between faces (Fig. 1).

The coefficient of piezoelectric activity $K_{\text{piezo}} = \Delta V / \Delta_\sigma$ was 10^{-3} V·cm^2/m·kg in the above experiments. The elastic stress drop during earthquakes is on the average several bars [3, 4]. The electric potentials developed in the process in granites may attain values of 10^{-2} V/m. These intensity values

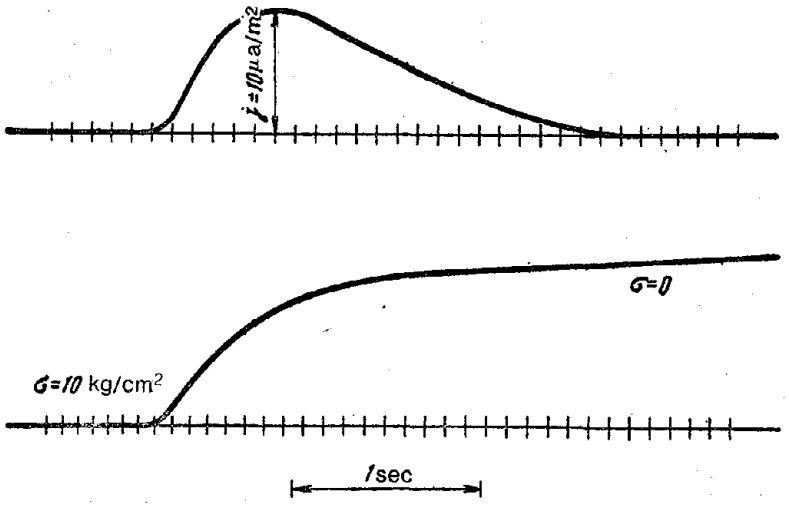

Fig. 1. Records of electric current in piezoelectric rock specimens during unloading.

should permit recording of electric fields of a piezoelectric nature in the neighborhood of epicentral zones. This estimate is based on laboratory measurements made at the elastic stress variation rate $\dot{\sigma} = 10^{-2}$ kgf/cm². Since the piezoelectric-type effect decreases in inverse proportion to $\dot{\sigma}$ and a field intensity of 10^{-6} V/m seems to be the lower limit of the experimentally recordable values, we can scarcely expect piezoelectric signals at elastic stress variation rates lower than 10^{-2} kgf/cm²·sec.

Another mechanoelectric effect common in rocks is produced by electrokinetic phenomena. Liquid movement through rock capillaries causes the positive electric charges occurring in the liquid to be isolated from the negative charges rigidly bound with the solid phase and facilitates development of a potential difference in the direction of movement. As a result of groundwater filtration electric fields of the intensity $E = (10^{-3}–10^{-4})$ V/m develop on hill slopes [5].

Knowing the hydrostatic pressure gradient from familiar hydrogeologic formulas [6], we can determine the coefficient of infiltration-electric activity by the equation

$$K_{\text{eff}} = \frac{E}{\Delta p} = (10^{-2}–10^{-3})\ \text{V}\cdot\text{cm}^2/\text{m}\cdot\text{kg}.$$

Moreover, direct flow potential measurements in rocks [7] also yielded the values

$$K_{\text{eff}} = 10^{-2}–10^{-3}\ \text{V}\cdot\text{cm}^2/\text{m}\cdot\text{kg}.$$

Hydrostatic pressure fluctuations of the order of 180 psi ($\sim$ 12 kgf/cm²) were recorded at boreholes 12 km from the earthquake focus zone in California [8]. Fluctuations of pipe water pressure in the pleistoseist zone of the Tashkent earthquake [9] reached 1 kgf/cm². Perhaps $\Delta p = 10^{-3}$ kgf/cm²·m would be the minimum hydrostatic pressure gradient in these cases, resulting in an expected electric potential of an intensity $10^{-5}–10^{-6}$ V/m. Electric potentials of such magnitudes can confidently be recorded.

Electric potentials are not the only mechanoelectric phenomena arising from the existence of double layers in rocks [10]. Our experiments disclosed that besides the electric potential difference along the solid-liquid phase boundaries, an electric field oriented perpendicular to the phase interface is also created by mechanical action on double layers. This mechanoelectric contact effect (MECE) is also observed in deformation of the interface of two solid bodies.

The mechanoelectric contact effect was studied in the laboratory at ultrasonic frequencies. The magnitude of electric potential increased steadily as the formation of the liquid (distilled water)-solid body (plexiglas) double layer progressed. The presaturation time was less when the experiment was conducted operating the ultrasonic sensor continuously than when the sensor

was operated intermittently. The effect did not change in magnitude when the electrode was carefully withdrawn from the liquid and inserted again, indicating the presence of a double layer strongly bound with the solid surface.

Experiments with solid specimens (Fig. 2) showed that the mechanoelectric effect arises not only due to deformation of rigid contacts, as for instance between metals and rocks, but also due to close disposition of the metallic electrode and the specimen. Similarly, in irradiation of a liquid-solid body contact the amplitude of the electric signal rises with the formation of the double layer, as observed on the oscillograph screen in the form of numerous high-frequency impulses. An interesting phenomenon was observed on transferring the electric potential difference to the specimen: the magnitude of the mechanoelectric effect can be greatly increased by changing the polarity of the battery. We observed the above phenomenon in the field as the elastic waves from detonations and earthquakes acted on the metallic receiving electrodes.

All three types of mechanoelectric phenomena are associated with the elattic deformation of rocks. Several electrical effects arise in the formation or growth of defects. The Stepanov effect, fairly well studied in crystals [11, 12], is one of those stimulated by the movement of dislocations. Recently this effect was produced in the laboratory by deforming an artificially created dispersed system [13]. Experiments with specimens composed of monomineral particles of various sizes revealed that the resulting electric discharge consists

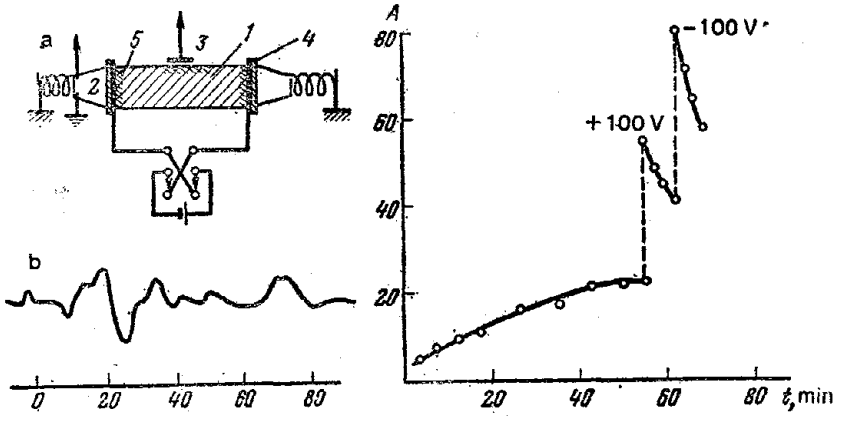

Fig. 2. Mechanoelectric effect of solid body contacts:
a—Measuring scheme: 1—rock specimen; 2—ultrasonic sensor; 3—receiving electrode; 4—electrode; 5—effect origin zone; b—Form of mechanoelectric contact effect; c—Amplitude variation of mechanoelectric contact effect with time and polarity variation of external field.

of a low-frequency component and higher-frequency impulses. The low-frequency component is associated with the failure preparation of the specimen as a whole. The higher-frequency impulses arise from the movement of the dislocations in isolated monomineral blocks. The duration of the electric discharge is proportional to the size of the block.

The potential difference of the low-frequency discharge on the faces of a concrete specimen deformed under room conditions reached 400 mV in these experiments. We observed electric discharges accompanying microfracture of rock specimens earlier [1]. The potential difference recorded was ~ 1 mV. The physical nature of this type of discharge may be linked with the adhesion phenomenon [14]. Triboelectricity, studied only qualitatively [15], may also be generated upon rock fracture. Besides the appearance of active electric sources in seismoactive regions, the electric potential of the earth may also be disturbed. In particular, our measurements in Kamchatka, described below, indicate the existence of calculable local electric fields. In such case a change in the tensor of electrical conductivity of rocks will lead to the appearance of fictitious electric sources inside the earth.

TECHNIQUE AND APPARATUS FOR FIELD STUDIES

The choice of Kamchatka as a region for field observations was dictated by three considerations. This is seismically the most active region in the USSR where several earthquakes of magnitudes higher than 5.5 occur annually [16]. A long-term (five-year) prediction schedule of places of strong earthquake occurrence has been prepared for the Kamchatka region [17], allowing the organization of electrotelluric observations in areas of expected strong earthquakes. Lastly the geoelectric profile of Kamchatka, where highly conducting sediments lie on the surface, is favorable for recording quasistationary electric fields of a deeper origin. Moreover, the low-resistance (ocean) and high-resistance (continent) medium boundary leads to current concentration [1] in the coastal strip, and becomes a natural amplifier. In consideration of these factors the electrotelluric field stations for studying earthquake warnings were located along the east coast of Kamchatka about 100 km apart (Fig. 23).

The natural electric field of the earth is complex in nature and varied in frequency composition. The ultrasonic sensing apparatus used in practice for recording temporary variations [18] allows a study of terrestrial currents in the time range of several seconds to several hours. We used such an apparatus for observations during 1966–1970. Along with its definite merits: high sensitivity, simplicity of operation, and great economy of current input—this apparatus also has notable drawbacks, which manifested in the study of quasiconstant electrotelluric fields. The main shortcoming is the sensitivity of the galvanometer to mechanical deformations and temperature fluctuations.

On the basis of the research carried out during 1966–1970, apparatus specifications were evolved for recording the natural electrotelluric field in seismoactive regions with a view to studying earthquake warnings and prediction. A new system of recording at the stations was introduced in 1971–1972.

The apparatus for the electrotelluric field (AETF) is meant for recording slow daily variations. A PS-1-08 automatic recording potentiometer is used as the recording device. The device measures and records the potential difference between points on the earth's surface as conveyed by the electrodes. The electrotelluric field apparatus also includes the ARP clock, a control unit, low-frequency filters, a timer, a transformer, and accumulators (Fig. 3).

The apparatus assembly can take 24 automatic measurements a day. The PS-1-08 potentiometer is multipoint and capable of measuring and recording 6 or 12 independent values. The scanning time of 6 channels is 1 min.

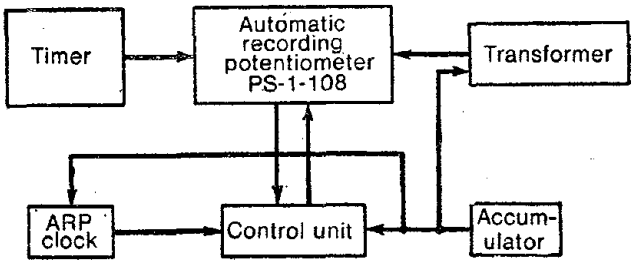

Fig. 3. Block diagram of apparatus for electrotelluric field (AETF).

The electrodes are lead bands 2500 cm² in area. The surface was cleaned before laying at a ground depth of 2 mm and they were then held in water in pairs to obtain an oxide film. Retention of the electrode in water facilitated curing, which reduced the time for attaining normal polarization. The potentials of normal polarization are stabilized in the course of 1.5 months after earthing the electrodes (Fig. 4).

The electrode couples were strewn with the same rock to reduce the potential difference of normal polarization of the pairs. It is very important that solders and connecting wires have high insulation properties, because contact between copper and moist soils results in the appearance in the recording line of parasite potentials varying with the moisture content of the soil. With a careful choice of lead in the couples and identical curing and earthing of electrodes in soils of the same composition the potential difference of normal polarization in the couples does not exceed 30 mV, making it possible to use PS-1-08 potentiometers with a more accurate scale.

Study of the properties of lead electrodes showed that in the Kamchatka environment the transient resistance of these electrodes with an area of 2500

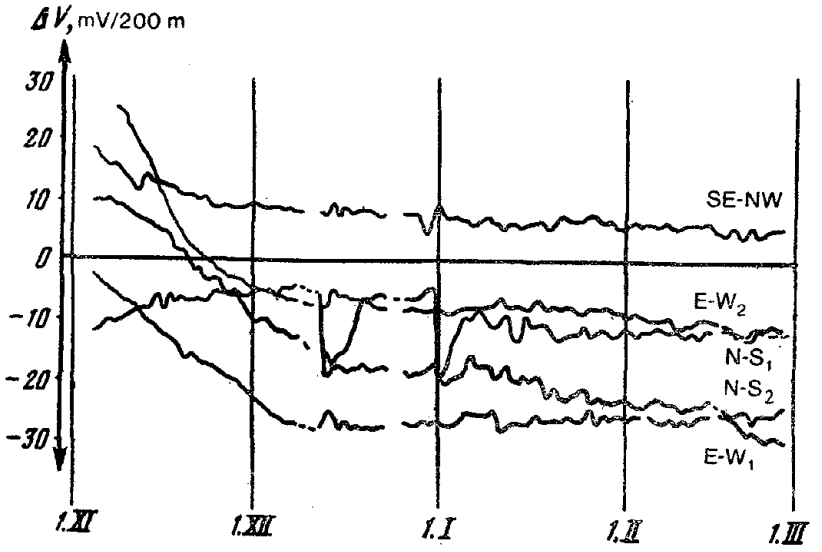

Fig. 4. Normal electrification of electrodes at station 4.

cm² is 1 k Ohm. Reduction of the electrode area to 100 cm² showed that the recorded potential difference of the external source was not affected, but the stability of the normal polarization is disturbed. When a branch resistance is provided in the measuring line the external signal is divided in accordance with Ohm's law. The normal potential of the line, for instance, in the absence of any external signal, does not alter in proportion to the introduced divider, with the result that the level of the field to be recorded alters spasmodically. A steep change in the record level also results from mechanical loading of the electrode. For instance, the field level altered by several millivolts when an explosion occurred near the electrode.

Since simultaneity of recording parallel measuring lines is very important for identifying earthquake warnings, in view of the difficulties involved the AETF operating on the principle of systematic electrode examination should ensure high reproducibility of recording of the channels. It is notable that much difficulty is encountered in multichannel measurement of the electrotelluric field using an array of sensors interlinked by the earth's distributed resistance. Different types of disturbances occurring in the earth are responsible for the appreciable divergence of the results of field tests of the apparatus assembly from the laboratory results.

The AETF for electrotelluric field measurement, which directly records the field level once an hour, enables us to analyze the field structure over a time span of several hours. The dynamic features of the record at each observation station are dependent on the geoelectric conditions in the area of

electrode earthing, the geographic location of the station, its proximity to the ocean, etc.

The potential differences in the main and backup lines are recorded at all stations in the N–S and E–W directions, maintaining the distance between the electrodes in the couples at 200 m. Besides, additional lines up to 1000 m long are installed at stations 2, 3 and 4. Fig. 5 shows the records of the field at these stations, displaying daily fluctuations due mainly to *sq*-variations. It is clear that the principal maxima and minima of the daily fluctuation appear synchronously at all stations.

The records of higher-frequency variations sometimes differ widely in amplitude even in parallel components. This is attributable to the fact that in systematic operation of the channels fluctuations may arise due to intense high-frequency variations at the instant of measurement. The daily electrotelluric field is polarized at all stations quasilinearly. Each measuring line has its own seasonal variation. The AETF enables us to detect anomalous variation in the electrotelluric field at least within a time span of several hours to several weeks.

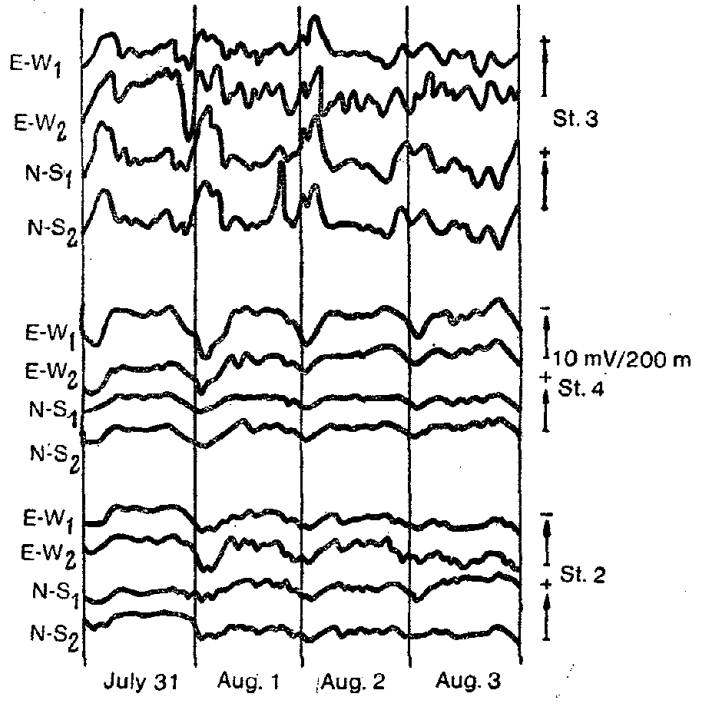

Fig. 5. Records of daily electrotelluric field variations in Kamchatka.

VARIATION IN ELECTROTELLURIC FIELD BEFORE STRONG EARTHQUAKES

According to the postulates of failure mechanics of statistically inhomogeneous media [19, 20] warnings of varying durations may be observed in the course of earthquake preparation. A general review of warnings [21] demonstrates that they may last from several minutes to several years in different geophysical fields. We are inclined to believe that there may be an almost continuous frequency spectrum of warnings, reflecting the process of fracture of blocks of rock on differing scales. Perturbations of the electric field before different earthquakes lasting for minutes or hours were cited in [1, 22, 23]. Electrotelluric field anomalies for several days are noted in [24–26]. Such warnings recorded before some earthquakes in Kamchatka are diagrammatically shown (in baylike form) in [27].

Analyses of anomalous fluctuations in the electrotelluric field lasting for several days are cited in the present paper because AETF operating intermittently does not allow analysis of field variations for periods shorter than several hours. On the other hand, the series of continuous observations made so far with the same sensor array is not adequate for analyzing slower changes lasting several months (due to problems involved in seasonal observations) or years. Thus the time range of analysis (several days) was chosen because of the great representative character of the data. It may be only part of a wider time range of the electric warnings.

In studies conducted during 1966–1970 using the ultrasonic sensing apparatus assembly appreciable background thermal and mechanical noise, specific for each channel, resulted in poor correlation of the records of parallel measuring lines (in the time range of several days). Consequently, even when the field variations before the earthquake markedly surpassed the background [26] it could not be ascertained whether the fluctuations in the parallel lines were synchronous. But it is essential to obtain this information so as to explain the nature of the warnings. The synchronous field variations and almost equal anomaly amplitudes in the parallel lines seem to mean that the anomalous variation is stimulated by a remote field source. Synchronous variation and inequality of amplitudes would have indicated that the source was located near the observation station. Lastly, lack of synchronism denotes that the alternations in the electrotelluric field level are induced by the process occurring in the immediate vicinity of the electrodes or at the electrode-soil contact.

Since 1971 use of the AETF immune to thermal and mechanical noise and its operation on the principle of systematic examination of electrodes in the same measurement recording tract has ensured improved channel correlation.

Average daily records of the electrotelluric field at station 1 situated 60

km away from the instrumental epicenter of the earthquake of magnitude 7.7 that occurred on December 15, 1971 are given in Fig. 6. At this time the station was equipped with a three-channel recorder, so it was not possible to record the potentials from the backup N–S line. These records show three occasions of intense field fluctuation, on November 8 and 27 and December 19. The first and last fluctuations correspond to period of heavy precipitation, which may have caused them.

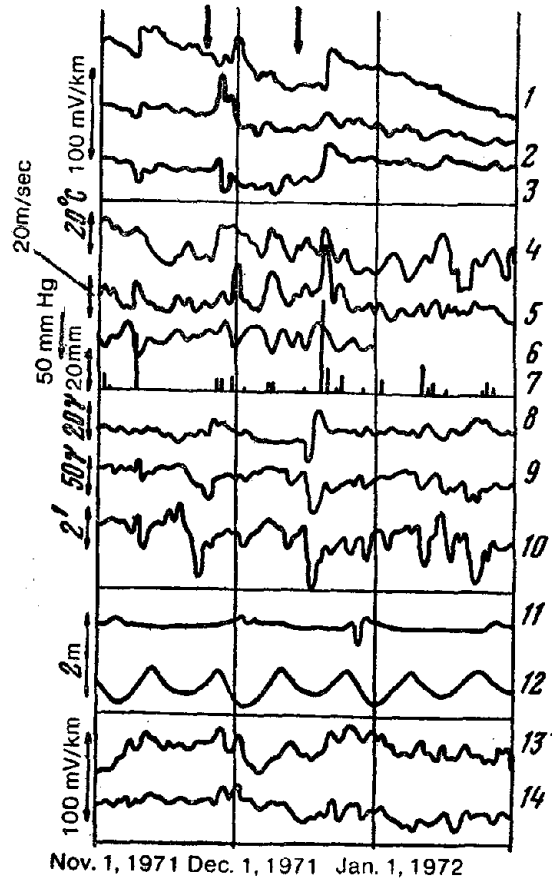

Fig. 6. Change of geophysical and meteorological factors during strong earthquakes in Kamchatka:

1-3—Average daily electrotelluric field level on N-S, E-W_1 and E-W_2 lines at station 1; 4-7—Air temperature, wind velocity, atmospheric pressure and precipitation at station 1; 8-10—*X*, *H* and *D* geomagnetic field components at Paratunka Observatory; 11,12—Height of high water and ebb tide in ocean; 13,14—Average daily electrotelluric field level at station 3. Occurrence times of deep earthquake on Nov. 24, 1972 ($M = 7.2$) and shallow earthquake on Dec. 15, 1971 ($M = 7.7$) are shown by arrows.

It should be noted, however, that numerous cases were observed during the functioning of the station when heavy precipitation did not cause field variations. The field variations that began on November 27 do not lend themselves to correlation with precipitation and other meteorological phenomena or with tides and geomagnetic perturbations. They can be correlated with the approach of the December 15, 1971 earthquake. Since these variations began three days after another strong, deep earthquake on November 24, 1971, 450 km from station 1, it is interesting to compare these records with the records of station 3 lying nearly 50 km away from the epicenter of this earthquake. The field was found to alter at station 3 too after November 27, but to a lesser extent than at station 1. This seems to suggest that these variations were not a direct consequence of the deep earthquake, but may have been a manifestation of the revived tectonic process over a vast area after a strong earthquake, as noted in [20].

The hourly records of the components of station 1 during the development of the above multidiurnal anomaly are cited in Fig. 7. It is noticeable that isolated variations vividly manifest in the main and backup lines in the E–W direction occurred against a background of slow change in the recording level after November 27. These changes are not observed at station 3 or in geomagnetic variations; the influence of the latter on the electrotelluric field can be assessed from the records of November 25. The ratio of the records of the $E–W_1$ and $E–W_2$ components measured at station 1 from observations of bays and *sq*-variations is close to 1. The variations on November 29–30 are similar in amplitude on both lines, while the variations on November 27 are different.

The next example of anomalous change in the field before an earthquake is given in Fig. 8. A deep earthquake of magnitude 6, very rare for this region, occurred on May 27, 1972 with its focus lying in Kamchatka at an epicentral distance of 250 km from station 3. Synchronous changes in the electrotelluric field level along all components were observed at station 3 about a week before the earthquake. It is difficult to determine the amplitude of the anomaly because the normal electrotelluric field level is unknown. It is dependent on the properties of the electrodes, conditions of earthing, meteorological factors, and, also, the seasonal pattern specific for each measuring line. Tentatively, taking the levels on May 20 as normal, the field change on the eve of the earthquake should be 10–13 mV/200 m on both E–W lines and 8–10 mV/200 m on the N–S lines. The hourly recording for this period shown in Fig. 9, indicates identical smooth variation in field level on all lines. As distinct from what is shown in Fig. 7, there were no pronounced perturbations in the present case in the higher-frequency range.

In most cases the electrotelluric field variations before earthquakes do not surpass the background limits; this renders impossible evaluation from the recording of one measuring line and necessitates standardization of the

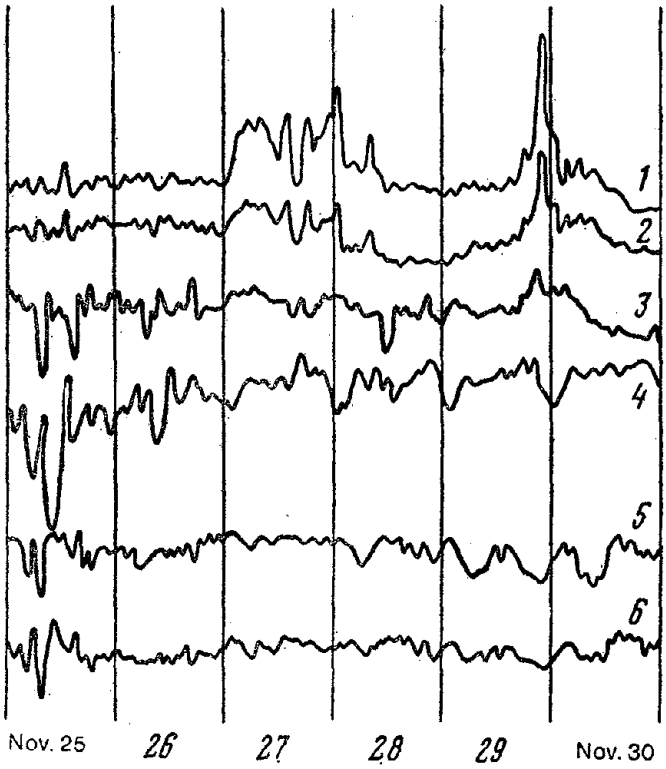

Fig. 7. Example of momentary fluctuations in electrotelluric field before strong earthquake:

1-3—Records of E-W and N-S main and backup lines at station 1 lying 60 km from earthquake epicenter; 4—Geomagnetic variations (*H*-component at observatory 480 km away); 5, 6—Records of E-W and N-S lines at station 3, 400 km away.

method for combined analysis of several synchronous recordings. One probable program of analysis is described below.

When analyzing electrotelluric field recordings with reference to seismicity the probable response of the field to meteorological changes should be taken into account. For instance, it is known that heavy precipitation may stimulate momentary development of filtration potentials and also affect polarization potentials [29–31]. The effects of rock temperature, geomagnetic storms and ocean gales, etc. are also to be expected. The average daily electrotelluric field level is shown in Fig. 8, also cited are data on wind velocity; the temperature of the air and of soil and rocks at a depth of 1.6 m, precipitation taken from the tables compiled by the Hydrometeorological Service,

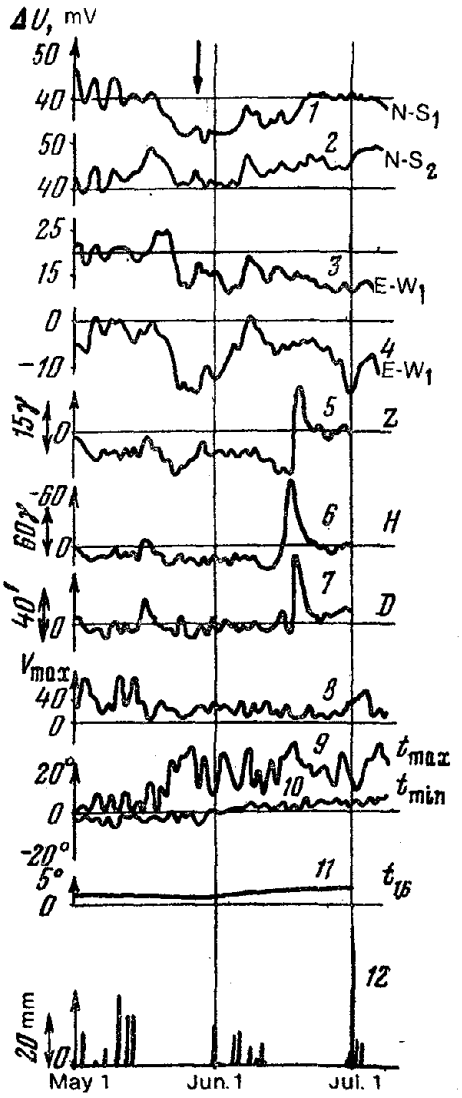

Fig. 8. Example of electrotelluric field variation before earthquake: 1-4—Average daily electrotelluric field; 5-7—Average daily geomagnetic field; 8—Wind velocity; 9, 10—Surface soil temperature; 11—Rock temperature at depth of 1.6 m; 12—Precipitation.

and average daily variation of three components of the geomagnetic field at an observatory 80 km away from station 3. Collation of these data prompts the conclusion that the electrotelluric field level cannot be correlated with temperature and velocity of wind or with geomagnetic perturbations. Further,

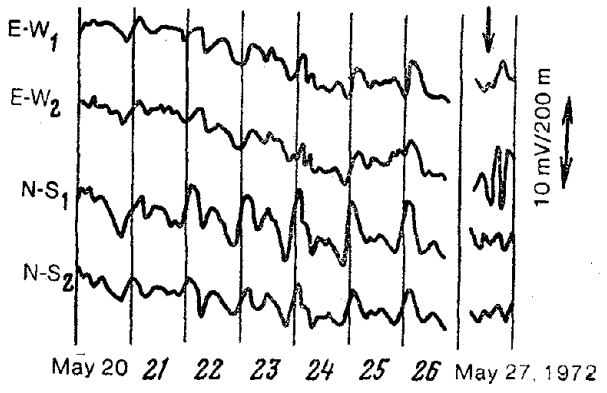

Fig. 9. Example of electrotelluric field variations before earthquake.

attempts were made at different times to correlate the electrotelluric field level with the ocean level and atmospheric pressure, but no relationship was observed among them. It can be inferred from Fig. 8 that the potential difference of isolated measuring lines often responds to precipitation.

STUDY OF STRUCTURE OF LOCAL ELECTRIC FIELDS

Special efforts to study the conditions of geoelectric observation and the properties of the electrodes used were made during the research on electrotelluric warnings. Let us review the experimental results in the station 3 region.

The arrangement of the electrodes is shown diagrammatically in Fig. 10. The principal lines of around-the-year observations using the AETF are represented by the N_1–S_1, N_2–S_2, E_1–W_1 and E_2–W_2 lines with an interval of 200 m, and E_3–W_3 with an interval of 560 m; all the electrodes were placed on the slopes of a coniform hill. Besides the electrodes E_4, "cliff"(c), and "shore"(s) were set to ascertain the effect of the ocean. Three additional electrodes differing in depth (electrodes E^{I}, E^{II}, E^{III} and W^{I}, W^{II}, W^{III}) and specially coated weakly polarized electrodes (E^{IV}, W^{IV} and N_3) were placed near each of the electrodes E_1 and W_1 to study the electrokinetic conditions in the zones adjoining the electrodes.

Figure 11 is a diagram of the arrangement of the groups of profiles near the electrode W_1. It also shows the profile along which regular observations of the natural electric field were made with the help of unpolarized calomel electrodes, electroprofiling, and the central points of vertical electric sounding (VES 1 and VES 2).

The center of VES 1 was chosen on the slope of the coniform hill so that

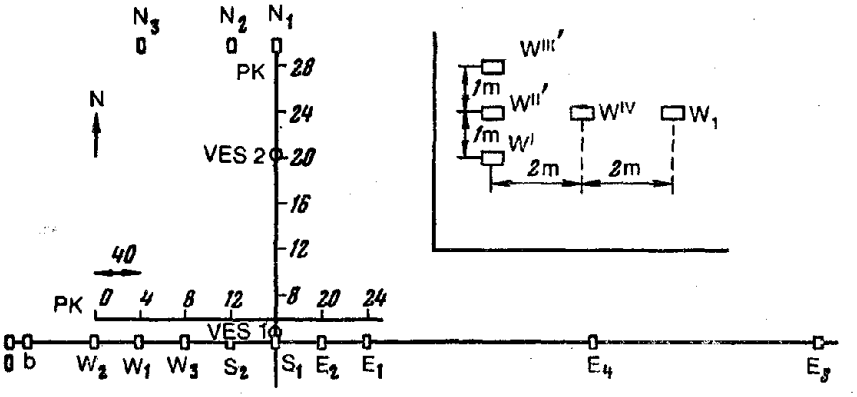

Fig. 10. Diagram of electrode arrangement and observation profiles: Arrangement of additional electrode groups is shown inset at right.

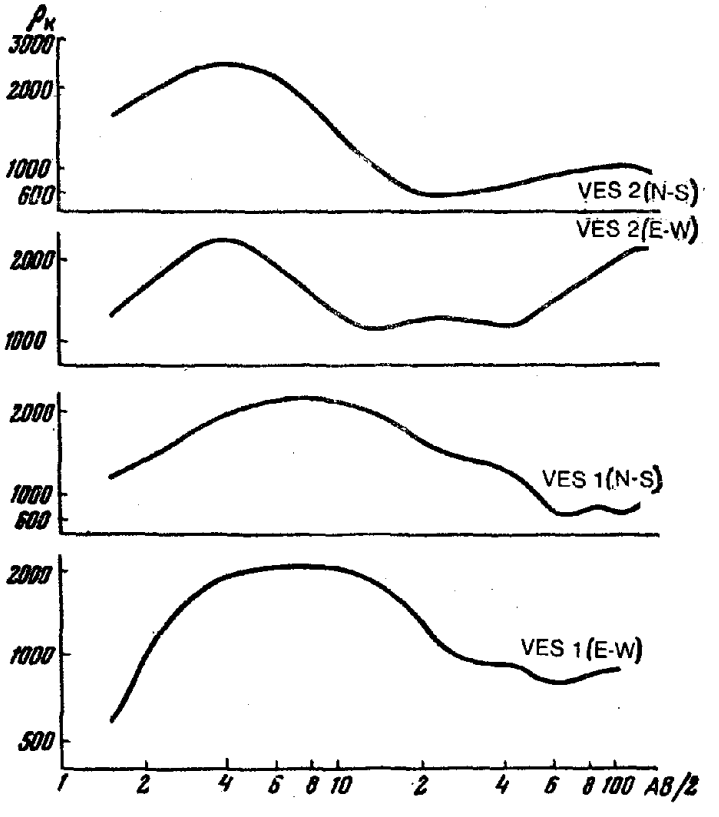

Fig. 11. Vertical sounding curve plotted at station 3.

the feeder electrode AB moved along the principal recording lines E_1–W_1 and N_1–S_1. The curves obtained for the apparent electric resistance ρ_k are shown in Fig. 11. The maximum spacing of $AB/2$ is 110 m. The ρ_k values determined in the forward and backward courses were almost the same. The flat maximum of the apparent electric resistance mounting to 2000 Ohm·m corresponds to a layer of homogeneous loam at depths of 1.5–4 m. All the principal electrodes for electrotelluric observations were located right in this layer. The minimum ρ_k values of $\sim$ 800 Ohm·m correspond to groundwater at depths of 10–20 m.

The second vertical electric sounding (VES 2) was carried out on the top of the coniform hill. The results obtained showed that even though the loam layer was 1–1.5 m thick and the water-resistant layer accordingly lay close to the surface, the shape of the VES curves did not alter, testifying to the homogeneous geoelectric section in the station area. The spacing for the electroprofiling $AB/2 = 50$ m was chosen in accordance with the VES curves, and the results are given in Figs. 12 and 13. A homogeneous field with its ρ_k increasing steadily from south to north is observed in the N–S profile. The central part of the E–W profile where most of the electrodes were located is also characterized by a steady ρ_k field. The variations in ρ_k in the eastern part of the profile are due to geological heterogeneities of the relief; an anomaly caused by metal wires laid in the ground was observed in picket 36. The engineering structures figure more prominently in the graph for the natural electric field. The measurement procedure is described below.

A reliable version of the calomel electrode was used for study of the earth's electrotelluric field. For effective contact with the earth the electrode was housed in a fine-grained ceramic casing 30 mm in diameter and 40 mm in length. The casing was filled with a gel of saturated KCl solution in agar-agar. The electrode was hermetically sealed with epoxy resin. The electrodes were held in the saturated solution for five days, after which the natural electrode potentials were measured with reference to a standard calomel electrode. An RN-340 instrument was used for measurement. In KCl solution the electrodes did not differ from the standard by more than $\pm$ 1.5 mV. The electrodes were compared under field conditions in the profile, placing the ceramic-encased electrodes not more than 10 cm apart in one socket. The electrodes were considered suitable for electrotelluric field measurements if the potential difference between them in the socket did not exceed 2 mV.

Control determinations of the stability of the natural potentials of the measuring electrodes were carried out at the end of the measurements in the profile. If the control measurements showed that the normal potentials of the electrodes deviated by more than 2 mV from the standard the electrodes were immersed in fresh gel.

The natural field was measured repeatedly by the potential method from July through September, 1973. The purpose of the measurements was to

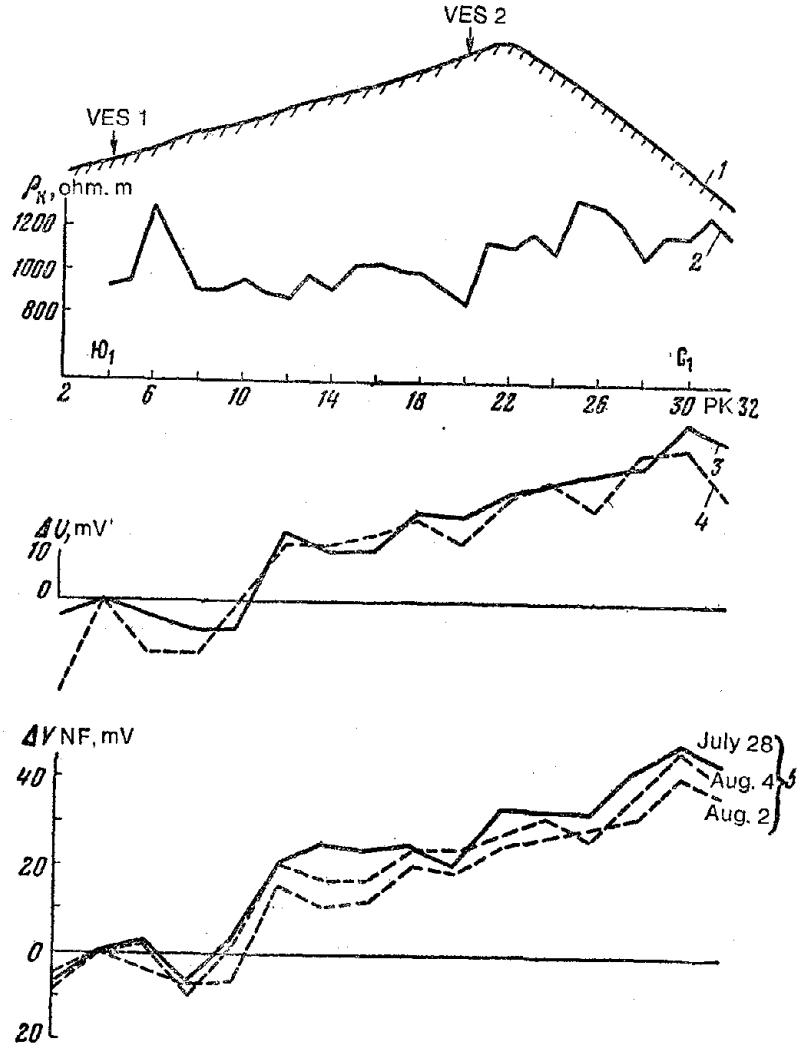

Fig. 12. Results of electrometric observations at station 3:
1—Relief; 2—Electroprofiling curve; 3, 4—Curves for natural field (NF) after precipitation; 5—Graphs for natural field repeatedly observed.

find out if the natural field was disturbed before the earthquake and during precipitation. The natural field measurements corrected for daily variations are given in Figs. 12 and 13. The corrections were determined from the oscillograms of the E_1–W_1 and N_1–S_1 lines of the PS-1-08 automatic recording potentiometers. The natural field curves show the accuracy of observation in repeated measurements. In most pickets the potential diverged, essentially due to changes in conditions at the electrosoil contact, by a few millivolts.

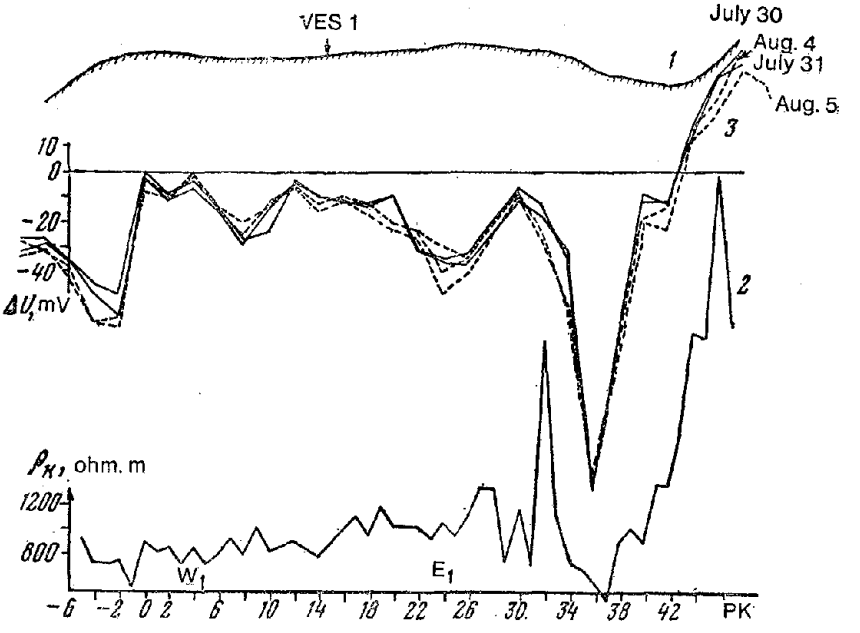

Fig. 13. Results of electrometric observations in E-W profile at station 3:
1—Relief; 2—Electroprofiling curve; 3—Graphs for natural field repeatedly observed.

The potentials in the forward and backward directions on the same day tallied within an accuracy of 3 mV.

It was also verified with the help of nonpolarized calomel electrodes how far the natural field on the earth's surface differs from the field at the electrode earthing depth and how it alters with time. For this purpose the potential was measured in the recesses of the vertical wall of the trench with reference to the "zero" electrode 2 m away from the trench. Repeated potential measurements at varying depths (Fig. 14) showed that the potential varied within 10 mV, but the relative variations of absolute potentials at varying depths were not wide. This gives an indication of the total potential variation in the trench wall relative to the zero electrode. This is also valid for precipitation.

A study of the N–S profile by natural field measurements revealed a steady south-to-north rise in potential at a gradient of 0.16 mV/m (Fig. 12). An average potential difference of 40 mV was observed in this case between the points on the earth's surface above the N_1 and S_1 electrodes; the potential difference did not vary by more than 10 mV in repeated observations over a period of one and one-half months. Around-the-year recording on the $N–S_1$ and $N–S_2$ measuring lines also showed a steady potential difference of 40–45 mV with an average seasonal variation of nearly 10 mV.

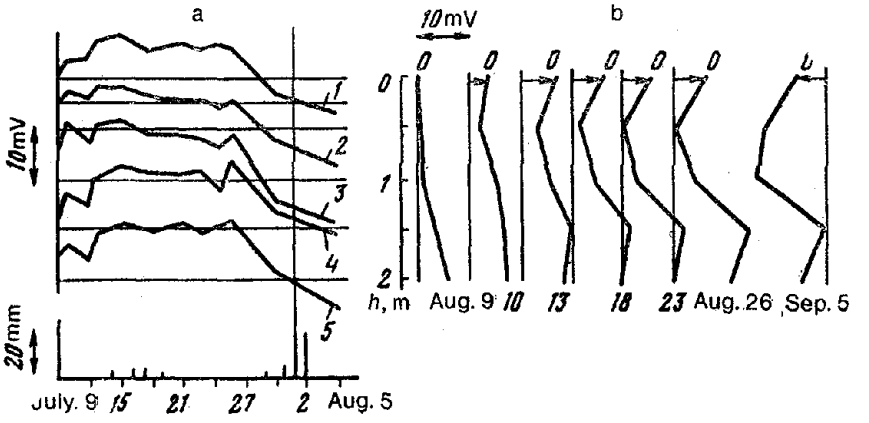

Fig. 14. Results of natural field measurements at varying depths:
a—NF variation with time at depths, m: 1—0, 2—0.5, 3—1, 4—1.5, 5—2; time and amount of precipitation are shown below;
b—NF variation with depth in repeated measurements.

The N_3–W^{IV} measuring line installed during the field work in July, 1972, which included poorly polarized electrodes specially coated with PbOHCl, also reached a steady level of 40 mV. For control, the normal polarization of the electrodes N_1, N_2, N_3, S_1, S_2, W^{IV} was measured with reference to the nonpolarized calomel electrode. In these measurements the same calomel electrode was successively placed over the measuring electrodes. The potential difference of the normal polarization of the N_1–S_1, N_2–S_2 and N_3–S_3 (W_1^{IV}) electrode pairs did not exceed 10–20 mV and had a polarization opposite to that of the existing field, as if to balance part of the field.

The results obtained show that in a given case the natural field in the earth is steady in time. Prolonged natural fields of redox processes, contacts, less steady filtrational and "time-variant" fields have been quite well studied in geophysics [28–30]. Background fields of a different nature, practically unstudied [5], were also noted.

Additional measurements of the natural field were also made beyond the coniform hill, where the electrodes of station 3 were earthed, to understand certain aspects of the observed phenomena. Recordings every 50 m along two 1 km long N–S and E–W profiles showed that no steady gradient of natural field is observed in such long profiles within the measuring accuracy of 5 mV. Quantitative study of the magnetic properties of rock specimens at station 3 did not show an increased proportion of magnetic minerals. There is no basis to expect sulfide minerals in the rocks of volcanic origin forming the coniform hill.

Measurements of the natural field after heavy precipitation (Fig. 12) did

not show marked deviation from the observed regularities. It should be noted that the gradual rise of potential throughout the N–S profile does not correspond to the topography of the locality, which on the southern slope has a polarity the reverse of that observed in filtration phenomena. Some relationship seems to obtain between the gradual potential changes of the natural field and apparent electric resistances (Fig. 12). Further studies are necessary for an understanding of the nature of this phenomenon and its impact on earthquakes.

Soon after the experimental studies began a sharp change in the electrotelluric field lasting for the two weeks preceding an earthquake of energy class 13 with its epicenter 200 km away (August 3) was observed on all the measuring lines at station 3. The average daily anomaly is shown in Fig. 15. The potential difference was found to fall by 7–17 mV from July 17 through 20 and to rise after July 20, more steeply in the E–W components.

Some analysis was carried out to get an idea of the location of the sources of the anomaly. Let us first analyze the anomaly area on a wider time base. The records of the permanently operating and additional lines at station 3,

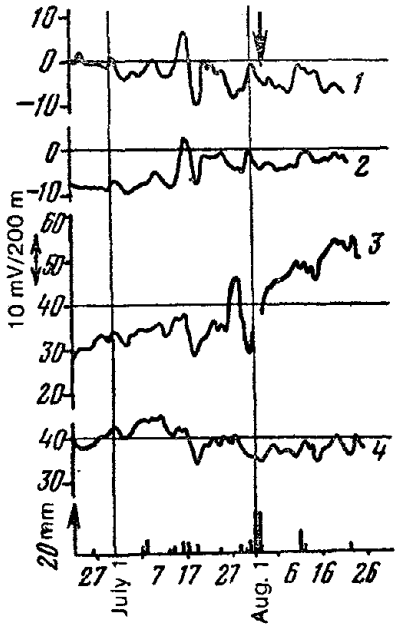

Fig. 15. Local change in electrotelluric field at station 3 before earthquake:

1-4—E_1-W_1, E_3-W_3, N_2-S_2 and N_1-S_1 components. Precipitation in station area is indicated below.

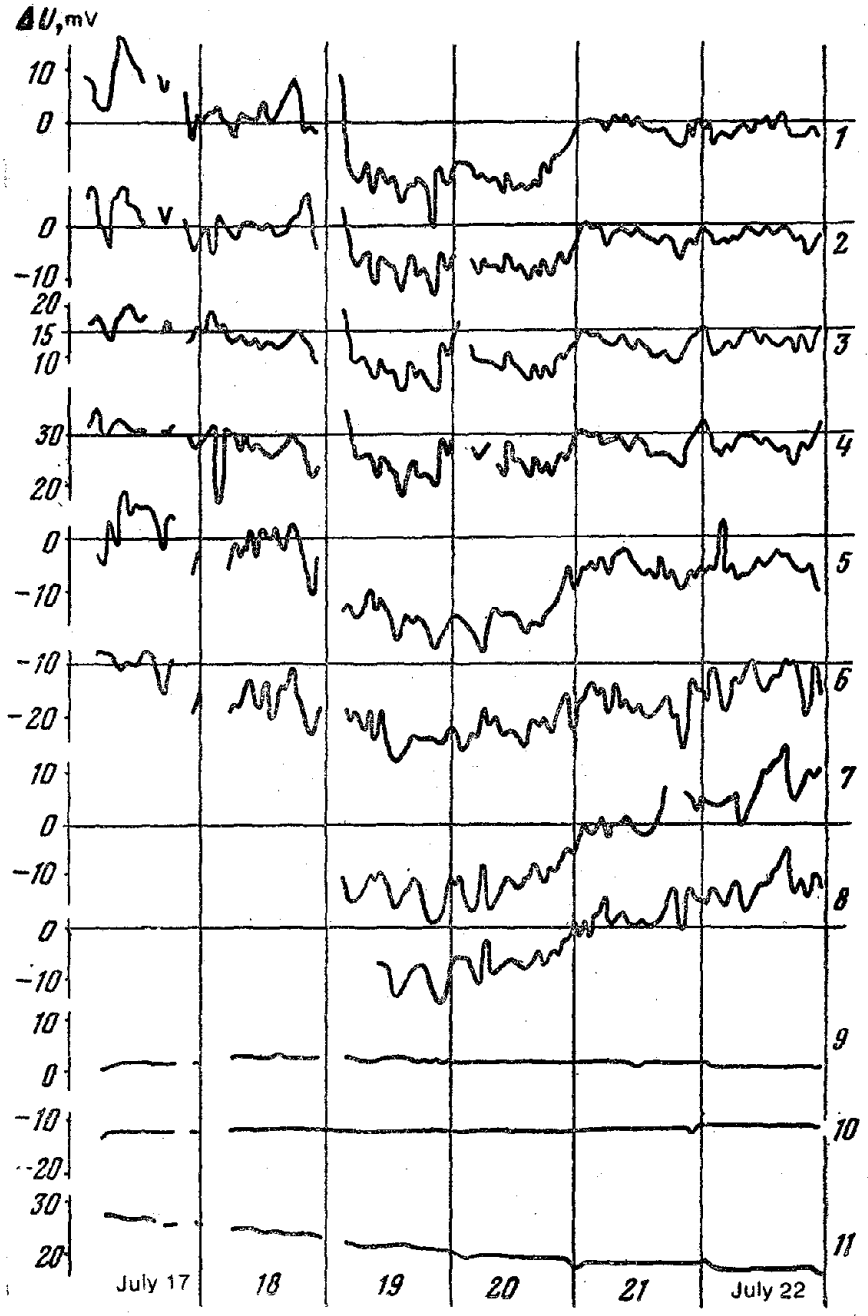
ΔU, mV
10
0
1
0
-10
2
20
15
10
3
30
20
4
0
-10
5
-10
-20
6
10
0
7
-10
8
0
-10
10
0
9
-10
-20
10
30
20
11
July 17
18
19
20
21
July 22

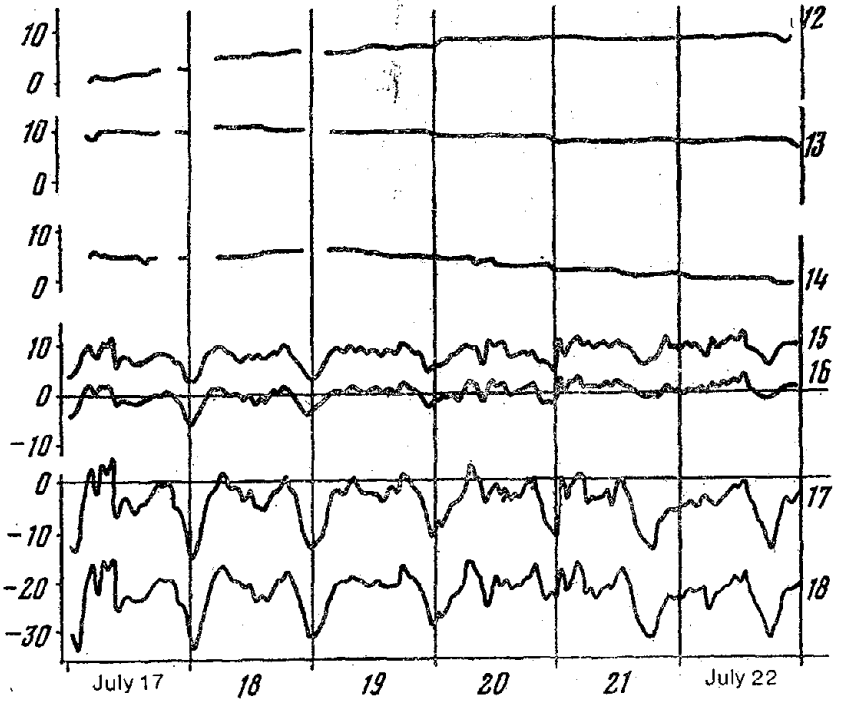

Fig. 16. Local variation in electrotelluric field at station 3:

1-4—E_1-W_1, E_3-W_3, N_2-S_2 and N_1-S_1 components; 5—Control recording of E_1-W_1 line made with another apparatus; 6—Recording of E_1^{VIII}-W_1^{IV} line using weakly polarized electrodes; 7—Recording of "cliff"-"shore" line; 8—Recording of control E^{IV}-W^{II} line; 9-14—Recording from short lines 1-2 m in length; 9, 10—Vertical; 11—Horizontal line of electrode E_1; 12, 13—Vertical; 14—Horizontal line of electrode W_1; 15-18—Recordings of E-W and N-S main and backup components at station 4.

are shown in the upper part of Fig. 16. These curves suggest that the electrotelluric field variation is not of a global scale (the effect is not observed at station 4) and is not induced by the near-electrode processes, including moisture variation in the adjacent zone (no change was observed in the recordings of the electrode group placed near the electrodes E_1 and W_1). However, variations are clearly noticeable on all the E–W measuring lines.

Let us correlate the electrotelluric field variations recorded on the E_3–W_3, N_2–S_2, N_1–S_1 measuring lines with the variation on the E_1–W_1 line and compare this correlation with the "normal background". The corresponding relationship based on *sq*-variations during seismically quiet periods is taken as the normal background.

The records of the electrotelluric field and geomagnetic variations during the quiet period are illustrated in Fig. 17. The ratio of daily variations on the

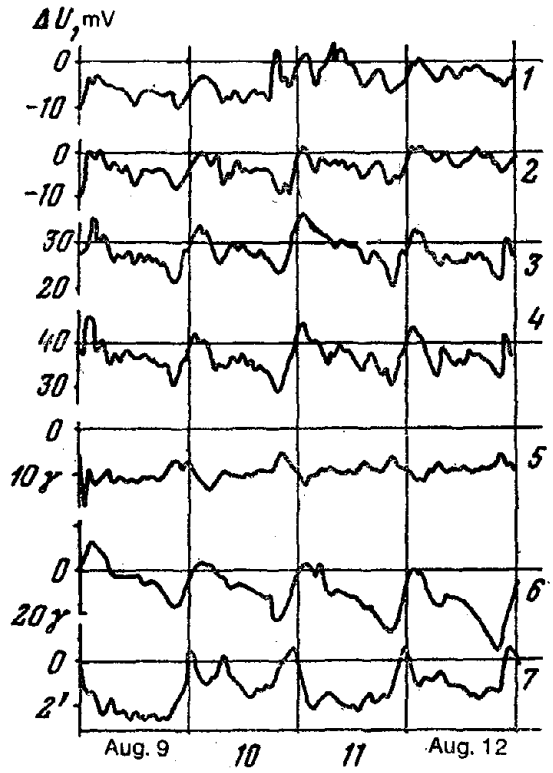

Fig. 17. Background of electrotelluric field and geomagnetic variations at station 3: 1-4—E_1-W_1, E_3-W_3, N_2-S_2 and N_1-S_1 components of electrotelluric field; 5-7—*Z*, *H* and *D* components of geomagnetic field.

E_3–W_3, N_2–S_2 and N_1–S_1 lines to variations on the E_1–W_1 line is roughly 1.2, 1.5 and 1.5 respectively. The corresponding variations in the field level noted during the anomaly (July 20–21) are 0.8, 0.6 and 0.6. It can be inferred that the orientation of the horizontal component of the electric vector during the anomaly differs from the orientation of the *sq*-variations. However, certain differences are observed in the ratio for parallel components. This may indicate the probable strong influence of local geoelectric conditions when the anomaly source is relatively close.

To know whether the field level altered on July 20–21 due to strong local distortion in some part of the E–W profile we will make use of the measurements made on the pickets of the E_1–W_1 profile using nonpolarized calomel electrodes. Subtracting the results of potential measurements on all pickets on July 20 from the corresponding values obtained on July 21, we find (Fig. 18) within the range of measuring accuracy a smooth slope of the difference

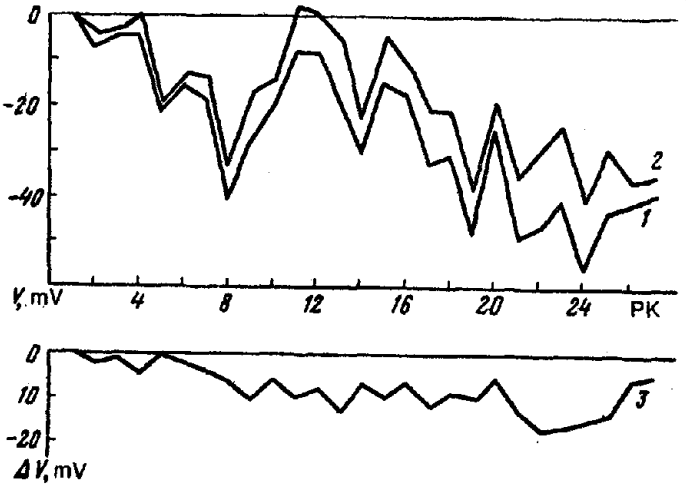

Fig. 18. Repeated natural field measurements in E-W profile by nonpolarized electrodes during local anomaly development:
1—July 20; 2—July 21; 3—Difference curve.

curve corresponding to the field level variation observed on the E_1–W_1 line.

These experiments revealed that an electrotelluric field of unknown nature with its source lying in the station region may vary before an earthquake.

ELECTRIC FIELD OF NATURAL SOURCES WITH SPATIALLY DISTRIBUTED ELECTROMOTIVE FORCES

It is obvious from physical concepts that any source of a natural electric field occupies a definite space and that sources with surfacially (orebodies) or spatially (piezoactive rocks) distributed emf occur under real conditions. Electrotelluric symptoms of seismic events appear due to spatial mechano-electric transformation. Specifically, the sources of low-frequency earthquake warnings can be regarded as the sources of quasisteady currents. Then the current density in the external space j_e and the current density inside the source j_i can be correlated with the electric field potential as follows:

$$\vec{J}_e = -\gamma_e \operatorname{grad} U_e, \quad \vec{J}_i = -\gamma_i \operatorname{grad} U_i + \vec{J}_0, \tag{1}$$

where J_0 is the current density of external emf sources; γ_e and γ_i are the electric conductivity outside and inside the source; U_e is the potential outside the source satisfying the Laplace equation:

$$\Delta U_e = 0,$$

where U_i is the potential inside the source satisfying Poisson's equation:

$$\Delta U_i = \frac{1}{\gamma_i} \operatorname{div} \vec{J}_0.$$

The electric potential and the normal component of current density should be continuous at the medium interface surrounding the source.

To a first approximation the local sources may be presumed to be spherical. It is known [32] that integral solution of the Laplace and Poisson equations for a sphere leads to the resolution, on the principle of spherical harmonics, of the unknown potential, the right-hand side of Poisson's equation, and the boundary conditions. However, for random dependence of intrinsic current on radial coordinates it is not always possible to compute the coefficient of resolution U_i obtainable in an integral form from the solution of the Eisler's inhomogeneous equation. The unknown coefficients can be obtained only for special cases, for instance, when the radial function of the external current can be represented by an exponential series. It should be noted that a similar approximation allows analysis of a fairly wide class of real sources having spatially distributed emf. In that case, knowing the series of the spherical functions for the right-hand side of Poisson's equation and the normal component of the external current, we have

$$\operatorname{div} \vec{J}_0 = \sum_{n=0}^{\infty} \sum_{m=0}^{n} \sum_{k=0}^{\infty} [\alpha_{kmn} \cos m\varphi + \eta_{kmn} \sin m\varphi] r^{k-1} P_n^m(\cos\theta);$$

$$J_{0r} = \sum_{n=0}^{\infty} \sum_{m=0}^{n} \sum_{k=0}^{\infty} [\lambda_{kmn} \cos m\varphi + \mu_{kmn} \sin m\varphi] r^k P_n^m(\cos\theta). \qquad (2)$$

The general solution of this problem can be obtained as follows:

$$U_e = \sum_{n=0}^{\infty} \sum_{m=0}^{n} \sum_{k=0}^{\infty} \frac{1}{(n+1)\gamma_e + n\gamma_i} \left\{ \left[\lambda_{kmn} - \frac{\alpha_{kmn}}{k+n+2} \right] \cos m\varphi \right.$$

$$\left. + \left[\mu_{kmn} - \frac{\beta_{kmn}}{k+n+2} \right] \sin m\varphi \right\} P_n^m(\cos\theta)\, r_0^{k+n2} r^{-(n+1)},$$

$$U_i = \sum_{n=0}^{\infty} \sum_{m=0}^{n} \sum_{k=0}^{\infty} \left[\left\{ \frac{1}{(n+1)\gamma_e + n\gamma_i} \right.\right.$$

$$\times \left[\lambda_{kmn} \frac{k+1+\frac{\gamma_e}{\gamma_i}(n+1)}{(k+1)(k+2) - n(n+1)} \alpha_{kmn} \right]$$

$$\left. \times r_0^{k-n+1} r^n + \frac{1}{\gamma_e} \frac{\alpha_{kmn}}{(k+1)(k+2) - n(n+1)} r^{k+1} \right\} \cos m\varphi$$

$$+\left\{\frac{1}{(n+1)\gamma_e+n\gamma_i}\left[\mu_{kmn}-\frac{k+1+\frac{\gamma_e}{\gamma_i}(n+1)}{(k+1)(k+2)-n(n+1)}\beta_{kmn}\right]\times r_0^{k-n+1}r^n\right.$$

$$\left.+\frac{1}{\gamma_i}\frac{\beta_{kmn}}{(k+1)(k+2)-n(n+1)}r^{k+1}\right\}\sin m\varphi\Bigg]P_n^m(\cos\theta), \qquad (3)$$

where r_0 is the radius of the sphere; r, θ and φ are the spherical coordinates of the observation point; $P_n^m(\cos\theta)$ are the associated Legendre polynomials.

The dipole moment is maximum in multiple resolution of spatial potential when the electrotelluric earthquake warnings are recorded far from the hypocenter. Taking this into account and assuming the current field inside the source to be homogeneous, we will analyze a special case of general solution of (3) corresponding to a source having an extrinsic dipole field ($m = 0$, $n = 1$; $\mu_{k01} = \beta_{k01} = 0$). For such a source it follows from (2) that

$$\alpha_{k01} = \frac{k(k+3)}{k+1}\lambda_{k01}. \qquad (4)$$

Deriving current density from (1), (3) and (4) and using the concept of total current I [5], we get the final result as

$$j_{er} = \frac{Ir_0}{2\pi}\frac{2\cos\theta}{r^3}, \qquad j_{e\varrho} = \frac{Ir_0}{2\pi}\frac{\sin\theta}{r^3},$$

$$j_{ir} = \frac{I}{\pi r_0^2}\cos\theta, \qquad j_{i\varrho} = \frac{I}{\pi r_0^2}\sin\theta, \qquad (5)$$

where

$$I = \int_0^{2\pi}\alpha\,\theta\int_0^r j_{ir}\,r^2\sin\theta\,dr = \frac{2\pi\gamma_e}{2\gamma_e+\gamma_i}\sum_{k=1}^{\infty}\frac{\lambda_{k01}}{k+1}r_0^{k+2}. \qquad (6)$$

It is noteworthy that in external effects sources having spatially and sufficiently distributed emf can be equivalent. In fact, in accordance with the known formula (5), correlating the contact potential difference ϵ_0 with the total current of the spherical source having the surface emf distribution

$$I = \frac{2\pi\gamma_e\gamma_i}{2\gamma_e+\gamma_i}r_0\epsilon_0,$$

and with formula (6), we find that for an equivalent source with the emf distributed on the surface the contact potential difference is given by the equation

$$\epsilon_0 = \frac{1}{\gamma_i}\sum_{k=0}^{\infty}\frac{\lambda_{k01}}{k+1}r_0^{k+1}. \qquad (7)$$

It should also be noted that the results obtained are valid for an unlimited external medium having isotropic and homogeneous geoelectric parameters. The potential should be doubled when there is a day surface. This will correspond to approximate evaluation of the mirror image of a source in a flat day surface [5].

Equation (5) permits us to derive the energy parameters of a source, e.g. the power, which, in conformity with the energy balance, should equal the total heat released outside and inside the source in unit time:

$$Q_e = \frac{1}{\gamma_e}\int_0^{2\pi} d\varphi \int_0^{\pi} d\theta \int_0^{\infty} (\vec{J}_e)^2 r^2 \sin\theta\, dr = \frac{2}{3\pi}\frac{1}{\gamma_e}\frac{I^2}{r_0},$$

$$Q_i = \frac{1}{\gamma_i}\int_0^{2\pi} d\varphi \int_0^{\pi} d\theta \int_0^{r_0} (\vec{J}_i)^2 r^2 \sin\theta\, dr = \frac{4}{3\pi}\frac{1}{\gamma_i}\frac{I^2}{r_0}. \tag{8}$$

Heating of the medium due to the Joule effect can also be computed from the known current distribution (5). This arouses interest in the physicochemical processes involved in the flow of electric current in the seismoactive zone. It is known [33] that the thermal field of the electric current is obtained from a thermal conductivity equation of the following type:

$$\Delta T = -\frac{1}{\varkappa\gamma}(\vec{J})^2,$$

where T is the temperature of the stationary thermal field; k is the thermal conductivity of the medium. The approximate solution of the thermal conductivity equation with γ and $\varkappa$ identical outside and inside the source takes the form

$$T_e = \frac{1}{\varkappa\gamma}\left(\frac{I}{2\pi}\right)^2\left[-\frac{1}{\sigma}\frac{r_0^2}{r_4} + \frac{2}{r_0 r}\right],$$

$$T_i = \frac{1}{\varkappa\gamma}\left(\frac{I}{2\pi}\right)^2\left[-\frac{2}{3}\frac{r^2}{r_0^4} + \frac{5}{2}\frac{1}{r_0^2}\right]. \tag{9}$$

Field observations permit evaluation of the parameters of the mechanoelectric sources whose appearance in the earth's crust might explain electrotelluric field variations in the earthquake preparation process. The parameters of anomalous perturbations of telluric currents for an earthquake of energy class 13 are the initial data (the anomaly is 30 mV/km on the average at a distance of 100 km from the epicenter and the duration of the anomaly is 10^6 sec) for the computation. The electric conductivity of the medium is taken as 10^{-4} ohm·m^{-1} and the thermal conductivity as 4 W/m·deg.

To a first approximation it can be assumed that the source in question is spherical, and that the external field of such a source coincides at a significant distance from the hypocenter with the electric dipole field. This implies

that for an anomaly recorded at a distance of 100 km the radius of the sphere should exceed 10 km. It should be pointed out that, on the one hand, the radius of the preparation zone of strong earthquakes is likely to exceed 10 km, on the other, solution of the inverse problem demands an increase in the electric capacity of the model of the source with any decrease in size. Thus, taking the radius of the sphere $r_0 = 10$ km, we get the maximum value of the real parameters of the mechanoelectric source.

In conformity with the initial data and formulas (6) and (9) the total current of a source is

$$I = \sqrt{2}\pi \frac{r^3}{r_0} \gamma E = 1.3 \text{ ka}. \tag{10}$$

However, the sizes of sources of varied physical nature can be chosen so that the total current will be the same. Therefore, it is convenient to characterize the source by the strength of the current obtainable from unit source surface, i.e. by the current density:

$$j = \frac{I}{\pi r_0^2} = 4.1 \ \mu\text{a/m}^2. \tag{11}$$

The current density obtained seems to be admissible for real sources. For instance, current of the order of 2000 μa/m^2 is discharged from the surface of an ore-body [5]. In a rapidly changing stressed state polarization current, e.g. piezoelectric, sources may also yield this current density, as was shown above.

The source energy comprising the heat liberated outside and inside the source is estimated from the known strength of total current and the duration of the anomaly using formula (8) as $W_e = 3.6 \times 10^{11}$ J and $W_i = 7.2 \times 10^{11}$ J, i.e. the source energy is estimated to be lower by two orders than the elastic energy of earthquakes of class 13. Estimation of the heating of the medium by formulas (9) and (10) shows that the maximum temperature rise inside the source is insignificant, namely $T_i = 2.7$°C.

Thus the hypothesis that active electric sources appear in the earth's crust during earthquake preparation does not contradict the scale, energy balance, and thermal regime of seismic processes and corresponds to the electric activity of natural sources.

ANALYSIS OF RECORDINGS OF ELECTROTELLURIC FIELD TO IDENTIFY ANOMALIES (SCHEMATIC PROGRAM)

An attempt will be made here to model the following procedure: An operator scanning a series of recordings made at a fixed instant of time t classifies the recording state at that instant either as "normal" or as "anomalous". Without going into details of the functions of the operator we will merely note that they are strictly speaking, of an intuitive nature, i.e. the

concept "anomaly" is undefined. The reason is the occurrence in the recording of unstudied interferences (probably of a regular nature) of an order approximating that of the "effective" signal produced by known factors.

The recording analysis program described below is an attempt to facilitate operator functions. Bearing the foregoing in mind, the proposed model, based, of course, on intuition, should be regarded as purely experimental, i.e. certain parts of the program and perhaps the whole of it can be altered in the course of the experiment.

The analysis program rests on the following premises: Isolated recording represents the potential difference $\Delta U_i(t)$ between two electrodes. The inter-electrode separation is l_i and the angle between the direction from one electrode to another and a certain fixed direction, e.g. N–S, $-a_i$; where i is the number of the channel.

It is assumed that

$$\Delta U_i(t) = \Delta U_i^{(0)}(t) + \Delta U_i^{(1)}(t) + \Delta U_i^{(2)}(t),$$

where ΔU_i is the natural telluric field and is proportional to the channel length l_i; $\Delta U_i^{(0)}$ consists of the "effective" sigual generated by the known factors and of unstudied noises; $\Delta U_i^{(1)}$ is the long-period component non-linearly dependent on l_i and regarded as interference; $\Delta U_i^{(2)}$ is the short-period low-amplitude component (noise). In other words, if $\omega_i^{(0)}$, $\omega_i^{(1)}$ and $\omega_i^{(2)}$ are average frequencies, then

$$\omega_i^{(2)} \gg \omega_i^{(0)} \gg \omega_i^{(1)}. \tag{12}$$

The first stage of the analysis consists of eliminating $\Delta U_i^{(1)}(t)$ and $\Delta U_i^{(2)}(t)$ on the basis of (12). Let this be done, i.e. let the potential difference $\Delta U_i^{(0)}(t)$ be ascertained. If α is the angle between the direction of electrotelluric field and the present direction (N–S) and $\Delta U(t)$ is the true potential difference over unit length, then

$$\Delta U(t) \cos(\alpha - a_i) = \Delta U_i^0(t)/l_i. \tag{13}$$

The second stage of analysis involves determination of $\Delta U^2(t)$ from (13) by averaging (squares method), whereby the influence of the unstudied interferences is eliminated to some extent provided these interferences are of a random nature.

The third stage of analysis consists of averaging the $\Delta U^2(t)$ values obtained in different methods of elimination of $\Delta U_i^{(1)}(t)$ and $\Delta U_i^{(2)}(t)$; how the elimination and averaging are to be done will be shown below.

The term "anomaly" denotes an abrupt jump of the $U_{av}^2(t)$ curve.

Schematic Program

To begin with we will describe the principal method employed in this program for smoothing the curve $f(t)$ ($t \geqslant 0$). T is a smoothing parameter.

The smoothed value of $f^*(t_0)$ at the instant $t_0 \geqslant T$ is determined thus: a linear function $at + b$ is chosen in the segment $[t_0 - T, t_0]$ for the function $f(t)$ using the least squares method, so that

$$f^*(t_0) = at_0 + b.$$

Such smoothing "cuts" fluctuations that are momentary as compared to T. The section $(0, T)$ remains unaffected and is taken as lost "for instruction".

Let us elaborate the procedure of analysis. For simplicity let us consider the recordings evenly numbered, h being the interval of numbering.

First stage of analysis. Let us take m and M as two integers such that $m < M$ and introduce the two smoothing parameters mh and Mh. Let us carry out smoothing of each recording with each of these parameters. Let us suppose that the smoothing with the parameter mh "cuts" the noise $\Delta U_i^{(2)}(t)$, leaving $\Delta U_i^{(0)}(t)$ and $\Delta U_i^{(1)}(t)$, and that with the parameter Mh "cut" the effective signals along with the noise, leaving $\Delta U_i^{(1)}(t)$. Then the difference between the recordings of the same channel smoothed with mh and Mh will be regarded as the telluric field $\Delta U_i^{(0)}(t)$ in the desired range. Let us ascertain such differences $\Delta U_i^{(0)}(t, m, M)$ for each of the channels.

Second stage of analysis. The potential difference per unit length is computed for each channel as follows:

$$\frac{\Delta U_i^{(0)}(t, m, M)}{l_i} = \mu_i(t, m, M).$$

Next the square of the average difference of all channels is found by the following formula:

$$\Delta U^2(t, m, M) = x^2 + y^2,$$

where

$$x = \frac{1}{\Delta}(c_1\gamma_1 - c_3\gamma_2); \quad \gamma_1 = \sum_{i=1}^{n} \mu_i \cos\alpha_i; \quad c_1 = \sum_{i=1}^{n} \sin^2\alpha_i;$$

$$c_3 = \sum_{i=1}^{n} \cos\alpha_i \sin\alpha_i;$$

$$y = \frac{1}{\Delta}(-c_3\gamma_1 + c_2\gamma_2); \quad \gamma_2 = \sum_{i=1}^{n} \mu_i \sin\alpha_i; \quad c_2 = \sum_{i=1}^{n} \cos^2\alpha_i;$$

$$\Delta = c_1c_2 - c_3^2,$$

n is the number of channels.

These formulas are obtained using (13) from the expression

$$\min \sum_{i=1}^{n} (x\cos\alpha_i + y\sin\alpha_i - \mu_i)^2.$$

If, specifically, there are two channels placed orthogonally to each other, then $x^2 + y^2 = \mu_1^2 + \mu_2^2$. The result of $\Delta U^2(t, m, M)$ is stored in the memory.

The first two stages of analysis are accomplished with fixed m and each

time independently with $M = m + H, m + 2H, \ldots, m + KH = M_{max}$, where H is an integer called the averaging step.

The third stage involves averaging of the results obtained

$$\Delta U^2(t, m, M_{max}) = \sum_{s=1}^{k} \frac{\Delta U^2(t, m, m + sH)}{k}$$

and getting the output $\Delta U^2(t, m, M_{max})$.

Thus three parameters, namely m, M_{max}, and H, which should be selected in the course of the computerized experiment, are supplied to the input.

Figure 19 demonstrates the dependence of the stability of the program on the magnitude of the parameters m and M_{max}. The sections of the actual recording of the N–S_1 and E–W_1 components at station 3 from April through June, 1972 were taken for checking. The parameter m affecting the recording of the high-frequency background varied from 3 to 15 days, and M_{max}, meant for recording the seasonal variation and the zero lines, varied from 45 to 120 days.

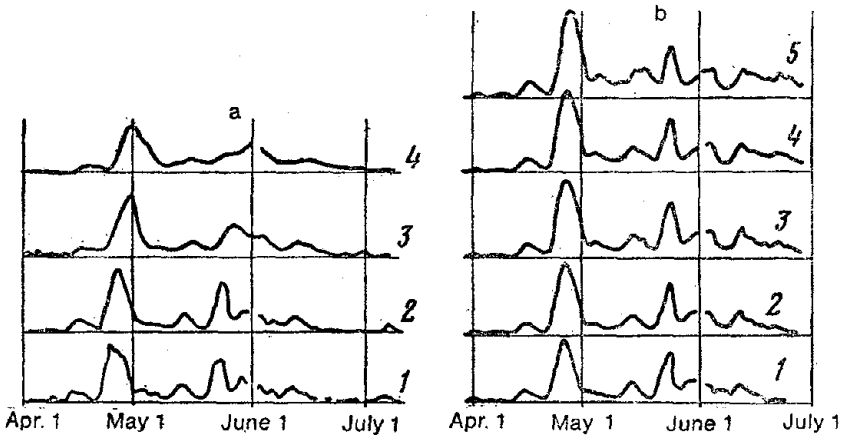

Fig. 19. Examples of dependence of output function ΔU^2 on smoothing parameters:
a: 1-4—Correspond to m = 3, 5, 10 and 15 when M = 60;
b: 1-5—Correspond to M = 60, 75, 90, 105 and 120 when m = 5.

Besides the stability of the program vis-a-vis the variation of the time parameters of the recording, it is necessary to evaluate its stability vis-a-vis the analysis of different numbers of recordings of the measuring lines at the same station. In that case steady values will also indicate that all recordings quite correctly reflect the variation in the field and the subjective features of each measuring line are of secondary significance.

The example of successive analysis of the realizations 2, 3 and 4 at station 3 is given in Fig. 20. Comparison of the curves reveals that even though the

inclusion of each new recording slightly alters the form of the output function, the principal maxima are retained and are hardly altered in form.

An example of analysis of observations at station 3 according to the program described is cited in Fig. 21. This check was done with the parameters $m = 10$ and $M_{max} = 60$. The high value of m directs the analysis essentially to identification of relatively prolonged variations in the initial recording of the electrotelluric field. The continuous arrows indicate the times of earthquakes of the energy class $K \geqslant 13$ whose epicenters lay up to 250 km away from the observing station 3 (Fig. 22) and of the April 2, 1972 earthquake of $K = 12$ whose focus was right under the observing station. The streaked arrows denote remoter earthquakes of $K \geqslant 13$.

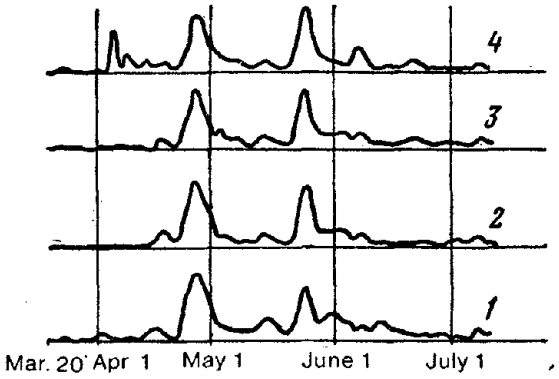

Fig. 20. Anomaly in simultaneous analysis of different recordings at station 3:
1—N-S_1 and E-W_1; 2—N-S_2 and E-W_1; 3—N-S_1, N-S_2 and E-W_1;
4—N-S_1, N-S_2, E-W_1, E-W and E-W_2.

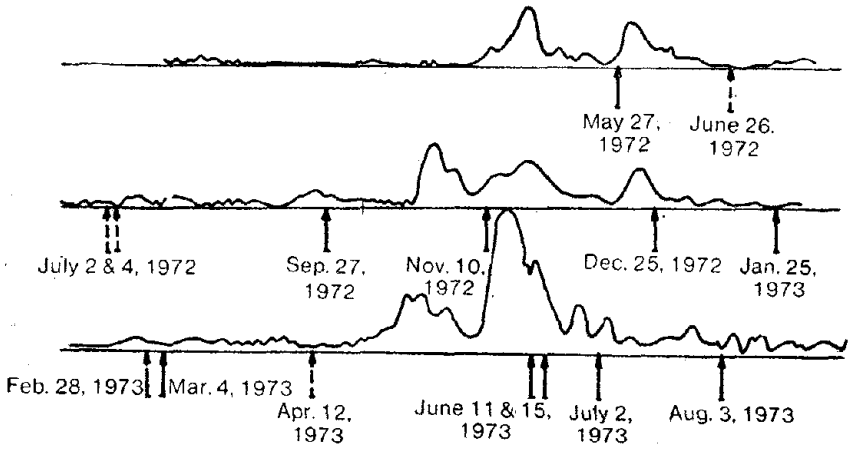

Fig. 21. Example of analysis of recording of electrotelluric field at station 3.

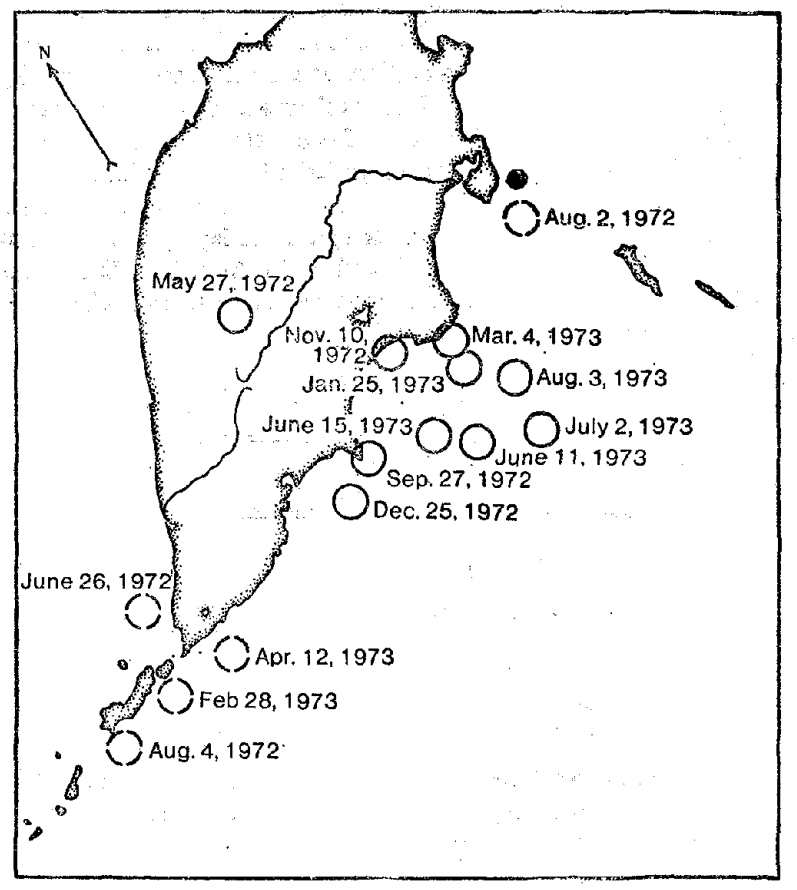

Fig. 22. Map of earthquakes of energy class $K \geqslant 13$ in Kamchatka for period January 1, 1972-September 1, 1973.

Comparison of Figs. 21 and 22 prompts the conclusion that the times of all earthquakes occurring at epicentral distances of up to 150 km from the observing station coincide with increased values of the function ΔU^2.

In interpreting Fig. 21 attention should be drawn to the fact that with the selected m and H_{max} values all the maxima of the ΔU^2 curve lag about 4–5 days behind the corresponding changes in the initially recorded field.

Mid-1973, when a series of strong earthquakes, two of them on June 11 and 15 being of energy class 13, occurred in Kronotskii Bay, seems to have been seismically the most active period in this region. The principal maximum of the function ΔU^2 is noted just before these events. The time of earthquakes 150–250 km away are less clearly correlated with the increased values of the graph. Lastly, change in the function ΔU^2 is almost unnoticeable for

earthquakes with their epicentral distances > 250 km.

A very encouraging fact is that the values in the graph did not increase during February–April, 1972 when strong earthquakes were conspicuous by their absence in the Kamchatka region. It can be inferred from analysis of the initial recordings at station 3 that the maxima of the curve in early May of 1972 and 1973 may correspond to the melting of snow, i.e. may reflect rapid change in the natural polarization of the electrodes at this time.

The series of observations so far made are not enough to assess the scope of this method of analysis for predicting earthquakes. It will be necessary to improve the quality of the initial recordings, to increase the number of measuring lines and to refine the program further.

EXPLORATORY ROUTINE PREDICTION OF KAMCHATKA EARTHQUAKES

Exploratory routine prediction of strong earthquakes in Kamchatka following a program prepared by S.A. Fedotov and G.A. Sobolev was initiated on January 1, 1972. It was based on an assessment of the seismic state as revealed by long-term seismic prediction, on prognostic symptoms diagnosed by seismostatistical and electrotelluric methods modified for Kamchatka, on the longitudinal to transverse seismic wave velocity ratio, and on space-time relationships of earthquakes. The exploratory routine prediction studies were conducted in 1972–1973 at the IFZ and the Institute of Volcanology of the DVNTs AN SSSR.

The current predictions were made twice a week on the basis of routine data monitored daily by radio from the observing station.*

The prediction was made by various methods separately and collectively. A two-point scale—0 to denote lack of signs of any approaching strong earthquake, and 1 to indicate the tentative alarm time—was used to assess the seismic hazard. The Kamchatka area was divided into subregions and the assessment was made for each of them.

Below we discuss some results of exploratory routine predictions made on the basis of electrotelluric field (ETF) measurements. Station 3, located at the center of the Kamchatka seismic region, is the reference station for making earthquake time predictions. The situations within an area of 2×10^5 km^2 lying between $\varphi = 50$–$56°$ and $\lambda = 156$–$164°$ was predicted from the data of this station. To determine the locality and time of the expected earthquake, additional use was made of the data of stations 1, 2, 4 and 6, with

*The siesmostatistical data were interpreted by O.V. Potapova, the electrotelluric data by A.A. Khromov, the longitudinal to transverse seismic wave ratios by L.B. Slavina and space-time relationships by A.M. Kondratenko. S.A. Boldyrev was responsible for the current work of the prediction team and party V.D. Feofilaktov for primary analysis of observations at the stations and for radiomonitoring of the routine data.

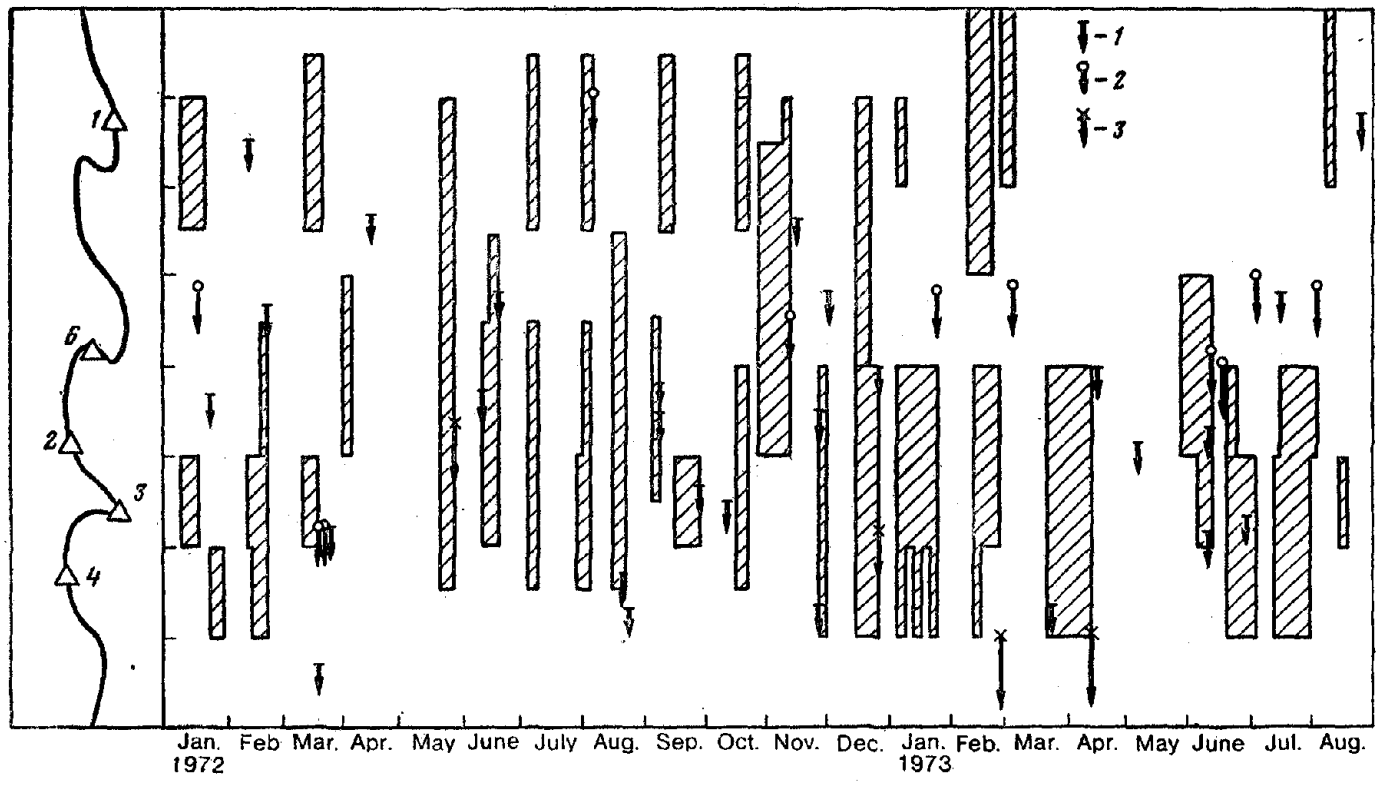

Fig. 23. Routine prediction chart of earthquakes in Kamchatka based on electrotelluric data:
1-3—Earthquake of energy class $12 \leqslant K < 13$; $K = 13$ and $K > 13$. Numbers on triangles indicate observation stations.

stations 4 and 6 functioning intermittently. The tentative alarm time was announced as soon as synchronous changes in the electrotelluric field of the type shown in Figs. 6, 8 and 15 were noticed in the recordings. The maximum duration of the alarm was 20 days. It was possible to record the alarm after the "realization", i.e. in the event of an earthquake of the energy class $K \geqslant 13$ throughout the area, or of a nearby earthquake having $12 \leqslant K < 13$. Moreover, the alarm could be recorded early if an aseismic cause of the anomaly (for instance, from meteorological data) was detected.

Figure 23 shows a routine prediction chart. The hatched zones denote periods of tentative alarm, the arrows, the times of earthquakes with $K \geqslant 12$; the length of the arrow corresponds to the energy class of the earthquake, and its place along the vertical axis, to the location of the epicenter in the subregion. The exploratory routine prediction was aimed mainly at ascertaining the scope and accuracy of electrotelluric field measurements for determining the time and location of the earthquakes and at resolving the problem of practical application of electrotelluric field measuring techniques.

The success of the first stage of the studies is attested by the fact that 12 out of 14 Kamchatka earthquakes of energy class $\geqslant 13$ and 19 out of 29 earthquakes with $12 \leqslant K < 13$ fell in the alarm periods. The long alarm time, comprising 37% of the total time, is a drawback.

The further task of refining exploratory prediction by electrotelluric field measurements involves reducing the alarm time through studies of physics of earthquake focus and the nature of electrotelluric precursors, in widening the time range of the precursors, and in creating a denser network of observation stations.

CONCLUSION

A multichannel apparatus assembly unaffected by mechanical or thermal noise has been developed on the basis of long experience to record electrotelluric fields in the infra-low-frequency range. This apparatus assembly allows recording of the field by an array of stations at each of which several measuring lines are installed.

The electrotelluric fields within a time span of several days have been analyzed and anomalous variations in the fields before several earthquakes have been recorded. The variations followed a baylike course and were observed at a distance of more than 100 km from the epicenters of earthquakes of $M \geqslant 5.5$. The nonsimultaneity of this type of anomaly at different stations and some differences in the results of parallel measuring lines suggest that the mechanoelectric sources of the anomalies were located near the observing stations.

The existence of a prolonged (several years) local electric field has been proved.

The anomalies before earthquakes can be ascribed to distortion of this field.

An algorithm and a program of analysis of multichannel recordings of electrotelluric fields, possessing high stability and directed to identification of anomalous variations of the fields before earthquakes, have been formulated for prediction.

Exploratory routine prediction of strong earthquakes has been practiced since 1972 by electrotelluric field measurements, allowing detection of "alarm" before almost all Kamchatka earthquakes with $M \geqslant 5.5$. The long alarm time of as much as 20 days is the main drawback of the procedure.

REFERENCES

1. Sobolev, G.A. and V.N. Morozov. 1970. Lokal'nye vozmushcheniya elektricheskogo polya na Kamchatke i ikh svyaz' s zemletryaseniyami (Local perturbations of the electric field in Kamchatka and their relationship with earthquakes). Sb. *Fizicheskie Osnovaniya Poiskov Metodov Prognoza Zemletryasenii*. Nauka, Moscow.
2. Volarovich, M.P. and G.A. Sobolev. 1969. P'ezoelktricheskii metod geofizicheskoi razvedki kvartsevykh i pegmatitovykh zhil (Piezoelectric Method of Geophysical Prospecting of Quartz and Pegmatitic Veins). Nauka, Moscow.
3. Brune, J.N. 1970. Tectonic stress and the spectra of seismic shear waves from earthquakes. *J. Geophys. Res.*, **75**, 426.
4. Wiss, M. and P. Molnar. 1972. Efficiency, stress drop, apparent stress, effective stress and frictional stress of Denver, Colorado earthquakes. *J. Geophys. Res.*, 77, 8.
5. Semenov, A.S. 1968. Elektrorazvedka metodom estestvennogo elektricheskogo polya (Electric Prospecting by Natural Electric Field Measurement). Nauka, Moscow.
6. Tkhostov, B.A. 1966. Nachal'nye Plastovye davleniya i geogidrodinamicheskie sistemy (Initial Bed Pressures and Geohydrodynamic Systems). Nedra, Moscow.
7. Reed, W.E. 1970. Transport of water away from a buried heat source with special reference to nuclear deformation. *J. Geophys. Res.*, **75**, No. 2.
8. Johnston, R.L. 1955. Earthquake damage to oil fields and Paloma cycling plant in the San Joaquin Valley in earthquakes in Kern County, Calif. during 1952. *Bull. Div. Mines, States California*, **171**.
9. Mavlyanov, G.A. 1973. Gidrogeokhimicheskie osobennosti podzemnykh seismoaktivnykh raionov uzbekistan (Hydrogeochemical Features of Underground Seismoactive Regions of Uzbekistan). Izd. FAN, Tashkent.

10. Sobolev, G.A. 1969. O mekhano-elektricheskom effekte kontakov (Mechanoelectric effect of contacts). Sb. *Fizika Gornykh Porod i Protsessov. Tr. MGI*, Moscow.
11. Stepanov, A.W. 1933. Ueber den mechanismus der plastischen Deformation. *Z. Phys.*, **80**, 560.
12. Polimov, N.G., N.V. Galustashvili and I.M. Paperno. 1970. Voznikno-venie raznosti potentsialov na poverkhnosti deforiruemogo kristalla LiF (Appearance of potential difference on the surface of deformable LiF crystal). *FTT*, **12**, 8.
13. Khatiashvili, N.G. and R.A. Chikovani. 1973. Elektricheskie yavleniya, svyazannye s protsessom razrusheniya tsementnogo kamnya (Electric phenomena related to fracture processes in concrete). *Soobshchenie AN GSSR*, **71**, No. 2.
14. Deryagin, B.V. and N.A. Krotova. 1949. Adgeziya (Adhesion). Izd-vo AN SSSR, Moscow.
15. Parkhomenko, E.I. 1968. Yavlenie elektrizatsii v gornykh porodakh (Electrification Phenomena in Rocks). Nauka, Moscow.
16. Atlas Zemletryasenii v SSSR. 1962. (Atlas of Earthquakes in the USSR). Izd-vo AN SSSR, Moscow.
17. Fedotov, S.A. 1967. O seismicheskom tsikle, vozmozhnosti kolichest-vennogo seismicheskogo raionirovaniya i delgosrochnom seismicheskom prognoze (The seismic cycle, scope for quantitative seismic zonation and perspective seismic prediction). Sb. *Seismicheskoe Raionirovanie SSSR*, Nauka, Moscow.
18. Troitskaya, V.A. and O.M. Barsukov. 1969. Sovetskie stantsii zemnykh tokov (Soviet Terrestrial Current Stations). Izd-vo AN SSSR, Moscow.
19. Myachkin, V.I., B.V. Kostrov, G.A. Sobolev and O.G. Shamina. Osnovy fiziki ochaga i predvestniki zemletryasenii (Fundamentals of physics of the earthquake focus forerunners). This collection, p. 1.
20. Sobolev, G.A. 1973. Perspektivy operativnogo prognoza zemletryasenii po elektrotellurichеskim nablyudeniyam (Prospects of routine earthquake prediction by electrotelluric observations). Sb. *Predvestniki Zemletryasenii*, VINITI, Moscow.
21. Myachkin, V.I. and S.I. Zubkov. 1973. Svodnyi grafik predvestnikov zemletryasenii (Average graph of earthquake forerunners). *Izv. AN SSSR, Fizika Zemli*, No. 6.
22. Bochkovskii, V.F. 1954. Izmenenie gradienta elektricheskogo potentsiala atmosfery kak odin iz vozmozhnykh predvestnikov zemletryasenii (Variation in the electric potential gradient of the atmosphere: a probable earthquake forerunner). Sb. *Problemy Prognoza Zemletryasenii*, Izd-vo AN SSSR, Moscow.
23. Tikhonov, A.N. et al. 1954. K voprosu o svyazi zemnykh tokov i zemletryasenii (Interrelation of terrestrial currents and earthquakes). *Tr.*

Geofiz. in-ta, No. 25/152.

24. Yanagihara, K. and T. Yosimatsu. 1968. Lokal'nye izmeneniya telluricheskikh tokov v Kanioke pered zemletryaseniyami (Local variations in telluric currents in Kanyoka before earthquakes). Sb. *Predskazanie Zemletryasenii*. Mir, Moscow.
25. Fedotov, S.A. et al. 1970. Investigations on earthquake prediction in Kamchatka. *Tectonophysics*, **9**.
26. Sobolev, G.A. et al. 1972. Elektrotellurichеskoe pole i sil'noe zemletryasenie na Kamchatka (Electrotelluric field and strong earthquakes in Kamchatka). *Izv. AN SSSR, Fizika Zemli*, No. 2.
27. Myachkin, V.I. et al. 1972. The study of variation in geophysical fields near focal zones of Kamchatka. *Tectonophysics*, **14** (3/4).
28. Tarkhov, A.G. 1946. O geoelektricheskom pole fil'tratsii (Geoelectric filtration field). *Izv. AN SSSR, Ser. Geogr. i Geofiz.*, **10**, 5.
29. Karev, A.P. 1951. Osnovy geoelektriki (Fundamentals of Geoelectricity). Gostekhizdat, Moscow.
30. Semenov, A.S. 1955. Elektrorazvedka metodom estestvennogo elektricheskogo polya (Electro-prospecting by Natural Electric Field Measurement). Nedra, Leningrad.
31. Lashkhi, A.S. 1956. O vliyanii temperatury, osadkov i groz na zemnye elektricheskie toki (Effect of temperature, precipitation and thunderstorms on terrestrial electric currents). *Tr. in-ta Geofiz., AN SSSR*, **15**.
32. Grinberg, G.A. 1948. Izbrannye voprosy matematicheskoi teorii elektricheskikh i magnitnykh yavlenii (Selected Aspects of the Mathematical Theory of Electric and Magnetic Phenomena). Izd-vo AN SSSR, Moscow.
33. Tikhonov, A.N. and A.A. Samarskii. 1966. Uravneniya matematicheskoi fiziki (Equations of Mathematical Physics). Nauka, Moscow.

UDC 550.34.01.013

Variation of Velocities of Ultrasonic Wave in Tectonically Dislocated Zones

O.I. Silaeva, A.M. Zamakhaev and V.A. Terent'ev

The paper reports the measurements of longitudinal wave velocities in rock specimens and massifs. Seismic data reveal a much larger tectonically dislocated zone than do geological data. Prolonged observation of ΔV (difference in longitudinal wave velocities in specimens and massifs) variation corrected for water saturation revealed the stressed state of rock massif to be variable.

One of the principal problems of modern geophysics, the prediction of strong earthquakes, consists of ascertaining the factors responsible for energy accumulation in stressed zones and understanding the mechanism of fracture in rock bodies, its development in time and space. Consequently, study of the stressed state of the earth's crust and of the fracture zones formed through tectonic dislocations is of great importance. A variety of methods—tensometric, geodetic, seismological, seismoacoustic, geological, etc. [1, 2]—is employed for ascertaining the stressed state of rock massifs.

Detailed studies of fracture zones to ascertain the variations in the stressed state and to clarify the mechanism of displacement along the fracture are currently being pursued, particularly in California, on the San Andreas fault system [3]. They consist of careful seismic recording of earthquakes by a network of permanent and mobile stations and of measuring the deformation of the earth's surface using strain gages and repeated levelings. We have not come across reports in the literature on systematic studies of the elastic properties of rocks in zones of tectonic dislocation to ascertain the stressed state of rocks and its variation in time and space. Only isolated results are available.

Systematic observations have been made since 1968 by the IFZ in collaboration with the Geophysical Studies and Explorations Division of the Gidroproekt in the dam construction region of the Inguri Hydroelectric Project (HES). Prolonged observations of ultrasonic wave velocities in rock massifs were carried out.

Apparatus. The elastic wave velocities in rock massifs and specimens were determined with the help of an S-70 ultrasonic device [4] modeled on

the conventional RS-5 instrument. The radiator and the receiver of elastic waves were piezoelectric seignette salt transducers with oscillation frequencies around 140 KHz. The S-70 seismoscope [4] was tested in laboratory and field conditions in highland Dagestan, the tunnels of the Inguri HES and Goroblagodat mines. The tests showed the apparatus to be fit for use in varied climatic conditions.

Method. The construction site of the Inguri HES lies in a narrow cayon of the Inguri River with sides comprising monoclinally deposited limestones and dolomites of Lower Cretaceous age. The site lies in the contact zone of the fold system on the southern slope of the Greater Caucasus and the Georgian block. The Ingirish strike-slip fault west of the dam site is the largest fault dislocation. Its formation was accompanied by a series of fault dislocations of a smaller order. Some of them dissect the Ingirish thrust fault. The rocks around the fault dislocations are highly fractured. Six crack systems are distinguishable, in which the cracks along the bedding plane, steeply dipping cracks oriented roughly along the slopes, and gently dipping cracks oriented toward the left and right slopes are widespread.

The Inguri River basin is a seismic area. Epicenters of earthquakes of $M \leqslant 4\frac{1}{2}$ have been recorded by seismic stations in the middle reaches of the Inguri River. The available earthquake records do not permit comparison of earthquake foci having deep faults.

Prolonged full-scale observations of variations in longitudinal wave velocities were made in tunnels up to 200–250 m long passing through the slopes of the valley. The tunnels of the right slope dissected the tectonically dislocated zone at various levels and the tunnels of the left slope passed through monoclinally disposed undislocated beds. The tectonic dislocation is represented by a strike-slip fault with a dislocation amplitude of as much as 100 m vertically and 60–80 m horizontally. The dislocator with a depth of 1–9 m dips toward the right slope roughly at an angle of 70–80°.

Numerous studies [2, 5] have shown that the elastic wave velocity is a function of the stressed state of the rock massif or specimen. Therefore the following sequence of prolonged observations of the velocity V was followed to determine its variation with the variation of the stressed state of the rock massif. Initially the longitudinal wave velocity V_M in the massif was determined for the walls of mine shafts at fixed pickets in four profiles 45° apart. Later, oriented specimens were collected from the picket sites and the longitudinal wave velocity V_0 in them was determined. Besides, oriented specimens were collected in the tunnel through the left bank of the Inguri River from three drillholes 5, 8 and 10 m deep. Further, the difference ΔV between the velocity V_M in the rock massif and the velocity V_0 in the specimen was determined as follows:

$$\Delta V = V_M - V_0.$$

The variation of ΔV with time was observed to ascertain the variation occurring in the rock massif due to variation in its stressed state.

The velocity was determined by the ultrasonic impulse technique using gating and longitudinal profiling methods [6, 7]. The error in velocity determinations did not exceed 1% in specimens and 2–3% in rock massifs.

Under natural conditions the choice of the location of the pickets on the wall of the adit and the length of the profile was dictated by the nature of the tectonic jointing systems. The place on the wall of the mine shaft where the observation profiles were located was chosen so that it was free from cracks. The profile length thus did not exceed 20 cm. The picket sites remained unaltered with time. The interpicket distance was 20–30 m but diminished to 2 m near the tectonic dislocation zone. Determination of longitudinal wave velocities in rock massifs and specimens (polyhedral) is shown in Fig. 1.

Weathering and water saturation processes exercise an influence on the elastic properties of rocks [8, 9]. Therefore evaluation of the influence of these processes is of primary importance for obtaining authentic data on the variation with time of longitudinal wave velocity in a rock massif due to variation in the stressed state.

It was shown in [8] that weathering processes bring down the longitudinal wave velocity in rocks. If the continuity of the rock is not lost thereby the nature of the spatial distribution of the velocity V (anisotropy of V) remains

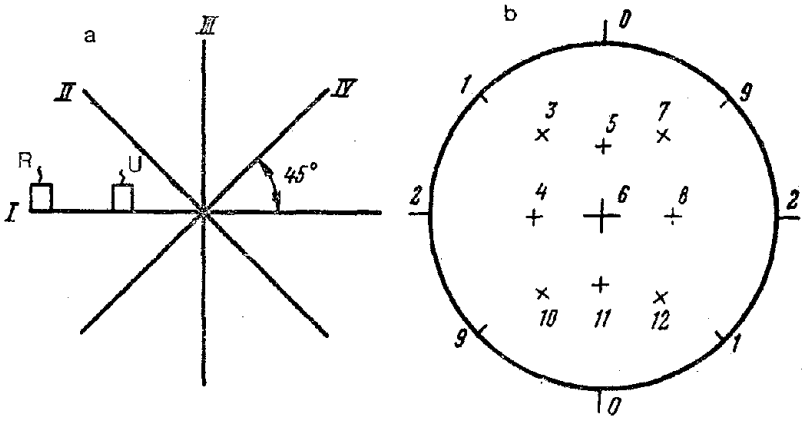

Fig. 1. Diagrams for determination of longitudinal wave velocities in (a) mine wall and (b) specimens (on Wulff's net):

a—I-IV are observation profiles; I—in horizontal direction along adit axis; III—in vertical direction; II and IV—intermediate through 45°; R—Radiator; U—Ultrasonic wave receiver; b—Direction 0 coincides with profile I; 5—with profile II; 6—with profile III; 11—with profile IV for recording velocity V on mine wall.

unchanged. Prolonged observations were made in deep adits to eliminate the influence of weathering processes.

Since the value of V and anisotropy of velocity is influenced by water saturation, studies were conducted to ascertain this influence. The results of these studies are partially compiled in [9].

Results of velocity V determination in specimens. Measurements of longitudinal wave velocity V in dry specimens of monoclinally bedded rocks from the left slope show that these rocks (limestones) possess high V values ranging from 3500 to 6500 m/sec. It was found that velocity anisotropy is a characteristic property of these rocks.

Earlier the influence of the structural orientation of rocks on the ultrasonic wave propagation velocity was clarified in the study [7] of Caucasian Jurassic and Cretaceous limestones, dolomites, and sandstone blocks collected from regions close to the Stepnoe-Bakuriani and Groznyi-Nakhichevan meridional deep seismic sounding (DSS) profiles.

The measurements showed that the rocks under study possess different elastic properties in different directions, i.e. the elastic wave velocities in them are anisotropic. The coefficients of velocity anisotropy for these rocks are on the average 3–10%, reaching 30–50% in isolated cases. Certainly, the structure of the rock reflects the circumstances that prevailed during its formation and subsequent deformation. It is therefore suggested that velocity anisotropy is a function of the stressed state of the rock bed and reflects a regular relationship of the microstructure orientation of the deformed rocks with the tectonic history of their geological evolution [6, 7].

Measurements of the velocity V in specimens collected at the Inguri HES construction site showed that the nature of spatial V (velocity anisotropy) distribution remains practically unchanged for the entire rock massif of the slope that we studied. Our measurements embrace roughly 500 m² of the massif. The area of maximum velocity lies almost in the horizontal plane roughly in the N–S direction, whereas the area of minimum velocity lies in the vertical plane almost perpendicular to the area of the maximum velocity. Since the rock beds dip at an angle of $\sim 50°$, the observed velocity anisotropy is not related to rock bedding.

The coefficient of velocity anisotropy calculated percentagewise as the maximum-minimum velocity difference referred to the minimum velocity reaches 10–30%. The spatial velocity distribution changes with the transition from rock beds of one mineralogical composition to another. The velocity data for specimens collected from two neighboring beds of marlaceous and crystalline limestones are shown as examples in Fig. 2a and b on a Wulff's net. According to these data, a definite spatial velocity distribution is typical of this rock massif. This average distribution expressed as the arithmetic mean of all distributions is shown in Fig. 2c. This cannot serve as a basis for determining absolute velocity values because it was plotted

from velocity values for rock specimens differing in mineral composition. However, it can give an idea of the general orientation of the axes of maximum and minimum velocities for the rock massif not subjected to stress.

The results of our studies (Fig. 2a and b) show that prolonged tectonic processes lead to such microstructural changes in the rock that only the influence of those tectonic processes are imprinted on the rock that it experienced during its geological evolution. The primary influence of rock bedding disappears.

Analysis of the velocity data for dry polyhedral rock specimens from the tectonic dislocation zone on the right slope of the Inguri River shows that the velocity is somewhat less in these rocks than in the rocks of the left slope. The limestones in the downthrow side along the adits, roughly from the adit mouth to the fracture site, show velocities ranging from 3000 to 5000 m/sec. The limestones in the uplifted side, near the fracture, have

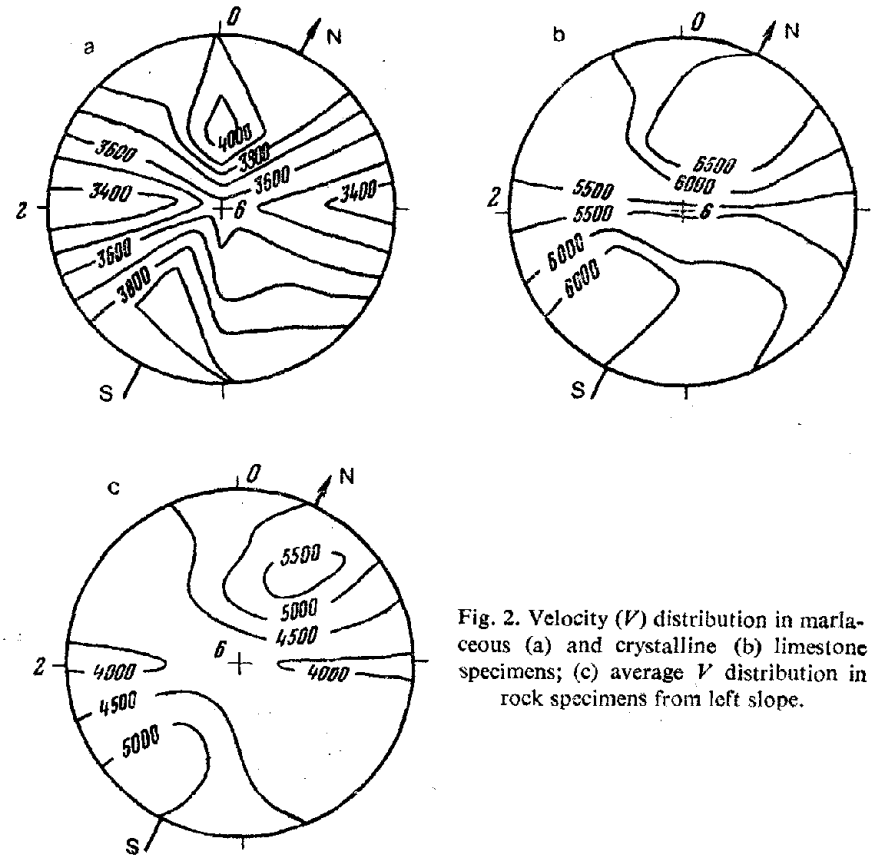

Fig. 2. Velocity (V) distribution in marlaceous (a) and crystalline (b) limestone specimens; (c) average V distribution in rock specimens from left slope.

lower V values of the order of 2500–3500 m/sec, and only near the adit face does the velocity increase to 5500 m/sec.

The measured velocities in dry limestone specimens collected from different beds in the zone of tectonic dislocation are shown in Fig. 3 on the Wulff's net. The spatial velocity distribution is not the same for all specimens taken from the tectonically dislocated zone along the adits. The velocity anisotropy coefficient for the rocks of the downthrow side varies from 10 to 60% and for those of the uplifted side from 6 to 30%. Thus the velocity in different directions in multihedral rock specimens from the zone of tectonic dislocation differs from that in specimens of rock bedded monoclinally. This difference can be attributed to the peculiarities of the tectonic processes.

In the monoclinally bedded zone the prolonged tectonic forces operating in a definite direction did not markedly disturb the continuity of the rock massif. This resulted in stable changes in the rock structure. The influence of these structural changes on the V values seems to be more important than

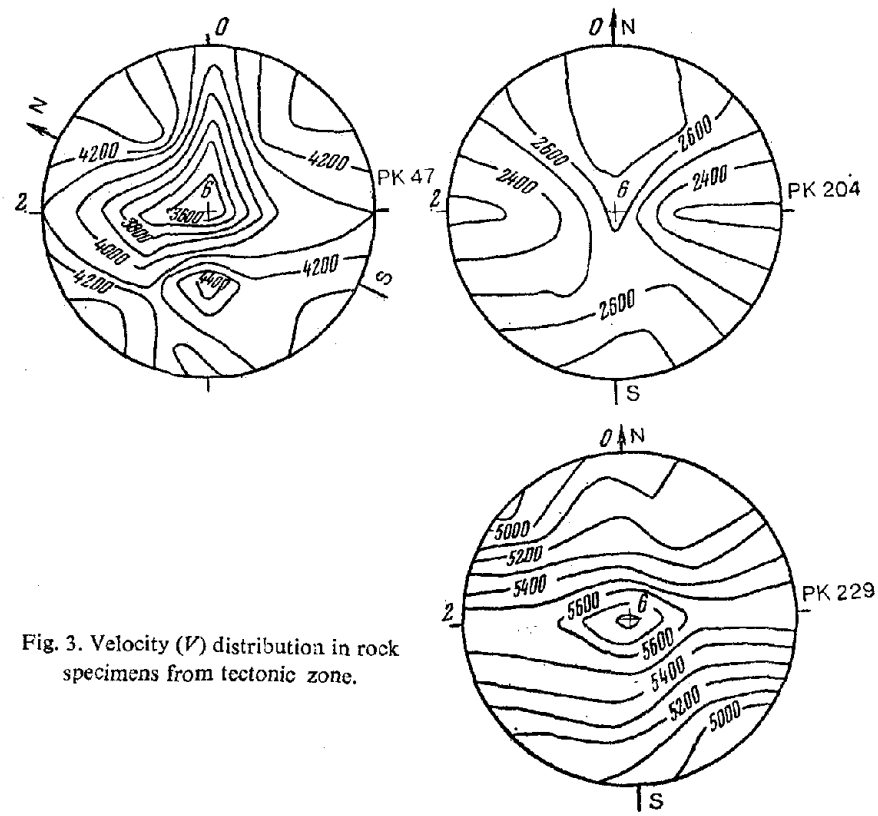

Fig. 3. Velocity (V) distribution in rock specimens from tectonic zone.

the influence of rock bedding. Similar structural changes are detectable by ultrasonic sounding. An almost unique spatial V distribution is obtained for the specimens from the left slope of the rock massif under study.

Repeated stress redistribution invariably occurred in the rock massif, because formation of supporting ruptures of the Ingirish fault, including the strike-slip fault of the right slope covered by the adits, was accompanied by repeated shoves. The stress field near the strike-slip fault was heterogeneous. The medium responded to this field in a definite way. The structural changes taking place with velocity changes in the specimens collected from the tectonic zone suggest the existence of such a heterogeneous stress field.

Thus, velocity determination in specimens showed that the tectonically dislocated zone identified by ultrasonic observations far exceeds (almost tenfold) the visible size of the dislocator zone given by geological data. According to ultrasonic data, the zone of tectonic dislocation is characterized by variable spatial distribution of longitudinal wave velocity. Constant spatial distribution of longitudinal wave velocity (velocity anisotropy) with increasing distance from the visible fracture site may be a sign that the wave has moved away from the tectonically dislocated zone.

Let us analyze the velocity measurements in specimens saturated with water. These data are elucidated in detail in [9]. Many researchers [8–10] have shown that water saturation exerts a great influence on the elastic wave velocity, which increases in some cases and decreases in others. The increase in velocity with water saturation of the specimen was attributed to an increase in the general elasticity of the system, while the fall in velocity with water saturation of the specimen was ascribed to the rupture of intergranular bonds under the influence of water.

In short, the results of our study of the influence of water saturation on the V values in rock specimens from the construction site lead us to the following conclusions:

Figure 4a, b and c shows typical graphs depicting the change of V (in the directions from 0, 1 and 2 to 12) as a function of water saturation of the specimen in terms of $(V_w - V_d)$ with increasing velocities V_d measured in the dry specimen in different directions.

Filling of the specimens with water leads in some cases to a general increase in velocity (Fig. 4a) level, where the nature of the spatial velocity distribution remains almost unchanged. The coefficient of velocity anisotropy also increases or decreases with water saturation. The coefficient of velocity anisotropy was calculated as the percentage ratio of the maximum-minimum velocity difference to the minimum velocity, ignoring the directions of measurements. In other cases filling the specimens with water results in an increase in velocity in the specimens, but a greater velocity increase with water saturation is observed in regions with lower V_d in dry specimens (Fig. 4c). Filling such specimens with water induces changes in the nature of the spatial velo-

city distribution in which the coefficient of velocity anisotropy diminishes. The difference between the nature of the water saturation of the specimens represented by the graphs in Fig. 4a and c seems to be attributable, mainly to the existence of oriented microfissures in the specimen. Oriented microfissures appear to be absent from the specimen PK 196 (Fig. 4a) because water saturation leads to a general increase in V_w. Orientation of microfissures is likely in the specimen PK 191 (Fig. 4c), for saturation occurs vigorously in directions in which reduction of V_d in dry specimens is observed.

In [10] the authors discussed at length the influence of the shape and size of pores and cracks filled with or free from water on the velocities to be measured in rock specimens. They concluded that the formation of microfissures is likely to increase with an increase in the difference $V_w - V_d$ in water-saturated and dry rock specimens. Thus, with $(V_w - V_d)$ varying from 1000 to 3000 m/sec the microfissures increase from $2 \cdot 10^{-3}$ to $5 \cdot 10^{-3}$ in granites.

The results of water saturation of the specimen PK 204 (Fig. 4b) show that for the majority of directions the intergranular bonds are severed as the velocity in the specimen falls with saturation.

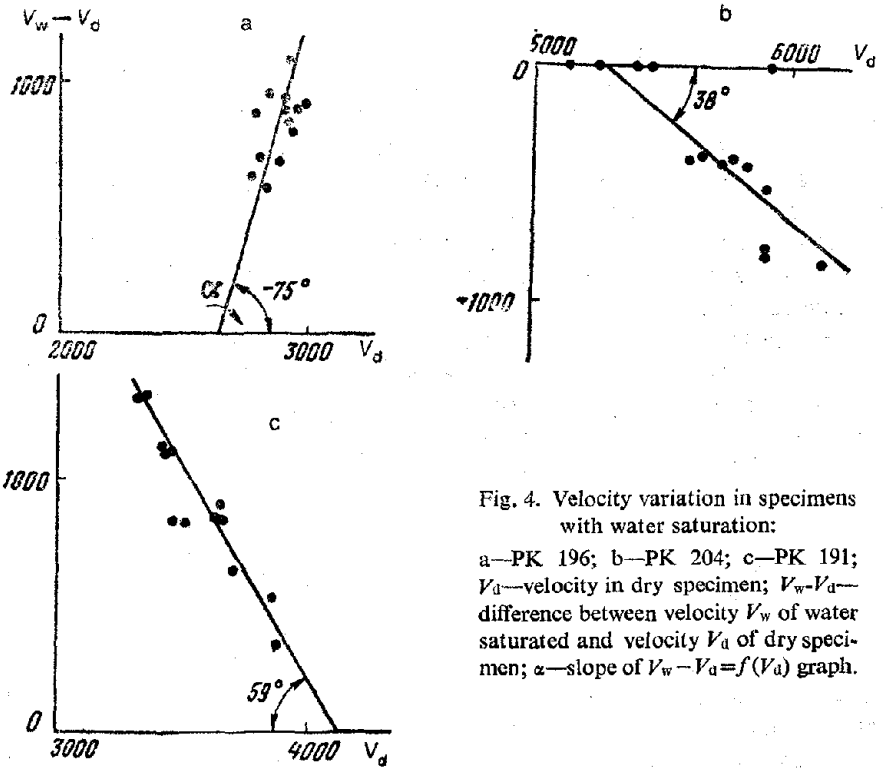

Fig. 4. Velocity variation in specimens with water saturation:

a—PK 196; b—PK 204; c—PK 191; V_d—velocity in dry specimen; V_w-V_d—difference between velocity V_w of water saturated and velocity V_d of dry specimen; α—slope of $V_w - V_d = f(V_d)$ graph.

The determination of the angles of inclination presented in Fig. 5 shows that with rare exceptions sufficiently stable α values of 20–40° are obtained for the downthrow part of the strike-slip fault (up to PK 188) even when $(V_w - V_d)$ values of velocity changes with saturation vary as shown in the graphs of Fig. 4. The uplifted side (191 m away) is characterized by unstable α values, being both positive and negative. Such directions of measurements were chosen for prolonged full-scale observations of velocities in the rock massif for which the calculated coefficients of velocity anisotropy changed little with saturation [9], even though the velocities might change with water saturation of specimens, as shown in Fig. 4.

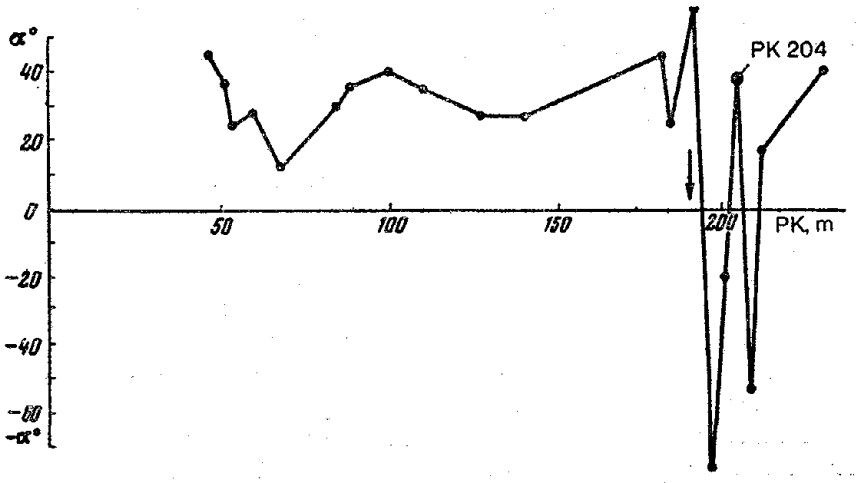

Fig. 5. Angle of inclination σ of $V_w - V_d = f(V_d)$ graph as function of distance for tectonically dislocated zone. Arrow shows fracture site based on geological data.

Thus, to obtain authentic data on velocity change with time in rock massifs due to change in the stressed state of the massifs it is necessary to clarify the influence of water saturation (preferably gradual) on the velocity distribution in rocks collected from the points where the ultrasonic probes are laid. These studies yield the most suitable directions for which the influence of water saturation on the coefficients of velocity anisotropy are negligible. Therefore the observed changes in the coefficient of velocity anisotropy in the massif with time should be attributed to the changes in the stressed state of the massif. In prolonged full-scale observations it is necessary to record the velocity not only in two directions but, if possible, in all directions, i.e. it is necessary to study the spatial velocity distribution in the rock massif.

Determination of velocity V in rock massif in tectonically dislocated zone. It follows from the review of the data obtained during 1968–1973 that regions of high ΔV values ($\Delta V > 1000$ m/sec) consistently occur on the wall of the mine shaft in the tectonically dislocated zone—a fact not to be explained by the influence of changes with time, in the water saturation of the massif, for these ΔV values are higher than the corrections to be introduced for water saturation. Besides, areas with low ΔV values of the order of 100–500 m/sec and even areas where ΔV values are negative (the velocity V_0 in the specimen is higher than the velocity V_M in the massif) are consistently observed.

Let us compile all the ΔV values corrected for water saturation in a Table, i.e. let us analyze a case where the velocity V_M in the rock massif is higher than or equal to the velocity V_W in the water-saturated specimen. In such a situation the record variations of ΔV with time should be attributed to the variations in the stressed state of the mine massif.

It is known that during mining the equilibrium of the stressed state of the massif is disturbed [2, 11] and that due to the redistribution of the internal strains around the mining drive three zones, namely, a low-pressure zone or a zone of rocks subjected to alteration, a high-pressure zone or a zone of maximum bearing pressure, and a zone of natural pressures where the rock massif remains unaffected by mining operations, are formed in succession with increasing distances from the pit wall. The drive into the rock massif stimulates a reaction, which leads to changes in the physical properties of the surrounding rocks due to changes in the stressed state near the mine pit. Complex seismoacoustic observations are made to determine the changes in the elastic properties of the rock massif [2, 11].

Seismoacoustic studies of the stressed state of rocks in mining operations revealed all three regions [11]. These regions spread in accordance with the physico-mechanical properties of the rocks, the distribution of the properties of the rocks and the configurations of the mining site. The region of weakened rocks is characterized by lower elastic wave velocities. The region showing maximum bearing pressures is distinguished by much higher elastic wave velocities normal for a deeper region of the massif not affected by mining operations. Thus absolute changes in the stressed state of a rock massif cannot be determined from the changes in the elastic wave velocities in the mine wall. However, the observed interrelation of stresses in the mining area and stresses in the rock massif permits an indirect evaluation of the changes in the stressed state of the rock massif from the velocities measured in the mine wall.

Experiments with rock specimens showed that the maximum velocity variation occurs at pressures varying from 0 to 30–50% of the failure pressure [5]. The failure pressure of the limestones tested ranges from 800 to 1000 kg/cm^2. It was found in experiments with specimens subjected to unidirectional pressure that along the compressive force, as expected, the V

variation with pressure is greater, the lower the velocity in the specimen under atmospheric pressure.

For instance, for specimens with $V_d = 2900–3600$ m/sec at atmospheric pressure, V_d increases by 900–1500 m/sec as the pressure p rises to 200 kgf/cm^2. For specimens with $V_d = 4000–5500$ m/sec at atmospheric pressure, V_d increases by 300–900 m/sec as the pressure p rises to 200 kgf/cm^2. The velocity V_w does not change much with pressure if the specimens are saturated with water [10].

Let us examine the data compiled in the Table in two groups: the data for profile I in the horizontal direction and for profile III in the vertical direction alongside the data for profiles II and IV inclined to profile III at 45°.

Prolonged observations of ΔV variations in the horizontal direction showed that areas of high and low ΔV values alternate (their places in the Table are left blank, for they lie below the level of correction for water saturation). It follows that the rock massif has areas of reduced stresses which might be assigned to zones of probable crushing of the massif. The zone is particularly stable in the uplifted side at PK 191, 196 and 199.

Prolonged observation of ΔV variations in the vertical direction (and in directions close to the vertical along profiles II and IV) showed that the area of relaxation of the slope extends roughly for 100 m. Farther on there is an area of increased ΔV which is consistently recorded irrespective of the locations of the observation pickets either on the downthrow side (up to 188 m) of the strike-slip fault or on the uplifted side up to PK 191. The area where PK 191, 196 and 199 are located is characterized by consistently low ΔV values. These pickets show an area of reduced stresses which might be assigned to the zones of probable crushing of the rock massif.

The observed values of $\Delta V > 1000$ m/sec show that the mine walls have areas under a compressive stress of ~ 200 kgf/cm^2, at least twice as large as the areas under geostatic load. Besides, there are areas where ΔV values are low. This is particularly true for an area on the uplifted side where tensile stresses are probable.

Geological data show that the rocks in the uplifted side are subjected to more severe crushing in the case of upthrust and strike-slip type disjunctive faulting. This is perhaps due to the fact that mainly the hanging side, which suffers maximum deformation, is set in motion. Therefore the occurrence of an area of reduced ΔV in the uplifted side does not contradict the general concepts.

The stressed state of the Inguri limestones bedded under natural conditions was estimated in a neighboring adit near the tectonically dislocated zone by measuring the strains in borehole cores [12]. The adit was not deeper than 60 m, and the tectonically crushed zone was found to occur at a distance of 23–25 m from the adit mouth. Experimental results showed that the influence

Variation of ΔV with respect to time

	Profile I, horizontal					Profile II, at an angle of 45°				
PK, m	1968	1969	1970	1971	1973	1968	1969	1970	1971	1973
47	400	0	0				850	300		
60	550	600	1050		500		450	350		550
100	0		500			0	450	1000		0
127	1700	800	1050	1050	2000	900	450	1600	1400	1700
181			1400					350	150	550
183		200			750	250	200		250	350
191	0	0	150	300			400	800	250	300
196							300	400	300	600
199										500
204	750	1400	1050	1350	1300	1900	1400	3000	2400	2400
207	1350	0		1150	0	550	500	1800	1400	1450
211								250		300
229			0	0						

	Profile III, vertical					Profile IV, at an angle of 45°				
PK, m	1968	1969	1970	1971	1973	1968	1969	1970	1971	1973
47	0	200	100				150	150		
60		0	0		250		200	250		300
100	1000	350	0							
127	900	1150	1400	1650	1650	150	1300	1000	1200	2000
181								1400	550	650
183	700	600	850		700	500	750	1250	1050	800
191	0	700	900	1100	500					700
196	200	450	750	450	900	750	1150	850	850	350
199									200	900
204	1900	2200	2250	2400	2450	1550	1600	1800		2100
207	750	750	2300	700	700	550		1800	900	400
211			100					250		200
229		150	200	700	—		1000		800	—

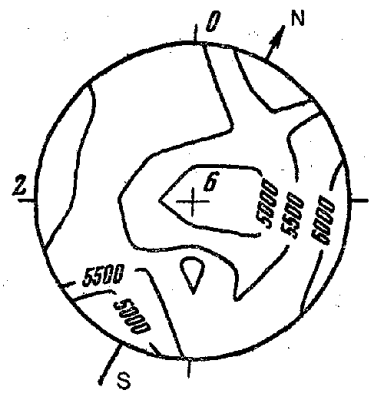

Fig. 6. Velocity (V) distribution in rock massif.

of the tectonically crushed zone manifests itself in a reduction of the principal compressive stresses and in a change in the stress orientation approaching the fault. The pattern of stressed state changes abruptly just after the zone and, in all probability, within the zone itself. Moreover, the principal stresses change not only in magnitude but also in sign.

The tensile stress gradually falls and turns into compressive as the distance from the fault increases. The stress variation ranged within $\pm$ 100 kgf/cm^2. Taking note of the great difficulties involved in full-scale measurements due to the complex geological structure of the area under study, the authors concluded that their results obtained by unloading cores describe the stresses in mountain blocks of diverse scale rather than the stressed state of the mountain rock as a whole. However, qualitatively the pattern of stress distribution around the fault obtained by the authors of [12] agrees with the results of our prolonged observations of the elastic wave velocity (V). The divergence lies in the evaluation of the stressed magnitude. Perhaps this is because the measurements reported in [12] were made in the sphere of influence of the slope (up to 50 m), resulting in a general reduction in the stress level.

Our measurements may contain systematic errors arising from velocity measurements in specimens not right after their extraction from the rock massif but after an interval. This may have resulted in strain release in the specimen and in gradual microfracturing and lowering of the velocity to be measured. This is a knotty question demanding special study.

Thus the salient findings of the prolonged observations of ΔV variations in mine walls are that the stressed state of rock massifs is variable.

The next stage of prolonged studies will involve observations of spatial ΔV variations in the rock massif beyond the sphere of influence of mining

operations so as to determine the variations of the stressed state in a region of the rock massif not affected by mining operations.

Such observations were started recently at PK 134 m where ultrasonic probes were installed at a depth of 4 m. The velocities V_M obtained by these probes are presented on a Wulff's net in Fig. 6. Interpretation of these velocity data suggests that the deeper limestones are characterized by high velocity values of the order of 5000–6000 m/sec. The spatial V_M variation is regular. The region of $V_{max} = 6000$ m/sec lies in the horizontal plane almost perpendicular to the V_{min} region. The region of $V_M = 5000$ m/sec lies in the horizontal plane in the N–S direction.

The spatial V_M distribution pattern in the massif is not related to rock stratification. The anisotropy coefficient of the velocity V_M reaches 20%.

CONCLUSION

Prolonged observations of ΔV (difference between longitudinal wave velocities in massif and specimen) variation, after allowing correction for water saturation revealed the stressed state of mountain rocks to be variable. In the downthrow side of the strike-slip fault and partly in the uplifted side near the dislocation the ΔV values are found to be high in the vertical direction, testifying to a region of compressive stresses almost twice as high as the geostatic load. Further, there are also regions of low ΔV values, particularly in the uplifted side and in the downthrow side in the horizontal direction where tensile stresses are possible. The low ΔV regions may be assigned to zones of probable crushing of the rock massif.

The results obtained provide the basis for suggesting that the spatial longitudinal wave velocity distribution (velocity anisotropy) resulting from the intrinsic microstructural peculiarities of a rock may be an indicator of the impact of the tectonic stress field on the rock and may reveal the zones of stress concentration. This provides a prospect for study of zones of active tectonic disturbances right up to the earthquake origin.

REFERENCES

1. Gzovskii, M.V. 1971. Sovremennye vozmozhnosti otsenki tektonicheskikh napryazhenii v zemnoi kore (Present scope for evaluating tectonic stresses in the crust). Sb. *Tektonofizika i Mekhanicheskie Svoistva Gornykh Porod*, Nauka, Moscow.
2. Myachkin, V.I. 1964. Ul'trazvukovye issledovaniya napryazhennogo sostoyaniya i svoistva gornykh porod v massive (Ultrasonic Studies of the Stressed State and Properties of Rocks in the Massif). Author's abstract of Doctoral Thesis, *IFZ AN SSSR*, Moscow.

3. Proc. Conf. on Tecton. Probl. of San Andreas Fault System. Stanford Univ. Press, 13, 1973.
4. Terent'ev, V.A. 1973. Malogabaritnyi polevoi impulsnyi ul'trazvukovoi seismoskop (A portable field impulse ultrasonic seismoscope). *Izv. AN SSSR, Fizika Zemli*, No. 11.
5. Sb. Ultrazuk v Geofizika (Collection: Ultrasonic in Geophysics). Mir, Moscow, 1964.
6. Silaeva, O.I. and E.I. Bayuk. 1969. Izmenenie anizotropii skorosti v gornoi porode pri gidrostaticheskom davlenii (Velocity anisotropy variation in rocks under hydrostatic pressure). *Izv. AN SSSR, Fizika Zemli*, No. 8.
7. Silaeva, O.I. et al. 1971. Anizotropiya skorosti prodol'nykh voln v gornykh porodakh Kavkaza (Velocity anisotropy of longitudinal waves in rocks of the Caucasus). *Izv. AN SSSR, Fizika Zemli*, No. 2.
8. Delitsin, I.S. and O.I. Silaeva. 1973. Vliyanie kontakta zeren kvartzita na skorosti prodol'nykh voln v gornoi porode (Effect of quartzite grain contact on longitudinal wave velocity in rock). *Izv. AN SSSR, Fizika Zemli*, No. 10.
9. Silaeva, O.I. and A.M. Zamakhaev. 1974. Izmenenie anizotropii skorosti v obraztsakh gornykh porod s vodonasyshchiniem (Velocity anisotropy variation in rock specimens with water saturation). *Izv. AN SSSR, Fizika Zemli*, No. 8.
10. Nur, A. and G. Simmons. 1969. The effect of saturation on velocity in low porosity rocks. *Earth and Planet, Sci. Lett.*, Dec.
11. Savich, A.I., V.I. Koptev and E.A. Grigor'yants. 1974. Izuchenie estestvennykh napryazhenii v massive gornykh porod seismoakusticheskimi metodami (Study of natural stresses in rock massif by seismoacoustic methods). *Tr. Gidroproekta*, No. 33.
12. Gaziev, E.G. and A.E. Krylov. 1972. Estestvennye napryazheniya v skal'nom osnovanii arochnoi plotiny Inguri GES (Natural stresses in the rocky base of the arch dam of the Inguri HES). Sb. *Izmerenie Napryazhenii v Massive Gornykh Porod*, Izd-vo SO AN SSSR.